VERTICAL SEISMIC PROFILING: THE ONE-DIMENSIONAL FORWARD AND INVERSE PROBLEMS

by

Robert R. Stewart
B.Sc., University of Toronto,
Toronto, Ontario, Canada
1978

SUBMITTED TO THE DEPARTMENT OF EARTH AND PLANETARY SCIENCES IN PARTIAL FULFILLMENT OF THE REQUIREMENTS FOR THE DEGREE OF DOCTOR OF PHILOSOPHY

at the

May 24, 1983

Signature of Author . . . . . .
Department of Earth and Planetary Sciences
May 24, 1983

Certified by . . . . . .
M. Nafi Toksöz
Thesis Advisor

Accepted by . . . . . .
Theodore Madden
Chairman
Departmental Committee on Graduate Students

VERTICAL SEISMIC PROFILING:

THE ONE-DIMENSIONAL FORWARD AND INVERSE PROBLEMS

by

ROBERT R. STEWART

Submitted to the Department of Earth and Planetary Sciences on May 24, 1983 in partial fulfillment of the requirements for the Degree of Doctor of Philosophy in Geophysics

ABSTRACT

In situ measurement of the seismic wavefield generated by a surface source is becoming an increasingly common geophysical surveying procedure. This measurement, known as a vertical seismic profile (VSP), furnishes the opportunity to investigate wave propagation in the shallow earth and to estimate the seismic values describing the lithologic section.

This study develops two one-dimensional (1-D) inversion procedures to estimate the seismic parameters (velocity, density, attenuation, upgoing and downgoing wavefields) from VSP data. A Marquardt-Levenberg traveltime inversion using 1-D ray tracing is designed and applied to synthetic and field data from the Gulf Coast, Sulphur Springs, Texas and Colorado. The errors in the data and parameters and their relationship to one another are considered. Optimal velocity layer thickness (40ft-150ft) in the inversion depends partly on the observation spacing and data noise. The traveltime inversion is found to provide a stable and accurate 1-D estimate of the velocity section. The VSP velocities are found to be consistently several percent smaller than the sonic velocities. Both P and SH velocities in the Gulf Coast survey are significantly reduced in regions of gas saturation.

Comparing the VSP traveltimes to the integrated sonic traveltimes from surveys conducted in the Anadarko Basin, Texas, the above field data and the literature uncovers a discrepancy between the seismic and sonic traveltimes. The seismic traveltimes are from 2.0 to 7.0 ms/1000ft longer than their corresponding sonic traveltimes. Wave equation synthetic data and field results indicate that this discrepancy may be well explained by wave propagation effects. Velocity dispersion associated with attenuation (nearly-constant Q) appears to cause the most significant time delays while short-path multiples have a smaller but observable effect. Equations to predict these effects are developed.

To allow usage of the full VSP waveform in constraining the seismic parameters, two wave equation based inversions are devised. The weighted damped least-squares inversion is used to simultaneously estimate the velocity, attenuation and upgoing and downgoing waves in a group of four vertically-adjacent VSP seismograms. This process is repeated for the

entire set of VSP seismograms. Results from both synthetic and field data show very good parameter estimation. Especially useful is the extracted upgoing wave; it may be used to pinpoint the depth of its generation and to estimate the underlying impedance mismatch. The separated downgoing wave provides a source signature as well as constraint on the velocity and attenuation of the medium.

Impedances are also included as independent parameters in the forward model of a stochastic inversion using the four trace group. In areas of large reflection coefficients, impedance contrasts are reasonably estimated. Basically, the algorithm finds the impedances which fit the reflection coefficient and are also closest to the initial guesses. A good first guess is critical. Density may be computed from these impedances. In the field example, the densities have been well estimated near a strong impedance contrast.

Several related theoretical results are developed. Analysis for the extension of the wave equation inversion to the elastic and dipping interface cases is outlined. A procedure for the simultaneous inversion of the complete VSP data set is devised. The lateral resolution (Fresnel zone) is calculated for the VSP geometry and wavelength.

The procedures developed and results found in this work provide a coherent and reasonably complete analysis of the 1-D vertical seismic profile.

Thesis Supervisor: M.N. Toksoz

Title: Professor of Geophysics

To my clan, especially Ronald and Emma

with fondest remembrance and admiration of Ida.

Acknowledgements

I am grateful to my advisors on the faculty and staff at MIT. In particular, I was encouraged, aided and supported by Prof. K. Aki, Prof. M.N. Toksoz and Dr. R. Turpening. I sincerely thank them for the insight that they provided. Prof. T. Madden offered valuable advice both on and off the hockey rink.

A significant part of my education has been provided by the geophysical industrial community. Many people at the Chevron Oil Field Research Co. and ARCO Exploration and Production Research Center were exceedingly generous with their time and knowledge.

The VSP group at ARCO consisting of J. DiSiena, J. Gaiser, P. Huddleston, H. James, C. Mosher, M. Osterhoudt and T. Fulp was always enthusiastic about the subject and supportive of new developments. I am appreciative of their critical review of numerous manuscripts. Special thanks to T.K. Kan for his particular insight into the science of rock physics and exploration seismology. Further thanks to him for his participation on the thesis defense committee.

I also wish to express my appreciation to the ARCO Oil and Gas Co., Dallas, Texas for releasing much of the data used in Chapters 3 and 4. and for providing gainful employment for a period during which part of this work was completed.

Discussions with G. Omnes of CGG and W. Dieckman of Chevron have been useful.

Many others also contributed to the intellectual and social enjoyment of the MIT experience. Without the jovial camaraderie of J. Nabelek and B. Tucker, this effort would be greatly diminished. May the great problems of existence (traveltime around the Charles River bridge circuit, ethics of scientific exchanges with the USSR, etc.) continue to fascinate and challenge.

A number of other friends and colleagues have created and enhanced the good experiences and while tempering the bad. Sincere thanks to D. McTigue, K. Tubman, M. Willis, C. Esmersoy, J. Pulli, K. Coyner, P. Huang, T. Keho, W. Beydoun and C. Barton for their scientific commitment and expertise and valued friendship.

Fondest thanks to B. Brennan, K. Forni, J. Peet and P. Telles for their patience, humor and civilization.

D. Roecker is legendary for her administrative touch. D. Frank word processed (and processed...) this thesis. Many Thanks.

Table of Contents

Forward

> I am in earnest, I will not equivocate, I will not excuse, I will not retreat a single inch and I will be heard.
>
> William L. Garrison
> (Bostonian Statesman, 1805-1879)

0.1 OVERVIEW

The Vertical Seismic Profile (VSP) is adding the third dimension to seismic observations. It is an in situ measurement or probe of the seismic wavefield in depth as well as time; that is, the wavefield is recorded at known points inside the medium for a several second duration. The physical methods of measurement (downhole receivers, surface sources, digital recorders) have advanced to the point where there is abundant coherent information in the recorded waveforms that has yet to be extracted and interpreted. Thus, the exciting and unusual situation exists where good data are available but fundamental interpretation is still developing. This thesis develops several forward and inverse analysis techniques and uses these methods to study a number of synthetic and field data sets.

0.2 OBJECTIVES

The ultimate objective of geophysics is to be able to make quantitative statements about the interior of the earth. The primary objective in this thesis is to use VSP data to estimate the seismic parameters (velocity, density and attenuation) describing the lithologic section.

En route to this goal, techniques are developed to analyse the VSP data-both in terms of forward modelling and data inversion. In this respect, ray tracing, wave equation modelling and classical inverse theory are brought to bear on the VSP data. The attempt has been made to develop simple, stable techniques which are intended to work on a wide variety of

data sets. As a necessary factor accompanying the velocity, density and Q estimation, upgoing and downgoing waves in the section need to be separated. Extracting the upgoing wave is of great interest itself, as it is this upgoing wave which is measured by the pervasive seismic reflection technique. The extracted upgoing wave may be used to show how each phase of the surface seismogram was generated. Secondary goals of this work are to understand which lithologic constraints (such as layering thickness) and wave propagation effects (velocity dispersion) have a dominant effect on the parameter estimation.

Having estimated the seismic parameters as the primary objective, it is necessary to correlate them with particular lithologies. In the field examples discussed, the methods developed here are used to solve problems concerning the lithology of the shallow earth. Thus, while considerable attention is given to the development of methods, the approach is "petro-geophysical"; the final goal in geophysics must always be to interpret the parameters in terms of "rocks". In summary, the attempt is made to extract all possible seismic information from the single source offset one-dimensional VSP and use it to enhance lithologic understanding.

0.3 CHAPTER DESCRIPTION

While it often seems that most seismological problems were solved, at least theoretically many decades ago (e.g. Lamb, 1898), new techniques and developments in both equipment and computing have lead to new challenges. The VSP technique and analysis are recent enough that a thorough review of the subject does not yet exist in the literature. Because of this, Chapter 1 provides an overview of previous work in "borehole seismology" and attempts to give an accurate assessment of where the field stands at present.

In accordance with the goal of developing techniques to extract the seismic properties of the geologic section from the VSP, this thesis presents several inversion techniques with accompanying examples.

Chapter 2 begins the discussion with the simple notions of 1-D ray tracing and traveltime inversion. This chapter is straightforward and serves as a primer on VSP data and inversion. Using only the first arrival times of a VSP is a minimal analysis yet still a very powerful one considering the quality and simplicity of these data. Concepts of inverse theory are introduced and applied to the traveltime data. Errors in the VSP traveltimes are considered along with the layer thickness resolution that is possible with a given VSP. Parameter covariances are studied in conjunction with several VSP data sets. The traveltime inversion of three field data sets demonstrates the effectiveness of the algorithm.

Comparing the VSP source-to-receiver traveltimes to those of the integrated sonic log leads us to believe that the propagation problem is more complex than simple ray tracing predicts. The concern with the traveltimes is that there may be systematic effects that are not understood in terms of experimental errors or ray tracing. As the sonic log is an important measurement, which is often compared to the VSP, some consideration is given to how the two measurements and their analysis differ. In chapter 3, wave equation modelling is used in attempt to understand how short-path multiples, Q and velocity dispersion can affect the VSP traces and in particular the traveltimes. Using the wave equation for the forward problem thus allows a more realistic earth model (attenuative and velocity dispersive) than does ray tracing. It also

provides a method to model the later arrivals in the seismogram and their amplitudes. A set of four VSP surveys conducted in the Anadarko Basin, Texas and one from Sulphur Springs, Texas are used to analyse these effects. It is established that short path multiples, and more importantly, body wave velocity dispersion (based on a nearly-constant Q theory) explain the observed differences between seismic and sonic traveltimes. This is an important and controversial result.

Chapter 3 is mainly concerned with the forward problem of modelling VSP data. In many cases, as in Chapter 2, the observed data are available but it is the underlying parameters which are of interest. Chapter 4 sets up the the one-dimensional VSP inverse problem with a wave equation forward model. Both the weighted, least-squares and stochastic inverses are used. The procedures proposed and developed use a group of four traces which are iteratively matched by the synthetics. In this manner the velocity, density, attenuation and upgoing and downgoing waves are simultaneously estimated for the group of traces. The whole VSP section is analysed four traces at a time. Several synthetic observations are inverted to test the algorithm. One set of field VSP data is also inverted with very good results. To the authors knowledge, this is the first VSP inversion to attempt to estimate density. It is also the first process which simultaneously calculates velocity, attenuation and density while separating the upgoing and downgoing waves.

Chapter 5 concludes this work with a summary and critique of the results from the forward and inverse problems. Because the analysis of VSP data is a relatively new endeavor, much work remains to be done. Chapter 6 presents a number of possibilities for future work. Many of the techniques in the thesis were explicitly developed because they could be generalized

to more complicated cases, thus some paths by which to proceed are discussed.

Tangential or involved concepts relevant to the body of this work are presented in 8 appendices.

Chapter 1

REVIEW OF BOREHOLE SEISMOLOGY

...The process of generation and propagation of seismic waves in actual media has not been pursued with sufficient vigor.

E.I. Galperin in Vertical Seismic Profiling, 1974

1.1 INTRODUCTION

Borehole seismology has a long if somewhat sporadic history of development. Beginning concurrently with the seismic reflection techniques (DeGolyer, 1935), it has developed much more slowly than the now mature procedures for surface recording and analysis. One of the earliest discussions of borehole seismology or "well-shooting" as it was called (McCollum and LaRue, 1931) indicated that a great wealth of geologic information could be recovered from in situ seismic measurements. These aspirations however, were not realized in practice, with several notable exceptions until recently. Borehole seismology has now rapidly advanced from well-shooting to the vertical seismic profile used for both structural and stratigraphic imaging and enhancement of surface-recorded data.

1.2 CHECK SHOT SURVEYS

The basic concept of "shooting a well" or check shot surveying is shown in Figure 1 (after Dix, 1952). The main purpose of the measurements was to provide a seismic time-to-depth curve or later to calibrate the sonic log , hence the name "check shot" survey. The components of the survey are a seismic energy source, a borehole, downhole motion sensor, suspension equipment for the sensor and recording instruments. The survey procedure is straightforward; the source fires for each receiver depth or position and the first break of the resulting wavefield is recorded as it passes by the receiver. Typical check shot data is shown in Figure 2.

Note that the gain of the recording equipment is generally set high enough so that the first arrival is unambiguous. This often precludes the observation of later arrivals.

The early borehole analysis was concerned strictly with the time of arrival of the first break. Slotnick (1936a; 1936b) developed the forward model or traveltime versus depth curve for rays propagating in an earth that has either a linear or exponential velocity structure. Dix (1939) commented that these curves did not actually solve the problem in well-shooting; "it appears to the author that the real problem confronting the interpreter of the data is, on the other hand: given the well shot data, find the relation between v and h [velocity and depth]". He thus proposed an approximate method to invert traveltimes for velocity using the traveltime or Bullen integrals. Much later Grant and West (1965) gave an exact velocity inversion method using the Bullen integrals. Dix (1945) outlined five different methods of conducting a check shot survey to determine interval velocities. These methods use data from several source offsets with ray theory applied to a horizontally-stratified medium to approximately derive the interval velocities. In a third interpretation paper, Dix (1946) discussed another approximate method to find the dip angle of tilted beds from well shot data. In this case, it is assumed that the velocities increase linearly with depth. By finding the depth of a common velocity point from several different wells the dip of the beds may be approximated. While the check shot survey neglects a large amount of information arriving at times after the first break, it can nonetheless provide well-constrained interval velocities (Galperin, 1974; Stewart, 1982). In Chapter 2, traveltime analysis is further developed by using inverse theory.

A variation of the well-shooting scheme is to put an energy source in the well with receivers on the surface. This is referred to as "uphole" or transposed surveying. Kokesh (1952) describes several experiments where an explosive, formation perforation tool was used as a downhole energy source. He displays traveltime curves and the corresponding interval velocities for depths up to 8000 ft. Brewer and Holtzscherer (1958) used multi-offset, multi-azimuth surface receivers and downhole shots to attempt to delineate faults in the Parentis Oil Field, France. They used from 200 to 400 meters of coiled primacord at depths up to 2500 meters and were able to record adequate energy at the surface. From differences in the traveltimes recorded at the surface receivers with different azimuths, they proposed very plausible but not definitive fault locations.

Several other authors began to probe later times in the recorded trace and became interested in the shape of the first few cycles of the seismogram. Ricker (1953) derived a mathematical theory for wavelet propagation ("wavelet theory") which was based on the viscoelastic wave equation. His theory predicted that the velocity amplitude of the wavelet should decrease with the minus 2.5 power of traveltime. The wavelet breadth was predicted to vary with the square root of traveltime and low frequncy attenuation varied with the square of frequency. To test these predictions, he conducted an experiment using three downhole geophones in the Pierre shale, Colorado. He claimed that the observations of pulse shape were in agreement with the prediction of the theory. He also noted, from the traveltimes in two experiments, that the horizontal velocities were 14% and 18% higher than the vertical velocities.

Jolly (1953) described a wall-locking downhole geophone which could be used to accurately receive later arrivals. From these more informative

records he found reflected energy which could be traced back to the first break to find its depth of generation. He also observed, in his experiment in Garvin County, Oklahoma, that the amplitude of the initial pulse decayed to the minus 2.6 power of traveltime. Another contribution was his proposal and testing of a method to find the reflection coefficients from check shot data. In a manner similar to finding the generation depth, the amplitudes of the direct and primary reflections throughout the section are calculated and tracked back to their point of intersection. The ratio of these amplitudes is used to define a reflection coefficient.

Riggs (1955) used shallow uphole and cross-hole surveys along with the regular check shot survey to investigate the types of seismic waves propagating in several boreholes in Dallas, Texas. Suspension cable waves, casing waves and fluid column waves were all found to exist. Velocities of these respective waves were 3000-9000 ft/s, 15500 ft/s and about 4300 ft/s. Direct P waves in this area had velocities of 6500 ft/s. The measured open hole tube wave velocities were found to be in agreement with Lamb's (1898) formula.

Levin and Lynn (1958) analysed the results of eight well surveys. They observed pulse broadening due to high frequency absorption and found that amplitudes decayed with the minus 2.4th power of traveltime. They too traced reflected energy back to its generation point to calculate a reflection coefficient. For the primary reflections observed they found an average reflection coefficient of 0.36.

McDonal et al. (1958) performed an experiment specifically to find the attenuation of seismic energy. In their carefully designed and executed experiment in the Colorado Pierre Shale, they found both attenuation (1.0 dB/1000 ft-Hz) and anisotropy (2% in perpendicular directions) to be

present. They claimed that if velocity dispersion (associated with attenuation) was present then it must be less than several percent compared to sonic measurements at 10 kHz. McDonal et al. (1958) also stated that the earth was not behaving visco-elastically as proposed by Ricker (1953). Wavelet broadening and attenuation with time were less than Ricker's (1953) work would indicate. Also attenuation was found to vary with the first power of frequency. Wuenschel (1965) reinterpreted these data of McDonal et al. (1958) according to the attenuation-dispersion theory of Futterman (1962). This theory showed that linear, causal wave propagation in an attenuating medium was necessarily accompanied by velocity dispersion. Wuenschel (1965) found that the data were consistent with Futterman's (1962) third attenuation-dispersion pair.

While measuring dispersive effects across the seismic band is somewhat contentious, comparing sonic and seismic velocities offers a greater bandwidth to compare differences. Gretener (1961) pointed out that there was a consistent discrepancy between integrated sonic traveltimes in the kilohertz range and check shot times in the hertz range. Strick (1971) later interpreted this discrepancy in terms of velocity dispersion. Results from Ward and Hewitt (1977), Ganley and Kanasewich (1980), Peyret and Mons (1981) and Stewart et al. (1982) indicate that body wave velocity dispersion does exist. This discrepancy and velocity dispersion are discussed further in Chapter 3.

1.3 VERTICAL SEISMIC PROFILING

Borehole seismology was largely abandoned by the western literature during the 1960's and early 1970's. Perhaps this was because of the preoccupation with the great revolution in surface seismic analysis precipitated by digital computer processing. Omnes (1983) has suggested

that with the advent of synthetic seismograms (Wuenschel, 1960; Goupillaud, 1961; Sherwood and Trorey, 1965) it was believed that the exploration problem of wave propagation and subsurface analysis was largely solved. There, in fact, would be less need for in situ probes of the wavefield because the geologic section could be predicted by matching the synthetics to the observed data. However, while surface data processing has illuminated a great deal of geology it is of course not free of inaccuracy or non-uniqueness. Michon (1982) addressed this problem, "In fact, my main concern is to find a way of objectively evaluating seismic results. The synthetic seismogram might be helpful, but it is not free of errors. Far too often, and probably on account of these possible errors, we judge according to similarities rather than identities. Development of VSP is changing this trend, and we can already observe more precision in the comparisons between synthetic seismograms, VSP and surface seismics."

As an outcome of the more sophisticated rock physical, check shot surveys and work proceeding in the U.S.S.R., the vertical seismic profile (VSP) was developing.

The VSP is basically an enhancement of the check shot survey in several aspects

i) the wavefield is recorded for several seconds at each receiver location.

ii) an attempt is made to preserve the true amplitude and phase of the seismic energy.

iii) the receiver levels are spaced much more closely together than the check shot (about 1/4 of the dominant wavelength versus several wavelengths).

iv) generally a three-component wall-clamping receiver is used to be able to record the full vector wavefield.

Much of the work in the U.S.S.R. was concerned with the traveltimes of different types of waves reaching the receiver (Demidenko, 1964; Rudnitskyi, 1968; Galperin, 1975) and the particle motion of those waves (Galperin and Frolova, 1961; Galperin, 1974) and their intensities (Galperin, 1966). These studies in largely one-dimension media, for large offsets especially, show a very complex assortment of wave types. Converted, refracted and transcritically reflected waves are all apparent. Converted waves are especially abundant. Reflected waves are reported to be the dominant wave type in the later parts of the seismogram. Head waves generally have smaller amplitudes than transcritically reflected waves (Galperin, 1974). These forward traveltime and amplitude studies may help considerably in understanding wave type and velocity structure.

The more complex VSP survey is shown schematically in Figure 3. Garriott (1981) has detailed the planning and instrumentation required for effective VSP data acquisition. He notes that the recording apparatus must have sufficient dynamic range and bandwidth to capture the complete signal. The receiver need not only provide optimum signal detection but must operate in a hostile environment (high pressure, high temperature, large tilt angles). Sample interval, geometry, recording procedure and wireline quality are all factors which need to be considered in an effective survey. Part of a typical VSP data set is shown in Figure 4. Shown here is the vertical component of a receiver in a well pumped dry. Note the consistency of the first arrivals as well as the unambiguous reflection. S waves are observed arriving later in the section. All of the surveys considered in this thesis used wall-clamping geophones and were recorded digitally, except for Well D discussed in Chapter 3. Most of the receivers also had three-component geophones.

At least partially due to advances in experimental technique, borehole seismology evolved from velocity curve analysis to rock physics evaluation. The close depth spacing of VSP receivers and more accurate recording allowed analysis of the structure of the geologic section. Thinner layers could be resolved and mapped. Perhaps most importantly to the exploration industry the surface traces could be much better understood because the VSP provided an in-depth probe of how and where each phase of the surface trace was generated.

With greater processing and interpretation possibilities plus more interest in high-resolution seismology, the VSP measurement has again become an area of considerable interest. The recent literature has contained the results of field experiments (mainly to find velocity and attenuation), as well as synthetic seismogram generation, filtering and correlation to surface data. These topics are reviewed briefly and respectively below.

1.4 FIELD EXPERIMENTS AND RESULTS

Wuenschel (1976) was one of the researchers who reintroduced borehole seismology to the western literature. One of the salient features of the VSP, he noted, was the high signal-to-noise ratio of the seismic trace at depth. This is because of

i) less surface wave contamination

ii) cultural noise decreasing with depth

iii) scattering from the surface inhomogeneities decreases or becomes plane-like and may be attenuated by array processing.

This greater signal-to-noise ratio aids in the identification of wave types and lithology.

Lash (1980; 1982) reported the results of several VSP surveys in

Mississippi. He showed compelling evidence (in a manner similar to that of Galperin, 1974) that SV waves were generated near the source explosion and that significant P to SV conversions were occurring at depth.

Omnes (1980) has also given considerable attention to shear waves propagating in the earth. He shows how S and P wave VSP surveys may be used to develop elastic parameter well logs. Michon et al. (1981) give examples of a shear wave VSP log and its relationship to surface shear wave reflection data. They also developed a Poisson's ratio log from P and S VSP surveys. DiSiena et al. (1981) have noted the similarity of the VSP derived Poisson's ratio log and the self-potential log in a shallow well in Texas. While shear wave analysis is still developing it appears from the previous authors that there is a significant amount of interesting information to be used.

Stewart et al. (1981) used both P and SH wave surveys to delineate a subsurface fracture zone. By comparing surveys that were done prior to the fracturing of the rock with those performed after the fracturing an anomaly was located. They found that attenuation, scattering and time delaying of seismic energy occurred as the wave passed through the fractured area. From these changes in the wavefield they were able to estimate the fracture zone geometry and porosity (see Appendix I).

One of the more difficult tasks in analyzing the properties of the shallow earth has been finding a consistent and interpretable seismic attenuation. Hauge (1981) used the spectral ratio method (see Appendix II) for five detailed VSP surveys on the Gulf Coast to calculate an attenuation value. Several factors caused significant scatter in his results:

i) source variations

ii) interference from reflectors

iii) variable geophone coupling

iv) inadequate bandwidth

He found attenuations varying from 0.1-0.9 dB/wavelength (Q = 273-30). He also noted that the attenuation values in sand intervals were consistently larger than those for shale. As had O'Doherty and Anstey (1971) and Schoenberger and Levin (1974; 1978), he claimed that the interfering effect of short-path multiples could be responsible for as much as 40% of the measured attenuation. Kan et al (1981) found a smaller effect on the attenuation due to multiples in an experiment conducted in Colorado. They used VSP field data to first find a total attenuation. Over a 1600 ft to 7400 ft depth the spectral ratio Q determined was from 40-100. Apparent Q values from the corresponding synthetics generated from the sonic log were at most 268. Stewart et al. (1982) showed that short-path multiples could delay the seismic pulse by up to 2.0 ms/1000 ft but only in areas of highly cyclic stratigraphy. The effect of short-path multiples is discussed further in Chapter 3.

Ganley and Kanasewich (1980) attempted to avoid the interfering effect of reflectors in attenuation estimation by effectively deconvolving (dividing the structural transfer function out of the measured data) the acoustic earth response out of the VSP traces. In a survey performed in the Beaufort Sea, they found some improvement in the scatter of their attenuation results using this technique. They calculated Q values of 43 across a 549 m to 1193 m depth and 67 through 945 m to 131 m depths.

Wingo (1981) and Zeitvogel (1982) both analyzed VSP field experiments to determine the seismic attenuation. They also used the spectral ratio technique but attempted to correct the spectral ratios of the seismograms at two different depths for source variations. This was achieved by using

the spectra of the source monitor geophone in ratio with the spectra of the traces recorded at the different depths. Both authors found that this correction improved results. In a Gulf Coast survey, Wingo (1981) identified a very high attenuation coincident with a high pressure gas sand. By using a traveltime inversion on the traveltimes picked from this Gulf Coast VSP, Stewart (1982) found low velocities for the gas sand. Zeitvogel (1982) made a rough correspondence between his attenuation values and the lithology of a section in East Texas. Both Zeitvogel (1982) and Wingo (1981) found that they were able to define attenuation intervals of about a minimum thickness of 500 feet.

Peyret and Mons (1981) used seismic traveltime delays (with respect to the sonic log) and associated these delays with an attenuation value. In thirteen VSP surveys conducted in the U.K., they were able to find a correspondence between this attenuation and the lithology.

Several recent authors have used downhole measurements to analyze the radiation pattern of surface sources. Robertson and Corrigan (1983), in several shallow experiments in shale sections, positioned a shear-wave vibrator at various shot points around a three-component downhole geophone to find the source radiation pattern. They found that SV and SH waves were well separated depending on whether the source motion was toward the well head or at 90° to it. The SV radiation pattern had a lobe which peaked at a 30 to 35 degree incident angle to the well. From the construction of wave surfaces they suggested that considerable anisotropy in the shale was present. Horizontal SH group velocities appeared to be 25-30% greater than the horizontal SV group velocities.

Keho (1983), using the Gulf Coast data of Wingo (1981), found that SV amplitudes decreased rapidly inside the earth as expected from geometric

considerations. He modeled the amplitudes received *in situ* using the formulation of Miller and Pursey (1954). At 400 ft the observed amplitudes were 0.05 of their maximum value. He found consistent agreement between the observed and calculated amplitudes. Keho (1983) also suggested that inhomogeneous wave propagation (Borcherdt, 1973) was occurring which could explain the elliptical particle motions which he observed in the field data.

1.5 EXPERIMENTAL DIFFICULTIES

A number of problems plague the VSP measurement. Some of these are equipment related while others are due to the complications of wave propagation. It seems that the most troublesome equipment problem has been the reliability and response of the downhole receiver. In part this is because of the large variety of borehole diameters and lithologies that are encountered as well as the hostile environment mentioned earlier. To record an accurate waveform, due to a wave propagating in the formation, a firm couple of the receiver to the formation must be made. Numerous clamping arms and arrangements (see Figure 5) have been designed to produce this coupling (Wuenschel, 1965; Garriott, 1981; Schlumberger, 1982). There appears to be some room for improvement yet.

Assuming perfect coupling, Beydoun (1982) analyzed the response of a cylindrical receiver in a borehole. He found that for a heavy enough receiver with a small contact surface and "soft" formation, the receiver could resonate in the seismic band when excited by a seismic wave. This produces an undesirable ringing. Therefore he suggested that the receiver must be quite light and have a large contact surface to put its resonant frequency above the seismic band.

The seismic source itself may also introduce complexity into the VSP survey. A significant problem with seismic sources is their lack of repeatability. It is desirable to have a constant source so that events may be easily correlated and changes in lithologic parameters estimated. Careful monitoring of source conditions (e.g. air gun depth, soil compaction with impulsive sources) can ameliorate this difficulty. As discussed earlier, certain variations can also be accounted for if a monitor geophone and signal processing are used.

As alluded to previously inadequate bandwidth causes uncertainty in many parameter estimates. The problem with inadequate frequency bandwidth is largely due to the fact that seismic attenuation in rocks increases with frequency. Aside from increasing the fidelity and bandwidth of the recording apparatus and source, an attempt to reduce noise is perhaps one of the more realistic methods of extracting higher frequencies of the signal. This has led some researchers to study the sources of noise in a borehole.

Hardage (1981) studied the borehole tube wave - one of the factors inherent in many VSP surveys which degrades the signal. He claimed that tube waves were generated by surface waves as they impinged on the shallow section of the well. Body waves encountering a casing diameter change and refracted waves impinging on the borehole also seem to generate tube waves. These waves travel at velocities similar to those of shear waves (White, 1965; Cheng and Toksoz, 1982) and often have large amplitudes. Thus, they can obscure shear wave arrivals as well as later P arrivals. Hardage (1981) noted that moving the source away from the well head is an effective method of attenuating the tube waves. Turpening

(1980) found that lowering the fluid column in the borehole also attenuated tube waves in the deeper section.

Beydoun (1982) also studied the generation of tube waves from a plane wave impinging on a crack which intersects the borehole. The volumetric change of the fluid-filled crack due to the impinging body wave causes fluid flow in the borehole which creates a tube wave. As Huang and Hunter (1980) observed and Beydoun (1982) calculated a large event may be generated. This may further obscure the body wave arrivals.

1.6 SYNTHETICS AND SIGNAL PROCESSING

To aid in understanding the complex shape of the VSP traces several authors have developed methods to calculate synthetic seismograms. Following a procedure similar to that of Goupillaud (1961), who used it to calculate reflection synthetics, Wyatt (1981) outlined a time-domain procedure to find VSP synthetic traces. Basically a 1-D propagator matrix technique, it can be used to find the zero source offset acoustic VSP traces at depth. Ganley (1981) developed a more sophisticated wave equation method based on the up and downgoing waves of Claerbout (1976). This frequency domain calculation allows the inclusion of attenuation and velocity dispersion. It is perhaps a more realistic method in that it does not require the traveltimes in each layer to be equal. In Ganley's (1981) method a wave equation solution is propagated through an attenuating layer then the boundary conditions are matched at the interface of the next layer. Propagator matrices are used to calculate the seismogram at any point in the medium. This wave equation procedure forms the basis of the forward model used in Chapter 4.

Temme and Muller (1982) have advanced an acoustic wave equation method similar to that of Ganley (1981) to produce synthetic seismograms. They

included a geometric spreading factor to simulate the effect of a spherical wave. This divergence can correct the direct and primary waves but overly suppresses multiples.

Aminzadeh and Mendel (1982) proposed a "state space" approach to computing seismograms. Their technique describes the response of an elastic layered medium to either a plane wave or a line source. The model is based on time-domain recursive relations to which are input initial ray take off angles and source waveforms. To find the response of the medium to a line source, numerous takeoff angles are summed to give an approximately cylindrical wave.

Mellen (1982) has altered the SEIS81 program (based on Cerveny, 1981) to accept a VSP geometry. The SEIS81 program uses asymptotic ray theory (a high frequency solution to the wave equation) in a two-dimension model to compute reflection seismograms. Both realistic phase and amplitude variations are accounted for in this formulation.

Prange (1983) has modified a program by Bouchon (1982) which computes synthetic VSP seismograms via the discrete wavenumber method. Again this approach is a method to solve the elastic wave equation, this time by representing the wavenumber integral as a discrete sum (Bouchon and Aki, 1977). To do this, surface fictitious sources are assumed as well as a small attenuation. Both of these factors are removed in the final calculation.

The details of upgoing and downgoing waves propagating in a layered medium had been described by Wuenschel (1960), and Claerbout (1968; 1976). Wuenschel (1976) discussed shifting and summing VSP traces to enhance either upgoing or downgoing waves. This separation of waves proves to be

very useful as for example the upgoing wavefield shows at what depths reflections are generated.

With this greater understanding of the forward problem it is possible to begin to consider the inverse problem. Rice et al. (1981) and Cassinis (1981) have described the advances and potential of inverse theory in geophysical interpretation. They note the importance of finding the parameter of direct lithologic significance; velocity, as opposed say, to the reflection coefficients. The inversion of seismic reflection data has been a goal for some time (Claerbout, 1968; Bamberger et al., 1982; Johnson and Nogami 1982). While results have been mixed for surface data, VSP data is better constrained and, because of fairly well-defined upgoing and downgoing waves, more amenable to inversion.

Seeman and Horowicz (1981) presented a type of inversion which separates upgoing and downgoing waves, assuming that the impedances are known. They take a number of traces (about 11) and assume that there is a downgoing wave and a primary reflection only. Downgoing and upgoing waves are computed via least-square fitting this model to the data. Stewart (1982) outlined a traveltime inversion scheme, using the Levenberg-Marquardt algorithm to find layer velocities in a 1-D medium. This will be discussed further in Chapter 2.

Aside from the above work relatively little effort has been devoted to VSP data inversion. There does exist, however, a large body of inversion literature in the earthquake seismology realm. Traveltime inversions have been used for some time (Flinn, 1961; Aki and Lee, 1976; Thurber, 1981) in determining earthquake hypocenters and gross earth structure. More recently the first few cycles of the seismograms have been considered. A number of body-wave waveform inversion schemes have been proposed (Mellman,

1980; Kikuchi and Kanamori, 1982; Nabelek, 1983). These are mainly concerned with either finding earthquake source parameters or gross earth velocity structure. Chapter 4 presents a new body wave inversion method, in the frequency domain, for separating the upgoing and downgoing wavefields as well as determining the interval velocities, densities and attenuations in a VSP survey.

Gaiser et al. (1982) and Lee and Balch (1983) have presented the industry's state-of-the-art processing flow for VSP data (see Figure 6). These are the steps that are generally applied to VSP data prior to interpretation (note the similarity to surface data processing). In the edit process, very bad traces may be eliminated and timing errors corrected. Noise muting may also be helpful. The stacking process is used to reduce random noise. Several recordings of the source may be taken at each depth position. The resulting traces are aligned and summed.

Wavelet shaping is the name given to the techniques which perform the corrections for source variations. The recordings from the monitor geophone are analysed for their spectral content. The downhole traces are multiplied by the operator which makes the monitor traces constant. This often results in a more continuous and interpretable VSP section (Zeitvogel, 1982).

In amplitude analysis or true amplitude recovery (TAR), the attempt is made to make the recorded traces similar to theoretical plane wave seismograms. This is accomplished by taking into account attenuation and spherical or refractive spreading (O'Doherty and Anstey, 1971; Newman, 1973; Lee and Balch, 1983).

The separation of upgoing and downgoing waves is a major goal of VSP processing. As it is only the upgoing waves which are recorded on the pervasive reflection surveys, it is of primary importance to analyse the

VSP upgoing waves for greater understanding of the surface data. Velocity filtering (via f-k analysis for example) has been used successfully to achieve this separation (Gaiser et al., 1982). The reason for this success is the clear distinction between upgoing energy with its negative slope in the f-k domain and downgoing energy with its positive slope.

Estimating the interval velocities may also be performed at this stage of the processing sequence. This can be accomplished by some type of traveltime inversion or trace coherency velocity analysis. These interval velocities are used in numerous ways among those being; calibration of the sonic log, lithologic constraint and migration.

Using the downgoing wavetrain (it is often several hundred milliseconds long) to design an operator to deconvolve the upgoing VSP traces and the surface data can enhance the interpretability of the data considerably (Hubbard, 1979).

As Lee and Balch (1983) point out there is a great deal of information in the VSP survey but "a considerable amount of computer processing of digitally recorded VSP data is required in order to obtain the full benefit of these data".

1.7 APPLICATIONS

Having discussed some of rock physical VSP experiments and various ways to model and analyze the data, several more of the applications of VSP data will be reviewed. Kennett et al. (1980) noted several ways that the VSP could be of use to the geophysical interpreter

i) bedding dips may be computed from the hyperbolic moveout curves of primary reflections evident on VSP data

ii) by finding the generation time and depth of energy on the VSP, it

may be determined whether an event is a primary or multiple reflection

iii) by effectively treating the deepest VSP trace as a reflection seismogram, it can be used to "guestimate" the impedances below the total depth of the well.

This last result is potentially very helpful to the drilling engineer who is concerned with overpressured zones or very hard strata.

If several source offsets are used, the VSP may be processed via normal moveout curves to find an actual velocity at depths beneath the deepest receiver (Alam, 1981). In shallow wells this is potentially a very powerful procedure.

Hardage (1981) suggested that it would be possible to view faults some distance from the borehole in which a VSP had been conducted. Wyatt (1982) demonstrated this quantitatively and gave several examples to show how the throw and distance of a thrust fault from the well could be calculated.

DiSiena et al. (1981) showed that the VSP could be displayed to provide a mapping from an arbitrary well-log to the surface data (see Figure 7). This very useful technique allows an exact correlation between a certain "wiggle" on the surface trace and a particular stratum of the elastic properties. Lang (1979; 1979b) uses the VSP to tie a particular seismic signature to the well. This signature may be extrapolated from the well using CDP data. In this manner lithologies away from the well may be tied to it.

Fitch (1981), Hardage (1981), Tango (1981) and Balch et al. (1982) have also qualitatively described numerous applications (many of which are yet unrealized) of the VSP. Several monographs currently in press (Balch, 1983; Hardage, 1983) develop these concepts further. Tango (1981)

summarizes in saying "the full performance and potential of VSP is at present as yet unrealized. Yet ...VSP demonstrates a "new" and viable concept in exploration and evaluation".

1.8 CONCLUSIONS

While borehole seismology has been practiced for many years relatively few studies have been published. Early studies were concerned only with interval velocities and traveltimes. Later on, the wave shape was scrutinized for its rock physical significance. Now the full trace is being thoroughly processed and modelled. Many of the techniques used in VSP analysis have been adapted from reflection seismic processing and earthquake seismology. It is expected that these areas will continue to contribute to the development of VSP methodology and analysis. The recent resurgence of interest in borehole seismology (Hardage, 1983; Balch, 1983) bodes well for our understanding of wave propagation and *in situ* seimic parameters.

Figures

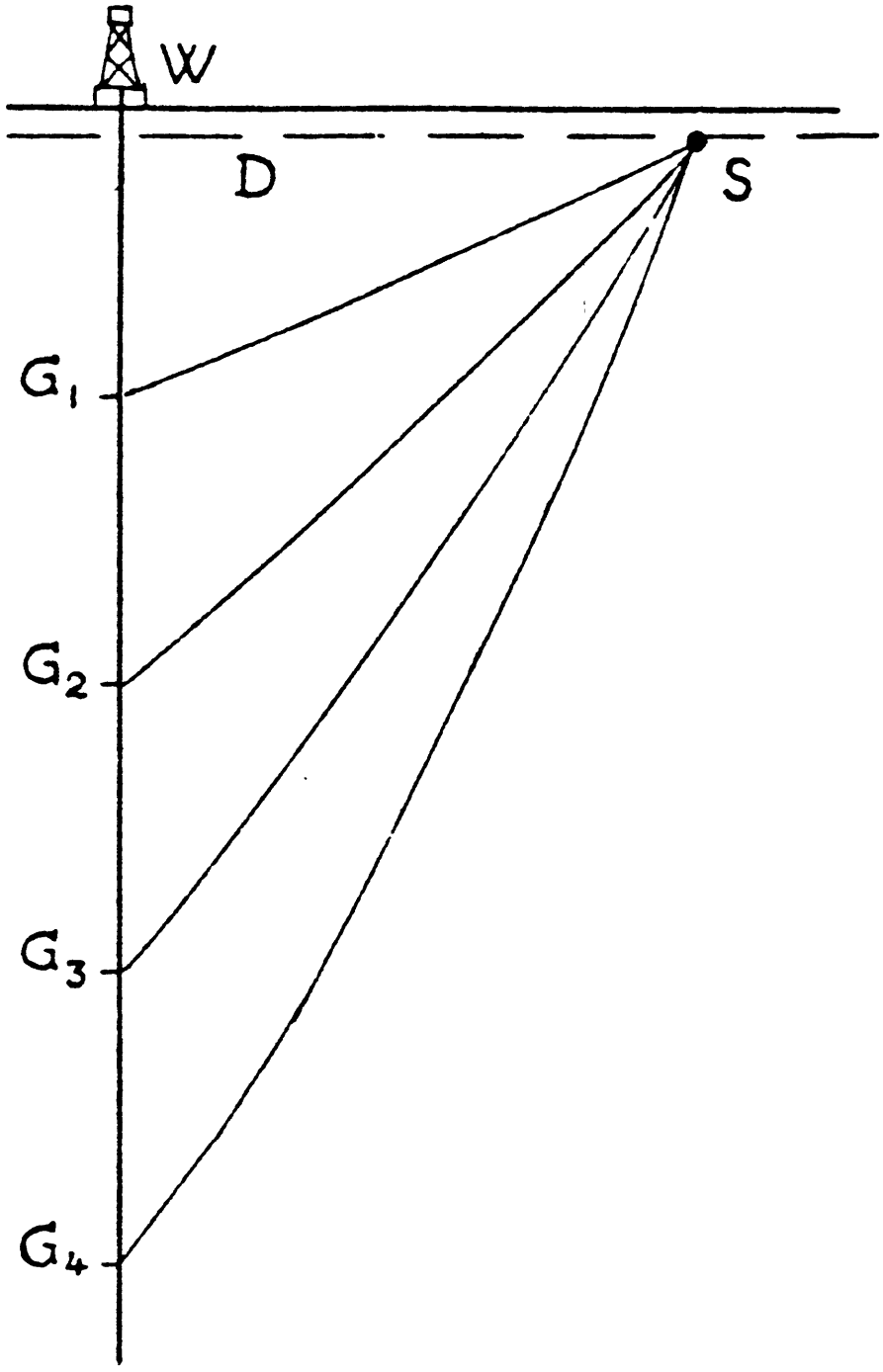

Figure 1.

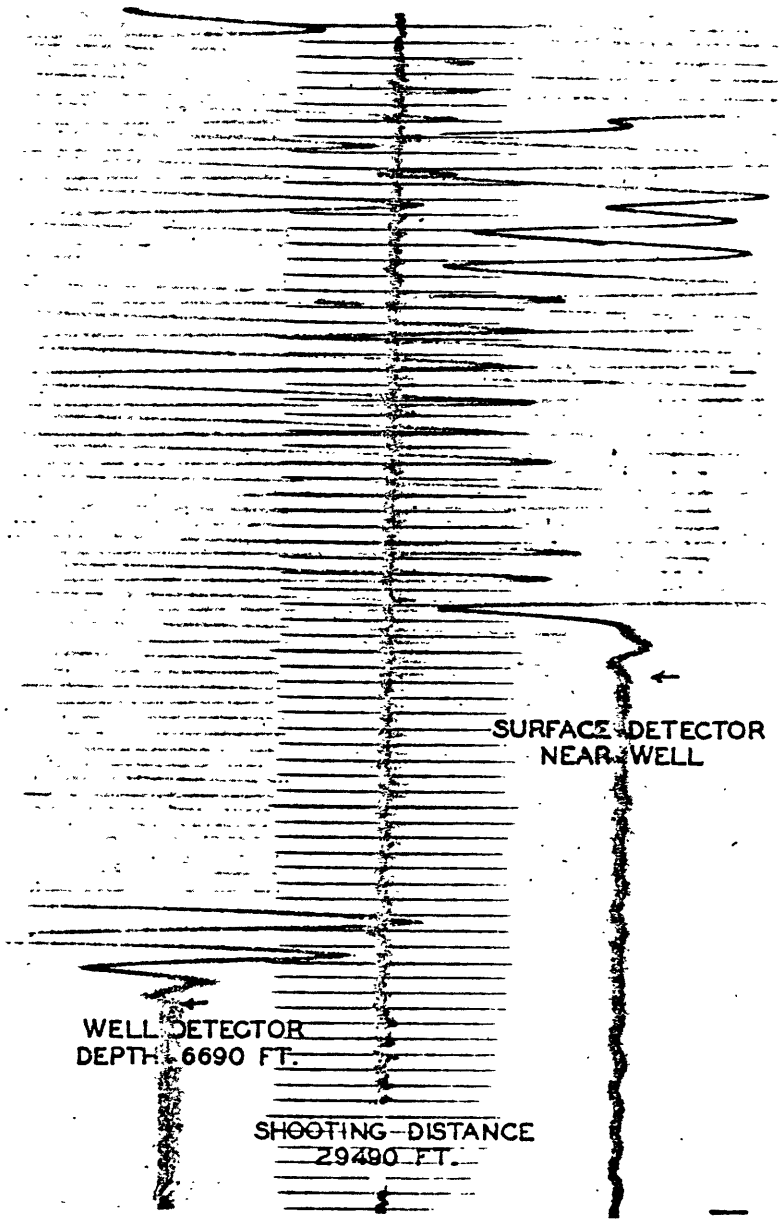
SURFACE DETECTOR
NEAR WELL
WELL DETECTOR
DEPTH 6690 FT.
SHOOTING-DISTANCE
29490 FT.

Figure 2.

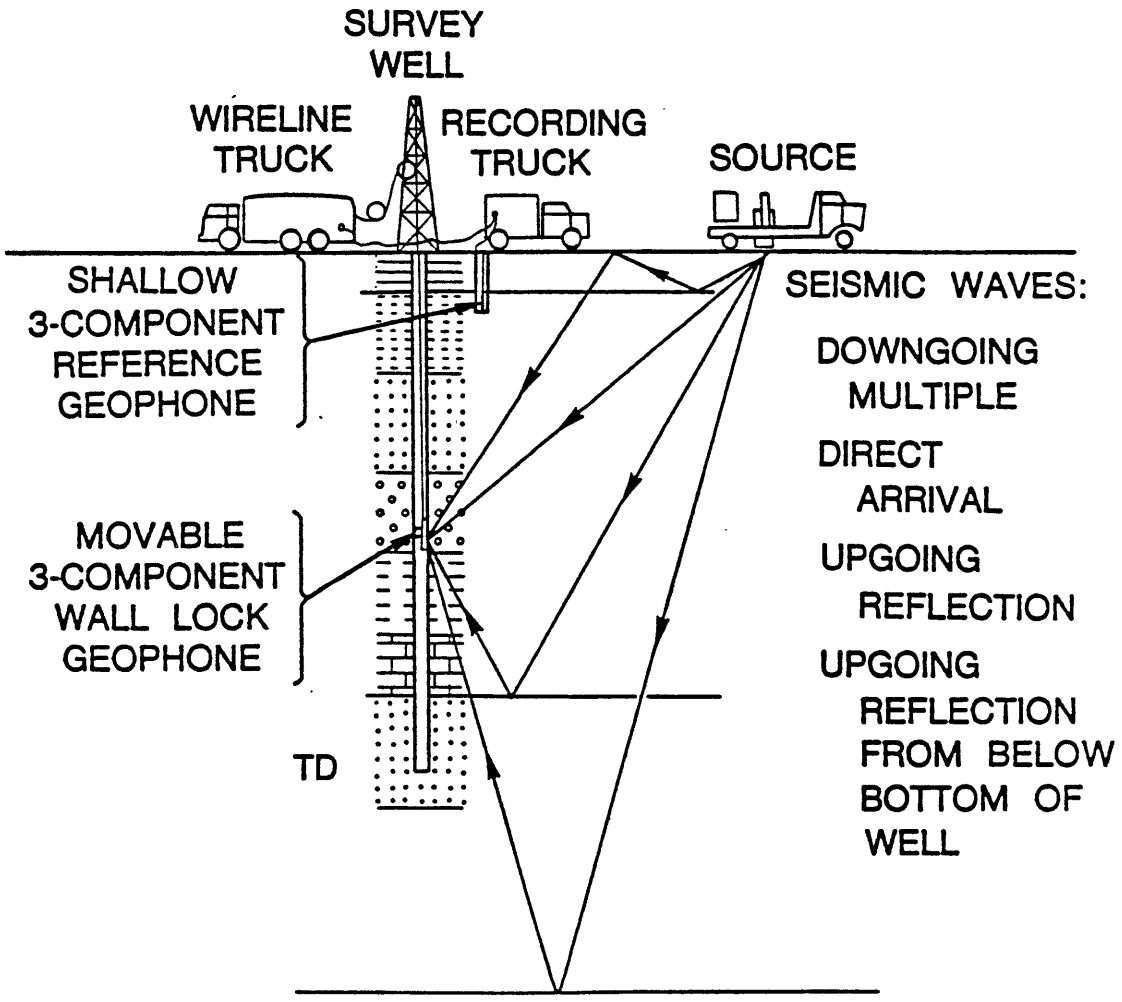
SURVEY
WELL
WIRELINE
TRUCK
RECORDING
TRUCK
SOURCE
SHALLOW
3-COMPONENT
REFERENCE
GEOPHONE
MOVABLE
3-COMPONENT
WALL LOCK
GEOPHONE
TD
SEISMIC WAVES:
DOWNGOING
MULTIPLE
DIRECT
ARRIVAL
UPGOING
REFLECTION
UPGOING
REFLECTION
FROM BELOW
BOTTOM OF
WELL

Figure 3.

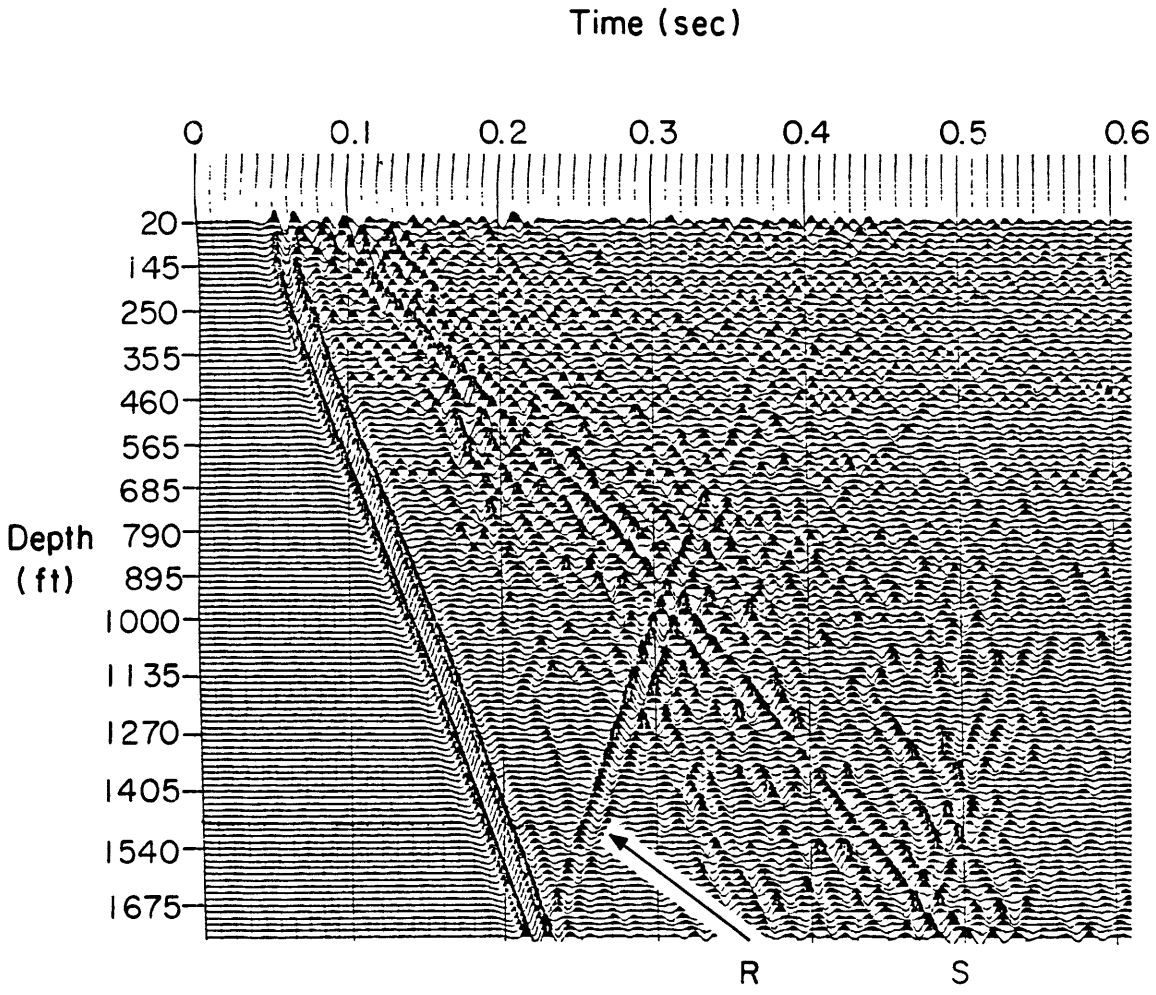
Time (sec)
0
0.1
0.2
0.3
0.4
0.5
0.6
Depth (ft)
20
145
250
355
460
565
685
790
895
1000
1135
1270
1405
1540
1675
R
S

Figure 4.

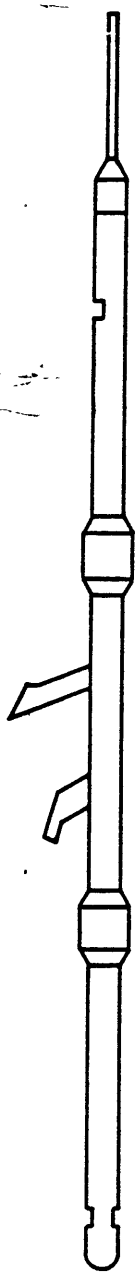

MAX. TEMP.	175° C (350° F)
MAX. PRESSURE	1400 Bars (20,000 psi)
TOTAL LENGTH	204"
TOTAL WEIGHT	273 Lbs
STANDARD ARMS	
Max. Hole Diameter	13½"
Min. Hole Diameter	5½"
LARGE ARMS (OPTIONAL)	
Max. Hole Diameter	19½"
Min. Hole Diameter	8"
MAXIMUM HOLE DEVIATION	45°

VELOCITY GEOPHONES
Geospace HSI-10 Hz. Four Used in Series
Bandwidth. 10 to 200 Hz at 3 dB.

DOWNHOLE AMPLIFIER
Gain. 60 dB.
Bandwidth. 0 kHz to 2 kHz at 3 dB.

Figure 5.

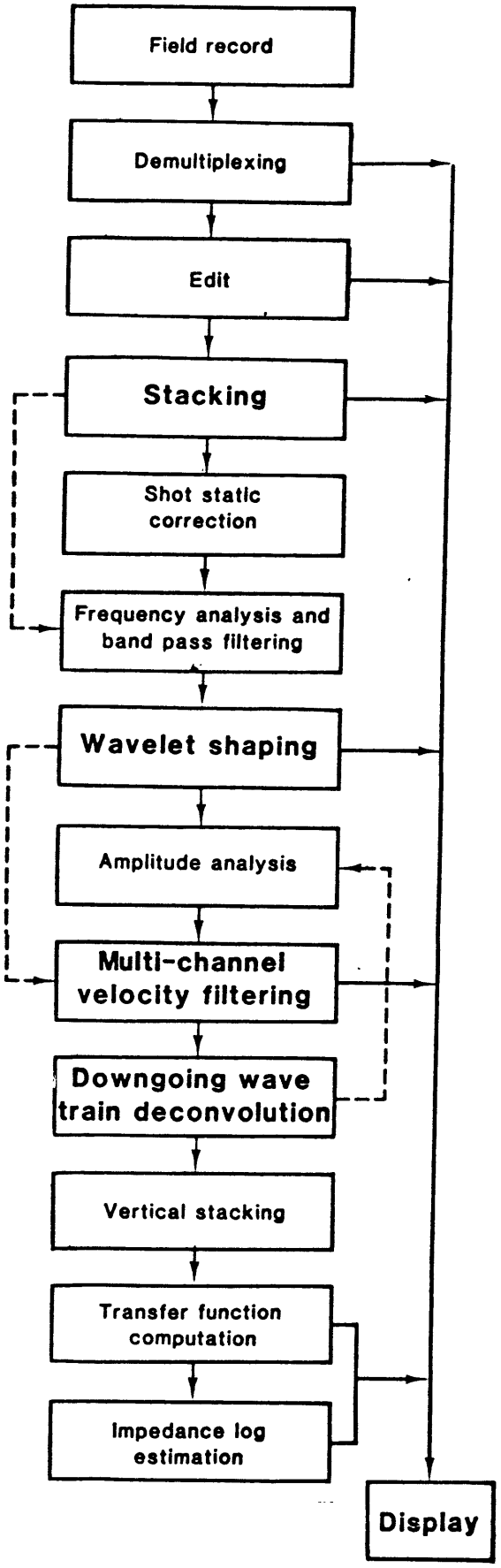
Field record
Demultiplexing
Edit
Stacking
Shot static correction
Frequency analysis and band pass filtering
Wavelet shaping
Amplitude analysis
Multi-channel velocity filtering
Downgoing wave train deconvolution
Vertical stacking
Transfer function computation
Impedance log estimation
Display

Figure 6.

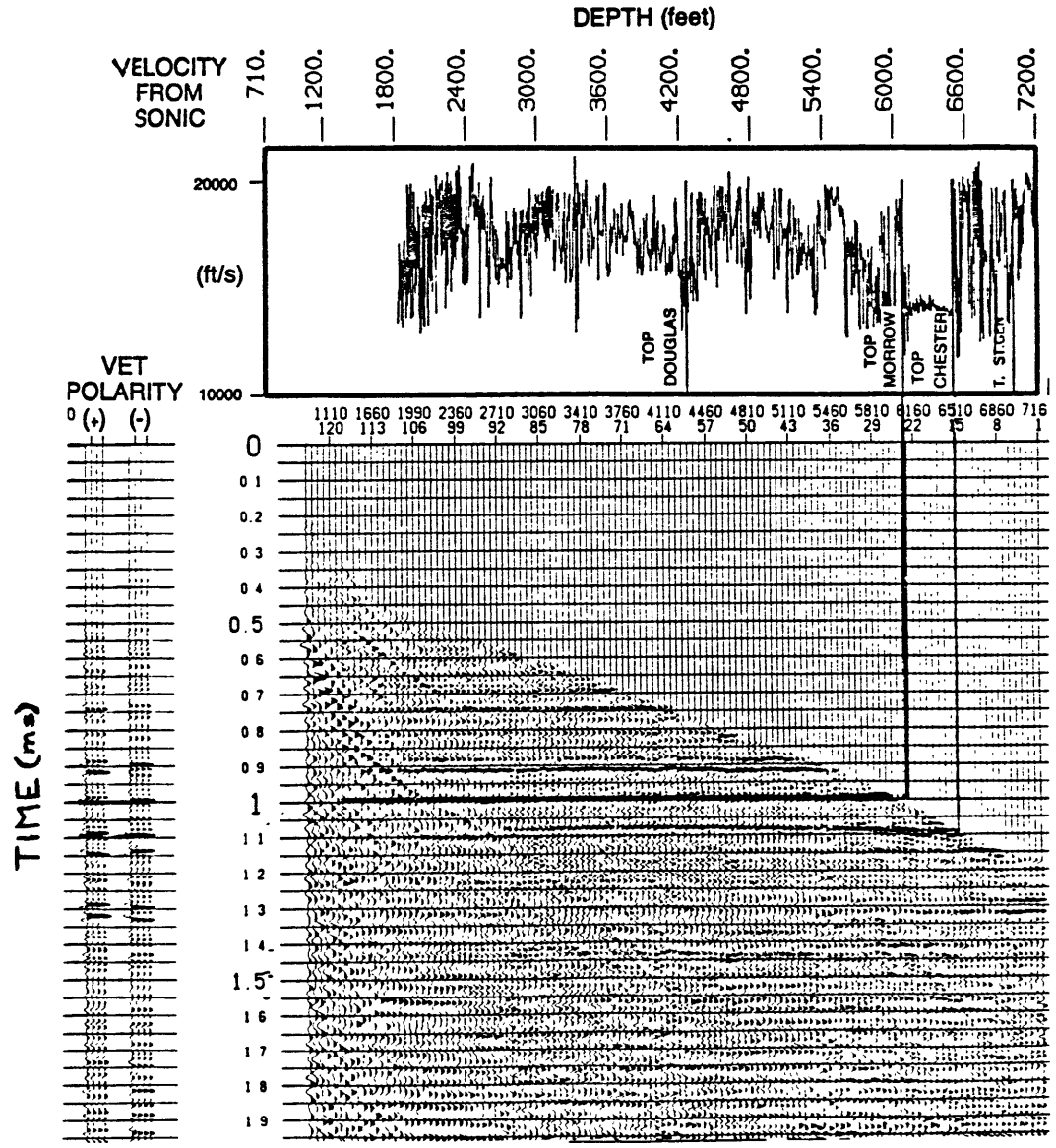
DEPTH (feet)
VELOCITY FROM SONIC
710.
1200.
1800.
2400.
3000.
3600.
4200.
4800.
5400.
6000.
6600.
7200.
20000
(ft/s)
10000
TOP DOUGLAS
TOP MORROW
TOP CHESTER
T. STOKN
VET POLARITY
0 (+) (-)
1110 1660 1990 2360 2710 3060 3410 3760 4110 4460 4810 5110 5460 5810 6160 6510 6860 716
120 113 106 99 92 85 78 71 64 57 50 43 36 29 22 15 8 1
TIME (ms)
0
0.1
0.2
0.3
0.4
0.5
0.6
0.7
0.8
0.9
1
1.1
1.2
1.3
1.4
1.5
1.6
1.7
1.8
1.9

Figure 7.

Chapter 2

TRAVELTIME INVERSION

...Why don't you use inverse theory? Everybody else does.

Prof. K. Aki
in General Examination of R. Stewart
May 1980.

2.1 INTRODUCTION

Perhaps the most basic information inferred from the VSP is the variation of seismic velocity with depth. Because of this, it is necessary to develop and use methods by which the velocity section may be calculated in an accurate and reliable manner. Currently, some classical techniques are being employed (Dix, 1945; Grant and West, 1965). These methods all use first arrival times picked from the VSP traces. Thus the VSP is being considered as a dense check shot survey. Simple assumptions are made concerning the ray propagation paths to calculate a velocity section. In only a few studies have the limits and errors inherent in the VSP observations and velocity calculation been considered (Gamburtsev, 1969; Beeston and McEvilly, 1977; Goetz et al., 1979).

In this chapter, the methods and assumptions involved in the techniques presently used to process VSP traveltime data are described. As part of this discussion, we consider some of the errors associated with a VSP survey and the problem that these pose for analysis techniques. To solve some of these difficulties and to allow quantitative estimation of the quality of the solution, while still limited to traveltimes, another technique is proposed. It is based on a damped least-squares linear inverse algorithm which simultaneously determines all the interval velocities from the traveltime data.

The testing of the inverse algorithm is accomplished by the use of synthetic data. The synthetic data are generated by ray-tracing through a model velocity section. Next, noise is added to the traveltimes determined from this ray tracing. The inverse algorithm then inverts the noisy traveltime data to arrive at a velocity structure. This calculated velocity section is compared to the original model velocity section.

Three field VSP examples (all land surveys) are also analyzed for velocity and are compared to their sonic logs. The inversion results are used to constrain the velocity layer thicknesses.

2.2 CURRENT TECHNIQUES

As described in Chapter 1, there are two fundamental approaches to the calculation of velocity from VSP traveltime data. It is possible to use the traveltime differences from a single source to different depths to compute an interval velocity (Dix, 1945; Grant and West, 1965). Alternatively, one may use a number of surface source offsets, with a fixed receiver at depth, to find an RMS velocity to that depth from the moveout curves (Dix, 1981). This second method is only rarely used, partially due to the expense of the many source offsets required to adequately define the moveout curves. Shooting up-hole (sources in the well with a surface spread of receivers) is the reciprocal of the previous techniques (Kokesh, 1952; Alam, 1981). This up-hole method is also used only occasionally and then at the near surface (because of down-hole source size limitations). In the future though, these alternate methods will no doubt become more widely used than they are at present.

Considered here is the routine, single source offset case. The basic data set upon which all of the current analysis methods operate is the traveltime vs. depth curve. The time vs. depth curve is calculated from a

trace section by picking the first-arriving energy. By using only the first arrival in the VSP trace, a great deal of information in the later part of the trace is being neglected . This is usually justified by noting that the first arrival has the best signal-to-noise ratio (at least 20dB higher than the primary reflection) and represents the most straightforward wavetype - the direct wave. Full waveform usage is discussed in detail in later chapters. Pulse height detection, eye picking or trace cross-correlation are all methods by which the first-arrival times may be deduced. These different picking methods are considered in the next chapter. It is found that interactive cross-correlation is the preferred time-picking technique.

The differences in the techniques for computing the velocity structure lie in the assumptions made about the ray path of the propagating energy. The simplest assumption is that the ray travels strictly vertically from the source to the receiver. This approximation is equivalent, in velocity terms, to finding an interval velocity (the apparent velocity) by differentiating the traveltime curve.

$$\text{Apparent velocity} = (\Delta t/\Delta z)^{-1} \tag{1}$$

where Δz is the depth interval between stations

Δt is the difference in traveltimes measured between the stations.

The usual correction that is applied to this vertical ray path is to assume that the ray travels in a straight line from the offset source to the receiver (Lash, 1980). This gives a slanted straight ray velocity as

$$\text{straight ray velocity} = \frac{\Delta z}{\Delta t} \cos\ \theta \tag{2}$$

where θ is the angle subtended by the line from receiver to wellhead and receiver to shot points.

It is possible to next assume that rays propagate through discrete flat-lying layers, bending at each interface in accordance with Snell's Law. Grant and West (1965) derive a relation between the velocity structure and traveltimes (see Appendix III for details).

They show that the total traveltime T, to some depth H, is related to the velocity structure V(z), and traveltime derivative $\frac{dT}{dz}$, as follows

$$T(H) = \int_0^H \{1-V^2(z)[\frac{1}{V^2(H)} - (\frac{dT}{dz})_H^2]\}^{-1/2} \frac{dz}{V(z)} \qquad (3)$$

Supposing that we have measured T(H) and its derivative $(\frac{dT}{dz})_H$, then equation (3) may be numerically integrated to determine V(z). This is done by first solving equation (3) for the surface layer, then the next layer and so on. This boot-strapping process is repeated until the complete velocity section has been calculated. Equation (3) does require a search for the velocity V(H) in each layer. A rapid search algorithm (after Bickle, 1981) based on the concepts of dynamic programming has been incorporated into the program to calculate velocities using equation (3).

To test briefly the validity of these different methods, synthetic traveltime curves [by offset one-dimensional ray tracing (after Comer, 1981)] are generated for a known velocity section. The model velocity section and corresponding traveltimes are shown in Figures 1(a) and 1(b). These traveltime curves were then processed by the three preceding techniques. The results for the apparent and straight ray velocities are shown in Figure 2. As may be expected, especially at shallow depths and high velocities, these two methods give poor estimates of the true interval velocities.

The ray trace approach gives much better results. Figure 3 shows the model velocity again with the velocities computed from ray trace integral [using the traveltime data from Figure 1(b) again]. The agreement is good. Again this is expected because the model traveltimes are ray-trace generated, while equation (3) is a ray-trace based inversion. Nonetheless, this demonstrates that for at least these noise-free data, the VSP velocity problem is well-behaved and invertible.

Figure 4, from Grant and West (1965), shows another velocity comparison for the different ray path assumptions. Again, it is observed that large discrepancies between the velocity estimations from the same traveltime data. Note that the ray trace integral gives unlikely velocities of about 30,000 ft/sec near the 7000 ft. depth. It appears that the ray trace integral inverts synthetic data well, but as it is a bootstrapping and exact method, it has some difficulty processing real data containing error or noise. This leads to an inquiry concerning the errors involved in a VSP survey.

2.3 ERROR ANALYSIS

Attempting to define the error associated with an observation is an arduous and generally unpleasant task. Nonetheless, understanding the errors in the survey will help in defining the accuracy of the calculated velocities. Two fundamental observations in the VSP survey are the total traveltimes from source to receiver and the depth of the receiver.

The true depth of the receiver is approximately known but difficult to specify exactly (Zeitvogel, 1982). Depth precision or repeatability is often claimed to be on the order of several tenths of a foot. But slippage of the tool in the well, without rerecording the final depth, could easily result in depth errors of several feet. This slippage is probably

systematic throughout the survey, as the tension on the cable is customarily reduced after clamping the tool (this procedure is designed to reduce cable wave propagation). The actual depths are probably biased several feet deeper than recorded. Random errors, such as operator error, cable stretching, and tool movements while clamping, probably introduce another several feet inaccuracy.[1] This means that the time error, due to the random depth inaccuracies, is about 0.5 ms (for an interval velocity of 6000 ft/s).

The errors involved in estimating the traveltimes are due to inaccurate time picking, inexact zero times, and instrument imprecision. Goetz et al. (1979) suggest that the instrument errors can be on the order of 1.0 ms. In general, the instrument errors are systematic delays and will cancel out in interval velocity calculations or provide a small shift to the shallow velocities (as do the systematic tool slippage errors). Gamburtsev (1969), in a series of shallow experiments estimates the standard deviation of the P-wave total traveltime to be 0.5 ms. Beeston and McEvilly (1977) also suggest that timing estimates are accurate to ±0.5 ms (see Appendix IV for picking error analysis). Adding these to the previously determined depth error (converted to time) gives an approximate total time error of about ±1.5 ms. Stewart et al. (1981) find maximum errors in a detailed Michigan VSP to be 2.0 ms for P-waves and 3.0 ms for S-waves. Very carefully executed surveys may have somewhat better precision than the above estimates.

---

[1]A British geophysicist related the following story at the 1981 SEG meeting. He and his colleagues were attempting to conduct an offshore VSP but were recording a great deal of noise with little signal. After many frustrating minutes, they realized that the tool was still on the deck and not in the hole at all. Such depth errors are difficult to quantify.

A more subtle type of error is associated with wave propagation effects. Anticipating the results of the next chapter, short path multiples may cause small delays in the seismic traveltimes. This effect is significant in only highly cyclically stratified sections where it may induce seismic delays of up to 2.0 ms/1000 ft with respect to the sonic log (O'Doherty and Anstey, 1971; Schoenberger and Levin, 1978; Stewart et al., 1982). If a cyclically stratified section is suspected this "drift" could be subtracted prior to analysis. Otherwise it will be largely negligible.

Assuming a simple geometry, it is possible to calculate what effect a given time error Σ_t, will have on an interval velocity. Using the geometry shown in Figure 5, the following worst case estimate may be computed for the error in velocity Σ_v

$$2\Sigma_v = \frac{\Delta z \cos \theta}{t1-t2-2\Sigma_t} - \frac{\Delta z \cos \theta}{t1-t2+2\Sigma_t} \qquad (4)$$

where Δz is the interval between recording stations

$\cos \theta$ is the cosine of the incidence angle

t_1, t_2 are the traveltimes to receiver positions 1 and 2

$\Delta t = t_1 - t_2$

Letting the velocity of the medium be $V = \frac{\Delta z \cos \theta}{\Delta t}$ and inserting this into equation (4) and assuming that $\Sigma_t/\Delta t$ small gives the relative velocity error

$$\frac{\Sigma v}{V} = \frac{2\Sigma_t}{\Delta t} \qquad (5)$$

If Σ_t = 1.5 ms, Δt = 6.0 ms (a depth interval of 50 ft for a velocity of 8333 ft/s), then the relative error in velocity is 50%! Evidently, time errors play a major role in the determination of an interval velocity.

Mismatches between noisy field observations and calculated values will still occur to an extent sometimes even greater than the errors predicted above. This is because of the simplified horizontally-layered earth model and one-dimensional ray tracing. Thus there is error in the analysis techniques as well as the observations.

By adding time noise to synthetic traveltimes, it is possible to directly investigate the effect of the observation errors on the computed velocity. In particular, the synthetic times of Figure 1(b) are used. The error or noise added to the times of Figure 1(b) has been pseudo-randomly generated from -1.0 ms to 1.0 ms. One of these random errors has been added to each traveltime point. This results in a perturbed traveltime versus depth curve. This curve is inverted using equation (3). The scatter in velocities so determined is evident in Figure 6. We notice that the scatter is greater in the deeper part of the section. This is due to the constant time error but decreasing time interval between stations of constant depth difference (i.e., Σ_t is constant, while Δt becomes smaller). There is also the cumulative effect of inaccurate previous (shallower) velocities.

To reduce traveltime scatter and thus arrive at a smoother velocity estimate, different time averaging techniques have been used. For example, smoothing the noisy traveltime curve with a three point average, then inverting the data with the ray trace integral, results in a better velocity estimate. Adding any more than about ±2.0 ms error causes the algorithm to abort.

It is seen that computed interval velocities are very sensitive to the input traveltimes. The velocity accuracy may be enhanced by using averaging techniques on noisy data. A definite criterion

for averaging is needed. It is not known, a priori, how many points to average over and what type of averaging to use. Even if an average that appears to work for the data is found, it is not certain about the quality of the solution. Large errors can cause inaccurate velocities, which, if incurred in the shallow depths, perturb the rest of the section. This is because of the bootstrapping nature of the algorithm. Large enough errors (>2.0 ms) cause the algorithm to abort. For these reasons, the previous techniques are operator intensive and require constant monitoring and interpretation.

2.4 INVERSE FORMULATION

As mentioned above, current techniques have certain shortcomings. It is anticipated, in addition, that VSP data will become increasingly complex. This will be due to multiple source offsets with different depth intervals of observations. To process all of this data simultaneously and optimally is very difficult with present techniques. With a least-squares inverse method, though, multiple data sets can be processed as a matter of course (Rice et al., 1981). The following discussion is a brief description of the classic linear inverse approach (Flinn, 1960; Crosson, 1976; Aki and Richards, 1980; Thurber, 1981).

In general, the inverse procedure is used to correct an initial guess at a number of parameters. In the VSP case, ray tracing through an estimated velocity model is performed. These calculated ray-traced traveltimes are compared (in a least-squares manner) to the observed field times. It is assumed that the difference between calculated and observed times (the residual) is linearly related to the change that needs to be made in the velocity model. This change is calculated using inverse matrix methods.

This process is repeated until either the difference in the observed and calculated traveltimes is within the experimental error or the velocity model is not changing significantly.

In detail, suppose (after Thurber, 1981) that the ray-traced traveltimes t^i_{cal}, for the i^{th} depth, have been calculated for some velocity model. The traveltime residual is defined by

$$r^i = t^i_{obs} - t^i_{cal} \qquad i = 1, M \tag{6}$$

where t^i_{obs} is the observed traveltime at depth i

M is the total number of observations

The goal is to perturb the model velocities v_j, such that the resulting change in the calculated traveltime Δt^i_{cal}, will make r^i small

$$t^i_{obs} - t^i_{cal} - \Delta t^i_{cal} \approx 0 \qquad i = 1, M \tag{7}$$

Equation (7) will never be exactly zero for all i because of errors in the traveltime data and model. Combining equations (6) and (7) gives

$$r^i \approx \Delta t^i_{cal} \tag{8}$$

Now t^i_{cal} is expanded in a Taylor series and truncated after the first term (the linearity assumption)

$$\Delta t^i_{cal} = \sum_{j=1}^{n} \frac{dt^i_{cal}}{dV_j} \Delta V_j \qquad i = 1, M \tag{9}$$

$$\Delta t^i_{cal} = t^i_{cal}(V^1_j) - t^i_{cal}(V^2_j) \tag{10}$$

where V^1_j is the first estimated velocity of the jth model layer. V^2_j is the second estimate.

N is the total number of layers

ΔV_j is the required velocity change $(V^1_j - V^2_j)$

In matrix form, equation (9) may be written:

$$Y = AX \tag{11}$$

where Y is a column vector of Δt^i's; i = 1,M

X is a column vector of ΔV_j's; j = 1,N

A is the matrix of partial derivatives, $\frac{dt^i}{dV_j}$

As mentioned previously, several problems, including noise, preclude an exact solution to equation (11). However, appealing to the least-squares criterion makes a solution possible. This constraint on equation (11) states that the sum of all the squares of the travel-time residuals must be minimized. Thus the following equations must hold

$$\frac{d}{dV_j} \sum_{i=1}^{M} (r^i)^2 = \frac{d}{dV_j} (Y^T Y) = 0 \qquad j = 1, N \tag{12}$$

This leads to the least-squares solution, $\hat{X}$

$$\hat{X} = (A^T A)^{-1} A^T Y \tag{13}$$

For more stability in the solution $\hat{X}$, the damped least-squares technique may be employed (Marquardt, 1963; Brown and Dennis, 1972). The solution is then given by

$$\hat{X} = (A^T A + \lambda^2 I)^{-1} A^T Y \tag{14}$$

where λ^2 is the damping parameter.

It may be shown (Aki and Richards, 1980) that the damping parameter, λ^2 is equal to the quotient of the variance of the data and the variance of the solution. In the present formulation, it is assumed that the observations all have the same variance, and that the velocity layers are uncorrelated. The algorithm continues to iterate (reduce λ^2) until the Δt_{cal} are within the assumed traveltime error or the new velocity estimate is negligibly different from the previous estimate. As λ^2 decreases to zero the resolution of the parameters becomes perfect; that is the parameter estimates are independent of each other.

The covariance matrix of the parameter changes C may be used to estimate the variance of the parameters (velocities) due to variance in the data

$$C = (\Delta X \Delta X^T) \equiv \sigma^2 \, (A^T A + \lambda^2 I)^{-1} \qquad (16)$$

where

σ^2 is the variance of the data = $\sum_{i=1}^{M} r^2_i$/(degrees of freedom)

ΔX is the parameter error vector

The traveltime problem is actually non-linear (Wiggins, 1972). Nonetheless, small enough changes in the velocity structure are approximately linearly related to the traveltime residual. Because only small changes are permitted, the process will need to be iterated to arrive at a final solution. Another quantity which is useful in examining the solution is the final traveltime residual. At every station or depth, the residual reflects the mismatch between the observed data and the calculated data. A single, large residual probably indicates a poor observed time. Several adjacent mismatches are often diagnostic of a poorly defined velocity layer. For example, a thick model layer covering two distinct real velocity layers will have a velocity that is approximately the average of the two real layers. However, the layer will have a polarity change in the sign of the residuals associated with it. This is an indication that an insufficient number of layers have been used. These measures, the parameter variances and data residuals, may be used to examine the quality of the solution.

The present inversion routine is operating on a mid-size computer system (VAX 11/780). The forward problem uses standard Snell's Law ray-tracing for horizontal layers and an offset source. This particular

two-point ray-tracing algorithm (after Comer, 1981) uses the method of false position to find the correct ray between the source and receiver. A finite difference Levenberg-Marquardt matrix inversion subroutine (Marquart, 1963; Brown and Dennis, 1972) performs the formal inversion. The next section describes the testing and usage of this inverse process on synthetic and real VSP data.

2.5 INVERSION RESULTS

Synthetically-generated data are used to test the algorithm. This determines the overall accuracy of the algorithm and the effect of noise on its stability. Also analyzed is the inversion of synthetic data that has some observation points missing. In particular, the top few observations are not used, but the velocity layers at these depths are kept. This leads to some interesting results.

Having examined synthetic VSP data, three field VSP data sets are analyzed. These results are also compared to their accompanying sonic logs.

2.5.1 Synthetic Examples

As previously used in synthetic examples, a theoretical traveltime curve is generated by ray tracing through a model velocity section. Traveltime noise may be added to the curve. This perturbed curve is then processed using the inversion algorithm. Figure 7 shows the results of an inversion performed on the traveltimes of rays traced through the interval velocities of Figure 1(a) with a 250 ft source offset. The velocities so determined are largely within one standard deviation of the model

velocities. The velocities are closer to the model values than those resulting from the ray trace integral.

In the next case, a large amount of noise (randomly generated from -3.0 ms to 3.0 ms) was mixed with the traveltime curve. Figure 8 shows the results for layers parameterized at the same depths as the model layers. The velocity estimates are generally within two standard deviations at the deeper depths. In the shallow section, the velocities are usually within one standard deviation. Recall that the ray trace integral method usually aborts when more than 2.0 ms noise is mixed with the traveltime data.

In a typical VSP survey, the top several hundred feet of data are often very poor (if recorded at all). This is due to cultural noise, multiple casings, and complex wave propagation. It is desirable, then, to use only the deeper traveltimes to constrain the surface velocities. This possibility has been investigated, using the synthetic traveltimes. Once again, ray tracing through the model velocity yields traveltimes. To these times was added random noise from -1.0 ms to 1.0 ms. In this case though, the top 500 ft of observations (observations were taken every 25 ft) were not used in the inversion. Two velocity layers were, nonetheless put in the top 500 ft. The results of the inversion are given in Figure 9. Note that the model velocities in the top two layers are closely approximated by the inversion results. The small standard deviations indicate that the algorithm was able to constrain the velocities fairly well. Intuitively, this is understandable for several reasons. In the first place, there are still many more observations (180) than layer velocities (15). Because the source was offset 600 ft, the upper two velocities have a large effect on the ray propagation direction and traveltimes to deeper observations. Thus these lower observations include information on the upper layers. The

inverse must find velocities for the upper layers to satisfy the observations in the deeper layers.

2.5.2 Gulf Coast VSP

This survey was performed in a cased well on the coast of Alabama by the Amoco Production Co. A slanted weight drop device (Toksoz et al., 1980) positioned 261 ft from the well-head was used to generate both P and right and left-polarized SH waves. The survey was recorded from a total depth of 1650 ft to the surface, at 10 ft receiver spacings with a three-component wall-clamping tool.

The well encountered only highly unconsolidated sediments. The top one-half of the section is mainly composed of silts and sands which trended into shale-sand interbedding for the lower half of the section. The sonic log (Figure 11) indicates that two gas sands were penetrated at 1327-1345 ft and 1496-1508 ft depths. "Kicks" on the drill string while drilling the well were evidence that the sands were highly pressurized with gas.

The P traveltimes were picked from the vertical component seismogram (Wingo, 1981). The SH times were found by overlaying the horizontal component traces from the right and left polarized source positions and picking the time of the opposing polarity arrivals. The traveltimes for P and SH waves were then input into the inversion routine which used layer thicknesses of 40 ft.

The P velocity so determined is shown in Figure 10. The velocities are quite low (about 6000 ft/s) due to the unconsolidated nature of the sediments. The errors in the velocities (about 500 ft/s) are fairly large even with four observations per layer. At 1300 ft there is evidence of the

gas sand. The velocity is dramatically lower both because of the sand and its high gas pressure (low differential pressure). The fact that the velocity is several standard deviations lower than the other velocities makes it unlikely that the result is spurious. Although 40 ft layers have been used, the velocity anomaly over the sand is quite visible. Generally, the VSP and sonic log show a similar velocity trend. However, the VSP velocities in the upper 1000 ft appear to be slightly lower than the sonic velocities. This observation is systemic through the VSP and sonic results and is the topic of the next chapter. The VSP also has several high (8000 ft/s) velocities, which judging by the magnitude of the error bars, are probably somewhat spurious. In this case it is appropriate to review the traveltimes in that region for error. If error is present then these could be edited or weighted to be less significant.

The SH velocities in Figure 12 show a greater trend with depth than the P velocities (Gregory, 1977). Errors in the estimates are about 100 ft/s. The low velocity at 1300 ft is indicative of the high pressure gas sand. Interestingly, the SH velocity is significantly lowered at 1500 ft also. It appears that this deeper but thinner gas sand has a larger effect on the SH waves than the P waves. This may be because the SH waves have a considerably shorter dominant wavelength than the P waves (about 100 ft versus 200 ft) and are thus more responsive to thinner anomalies.

The final traveltime residuals for the P survey inversion are less than 1.0 ms, while the S survey has residuals less than 2.0 ms. The error in the velocities due to the traveltime error for both cases is less than 10%. For the previous cases, the inverse algorithm requires about fifteen

iterations for convergence to the final solution. Each iteration takes on the order of several minutes of computer CPU time on the VAX system.

Numerous other layering-thicknesses have been used in the SH inversions. For example, one case computed the velocity section for 20 ft layers. The RMS value of the residuals was 0.6, but the errors were about 500 ft/s. Thus the attempted fine resolution produced excessive error.

We note also the very high Vp/Vs ratio; it changes from a near-surface value of nearly 7.0 to a minimum of 2.9 at depth. This variation is not unreasonable in light of the unconsolidated nature of the sediments. Such high and variant ratios are a factor in making the correlation of P and S reflection surveys somewhat difficult.

Using the velocities measured in the gas sand V_p = 4400 ft/s and V_s= 1530 ft/s gives a V_p/V_s = 2.88. This translates into a Poisson's ratio (σ) of 0.43. Nearby brine-saturated sediments have V_p = 6400 ft/s and V_s = 1750 ft/s. This gives V_p/V_s = 3.66 and σ = 0.46.

The small traveltime residuals, reasonable velocity errors and correspondence of the VSP velocities to the sonic log indicate a good solution.

2.5.3 ENIX VSP

A VSP was conducted in early 1980 in East Texas by the ARCO Oil and Gas Co. Six Dinoseis® guns were positioned 100 ft away from the wellhead to perform the survey. Recordings were made with a wall-clamping, three-component tool, every 25 ft from T.D. at 2175 ft to the surface.

The geologic section is composed primarily of Cretaceous and Tertiary sediments. Shales and limestones extend from the near surface to a depth of 780 ft. From here, the Arkadelphia marl trends into the Nacatoch sandstone at 1080 ft. Below this is the Taylor Group (sandstone, shale, marl) to 2000 ft. This in turn is underlain by the Pecan Gap chalk.

Figure 13 shows the results of a traveltime inversion for 75 ft thick layers. An inversion was also performed on a model with 100 ft layers. The velocity estimates for the two cases are quite similar. However, some differences do exist. For example, on the 75 ft layer model the bottom

®registered trademark of ARCO Oil and Gas Co.

group (2000-2200 ft) is bounded by lower velocities, whereas, on the 100 ft layer case, there is but one layer. The lithologic section indicates that there is, in fact, a high velocity chalk layer underlain by a slower marl.

Referring to the sonic log, (Figure 14) it is seen that while the overall trends of the sonic and VSP velocities are similar, the VSP velocities are consistently lower. In fact, this area has high attenuation and thus large velocity dispersion (Wuenschel, 1965; Strick, 1971; Ganley and Kanasewich, 1980; Stewart et al., 1982). Thus the VSP velocities should theoretically be a few percent lower than the sonic velocities as is observed (discussed further in Chapters 3 and 4).

The standard deviation of the velocity (about 5% relative error) and small traveltime residuals (<1.0 ms) indicate a high quality survey and reasonable velocity model.

2.5.4 COLORADO VSP

A thorough geophysical survey was conducted by ARCO Oil and Gas Co. in Colorado. It included a full spectrum of logs and a VSP. The VSP was recorded in Well #100 from a total depth of 7370 ft to 950 ft at 75-ft intervals. The survey used a group of four vertical vibrators offset at a distance of 1000 ft from the wellhead. A wall-clamping, three-component receiver provided good vertical but poor horizontal traces.

In this area, the geologic section is largely composed of shale (Pierre and Niobrara) to a depth of 4100 ft. From here to the bottom of the well there are alternating sandstones (e.g., Dakota), shales (Morrison), and limestones (Timpas). The Sangre de Cristo redbeds are encountered at 5375 ft.

Figure 15 shows a thick layer (approximately 600 ft) velocity interpretation of the Raton VSP from the inverse algorithm. The traveltime

residuals for this interpretation are rather large, often up to 2.0 ms, which is more than expected. The RMS value of the residuals is 0.7 ms. The standard deviations of the velocity are quite small. These highly constrained velocities (with unrealistic standard deviations) indicate that the resolution was too poor (i.e., velocity layers are too thick). Accordingly, the model is reparameterized with thinner layers (150 ft thick). In Figure 16, the results of the velocity inversion are shown. The high velocity redbeds are apparent at 5400 ft. The standard deviations of the velocity are more realistic (6-10% relative error), and the traveltime residuals are around 1.0 ms. The standard deviation of all the residuals is 0.3 ms. This appears to be a better solution. Figure 17 is a plot of the unedited sonic log velocities. Note the great deal of scatter in the sonic log. While much of this scatter may be edited out of the sonic log, questions of accuracy still remain. The VSP velocities are less sensitive to, for example, borehole conditions and can give more constrained velocities. The shallow VSP velocities are somewhat lower than those of the sonic log. This is similar to the findings in the ENIX and Gulf Coast wells. Again, this is perhaps due to higher attenuation in the shallow section which causes velocity dispersion (as will be discussed later).

2.6 CONCLUSIONS

For simple check shot surveys (small source offset, large observation intervals) elementary velocity analysis techniques are often adequate. However, as more complex VSP surveys are performed and from which more information is expected, increasingly sophisticated analysis techniques are required.

Trial and error ray tracing for velocity or using the integral method can produce reasonable results in data sets with low noise. But the procedure is operator intensive, can sometimes give erroneous velocities and leaves solutions without a statement concerning their quality.

The linear inverse method (Levenberg-Marquardt) solves some of these problems through the usage of the damped least-squares criterion. Synthetic results discussed demonstrate the accuracy and stability of the algorithm. Three field VSP surveys analyzed show the type of resolution and confidence that may be achieved with the linear inverse. VSP velocities appear to be slightly lower than those evidenced on the sonic log. The VSP is able to delineate several thin gas zones due to their velocity anomalies. The exact depth of specific lithology changes in the ENIX, Gulf Coast and Colorado field data has been determined using the velocity variation as computed by the inverse procedure.

This page is blank.

FIGURE CAPTIONS

Figure 1. Graphs of the model used to test various ray path assumptions. (a) The interval velocity vs. depth. (b) The ray-traced traveltimes through the velocity structure of (a). Source offset is 500 ft, and observations are made at 50-ft intervals. (c) The rays themselves are graphed as they would propagate through the velocity layers. Note the horizontal exaggeration.

Figure 2. Velocities calculated from Figure 1(b) using vertical rays (apparent velocity) and slanted straight ray assumptions. The deeper velocity estimates are more valid, as the assumed and actual rays are both nearly vertical. In the shallow section, the actual rays are more horizontal than the assumed rays.

Figure 3. Velocities calculated from the traveltimes of Figure 1(b) using the ray path integral, equation (3).

Figure 4. A VSP performed in Louisiana and analyzed by Grant and West (1965). Source offset was 1000 ft. Three velocity estimates are plotted using the ray path assumptions underlying equations (1) and (3). Note The differences in these velocities are quite substantial. Note the unrealistic velocities at about 7000 ft.

Figure 5. Simplified geometry of rays arriving with some angle, θ, at two receiver depths separated by distance, Δz. Each ray arrives at a time, t_i, and has an error associated with it, Σ_t.

Figure 6. Velocities calculated by the ray integral method from noisy travel times. The traveltimes are generated by ray tracing through the structure of 1(a) with a 1000 ft source offset. They are then mixed with random noise from -1.0 ms to 1.0 ms.

Figure 7. Interval velocity vs. depth as determined by the linear inverse. Noise (-1.0 ms to 1.0 ms) and interval velocities are the same as that of Figure 6 but the source is now offset only 250 ft. Horizontal bars are the one standard deviation of velocity limits.

Figure 8. Interval velocity vs. depth from the linear inverse. Random noise from -3.0 ms to 3.0 ms mixed with the travel times from Figure 1(b). This noisy data has been inverted.

Figure 9. Interval velocity vs. depth from the linear inverse. Traveltimes are calculated through the velocity structure shown with a solid line. Random noise from -1.0 ms to 1.0 ms has been added to these times. The top 500 ft of observations have been discarded and inverse performed. Note the small errors associated with the velocity estimate.

Figure 10. P interval velocity versus depth for Gulf Coast well from linear inverse. The well below 1600 ft was plugged with cement before the VSP was run. The depth interval between observations is 10 ft., and the velocity layers are 40 ft. thick. The P traveltimes were picked from the traces of the vertical geophones. The horizontal bars give the standard deviation of the velocity due to errors in the data.

Figure 11. Sonic log versus depth for Gulf Coast well. Note the two low velocity gas sands.

Figure 12. S interval velocity versus depth for Gulf Coast well from linear inverse. Observations were made every 10 ft. S traveltimes were picked by overlaying left and right polarized shear wave traces (from the horizontal geophones). S velocity increases with depth. The two low velocity gas sands are identifiable at about 1300 ft and 1500 ft depths. The horizontal bars give the standard deviation of the velocity due to errors in the data.

Figure 13. Interval velocity vs. depth from linear inverse for ENIX VSP. Layer thicknesses of 75 ft. are used. The depth between observations is 25 ft. A P traveltime is picked from the trace of the vertical component geophone at each level. The horizontal bars give the standard deviation of the velocity due to errors in the data.

Figure 14. Sonic log vs. depth for ENIX well.

Figure 15. P interval velocity versus depth for the Colorado VSP (Well #100) from the linear inverse. Observations were made every 75 ft. The P traveltimes were picked from the vertical geophones. Velocity layers are 600-800 ft thick. The horizontal bars give the standard deviation of the velocity estimate.

Figure 16. P interval velocity versus depth for Well #100 as in Figure 15. Velocity layers are 150 ft thick and standard deviations are shown.

Figure 17. Unedited sonic log versus depth for the Colorado Well #100.

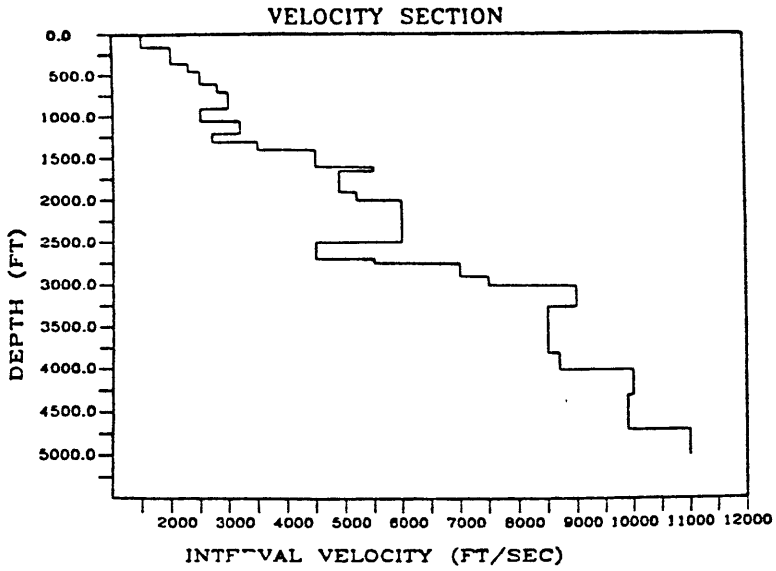
VELOCITY SECTION
DEPTH (FT)
0.0
500.0
1000.0
1500.0
2000.0
2500.0
3000.0
3500.0
4000.0
4500.0
5000.0
2000 3000 4000 5000 6000 7000 8000 9000 10000 11000 12000
INTERVAL VELOCITY (FT/SEC)

a)

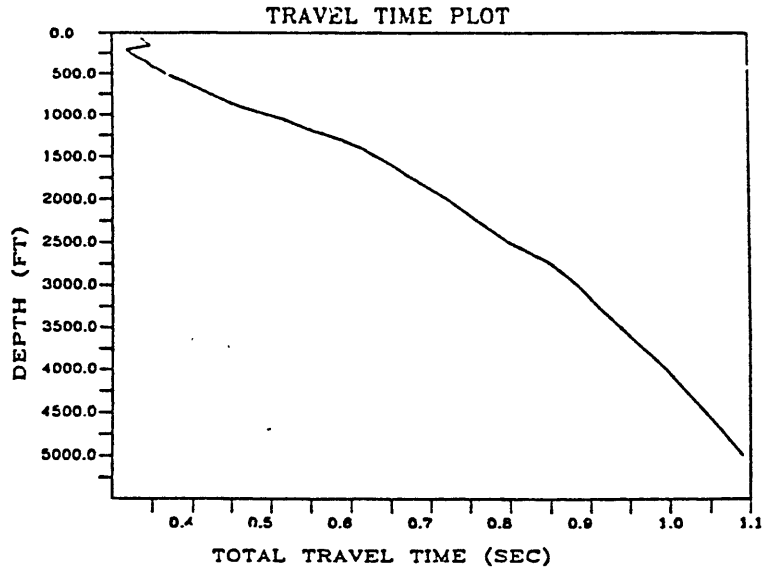
TRAVEL TIME PLOT
DEPTH (FT)
0.0
500.0
1000.0
1500.0
2000.0
2500.0
3000.0
3500.0
4000.0
4500.0
5000.0
0.4 0.5 0.6 0.7 0.8 0.9 1.0 1.1
TOTAL TRAVEL TIME (SEC)

b)

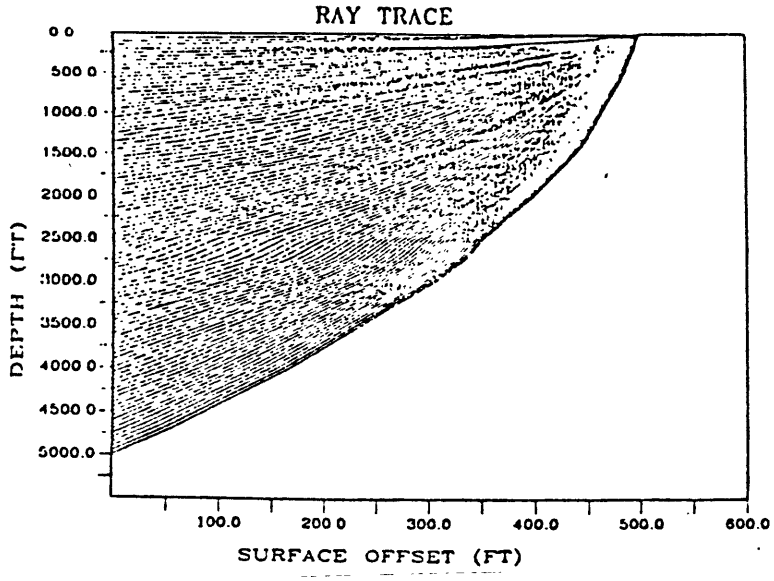
RAY TRACE
DEPTH (FT)
0.0
500.0
1000.0
1500.0
2000.0
2500.0
3000.0
3500.0
4000.0
4500.0
5000.0
100.0 200.0 300.0 400.0 500.0 600.0
SURFACE OFFSET (FT)

c)

Figure 1.

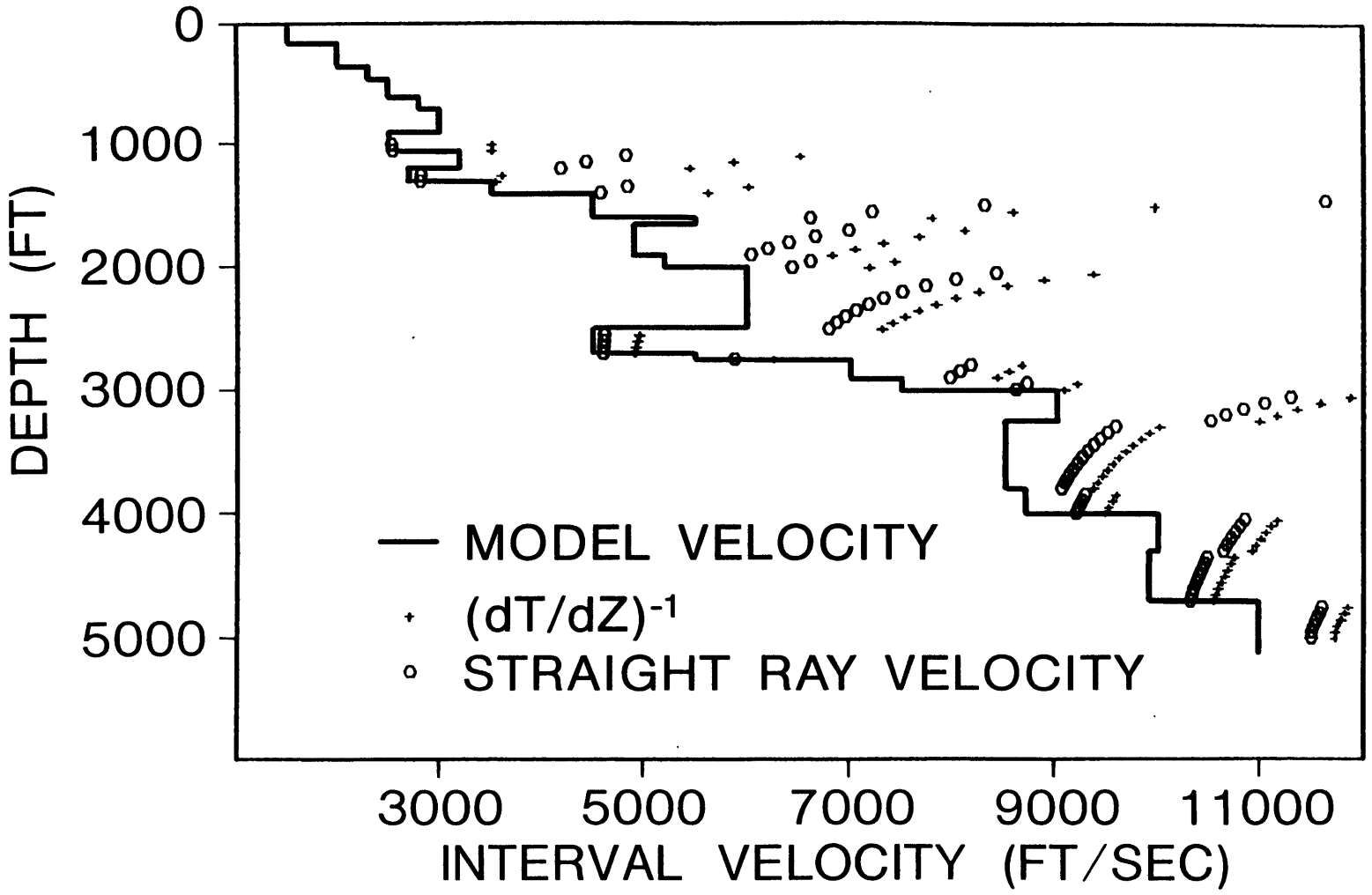
INTERVAL VELOCITY COMPARISON
NO NOISE, 1000′ OFFSET, 50′ SPACING, NO AVG
DEPTH (FT)
0
1000
2000
3000
4000
5000
MODEL VELOCITY
(dT/dZ)-1
STRAIGHT RAY VELOCITY
3000
5000
7000
9000
11000
INTERVAL VELOCITY (FT/SEC)

Figure 2.

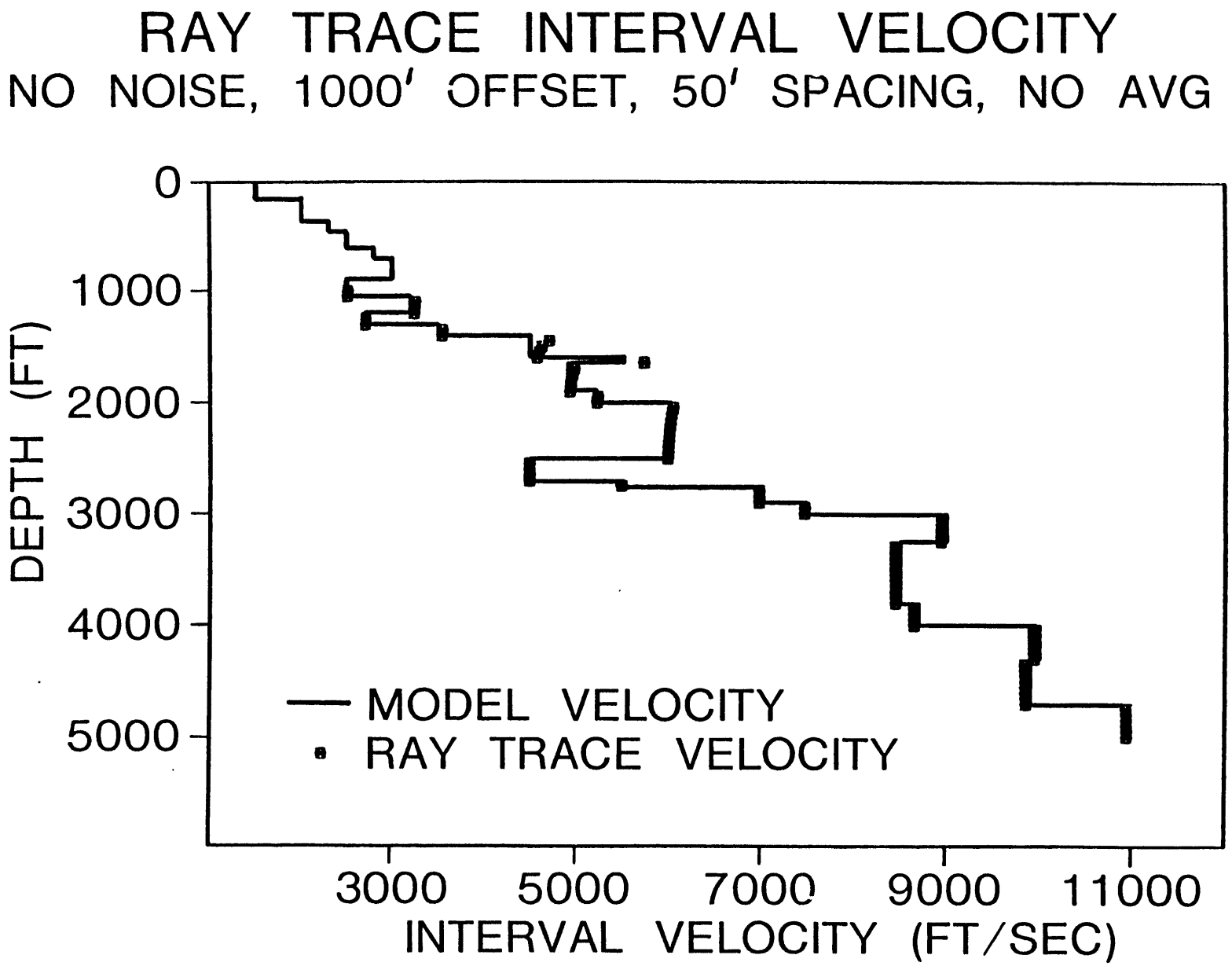
RAY TRACE INTERVAL VELOCITY
NO NOISE, 1000′ OFFSET, 50′ SPACING, NO AVG
DEPTH (FT)
0
1000
2000
3000
4000
5000
MODEL VELOCITY
RAY TRACE VELOCITY
3000
5000
7000
9000
11000
INTERVAL VELOCITY (FT/SEC)

Figure 3.

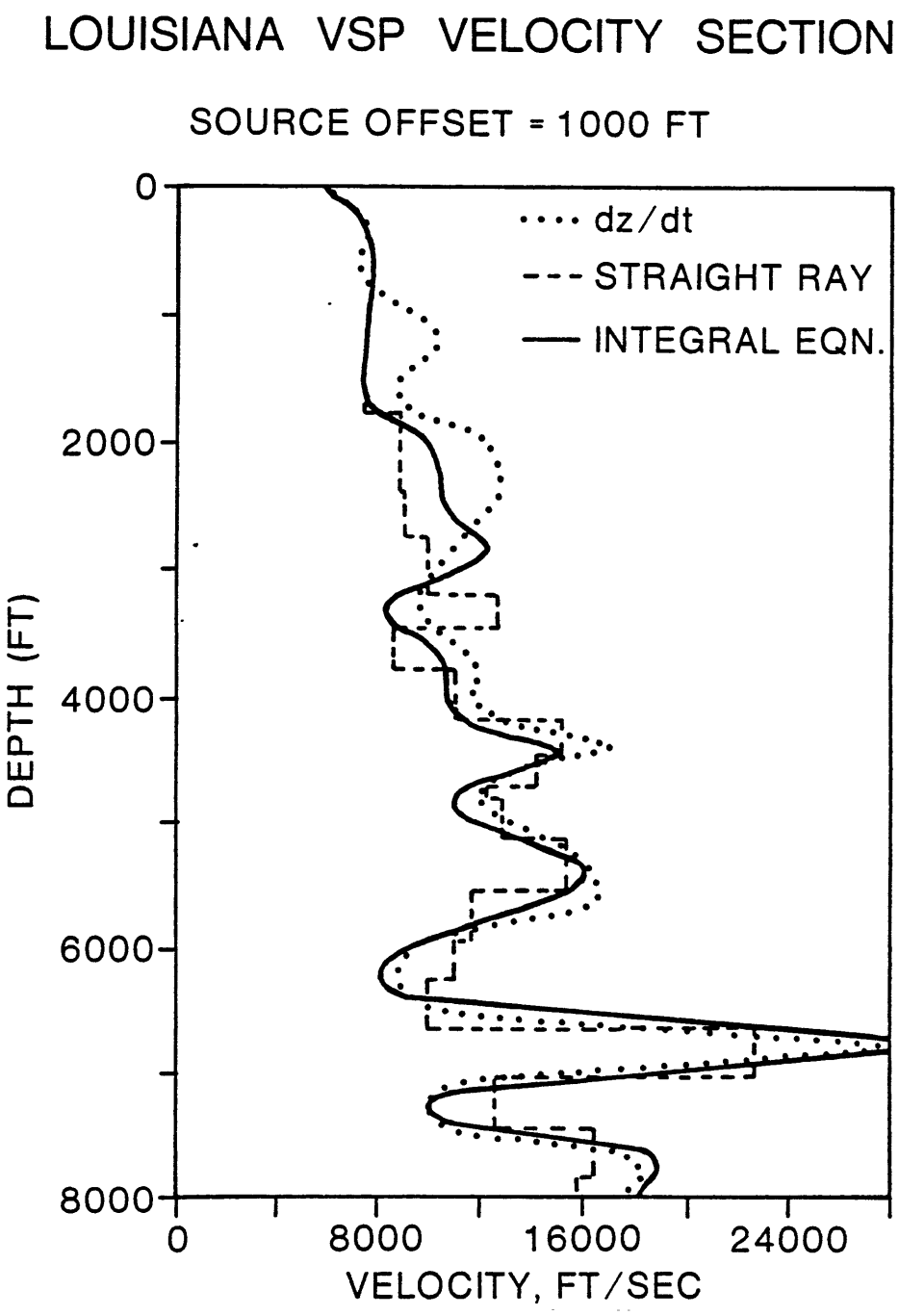
LOUISIANA VSP VELOCITY SECTION
SOURCE OFFSET = 1000 FT
dz/dt
STRAIGHT RAY
INTEGRAL EQN.
DEPTH (FT)
0
2000
4000
6000
8000
0
8000
16000
24000
VELOCITY, FT/SEC

Figure 4.

SCHEMATIC FOR ERROR CALCULATION

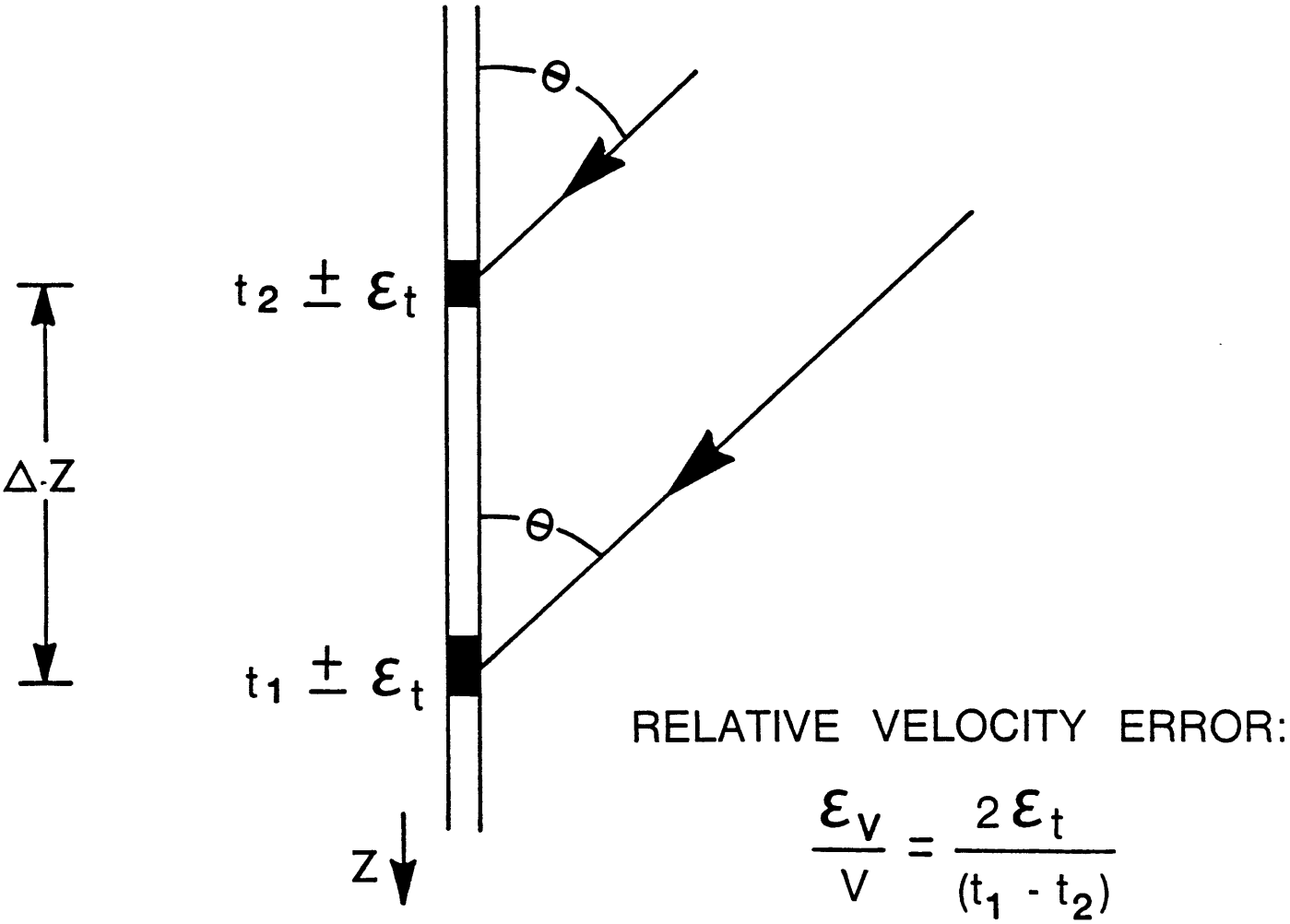

RELATIVE VELOCITY ERROR:

$$\frac{\varepsilon_V}{V} = \frac{2\varepsilon_t}{(t_1 - t_2)}$$

Figure 5.

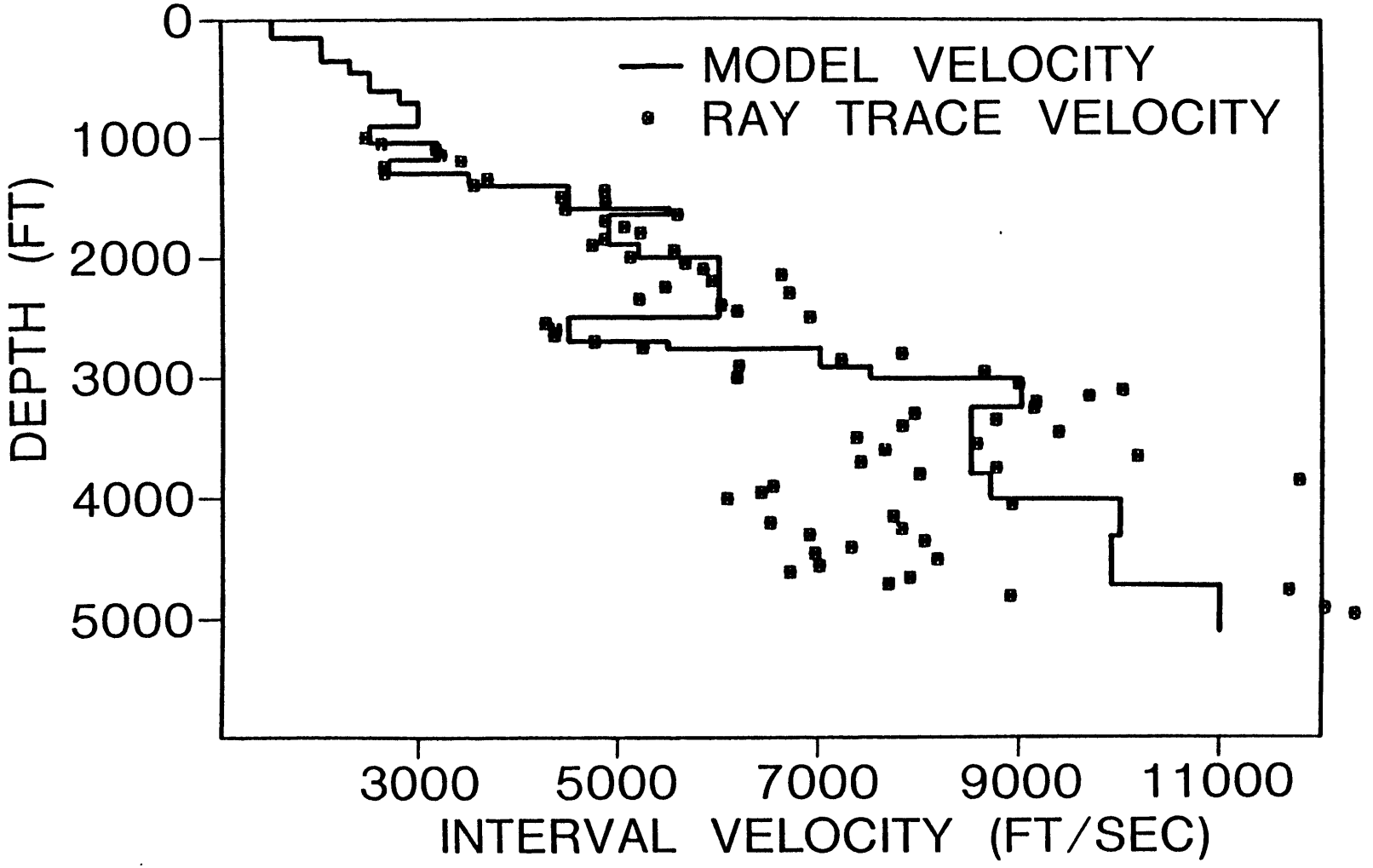
RAY TRACE INTERVAL VELOCITY
1.0MS NOISE, 1000′ OFFSET, 50′ SPACING, NO AVG
MODEL VELOCITY
RAY TRACE VELOCITY
DEPTH (FT)
0
1000
2000
3000
4000
5000
3000
5000
7000
9000
11000
INTERVAL VELOCITY (FT/SEC)

Figure 6.

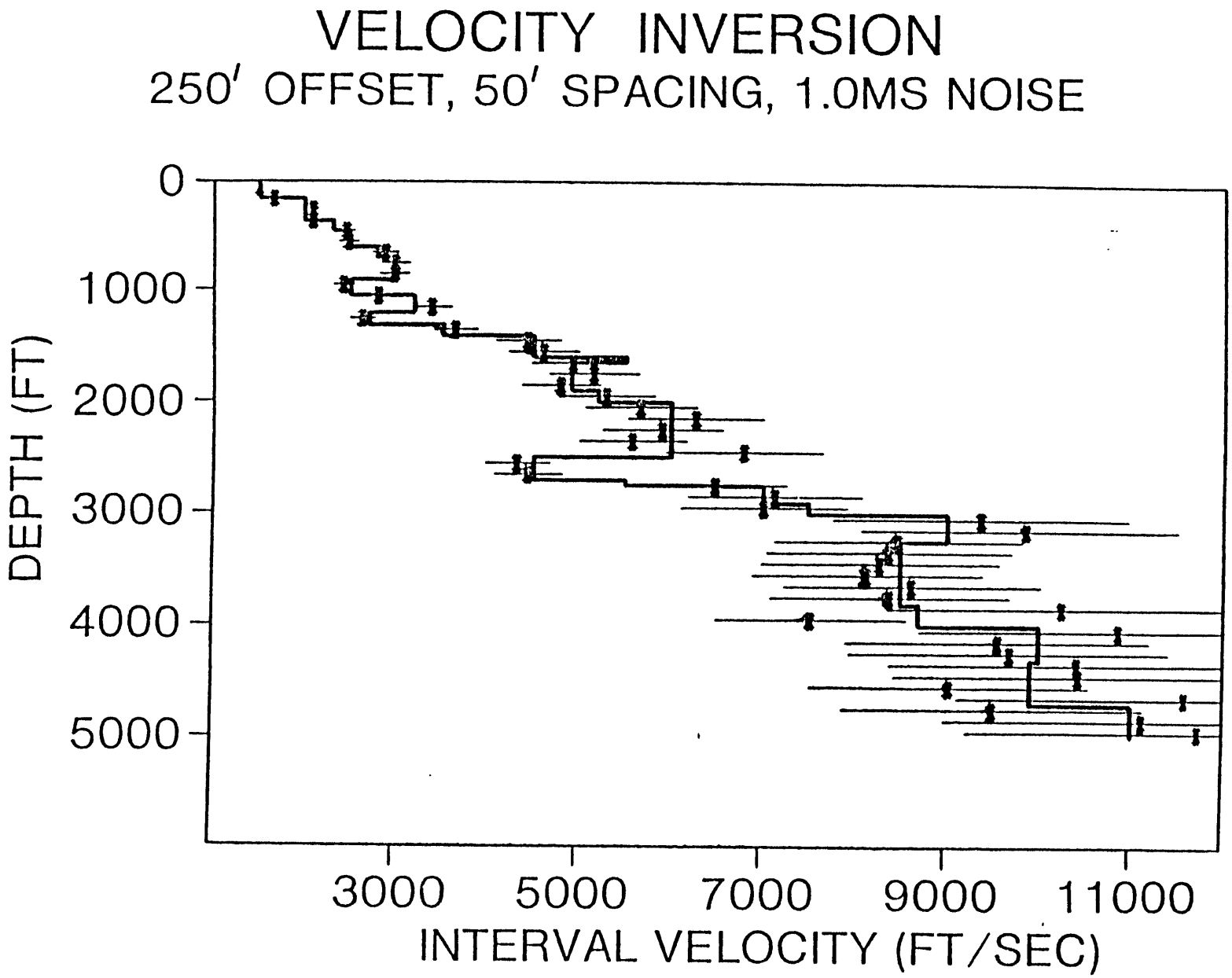
VELOCITY INVERSION
250′ OFFSET, 50′ SPACING, 1.0MS NOISE
DEPTH (FT)
0
1000
2000
3000
4000
5000
3000
5000
7000
9000
11000
INTERVAL VELOCITY (FT/SEC)

Figure 7.

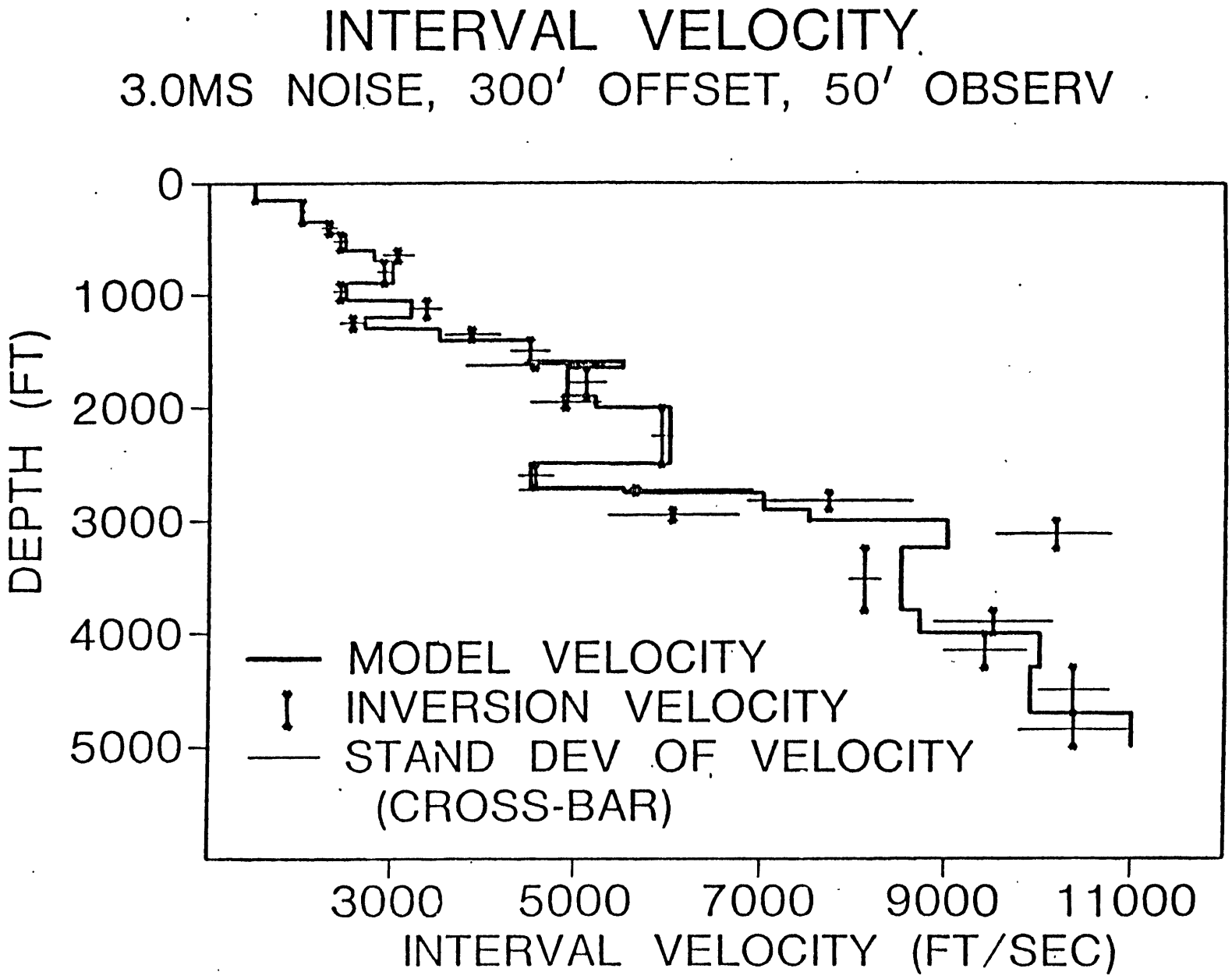
INTERVAL VELOCITY
3.0MS NOISE, 300′ OFFSET, 50′ OBSERV
DEPTH (FT)
0
1000
2000
3000
4000
5000
MODEL VELOCITY
INVERSION VELOCITY
STAND DEV OF VELOCITY
(CROSS-BAR)
3000
5000
7000
9000
11000
INTERVAL VELOCITY (FT/SEC)

Figure 8.

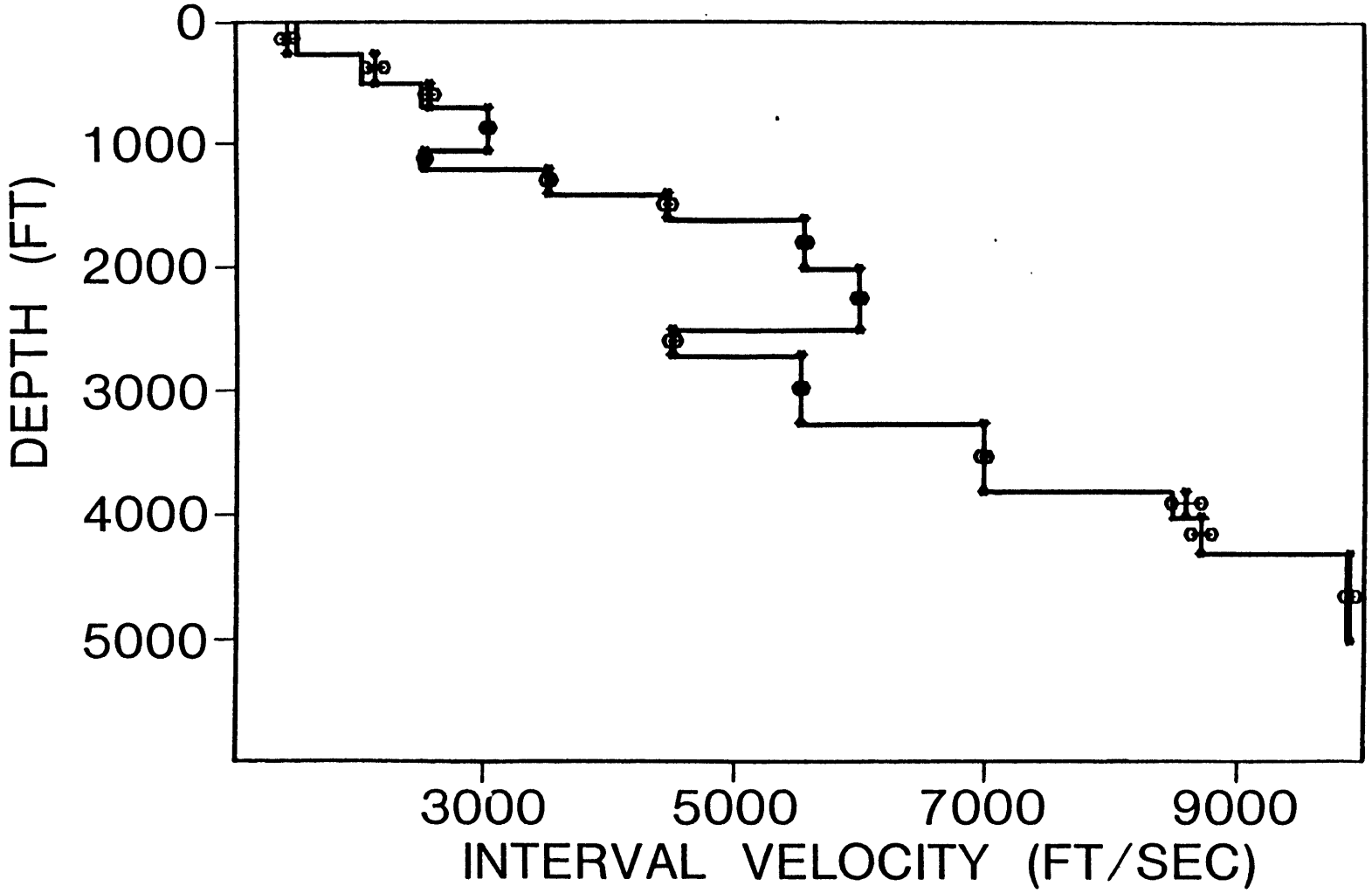
VELOCITY INVERSE: NO TOP 500′
600′ OFFSET. 25′ SPACING, 1.0MS NOISE
DEPTH (FT)
0
1000
2000
3000
4000
5000
3000
5000
7000
9000
INTERVAL VELOCITY (FT/SEC)

Figure 9.

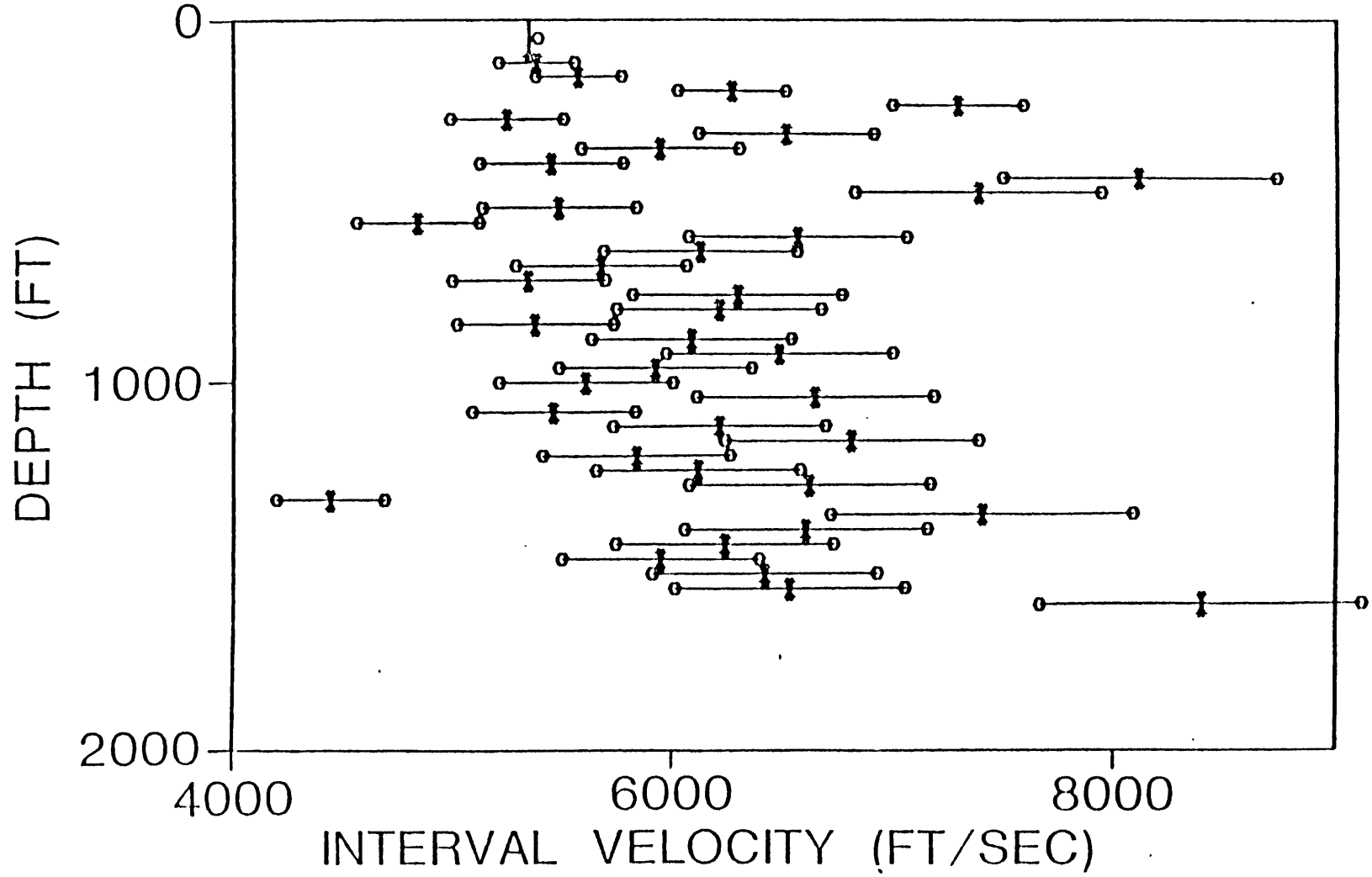
P VELOCITY — GULF COAST
260′ OFFSET, 10′ SPACING
0
1000
2000
DEPTH (FT)
4000
6000
8000
INTERVAL VELOCITY (FT/SEC)

Figure 10.

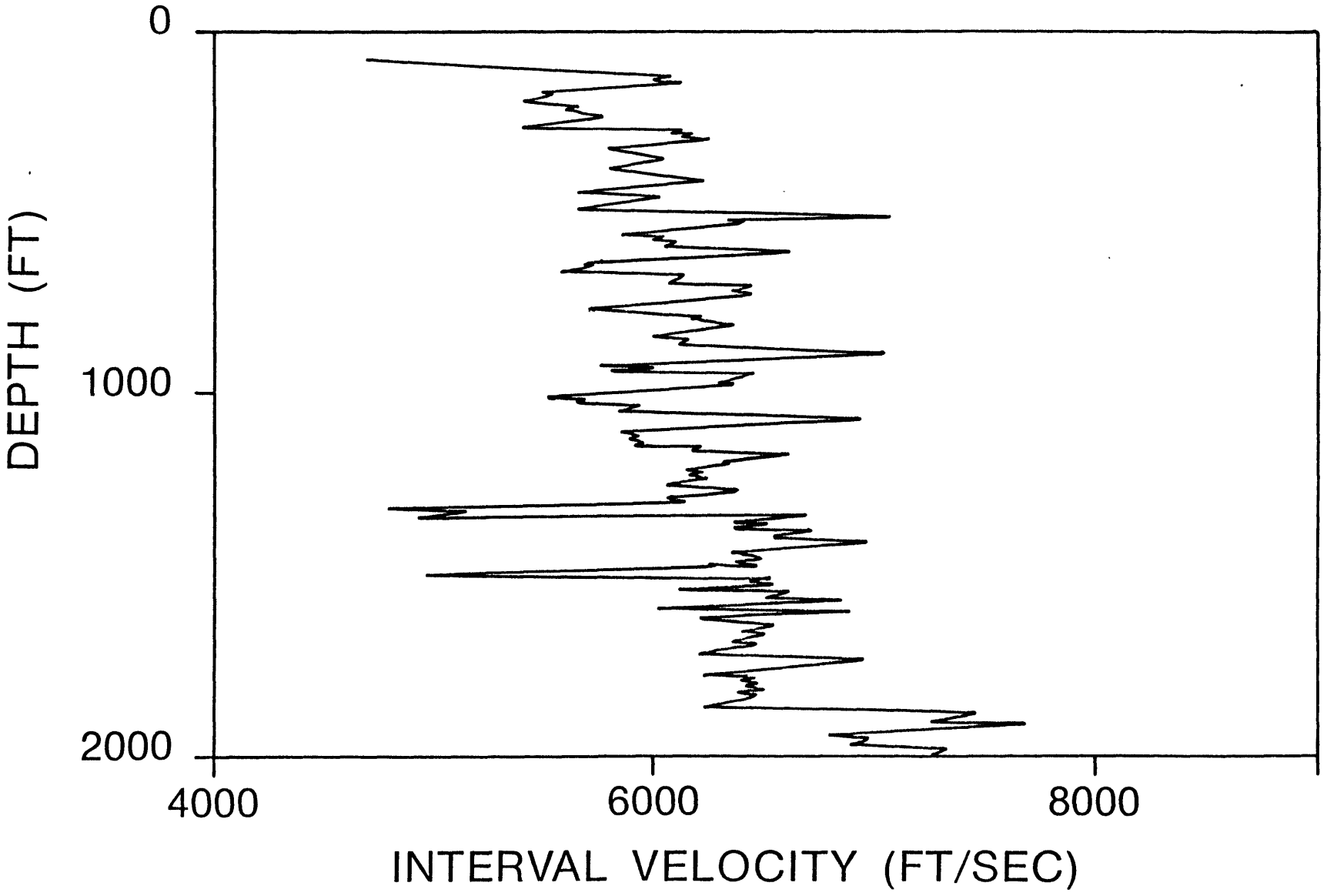
SONIC LOG — GULF COAST
0
1000
2000
DEPTH (FT)
4000
6000
8000
INTERVAL VELOCITY (FT/SEC)

Figure 11.

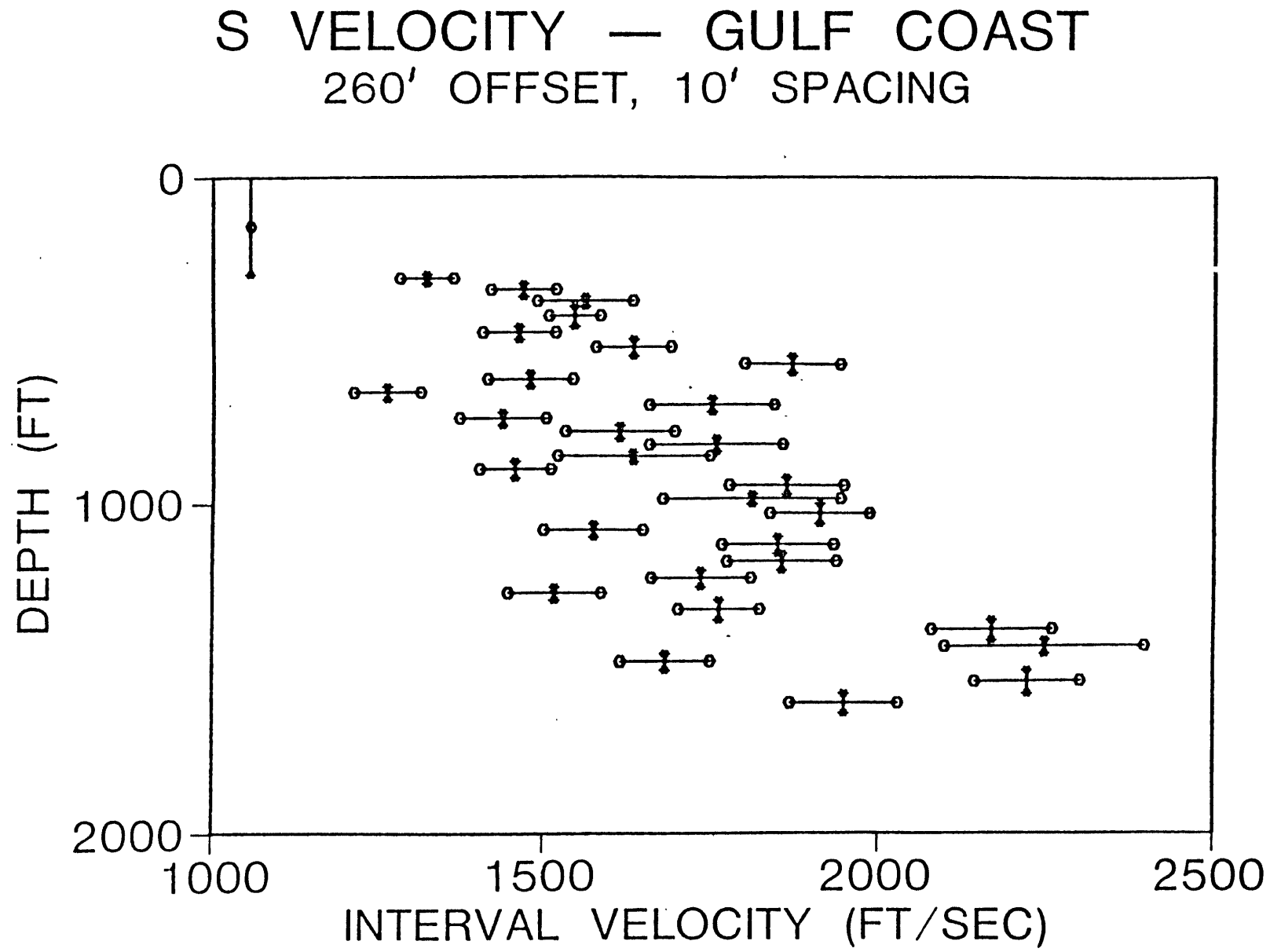
S VELOCITY — GULF COAST
260′ OFFSET, 10′ SPACING
DEPTH (FT)
0
1000
2000
1000
1500
2000
2500
INTERVAL VELOCITY (FT/SEC)

Figure 12.

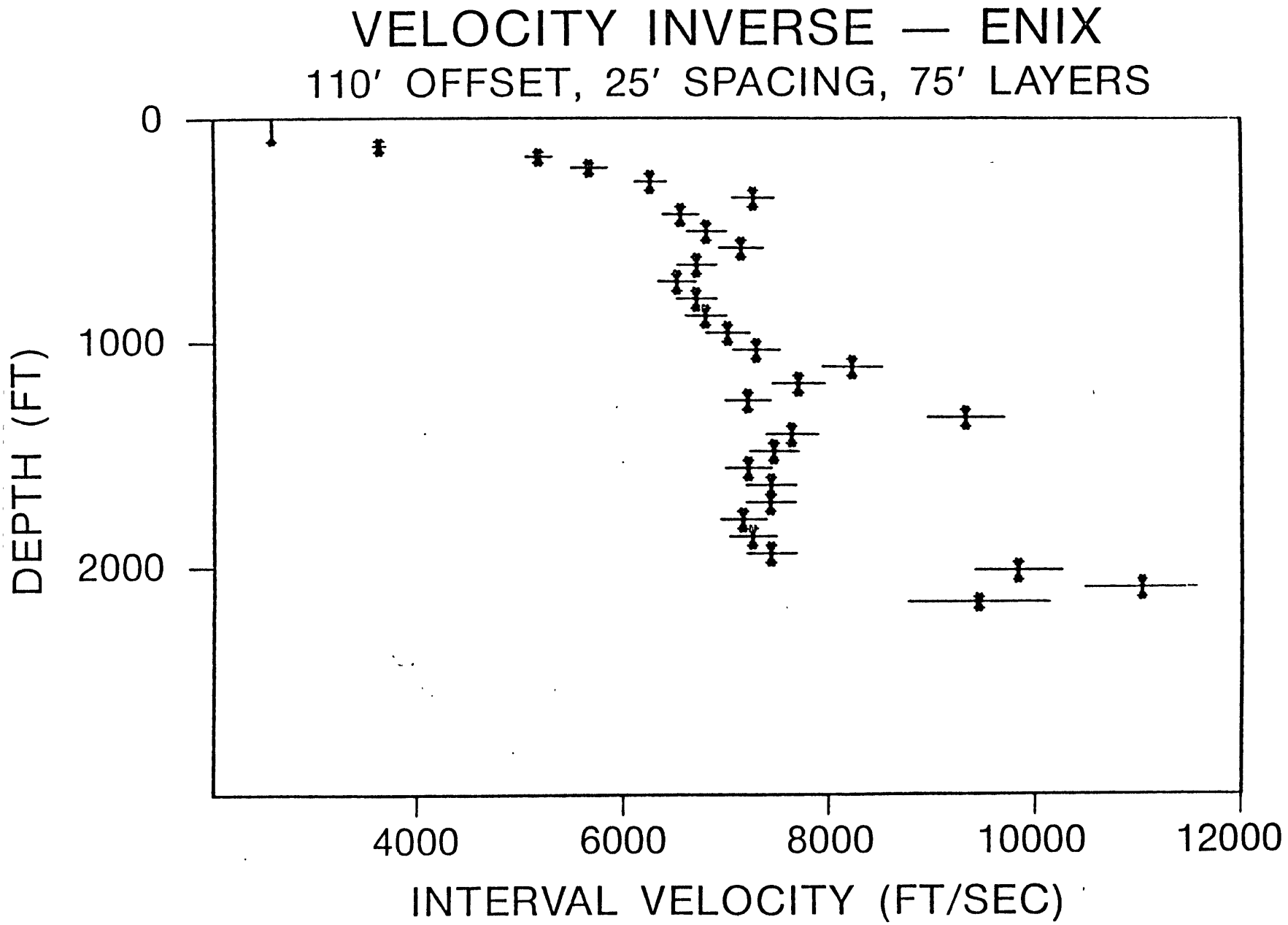
VELOCITY INVERSE — ENIX
110′ OFFSET, 25′ SPACING, 75′ LAYERS
DEPTH (FT)
0
1000
2000
4000
6000
8000
10000
12000
INTERVAL VELOCITY (FT/SEC)

Figure 13.

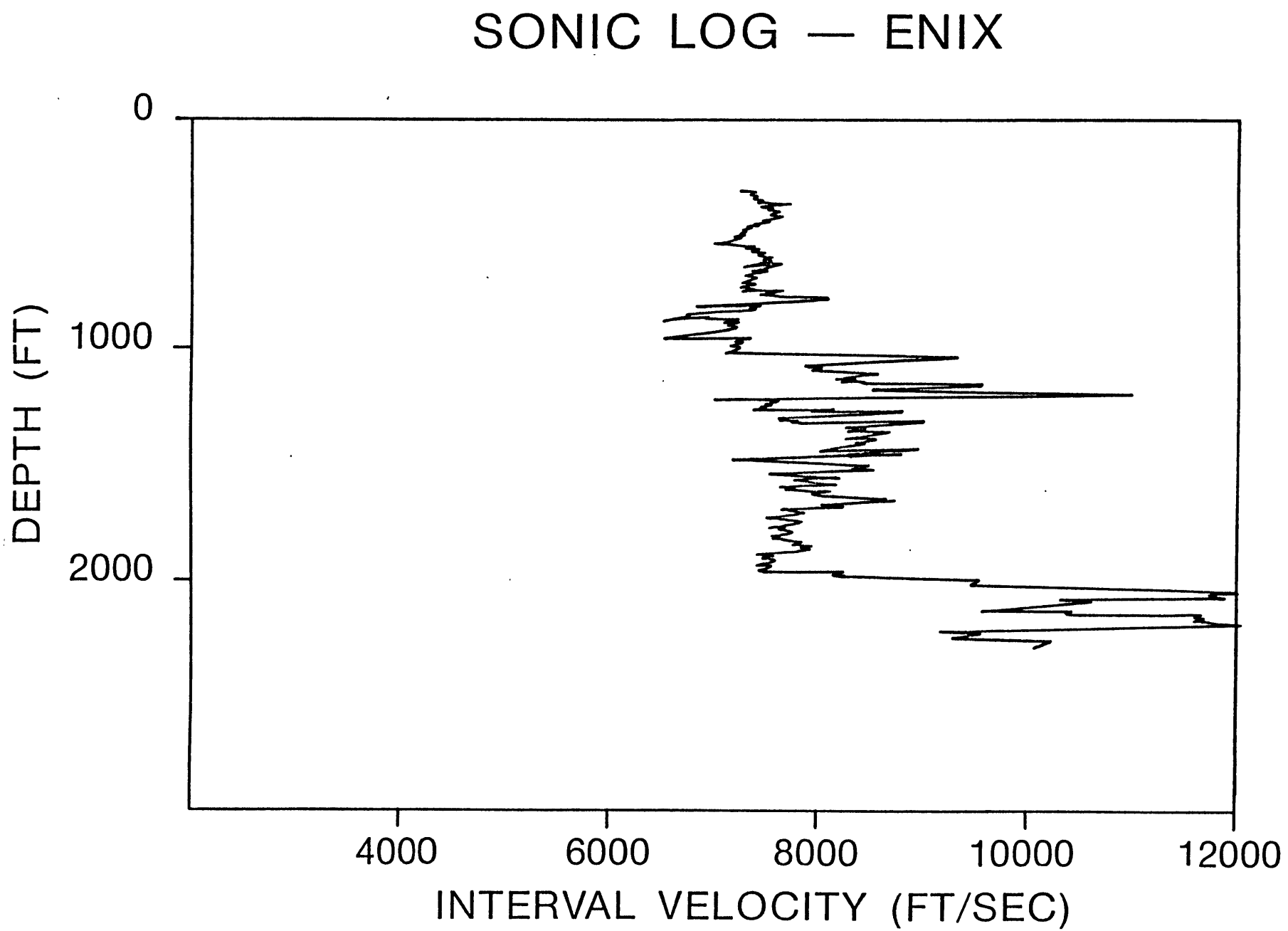
SONIC LOG — ENIX
0
1000
2000
DEPTH (FT)
4000
6000
8000
10000
12000
INTERVAL VELOCITY (FT/SEC)

Figure 14.

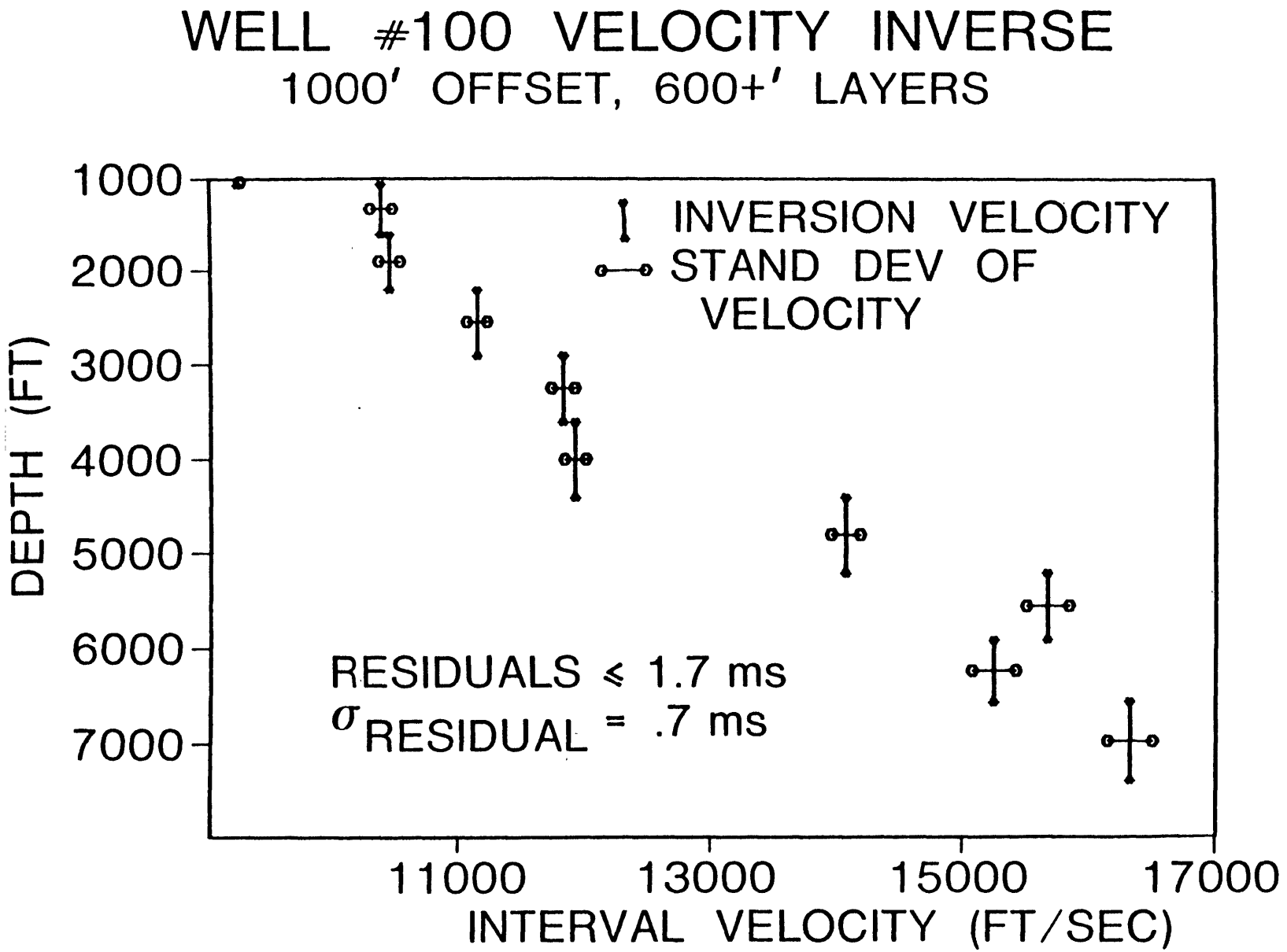
WELL #100 VELOCITY INVERSE
1000′ OFFSET, 600+′ LAYERS
DEPTH (FT)
1000
2000
3000
4000
5000
6000
7000
INVERSION VELOCITY
STAND DEV OF VELOCITY
RESIDUALS ≤ 1.7 ms
σRESIDUAL = .7 ms
11000
13000
15000
17000
INTERVAL VELOCITY (FT/SEC)

Figure 15.

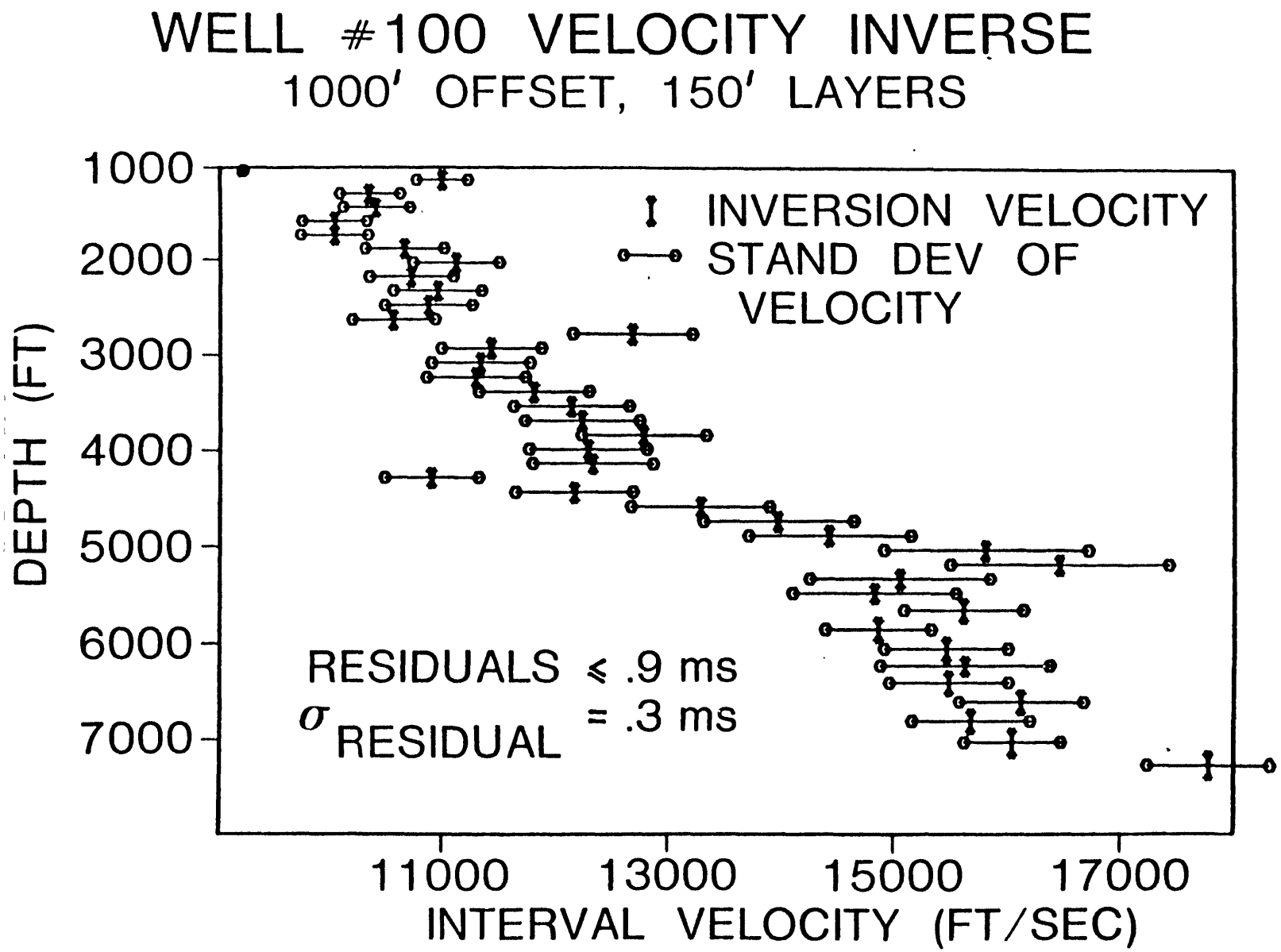
WELL #100 VELOCITY INVERSE
1000′ OFFSET, 150′ LAYERS
DEPTH (FT)
1000
2000
3000
4000
5000
6000
7000
INVERSION VELOCITY
STAND DEV OF VELOCITY
RESIDUALS ≤ .9 ms
σ RESIDUAL = .3 ms
11000
13000
15000
17000
INTERVAL VELOCITY (FT/SEC)

Figure 16.

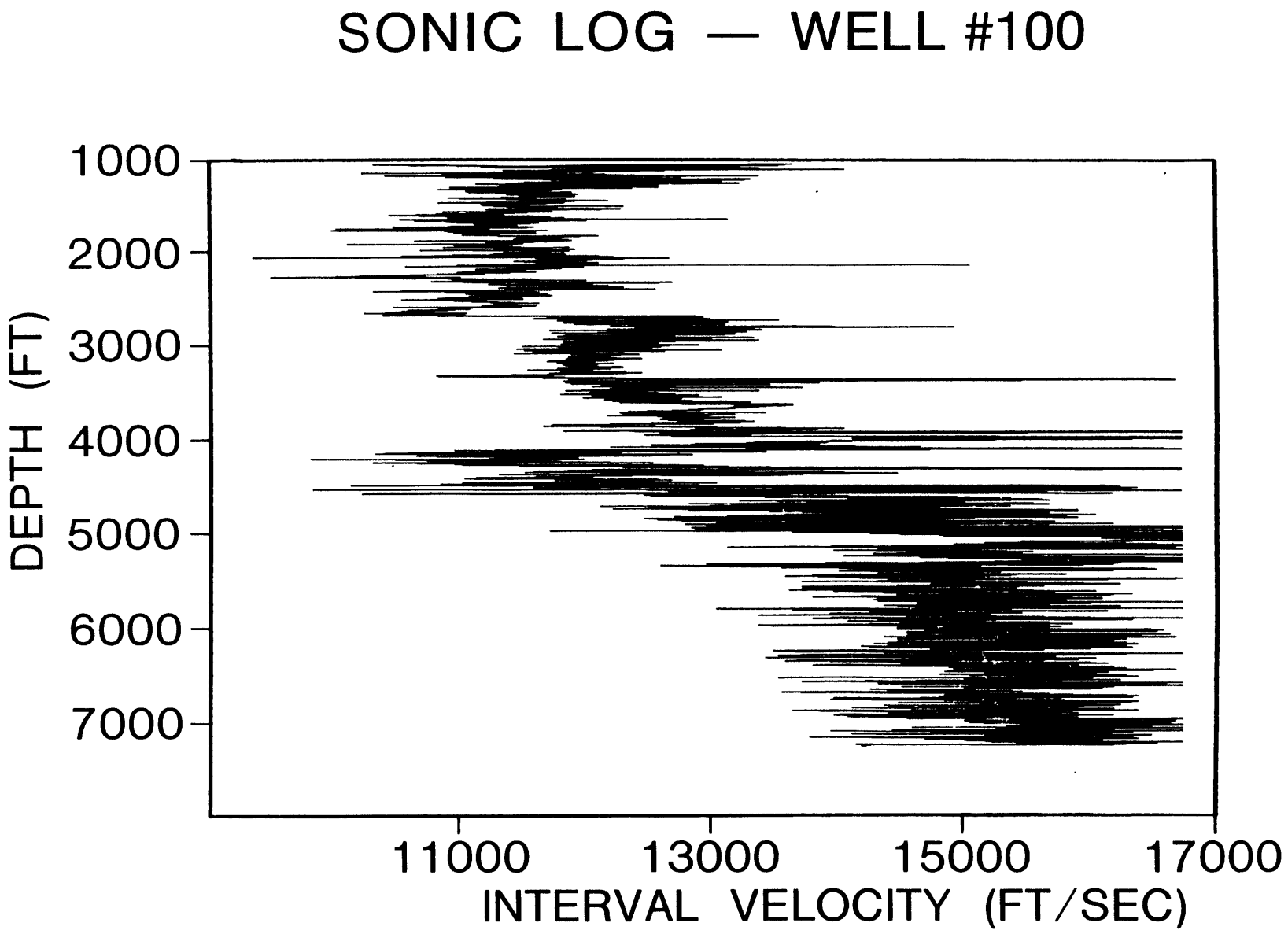
SONIC LOG — WELL #100
DEPTH (FT)
1000
2000
3000
4000
5000
6000
7000
11000
13000
15000
17000
INTERVAL VELOCITY (FT/SEC)

Figure 17.

Chapter 3

SEISMIC VS. SONIC TRAVELTIMES

...when you start looking at geophysical data, anything can happen.

Prof. J.F. Claerbout
Lecture at M.I.T.,
March 31, 1982

3.1 INTRODUCTION

Exploration geophysics involves finding a number of parameters that describe the type and state of rocks in a given region. Many tools and techniques are commonly used in this pursuit, among those being the sonic log and vertical seismic profile (VSP). One of the prime purposes of these in situ, surveys as discussed in Chapter 2, is to find a rock velocity or traveltime as a function of depth; this velocity is then used in the lithologic delineation and mapping process. The surveys can also help us understand wave propagation in an often complex medium.

Generally, the traveltime results of the two surveys show some discord. Because for example, the VSP or a check shot survey is often used to calibrate the sonic log, which is used to generate reflection synthetic seismograms, it is important to understand why the sonic and seismic surveys disagree.

There are several reasons for the observed differences (Thomas, 1978):

(a) The sonic and seismic tools investigate different volumes of rock because of their geometry and source frequencies.

(b) Each system has instrumental errors associated with it as well as analysis inaccuracy.

(c) Different wave propagation characteristics are in effect for the two measurements.

Fortunately, there are data sets available concerning the discrepancies observed between the sonic log and seismic survey (Gretener,

1961; O'Brien and Lucas, 1971; Goetz et al., 1979; Peyret and Mons, 1981). Several papers have advanced hypotheses as to the observed discord and its reconciliation (Strick, 1971; Ward and Hewitt, 1977).

Note here that sonic data are measured as slownesses - μs/ft; the transit times of sonic energy across a several foot interval. These data are summed to any depth to give a total traveltime called the integrated sonic times.

Both check shot and VSP surveys are considered in this chapter and compared to the integrated sonic log. Recall that the check shot survey is similar to the VSP except that in the check shot survey only the first break is recorded carefully and there is larger depth between receiver stations. The seismic traveltimes are corrected to the vertical to measure their time delay with respect to the sonic log.

In this chapter, the observed differences between seismic and sonic measurements and their causes are reviewed , but only factors affecting the traveltimes measured from the VSP are analysed.

The use of VSP traveltime picks is complicated for several reasons. Discrete sampling and band-limited traces limit the resolution obtainable in traveltime. There is also the problem of amplitude noise which results in a smeared first arrival. Thus, time picks can be made only approximately (Aki and Richards, 1980). The source waveform itself may change from shot to shot, making correlation difficult.

Propagation effects cause a discrepancy between the measured velocity and the expected velocity of the medium. Dispersive media distort the phase of the propagating waveform (Wuenschel, 1965; Strick, 1971; Ganley and Kanasewich, 1980). Attenuation degrades the frequency content of the waveform as it travels through the section (Hauge, 1981; Kan et al., 1981;

Zeitvogel, 1982). Finally, short-path multiples can cause an appreciable delay in the arrival of the maximum energy (O'Doherty and Anstey, 1971; Schoenberger and Levin, 1978). Small errors in traveltime, from the above origins, can cause large errors in the velocity. For example, a 0.5 ms error in time over a 25 ft VSP interval with a true interval velocity of 15000 ft/s gives an observed velocity of 11537 ft/s, a 23% error. To find the effect of these different parameters and propagation factors on the traveltimes, one-dimensional frequency-domain wide-band VSP synthetic seismograms are generated from field sonic logs. Both a Q structure and velocity dispersion may be incorporated into the synthetic data. The synthetic may also be generated with 1) primaries only or with all multiples, 2) with or without Gaussian noise added, 3) using different layer thicknesses and 4) can be convolved with either source wavelets extracted from field data or zero-phase Ricker wavelets. After a synthetic is generated with a particular set of parameters and picked using a particular method, the results are compared with the integrated sonic log from the well.

The above methods are used to analyze a set of VSP surveys from the Anadarko Basin, Texas and a survey conducted near Sulphur Springs, Texas. Short-path multiples and velocity dispersion are both found to have an effect on the seismic traveltimes. The combination of these two effects can explain the observed difference between the seismic and sonic traveltimes.

3.2 LITERATURE OBSERVATIONS

A number of authors, and certainly many practicing geophysicists, have noted the differences between the traveltimes and thus velocities observed by the integrated sonic log and the VSP (or check shot) survey. A typical

example of this discrepancy or "drift" is shown in Figure 1. Gretener (1961) made observations of drift in data from 50 wells in Alberta that had been shot for velocity using dynamite and had also been sonic logged. He found that the check shot times were consistently longer than the integrated sonic times. Shallow (<4000 ft) times were found to have drifts or residuals ($t_{seismic}-t_{sonic}$) of 1.7 ms/1000 ft, while the deeper (>4000 ft) residuals were 1.5 ms/1000 ft.

Boss (1970) states qualitatively that most residuals are positive and in extreme cases may be up to 10.0 ms/1000 ft. Kennett and Ireson (1971) used 44 wells in the North Sea to find an average time residual. They used data from both air gun and dynamite surveys (22 of each) in comparison with their corresponding sonic logs. These surveys were conducted in areas where the Tertiary sediments were thin or negligible. On the average, they found that the time residual was not significantly different from zero. A number of wells shot through the Tertiary sediments were also examined. In the very shallow depths (<1500 ft) the residuals were found to be, on the average, -3.0 ms/1000 ft for the air guns and -2.0 ms/1000 ft for dynamite. This shallow residual effect became more pronounced as the source was offset farther from the wellhead. At greater depths the average residual tended to zero. In another set of experiments (with 6 wells), a direct comparison was made between the times measured to given depths from the air gun and dynamite. Again on the average, the air gun times were 3.0 to 4.0 ms longer than the dynamite times, but this is a constant shift and not depth dependent.

O'Brien and Lucas (1971) analyzed a total of 66 wells from Libya, Alaska, Abu Dhabi, and the North Sea. All sonic results were obtained using a borehole-compensated sonde, and an effort was made to edit out

"caved" borehole sections, highly oscillatory records, and check shots with shot-to-geophone angles of greater than 30°. They found an average traveltime residual of .034 ms/1000 ft - a positive but statistically insignificant value.

Ward and Hewitt (1977) performed a unique experiment near Tulsa, Oklahoma. They used continuous wave vibrators with a 10.0 s signal duration and attempted to measure the phase differences recorded by the vibrator base plate accelerometer and a downhole wall-clamping geophone. Both digital and analog phase determinations were made. The results from both of the methods agreed closely. From the phase differences it was possible to calculate the traveltime necessary for a particular peak or trough to travel from the source to the receiver. In the experiment, 35 Hz and 55 Hz signals were recorded at 50-ft intervals from 600 ft to 2500 ft. Dynamite check shots were also recorded at depth intervals of 200 ft.

The seismic traveltimes, corrected to the vertical, were longer than the integrated sonic times. The dynamite residual, compared to the integrated sonic was about 5.0 ms/1000 ft. The 55 Hz and 35 Hz surveys had 5.5 ms/1000 ft and 6.5 ms/1000 ft residuals, respectively. This evidence of velocity dispersion, or higher frequency waves traveling faster than low frequency waves, is supplemented by the results of Ganley and Kanasewich (1980) who analyzed an air gun check shot survey in the Beaufort Sea. They measured the phase velocity and attenuation as a function of frequency for depth intervals of 3070 to 4260 ft and 1785 ft to 3880 ft with frequencies of 10-80 Hz and 30-80 Hz, respectively. The relative increase in the phase velocity as a function of frequency across the first interval was about 1.0%, while across the second it was near 0.6%. They show that these results are fairly consistent with the absorption-dispersion relationship

given by Futterman (1962) which predicts that velocity should increase with increasing frequency.

Goetz et al. (1979) have compiled the results of check shot surveys and sonic logs from 159 wells in the Far East. Many different sources, tools, and editors of varying quality were employed in the surveys. In the shallow depths (<3000-4000 ft) they found that negative residuals, about -4.0 ms/1000 ft, predominated. There was, nonetheless, considerable scatter from -8.0 ms/1000 ft to 8.0 ms/1000 ft. However, in the deeper intervals, the vast majority of residuals were positive with an average value for all measurements of about 2.0 ms/1000 ft (see Figure 2).

Peyret and Mons (1981) report interesting results from thirteen shallow VSP surveys conducted in Yorkshire County, U.K. They found unambiguous positive residuals in all of the wells analyzed. In fact, they were able to correlate the magnitude of the residual with the formation type in which it was measured. The mean residual was 8.3 μs/ft in the Bunter Sandstone, 3.0 μs/ft in the Permian (carbonates and anhydrite), 5.7 μs/ft in the Carboniferous coals. They suggest, as is derived in Appendix 4, that the residuals vary with Q^{-1} and that this is due to velocity dispersion.

In summary, there appears to be considerable scatter in the shallow residuals. Some of the early evidence in the literature suggests that they are negative (sonic times greater than seismic times). Later studies have found positive residuals.

All the evidence for the deeper intervals indicates that the seismic traveltimes are greater or equal to the integrated sonic times. Peyret and Mons (1981) have suggested that spurious negative drifts (see Appendix VI) due to measurement problems in some studies may mask the more

physically-caused positive drift. The most extensive and recent data set (Goetz et al., 1979) gives a time residual of about 2.0 ms/1000 ft.

3.3 FIELD DATA

A problem with many of the results quoted in the literature is that the VSP surveys and sonic logs were often performed in the same area but not the same well. In the main study area considered here - the Anadarko Basin - VSP data and sonic log data from the same wells are compared.

The geology of the Anadarko Basin (Figure 3) is well known from the many wells drilled in the area. It is a very deep basin with in excess of 40,000 ft of Paleozoic sediments. A major unconformity lies at the base of the Pennsylvanian below which are carbonates and above which are mainly clastics (see Figure 4). The cyclically stratified sequences at 8000-8800 ft on the sonic log (see Figure 5) are the result of the Wichita Mountain uplift (McCaslin, 1979; Evans, 1980; McCaslin, 1981).

Four VSP (or check shot) surveys in distinct wells are used. These are named Well A through D. Well D was surveyed in 1956 while the other three surveys are more recent (after 1978).

VSP data from well A are shown in Figure 6. This survey was performed with a vertical vibrator with a 15-56 Hz sweep, offset 1000 ft from the well-head. A wall-clamping geophone was used to give the true vertical amplitude shown in Figure 6. The survey was conducted over the depths 100 ft to 9350 ft at 75 ft intervals. Well B was also "shot" with a vertical vibrator offset 1000 ft from the well-head. Recordings were made every 50 ft from depths 2110 ft to 7160 ft.

The vertical vibrators for Well C were placed 675 ft N of the well-head and 794 ft SW of the well-head for a check shot survey. Dynamite

check shots were also recorded in this well from sources at 700 ft N and 750-780 ft SW of the well-head.

Well D was a dynamite check-shot survey with sources 600-700 ft both E and W of the well head.

The difference between the seismic traveltimes and integrated sonic times, according to the drift curves obtained by the VSP contractors, is approximately 2.0 ms/1000 ft for all of these surveys (see Figure 7). The full VSP sections were repicked for this study with similar results (see Figure 24 for an example). These results are discussed in more detail later.

One other VSP survey (the ENIX well) is included in this paper. It was recorded near Sulphur Springs, Texas and used an impulsive source (DINOSEIS®) offset 100 ft from the well-head. The survey was recorded over the depths 300 ft to 2175 ft at 25 ft intervals. This shallow VSP was conducted through Cretaceous and Tertiary sediments composed largely of shales and limestones.

The sonic log is shown in Figure 8 and the true amplitude VSP data are displayed in Figure 9. In this case, there is about a 7.0 ms/1000 ft positive traveltime residual (see Figure 25).

3.4 DIFFERENCES IN METHODS

As discussed in the previous sections, there is a systematic difference between the seismic and sonic traveltimes. The literature has recorded positive residuals as have the Anadarko and East Texas studies discussed here. Again, there are three somewhat interdependent causes for the discrepancies between the sonic and seismic results. First, the sonic traveltimes are for high frequency waves (about 15 kHz) propagating for several feet along a path adjacent to the borehole. The VSP survey uses a

seismic source with a bandwidth from approximately 10 Hz to 100 Hz that may be offset several hundred feet from the wellhead. Thus, while the sonic waves sample the formation on the order of a foot from the borehole, the seismic waves explore a region many tens of feet from the borehole (see Appendix V for a VSP Fresnel zone calculation). Of course, the actual properties of these two different volumes may be dissimilar.

Associated with these different volumes of investigation is the fact that the actual drilling of a well with circulating fluids causes alteration of the formation near the borehole. This formation alteration is due to several factors, among which are mud invasion, mechanical damage, shale hydration, and stress relaxation of the adjacent rocks (Thomas, 1978; Goetz et al., 1979; Castagna, 1982). The altered zone or annulus will often have a velocity not representative of the virgin formation.

The second type of discrepancy in the measurements is due to instrument analysis errors. In the sonic measurement for the simplest case, pulse traveltimes (Δt) are measured between two receivers and expressed as $\mu s/ft$. Alternatively, the VSP survey measures the traveltime from the surface source to downhole receiver. There are a host of reasons why both of these times may be in error. Brief comments on these instrumental problems and their minimization are given in Appendix VI.

The third class of differences includes the impact on the measurements of the different wave propagation effects.

Summarizing the observations thus far and the differences in the methods it is possible to say that many of the errors or differences in the sonic log and VSP survey may be minimized by carefully considering the equipment used, editing techniques, and analysis methods. The sonic log, however, especially in the past, is likely to have integrated times which

are longer than those of the true formation. This is mainly due to formation alteration, cycle skipping, and Δt stretches.

In the shallow depths, the check shots are perhaps more likely to have calculated vertical traveltimes which are shorter than the true vertical times. This can be at least partially explained by the significant anisotropy of surficial sediments and the commonly-used, straight ray path over-correction (Appendix VI). The common result of these factors in the shallow section is to give a negative residual.

In the deeper section, dispersion, Q, short-path multiples and picking errors are all expected to play a role in the observed delay of the arrival of the maximum seismic energy. The next section describes procedures to study what factors cause traveltime discrepancies. By adjusting these factors, their effect on the discrepancies will be observed and significance judged accordingly.

Further problems with the sonic log, and these are numerous (Willis, 1983), will not be treated in this paper. The focus of the discussion will be on the seismic traveltimes in the deep section.

3.5 COMPUTATIONAL METHODS

The validity of much of the study is based upon the ability to generate realistic seismograms that have controllable parameters. The synthetic seismograms are generated using a one-dimensional wave equation approach (Ganley, 1981; Kan et al., 1981). In this method a wide-band synthetic trace is generated from a sonic, density and Q log for each downhole position. This synthetic seismic response is computed in the frequency domain by a recursive formula, which may include an attenuation-dispersion pair, then Fourier transformed back to the time domain. This approach includes all multiples and does not require blocking

of the sonic log into equal time increments. Source frequencies, noise and layer thicknesses may be varied in the synthetic seismograms.

Three traveltimes picking techniques were used. For impulsive sources pulse height detection (PHD) was employed. In PHD, the noise level is measured before the signal's arrival and several times this level is used as a threshold value for signal detection. Once the signal is detected in this manner, the point of maximum curvature (largest second derivative) preceding the threshold point is picked as the signal arrival time. For zero-phase waveforms (Vibroseis® analogies), the Fourier interpolated point of maximum amplitude was picked as the signal arrival time.

In the second picking technique, sets of the VSP traces are displayed by computer on an interactive graphics tube. A cursor may be positioned by hand for an "eye-ball" pick. This manual picking scheme uses approximately the same ideas as the automatic signal detection method above, with the added ability of the eye to cross-correlate traces.

The third picking technique is a constrained cross-correlation method (CCM). The manual picks are used as the centers for specified time windows over which a trace-by-trace cross-correlation is computed. Time differences between the traces are stored and calibrated to the total time to a specified depth. This yields the time versus depth curve. A schematic diagram of these picking methods are shown in Figure 10.

The field traveltimes are reduced to their vertical components before comparison with the sonic log. This is accomplished by finding correction factors from ray-tracing through a 1-D velocity structure (from the sonic log) with an offset source.

An interactive processing package has been designed to incorporate the above algorithms and perform the complete analysis. It computes a series

of synthetic VSP traces from the input sonic log and Q log, mixes specified noise with the traces, convolves the source waveform and plots the results. Different picking algorithms, as described before, may be specified and the resulting picks plotted. This system is implemented on an IBM 4341 computer with graphics display and hardcopy capability. Field traces may also be input into the above processing flow. A block diagram of the procedure is shown in Figure 11.

3.6 NUMERICAL EXPERIMENTS

In this section, some of the mechanics of traveltime picking and synthetic generation are analyzed. As mentioned previously we are interested in finding which parameters have a significant effect on the traveltimes.

The Well A study uses synthetics generated using the sonic and density logs. Traces are calculated from 2675 ft to 9350 ft at 75 ft intervals. The traces are sampled at 2.0 ms and unless specified otherwise have a 5-125 Hz bandwidth.

The ENIX study uses VSP synthetics generated from the sonic and density logs with a 1.0 ft layer thickness. The synthetic wavefield is calculated from 50 ft to 2175 ft at 25 ft intervals. The output traces are sampled at 1.0 ms and have a 5-125 Hz bandwidth. They were computed using a 4096 point FFT.

3.6.1 Picking Methods

Generally VSP data has a high signal-to-noise ratio for the first arrivals (about 40 dB). Thus a fairly unambiguous timepick may be made. Nevertheless, it is of interest to observe the magnitude of the discord between picking methods and to find whether any bias is introduced. The raw field data shown in Figure 9 have been picked using the three methods

outlined in the previous section. The integrated sonic times are subtracted from these picks and the resulting residuals are graphed in Figure 12. In this case, the pulse height detector (PHD) performs the most poorly with several severe mistakes. This is attributable to the infrequent but ever present noise (systematic or glitches) in the data. This PHD (with maximum curvature picking) may be somewhat enhanced by interactively fine-tuning the detection threshold or using a moving average of the signal. The two other methods give results that are quite similar to each other. Recall that the manual picks are used to provide a starting point for the cross-correlation algorithm. The scatter in the manual picks is consistent with that which was proposed by Aki and Richards (1980) using earthquake data (see Appendix IV) and observed by Stewart et al. (1981) in a Michigan VSP. For the present frequencies and S/N levels, the expected and observed errors are about 1.0 ms. Hand-picking all of the arrival times of seismic energy, even with the aid of an interactive graphics screen, is a very tedious and time-consuming process. While perhaps more accurate than PHD, it is still not an attractive technique.

Because of the consistency of much VSP data, cross-correlation techniques are often used. When an unconstrained cross-correlation is used however, several problems arise. If the source waveform changes radically, or several traces are poor, a cross-correlation method will have difficulty following the first arriving energy. The cross-correlation may also start to follow a strong reflection as opposed to the first arrivals. However by manually-picking several first arrivals and using these to constrain the correlation (CCM) a good pick is almost always achieved. In Figure 12, the CCM has the least scatter.

A number of synthetic VSP sections were generated and picked. The results from one of these cases is shown in Figure 13. The synthetics were calculated with all multiples included from the sonic and density logs shown in Figure 8. A Q structure (without velocity dispersion) was used in the model (see Table 1; uncorrected Q) and the resultant wide-band traces were convolved with a 40.0 Hz Ricker wavelet. White noise with a maximum amplitude of -40.0 dB relative to the amplitude of the first arrival in the bottom trace was added to the traces.

The CCM again provides the most accurate traveltime picks. The PHD performs sub-optimally with several spurious picks. The manual picks have about a 1.0 ms scatter with a slight positive drift. Thus while the traveltime picks from the various methods are generally within several milliseconds of one another, the constrained cross-correlation is the most consistent and accurate method. There appears to be little systematic drift introduced by the picking method itself. Except for the noise study discussed in the next section, the traveltime curves used in the following considerations were generated using the CCM.

3.6.2 Noise

Gaussian noise, with signal-to-noise ratios of 20, 30 and 40 dB down from the maximum amplitude of the bottom trace, was mixed with the wide-band traces generated from the ENIX sonic log. The manually-picked and CCM time residuals for all of these cases were still within ±1.5 ms of the integrated sonic (see Figure 21). Thus greater than realistic values of noise do not perturb the traveltime picks significantly in this case.

3.6.3 Source Frequency

A very wideband synthetic (3-200 Hz) was calculated from the ENIX sonic log and synthetics convolved with 15, 25 and 50 Hz Ricker wavelets. For cross-correlation picks the RMS errors of the residuals from zero were 0.6, 0.37 and 0.34 ms respectively. The picks from the very wideband synthetic alone had a traveltime residual RMS error of 0.3 ms. Thus the bandwith of the trace has a consistent but only weak influence on the CCM traveltimes.

3.6.4 Layering Thickness

The Well A sonic log is sampled at 1, 2, 5 and 10 ft intervals to test the effect of layer thickness on the traveltimes. Synthetics (Figures 17 and 18) were generated (from 5-125 Hz) for all of these logs and traveltimes were picked (e.g. Figure 19). The RMS error from zero of the traveltime residuals, in order of increasing layer thickness, are 2.1 ms, 2.0 ms, 2.6 ms, 1.9 ms. These errors are large because there is a positive drift to the residuals (discussed in the next section). Nonetheless, the travel time of the first arrival appears to be fairly insensitive to the layer thickness of the sonic log, at least in these cases when the seismic wavelength is considerably longer than the layer thickness.

In summary, it appears that picking methods do not have a large consistent effect on the traveltimes. Likewise source frequency, noise and layering thicknesses do not cause significant alteration in the traveltimes. It appears that the systematic drift observed in the preceding sections must be due to other causes. In the next sections the wave propagation effects are considered.

3.7 MULTIPLES

O'Doherty and Anstey (1971) suggested that short-path multiples have a significant effect on the shape of the seismic waveform propagating through the earth. One of the effects of the multipathing of the various order multiples was to cause an apparent delay of the maximum energy in a pulse. Schoenberger and Levin (1974) alluded to this effect, also, and in a later paper [Schoenberger and Levin (1978)] showed quantitatively that multiples could cause both attenuation and time delays. In this later study they used time-domain synthetic seismograms calculated from the sonic logs of 23 wells around the world. An input wavelet was convolved with the reflection impulse response of each well, and the trough of the first arrival was picked. It was found that the troughs in these seismograms were delayed from 0.0 ms to 14.0 ms from the integrated sonic times over the total two-way depth of the wells. In several other wells, they note that there are time delays of up to 40.0 ms. They plotted the 23 previous time delays against the apparent cumulative caused by the multiples and found a linear relationship between the two. These results suggested that there is a 10.0 ms delay per 0.3 dB/Hz apparent attenuation.

Kan (1981) gave a graphic demonstration of this delay effect by calculating synthetic seismograms transmitted through a structure consisting of 680 layers with alternating velocities of 8000 ft/s and 12000 ft/s (see Figure 14). Using the one-dimensional wave equation approach, he calculated a transmitted waveform through the structure. He found that this waveform was similar in shape to the source pulse but considerably reduced in amplitude and delayed about 15 ms from the expected time of a wave transmitted directly through the structure (see Figure 15). Intuitively speaking, this is reasonable after considering the effect of

the transmission coefficients. For the above case, the transmission coefficient for an interface is 0.8. The direct wave (suppose a spike) transmitted through the structure will thus have an amplitude reduced from its initial amplitude by $(0.8)^{680}$. This final amplitude is a very small number and not resolvable on present computers. Thus, there is effectively no energy arriving at the inferred time of the direct wave. Numerous short-path multiples may sum, however, to give a significant arrival at some later time.

Spencer et al. (1982) also considered the effect of layering (or stratigraphy) on the seismic waveform. They used statistical mixes of layer thicknesses and velocities, with synthetic seismograms to observe the effects on the attenuation determined from the spectral ratio method. They found that the attenuation estimate was influenced by stratigraphy but remained constant when measurements were separated by a critical distance (about 300 ft in their example). They also noted that the attenuation value was not only dependent on the transmission path, but on the interference from waves reflected from stratigraphy above the upper receiver and below the lower receiver.

We consider now the surveys conducted in the Anadarko Basin, focussing attention on Well A. First the primaries only synthetics were generated (Figure 16) as discussed in the previous section. The zero phase peak was picked (using the CCM) and compared to the integrated sonic log (Figure 19). There is very little difference between the two. Next a synthetic VSP section was calculated which included all the multiples (Figure 17). Again the zero-phase peak was picked and compared to the integrated sonic log (Figure 19).

In this case, there is a definite increase in the traveltime residual as a function of depth. The short-path multiples cause a delay in the maximum energy of the propagating seismic wave. Referring to Figure 17, we can see that the first arrival is being reinforced by the short path multiples as opposed to the primaries only synthetic with its rapidly decreasing first arrivals (Figure 16). The total time delay over 6675 ft of propagation is 4.1 ms (shown in Figure 17). Note the large delay associated with the zone of cyclic stratigraphy from 8000-8800 ft. The sonic log (Figure 5) shows velocities oscillating rapidly from about 7500 ft/s to 18000 ft/s.

The same analysis was conducted for the Well B data. This well penetrated the same formations as Well A but was about 2300 ft vertically updip with respect to the surface. The cyclic stratification in this well is not quite as severe in the 7000 ft region as previously in the 8000-8800 ft depths. Nonetheless, the delay of seismic energy is again apparent (Figure 20).

Thus as indicated by previous studies in the literature and according to the present results, short-path multiples cause seismic traveltime delays.

Richards and Menke (1982) proposed an empirical relationship connecting the apparent attenuation due to scattering (multipathing) to the variance of the reflection coefficients of a set of layers and the average velocity (Appendix VII). In a similar manner, the traveltime delay, due to seismic energy propagating in a layered medium with impedance contrasts, is intuitively related to the magnitude of the reflection coefficients, the number of layers, and the traveltime through each layer. Thus an empirical traveltime delay equation is suggested here (see Appendix VII). The

proposed difference between VSP traveltimes and the integrated sonic times due to short-path multiples is

$$t_{delay} = K\sum_{i}^{N} |R_i|^2 \Delta t_i \qquad (1)$$

where K is an empirically-derived constant, $|R_i|$ is the magnitude of the reflection coefficient at the bottom of layer i, N is the number of layers, Δt_i is the layer traveltime. Consider the case for the sonic log shown in Figure 5 and the time delays plotted in Figure 19. If the time delay (1.9 ms) for the depths 3500 ft - 8000 ft and reflection coefficients (computer-derived from the well-logs) are used to find the constant K in equation (1) then

$$K \sim 10^4$$

Now using this K in equation (1) and the well-log to predict the time delay from the depths 8000 ft - 9000 ft gives a delay of 2.2 ms. This compares favorably with the observed value of about 2.0 ms.

Equation (1) can be used in an approximate fashion to predict the effect that short-path multiples will have on the VSP traveltime. Referring to Figure 24, it is noted that there is approximately a 17.5 ms delay over the depths surveyed, thus while short-path multiples play a role in the delay they are not the whole problem.

A similar analysis has been conducted with the ENIX data. The VSP synthetics were generated using the sonic and density logs. They were also mixed with random noise which causes some scatter in the traveltimes. Nontheless, there is a small positive drift of about 1.0 ms over the total depth of the well. The computer-derived time delay from equation (1) gives a value of 0.5 ms. Again the total observed delay in the field data is about 13.0 ms (Figure 25), which cannot be explained by the effect of short-path multiples.

3.8 Q AND VELOCITY DISPERSION

For many years it has been recognized that causal and linear wave propagation imply that attenuation and velocity dispersion must be related (Futterman, 1962). In situ attenuation has received some consideration (McDonal et al., 1958; Tullos and Reid, 1969; Morris, 1979; Ganley and Kanasewich, 1980; Hauge, 1981; Kan et al., 1981; Wingo, 1981; Zeitvogel, 1982) as has in-situ dispersion (Wuenschel, 1965; O'Brien and Lucas, 1971; Strick, 1971; Ganley and Kanasewich, 1980; Brennan and Smylie, 1981; Peyret and Mons, 1981).

Although it is generally believed that rocks do possess some measurable intrinsic attenuation which degrades both the amplitude and frequency content of a propagating wave, body wave dispersion has been the subject of greater contention. This is mainly because, while some attenuation effect is clearly visible on most recorded surface or VSP seismic traces, body wave dispersion is difficult to measure consistently from bandlimited traces recorded in a medium with structure.

For body waves, dispersion means that velocity increases as a function of frequency. Thus because seismic traveltimes are generally observed to be longer than sonic traveltimes, it has been postulated that dispersion is the responsible mechanism (Strick, 1971). As several authors (Ward and Hewitt, 1977; Ganley and Kanasewich, 1980) have shown, dispersion does appear to be operating across the seismic band. The dispersion model of Aki and Richards (1980, pp. 170-182) relates the phase velocity at two frequencies of a medium to its attenuation. This model may be found via Hilbert transform theory or experimental creep observations (Lomnitz, 1956; 1957)

$$\frac{C(\omega_1)}{C(\omega_2)} = 1 + \frac{1}{\pi Q} \ln \left(\frac{\omega_1}{\omega_2}\right) \qquad (2)$$

where $c(\omega_1)$ is the phase velocity at frequency ω_1 and Q is constant between ω_1 and ω_2).

Assuming that Q is nearly constant over the seismic to sonic frequency band, it is possible to calculate the amount of traveltime delay (see Appendix VIII) that a pulse would have as a function of the distance traveled d, attenuation Q, sonic velocity $V(\omega_2)$, and seismic center frequency ω_1. The time delay is given by

$$t_{delay} = \frac{d\ln(\omega_2/\omega_1)}{\pi\, Q\, V(\omega_2)} \qquad (3)$$

Thus, using a measured Q and a dispersive model, positive traveltime differences are predicted.

Again now, the Well A data are considered. Equation (2) has been used to include dispersive effects in the synthetics. The reference sonic frequency was taken to be 20.0 kHz. Figure 22 shows two synthetic seismograms computed from the Well A sonic and density logs. The top trace at a 9350 ft depth has no attenuation or velocity dispersion included. The bottom trace uses the dispersive model with a Q value of 80.0 over the total depth. Note the pulse broadening and traveltime delay in the second case.

The next set of synthetics used Q values determined from the spectra of the raw Well A data (see Table 1; Figure 23). Along with the amplitude decrease with depth was the change in the pulse shape from a symmetric shape to a "front-end loaded" or more minimum phase shape. The total time delay to 9350 ft was about 27.0 ms. This is a greater traveltime delay than observed in Figure 24.

As mentioned above, the raw field data was analyzed using a spectral comparison method (Kan et al., 1981) to find a Q structure. Multiples however, should cause an apparent attenuation in the field data (Schoenberger and Levin, 1978). To remove the effect of these multiples

before including Q in the dispersive synthetics, the apparent Q from non-dispersive synthetic seismograms that included primaries and multiples only, was found. This Q (actually Q^{-1}) was subtracted from the field data before the dispersive synthetic was computed. The final Q structure is also given in Table 1.

These synthetics were picked and the total peak delay was 20.0 ms. This synthetic traveltime drift is compared with that of the field data (Figure 24). The correspondence between the synthetic traveltimes with all multiples and dispersion and Q included is found to agree closely with the field data traveltimes. It seems that the multiple-induced delay in addition to the dispersion effect accounts reasonably well for the observed time discrepancies between the sonic and seismic measurements in the deeper parts of a section.

The data from the Sulphur Springs experiment also show considerable seismic traveltime delay over the 2175 ft depth. The average velocity for this well as measured by the sonic log using a 15 kHz signal was 7500 ft/s. The attenuation for the section was computed from the spectra of the traces. The harmonically averaged Q value of the field data was 50. The seismic pulse was centered at about 50 Hz. The delay between the sonic and seismic pulses over the 2175 ft from equation (3) using the above values is 10.0 ms. Earlier it was observed that the multiple-induced delay was about 1.0 ms (Figure 21). Thus the time delay predicted from the formulae is approximately 11.0 ms

Note that the time delay measured between the field VSP traveltime to 2175 ft and the integrated sonic was actually 13.0 ms. This gives a drift of about 7.0 ms/1000ft.

Dispersive synthetic traces were computed with the Q values from above and with all multiples. Picking the maximum arrival peak gives the residuals as shown in Figure 25. Again the observed and synthetic data are quite similar.

3.9 SONIC LOG CALIBRATION

Because wave propagation effects may significantly alter the traveltimes picked in a VSP survey, some care is required in using these times to calibrate the sonic log. Short-path multiples can cause small time delays. These may be corrected using equation (1). Generally this correction will be negligible. If non-dispersive synthetics are generated from the sonic log then the synthetics will have velocities that are too high. The sonic log should be shifted to agree with the longer seismic times.

A better approach is to calculate the full-waveform VSP synthetics, including a dispersion-attenuation pair and multiples, from the sonic log and vary the sonic log until the VSP synthetics and VSP field data are consistent.

3.10 CONCLUSIONS

Both VSP and sonic log surveys are routinely conducted and used to correlate traveltimes with depth as well as estimate interval velocities. Many empirical studies and synthetic seismogram generation show that there are differences between the integrated sonic times and vertically-corrected VSP times. There is no unanimous agreement on the magnitude of the discord, but the most recent studies indicate that seismic times are at least 2.0 ms/1000 ft longer than integrated sonic times below about 3000 ft. Numerous errors and difficulties plague the measurements, but

with carefully conducted data gathering, editing, and interpretation, many of the difficulties may be overcome.

Wave propagation effects in the VSP survey should be modeled to be understood thoroughly. But, in the experiments discussed here, simple formulae may be used to estimate the effects of velocity dispersion and short-path multiples on traveltimes. Velocity dispersion appears to be a large contributing factor to the observed discrepancies (multiples contribute to a lesser extent). The observed traveltime delays in the Anadarko Basin and Sulphur Springs studies are well explained through the use of wave equation synthetic seismograms with Futterman's velocity dispersion model.

TABLE CAPTION

Table 1. Attenuation values from Well A. Uncorrected values are from spectral analysis of the raw data. Corrected values have the effect of short-path multiples removed.

Uncorrected Q		Corrected Q	
1000-2400 ft	Q = 150	1000-2400 ft	Q = 150
2400-5100 ft	Q = 30	2400-5100 ft	Q = 40
5100-7200 ft	Q = 160	5100-7200 ft	Q = 160
7200-9350 ft	Q = 30	7200-10000 ft	Q = 40

Table 1

FIGURE CAPTIONS

Figure 1. Contractor's drift curve for Well A. The seismic traveltime from source to receiver (reduced to the vertical using cosine correction) minus the integrated sonic time to the receivers depth is plotted against depth.

Figure 2. Histogram of traveltime residuals. Data is compiled for 159 wells in the Far East from depths greater than 3000 ft (after (Goetz et al., 1979). The residual is defined as the check shot time minus the integrated sonic time over a particular depth.

Figure 3. Map of the VSP study area in the Anadarko Basin. Several structural features are indicated.

Figure 4. Typical geologic section for the Anadarko basin (after Evans, 1980).

Figure 5. Sonic and density logs for the Well A in the Anadarko Basin.

Figure 6. VSP section for Well A in the Anadarko Basin. The vertical geophone output is plotted versus time. The vertical vibrator source was offset 1000 ft from the well-head.

Figure 7. Drift curves for seismic and sonic surveys conducted in the Anadarko Basin. These results are from the contractors' logs.

Figure 8. Sonic and density logs for ENIX well at the ARCO geophysical test site near Sulphur Springs, Texas.

Figure 9. VSP section for ENIX well in East Texas. The vertical geophone output is plotted versus time. The impulsive source was offset 100 ft from the well-head. Note the rapid decrease in amplitude.

Figure 10. Schematic diagram of the different techniques picking the traveltime. The first trace has been picked manually. The third and fourth traces have been cross-correlated to find a traveltime

difference which is related to a known arrival. The fifth trace uses pulse height detection then a maximum curvature algorithm to find the first break.

Figure 11. Block diagram of the computer package used to generate and analyze VSP data.

Figure 12. Comparison of traveltime picking methods using the raw ENIX VSP. Pulse height detection (P), manual picks (M) and constrained trace crosscorrelation (C) results are displayed.

Figure 13. Comparison of traveltime picking methods using synthetically-calculated data. Synthetics were generated using the ENIX sonic and density logs plus field-determined Q values. The traces were convolved with a 40.0 Hz Ricker wavelet and mixed with 40 dB Gaussian noise. Pulse height detection (P), manual picks (M) and constrained trace crosscorrelation (C) techniques were used.

Figure 14. Cyclic sonic log model used to find the effect of short path multiples on the transmitted pulse.

Figure 15. The first trace is the pulse transmitted through the structure in Figure 11 when no multiples are allowed. The second trace has all multiples included for energy transmitted through the structure in Figure 11. Note the pulse delay and waveform shape change (amplitudes are normalized).

Figure 16. Synthetic traces with primary-only reflections for Well A. Note the rapid decrease in the amplitude of the first arrival, especially in the 8000-8800 ft zone.

Figure 17. Synthetic traces with all multiples included for Well A. The down-going multiples reinforce the first pulse.

Figure 18. Synthetic traces with all multiples included for Well A. In this section the sonic log has been blocked 10 ft intervals for the synthetic computation.

Figure 19. Drift curve for Well A synthetic - primaries only and with all multiples. Note the large residuals in the 8000-8800 ft interval coincident with cyclic stratigraphy.

Figure 20. Drift curve for Well B synthetic. The cyclically stratified region in this well extends from 5800 to 6400 ft depths. The velocity contrasts in this well are greater than those in Well A.

Figure 21. Drift curves for ENIX synthetic seismograms using manual (M) and constrained crosscorrelation (C) traveltime picks. Traces have been convolved with a 40.0 Hz Ricker wavelet and mixed with 20 dB Gaussian noise.

Figure 22. The first synthetic trace for Well A at 9350 ft has all multiples included but no dispersion and attenuation. The second synthetic trace for Well A at 9350 ft has a Q value of 80 and concomitant dispersion (amplitudes are normalized).

Figure 23. Synthetic section for Well A with corrected field attenuation and concomitant dispersion.

Figure 24. Drift curves for synthetic traces with attenuation and dispersion (dotted line) and field data (solid line) for Well A.

Figure 25. Drift curves for synthetic with attenuation and dispersion (dotted line) and field data (solid line) for the ENIX well.

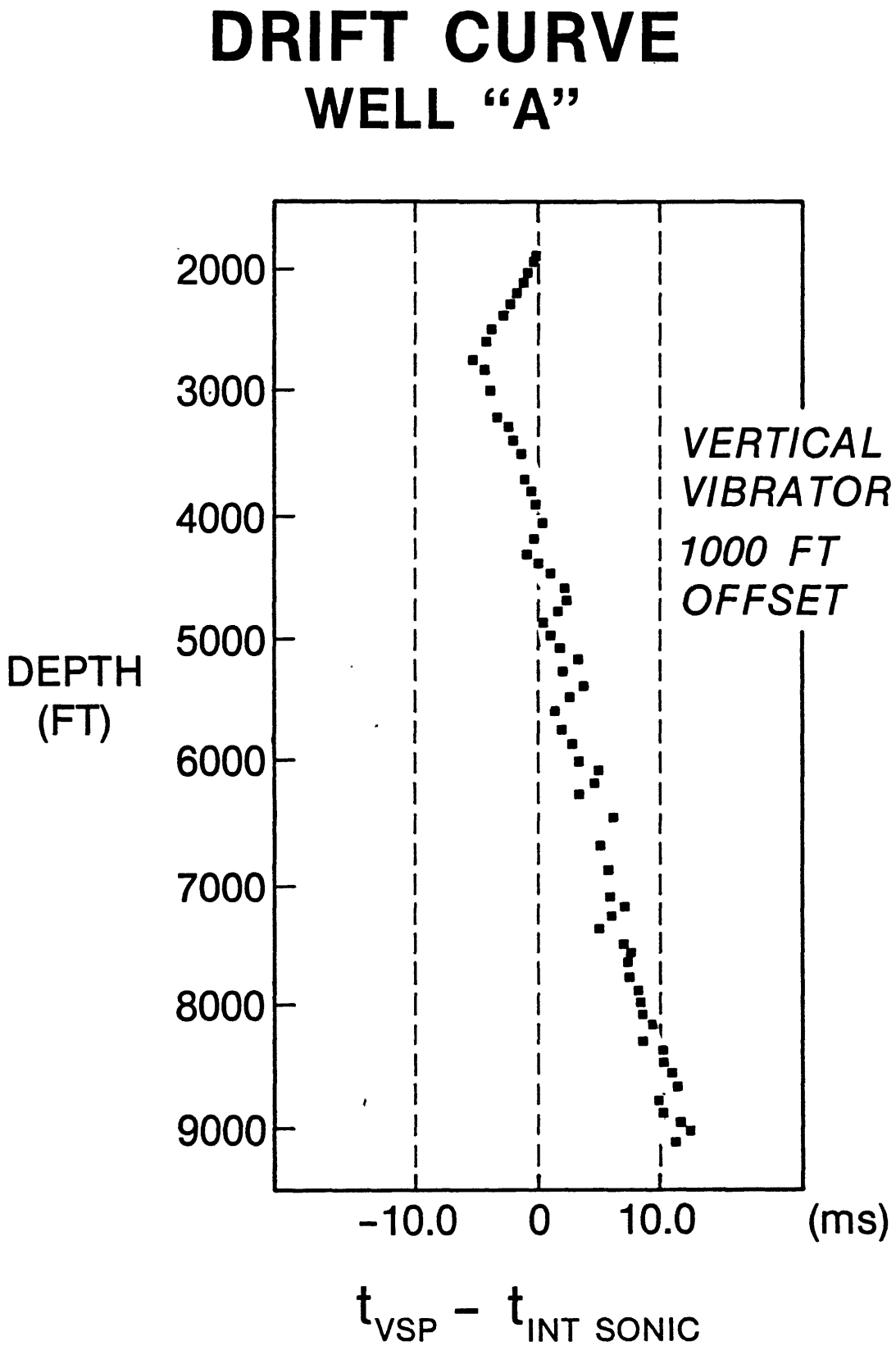
DRIFT CURVE
WELL "A"
2000
3000
4000
5000
6000
7000
8000
9000
DEPTH
(FT)
VERTICAL
VIBRATOR
1000 FT
OFFSET
-10.0
0
10.0
(ms)
$t_{VSP} - t_{INT\ SONIC}$

Figure 1.

HISTOGRAM OF DRIFT

(GOETZ ET. AL., 1979)

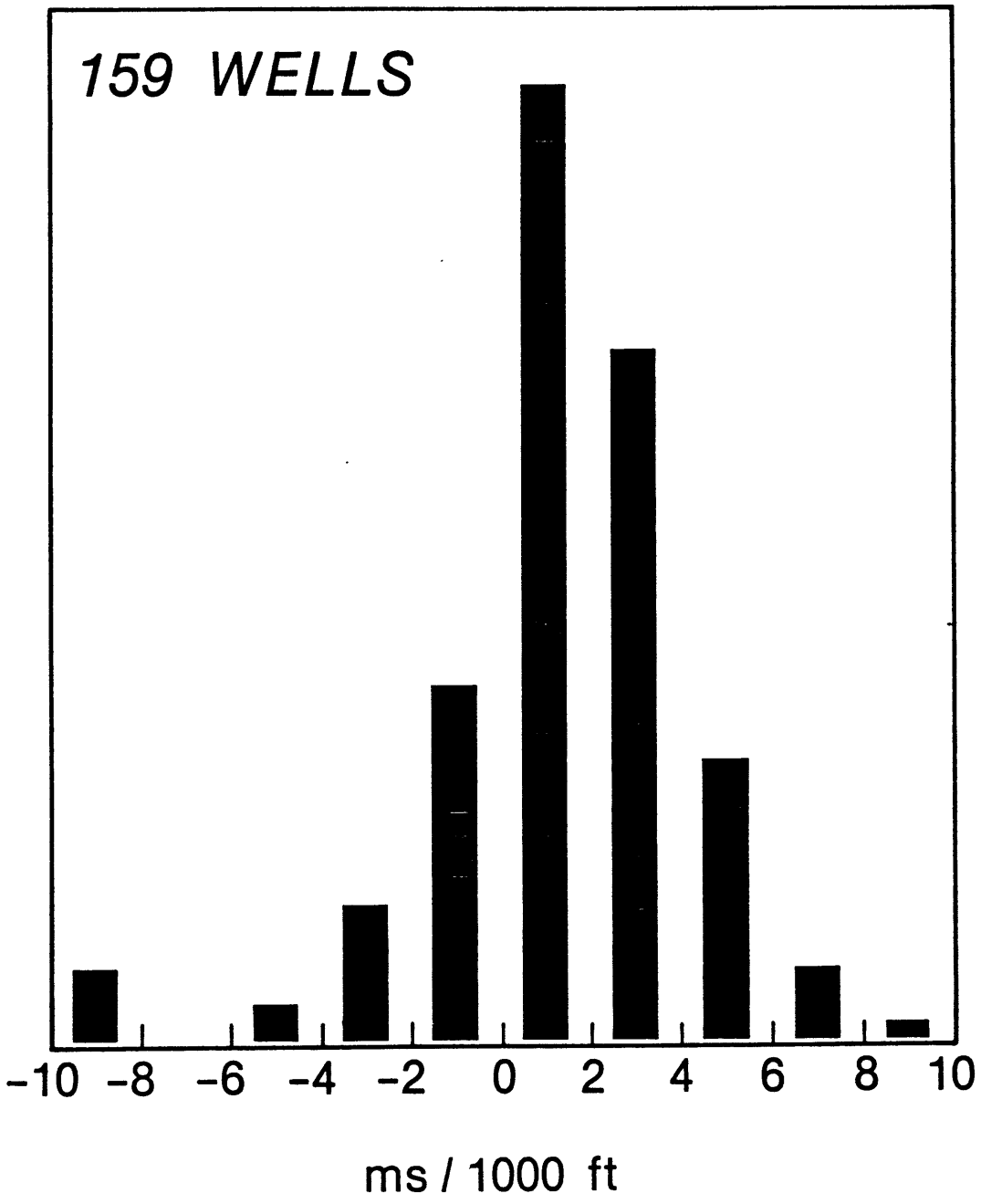

Figure 2.

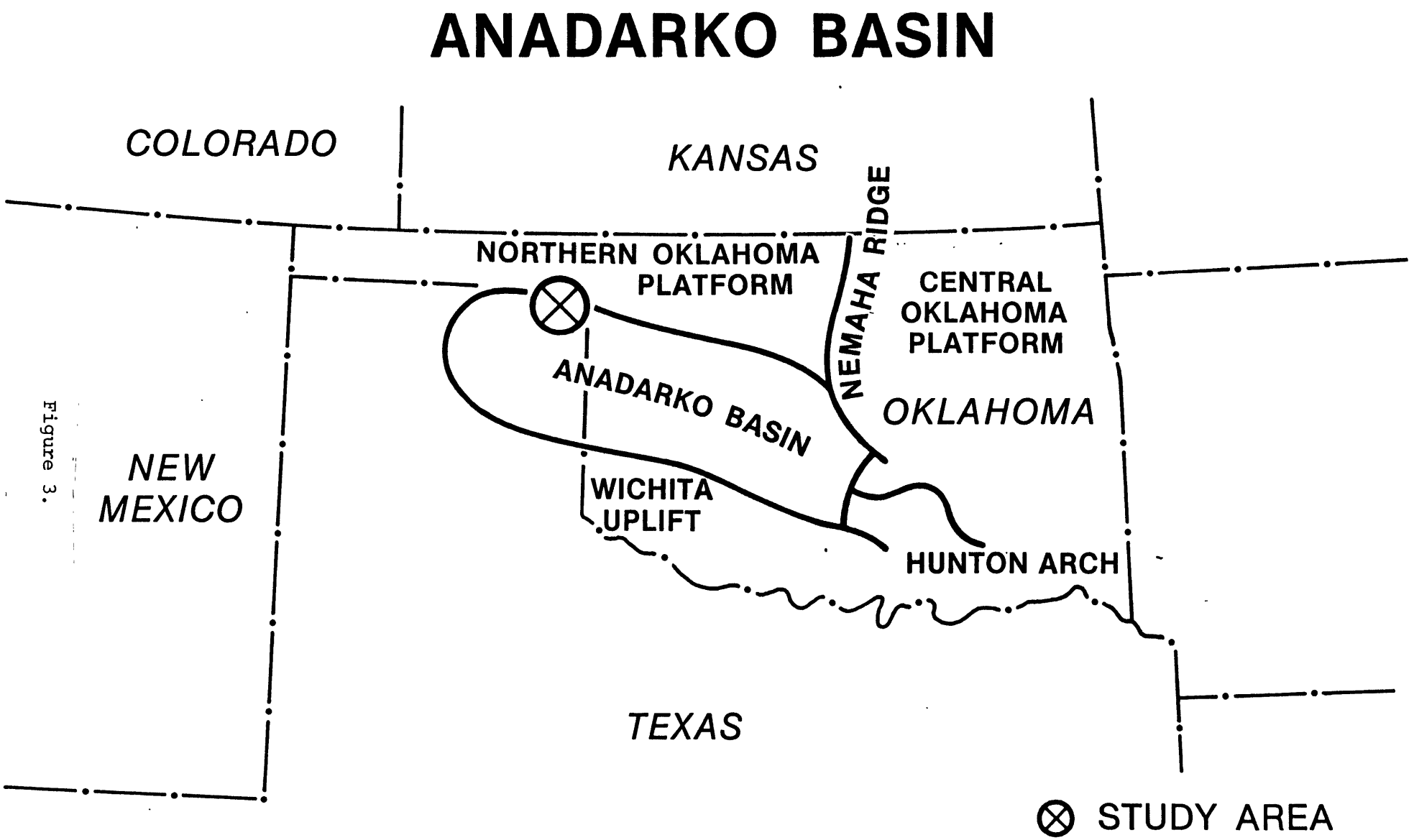
ANADARKO BASIN
COLORADO
KANSAS
NEMAHA RIDGE
NORTHERN OKLAHOMA PLATFORM
CENTRAL OKLAHOMA PLATFORM
ANADARKO BASIN
OKLAHOMA
NEW MEXICO
WICHITA UPLIFT
HUNTON ARCH
TEXAS
STUDY AREA

Figure 3.

TYPICAL COLUMNAR SECTION

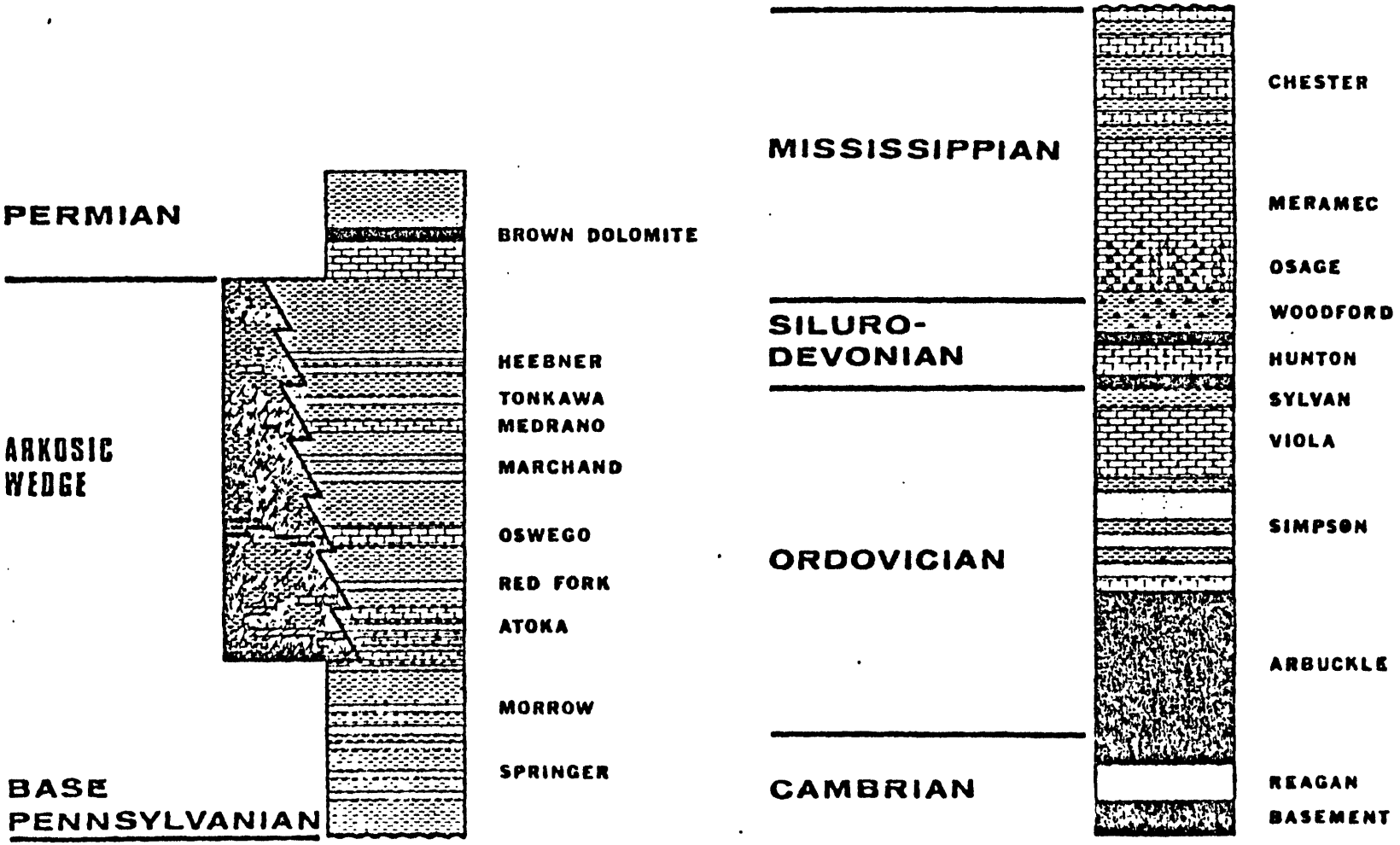

Figure 4.

SONIC AND DENSITY LOGS
WELL "A"

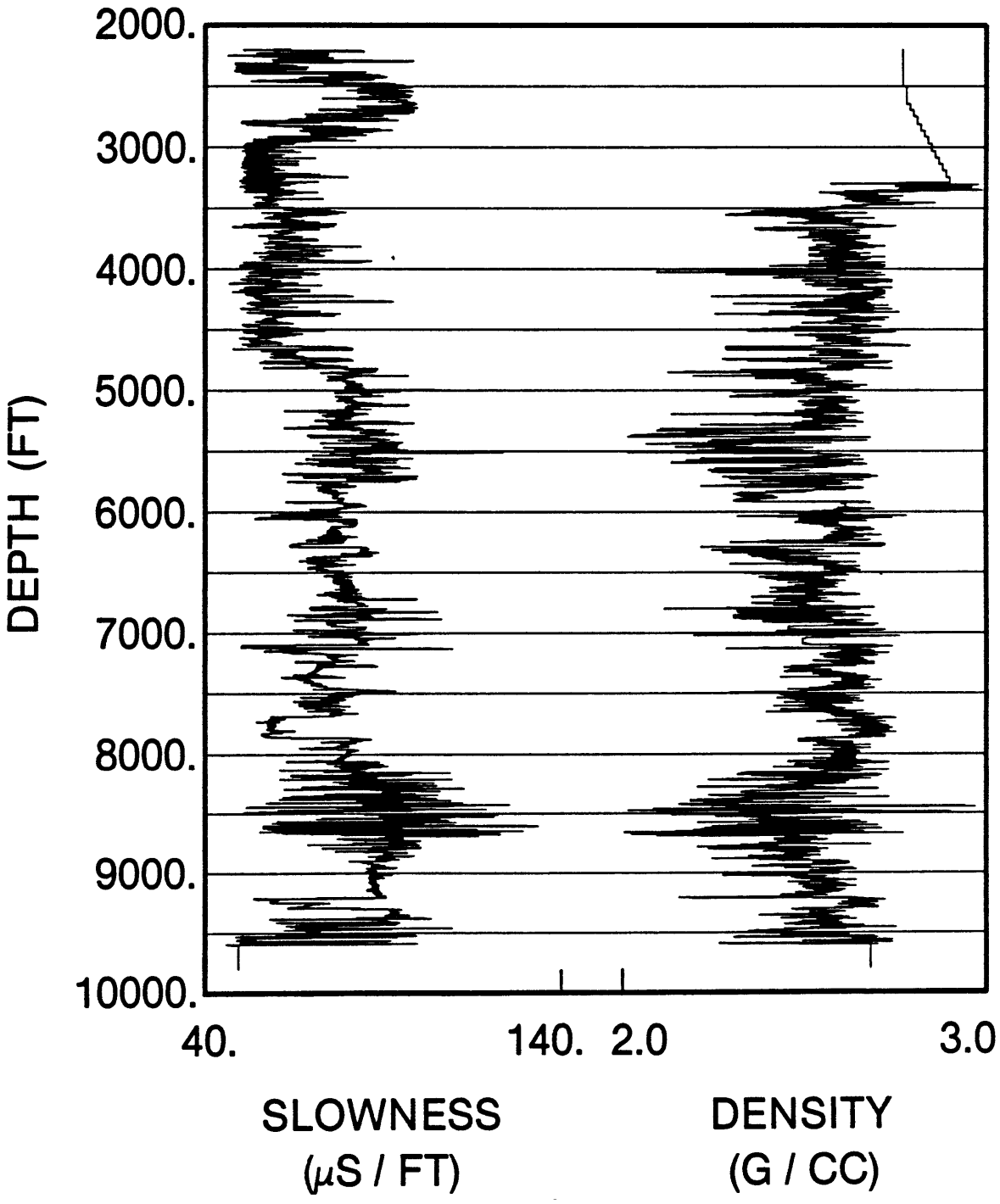

Figure 5.

VERTICAL VIBRATOR, WELL "A"

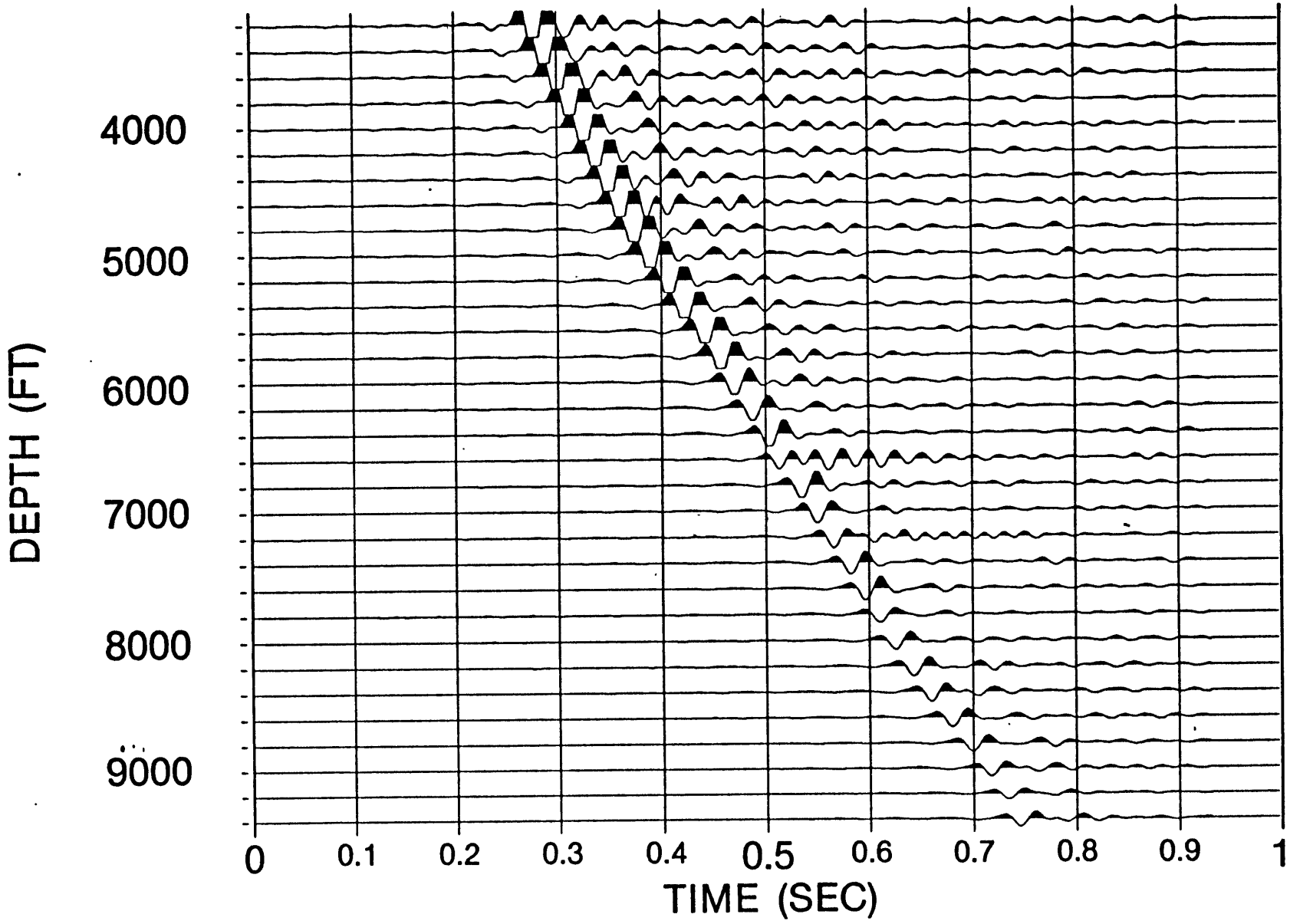

Figure 6.

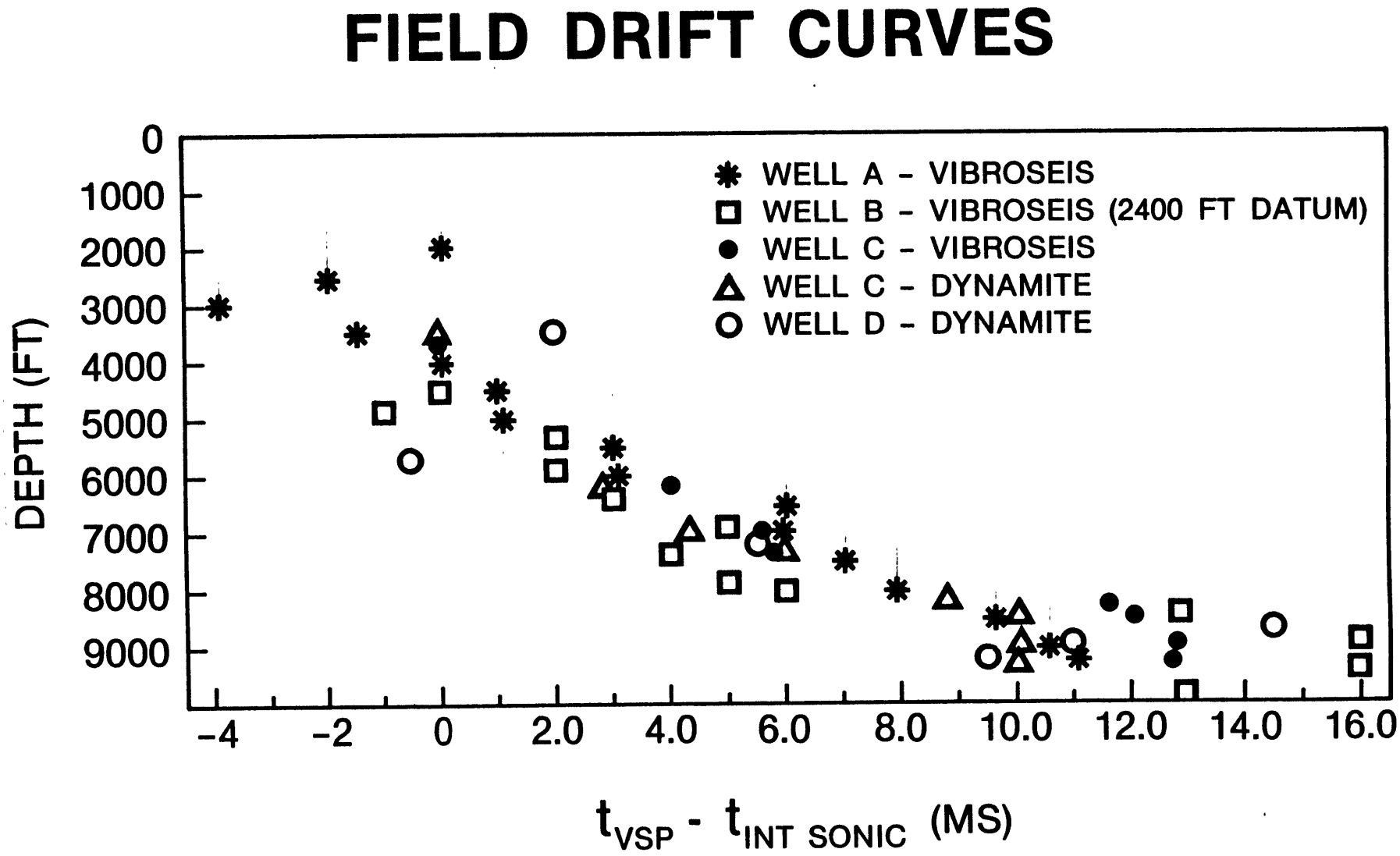
FIELD DRIFT CURVES
DEPTH (FT)
0
1000
2000
3000
4000
5000
6000
7000
8000
9000
WELL A - VIBROSEIS
WELL B - VIBROSEIS (2400 FT DATUM)
WELL C - VIBROSEIS
WELL C - DYNAMITE
WELL D - DYNAMITE
-4
-2
0
2.0
4.0
6.0
8.0
10.0
12.0
14.0
16.0
$t_{VSP} - t_{INT\ SONIC}$ (MS)

Figure 7.

SONIC AND DENSITY LOGS
ENIX WELL

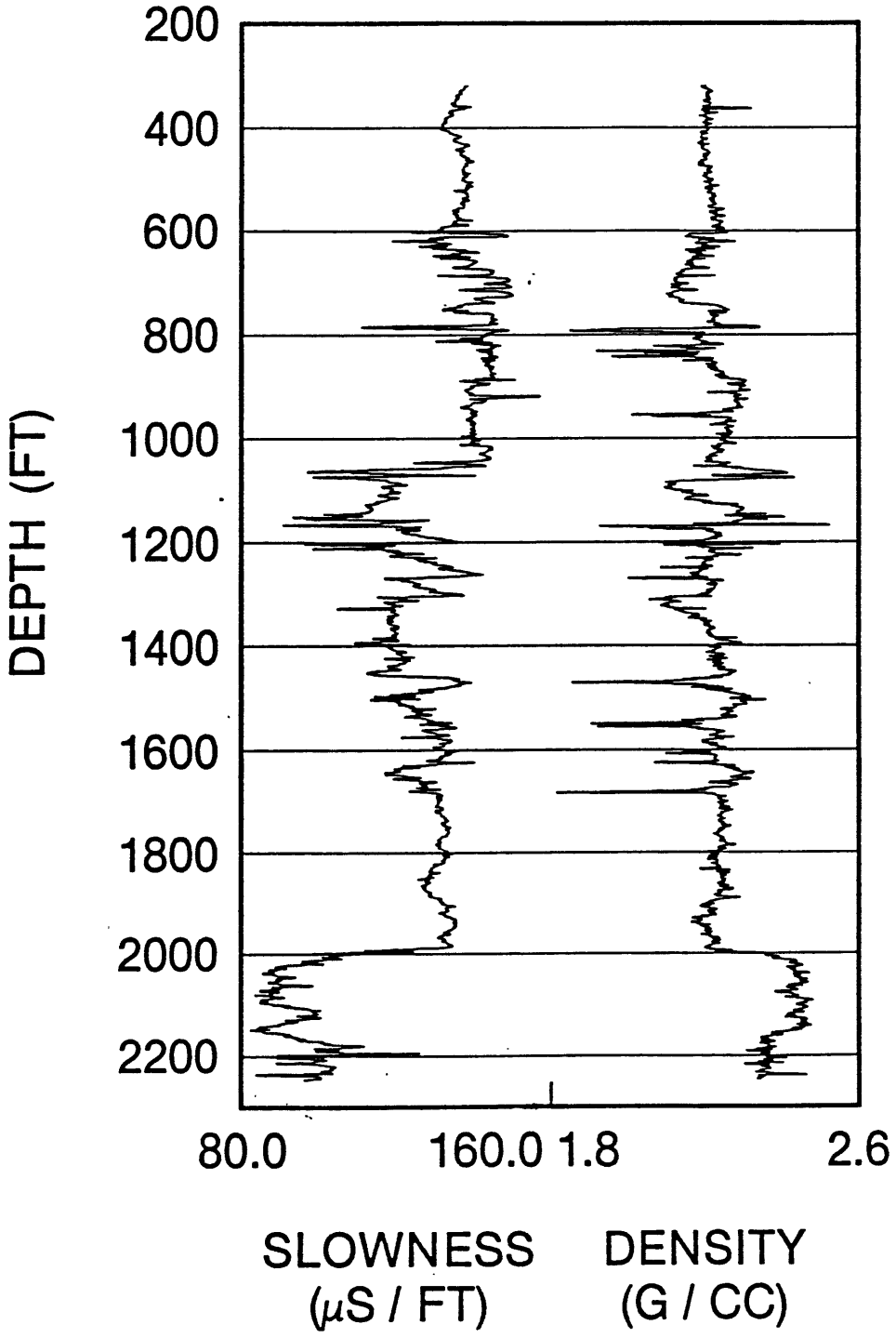

Figure 8.

DINOSEIS©, ENIX WELL

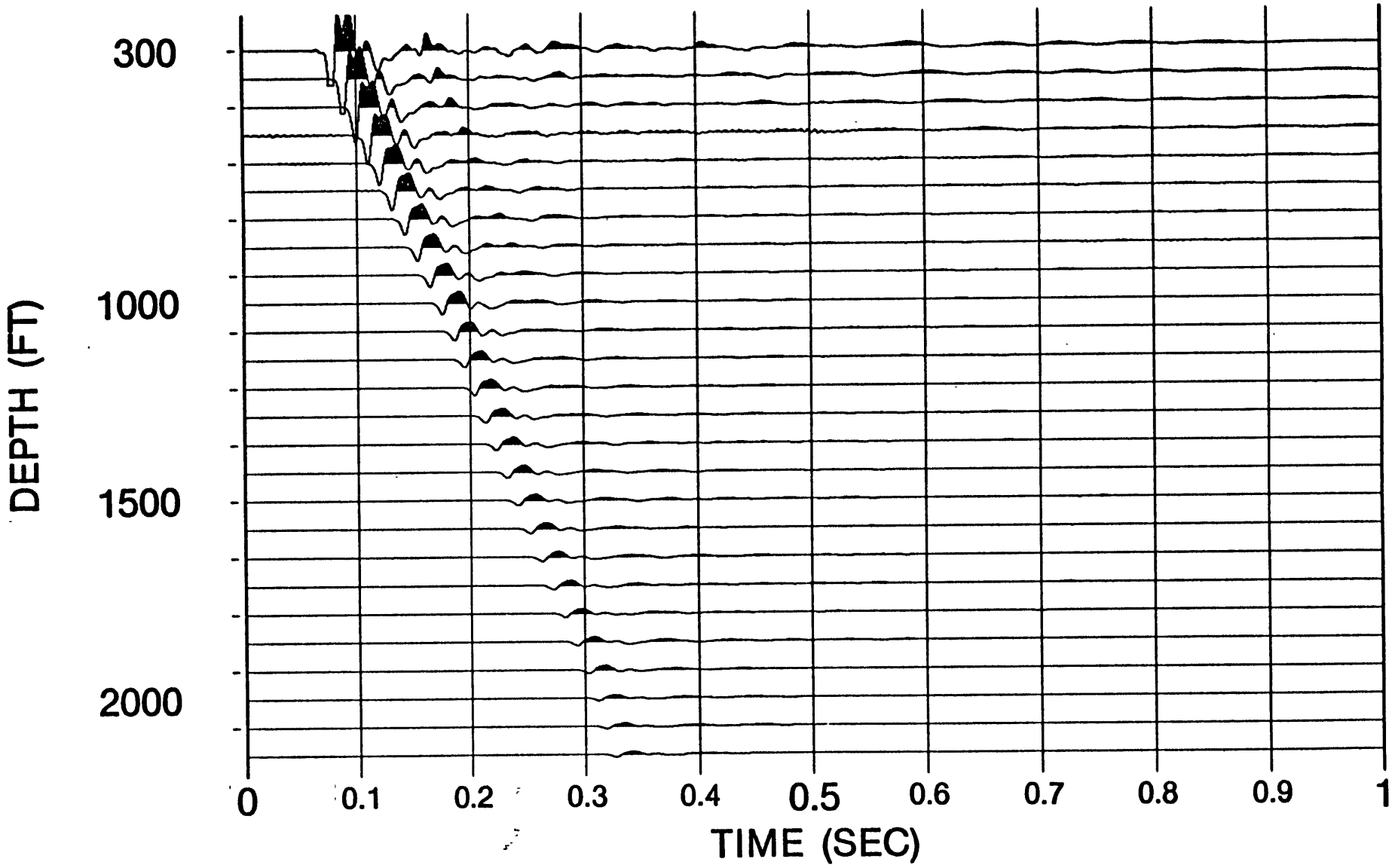

Figure 9.

TRAVELTIME PICKING METHODS
WELL "E"

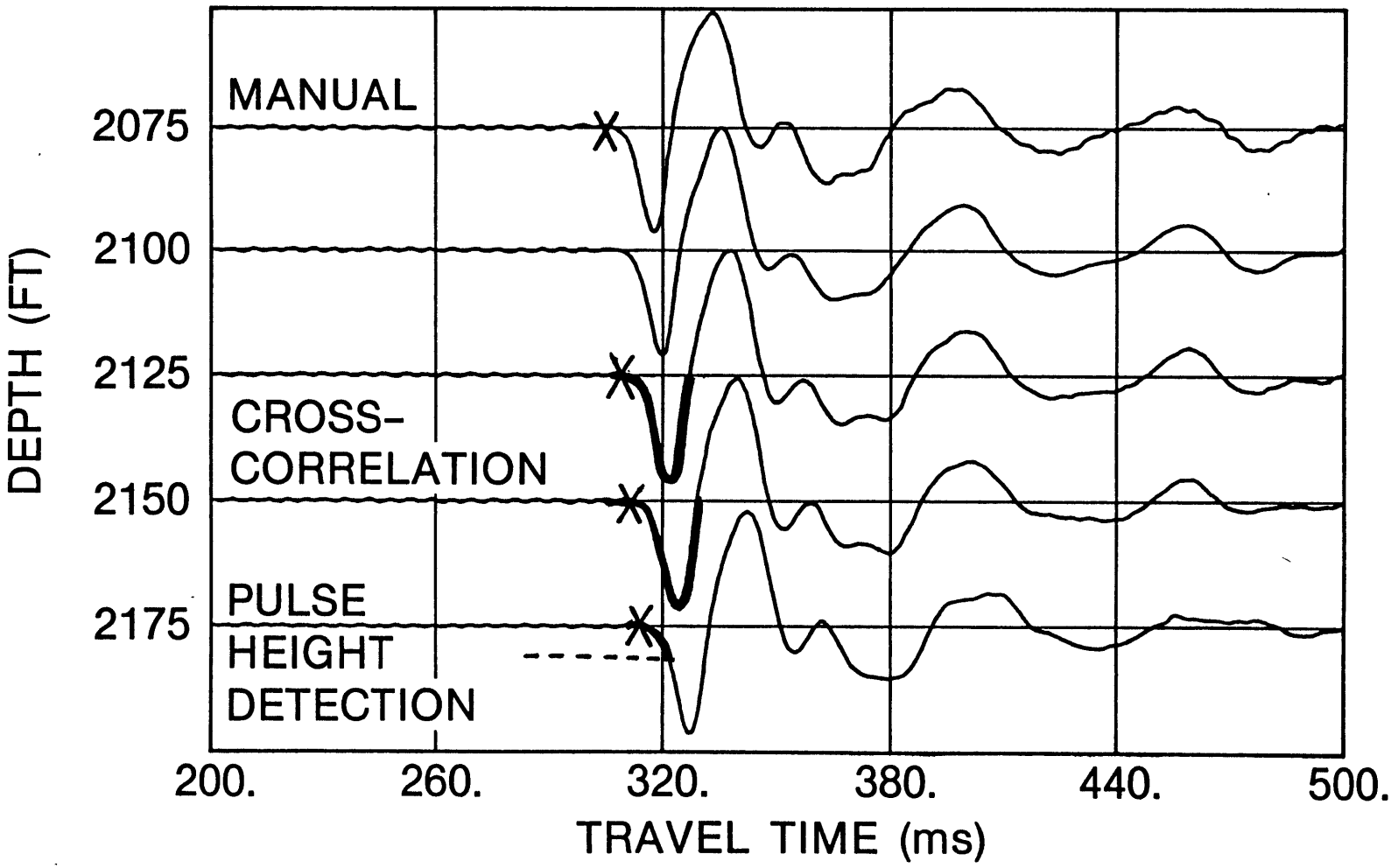

Figure 10.

VSP TRAVELTIME ANALYSIS

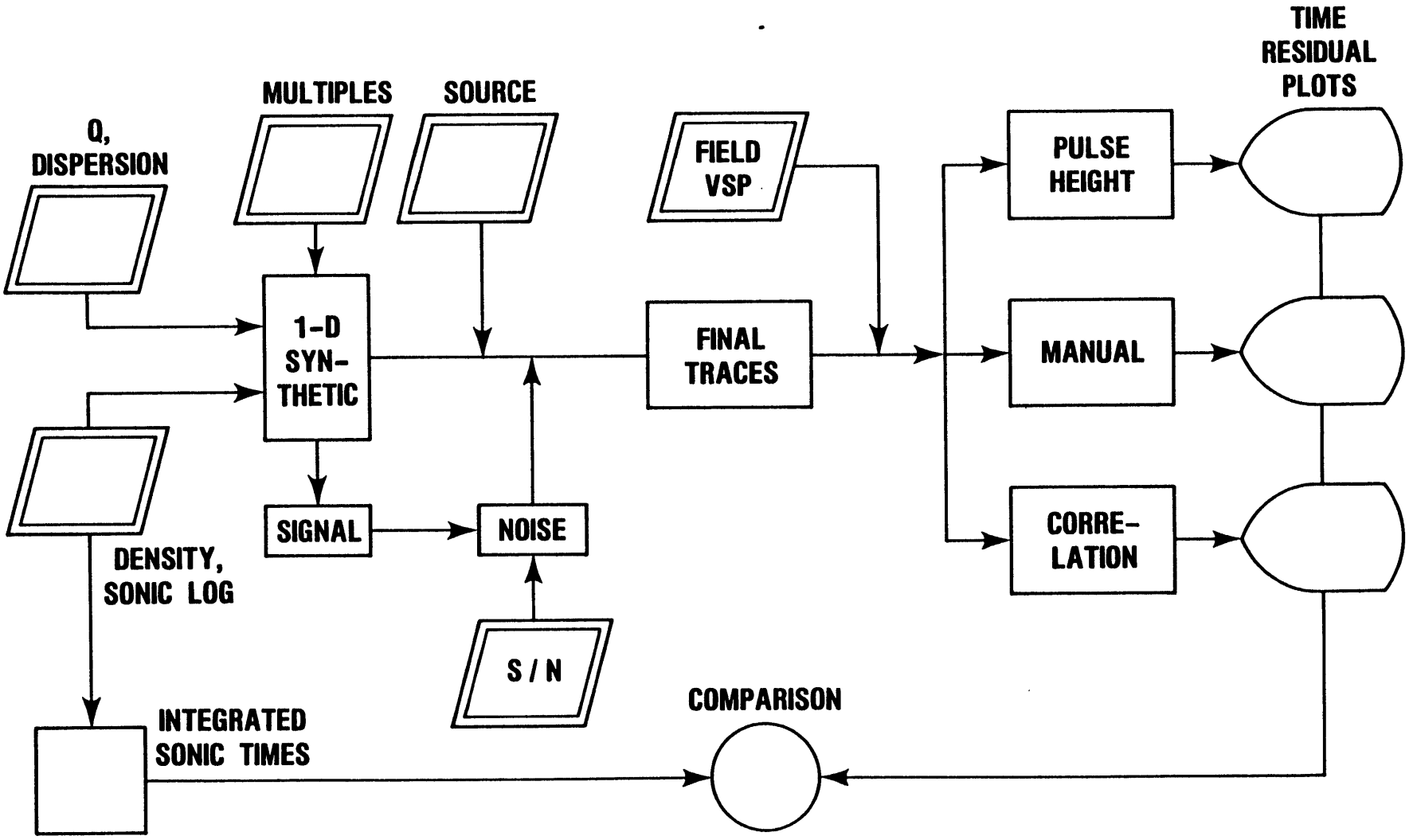

Figure 11.

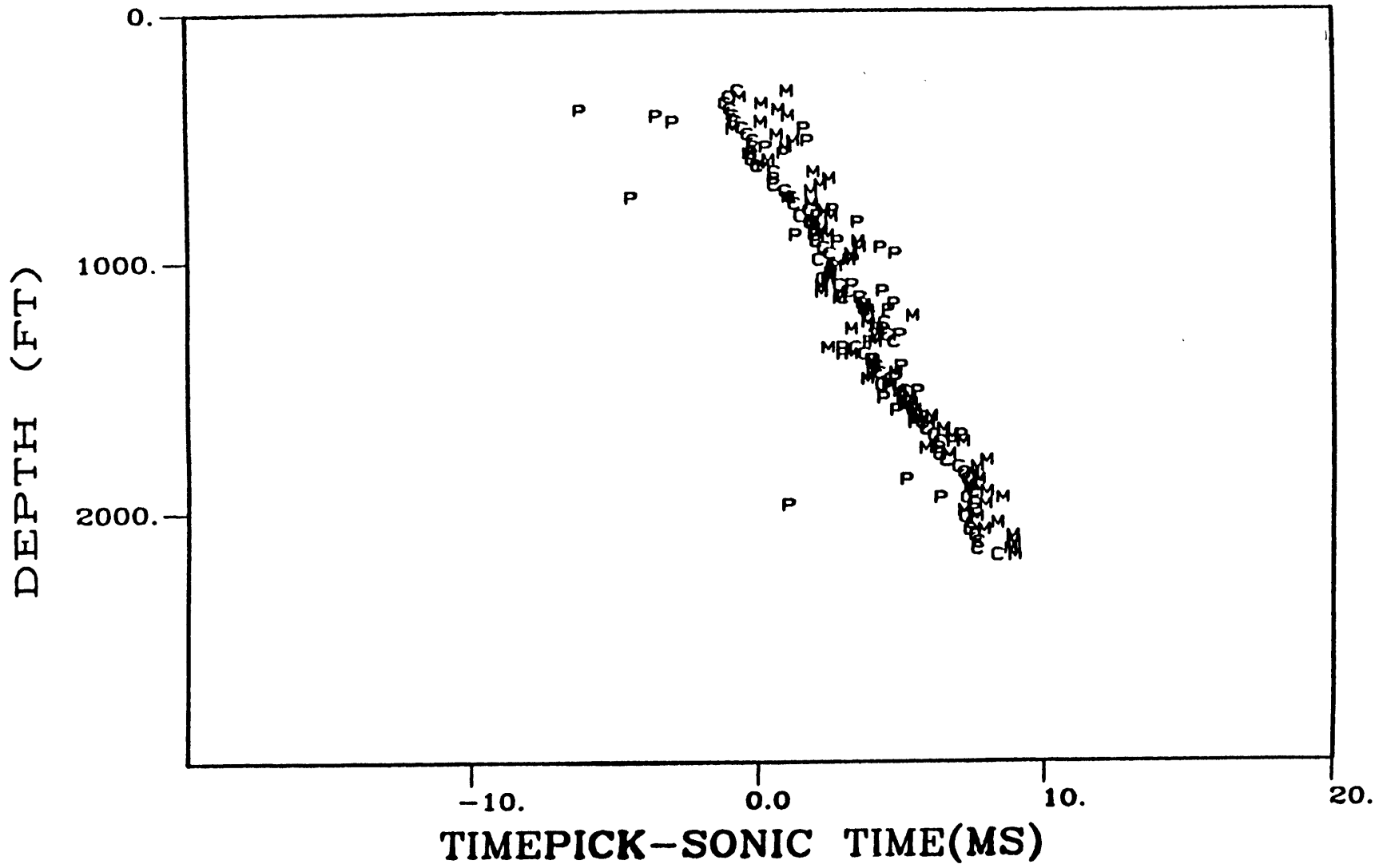

Figure 12.

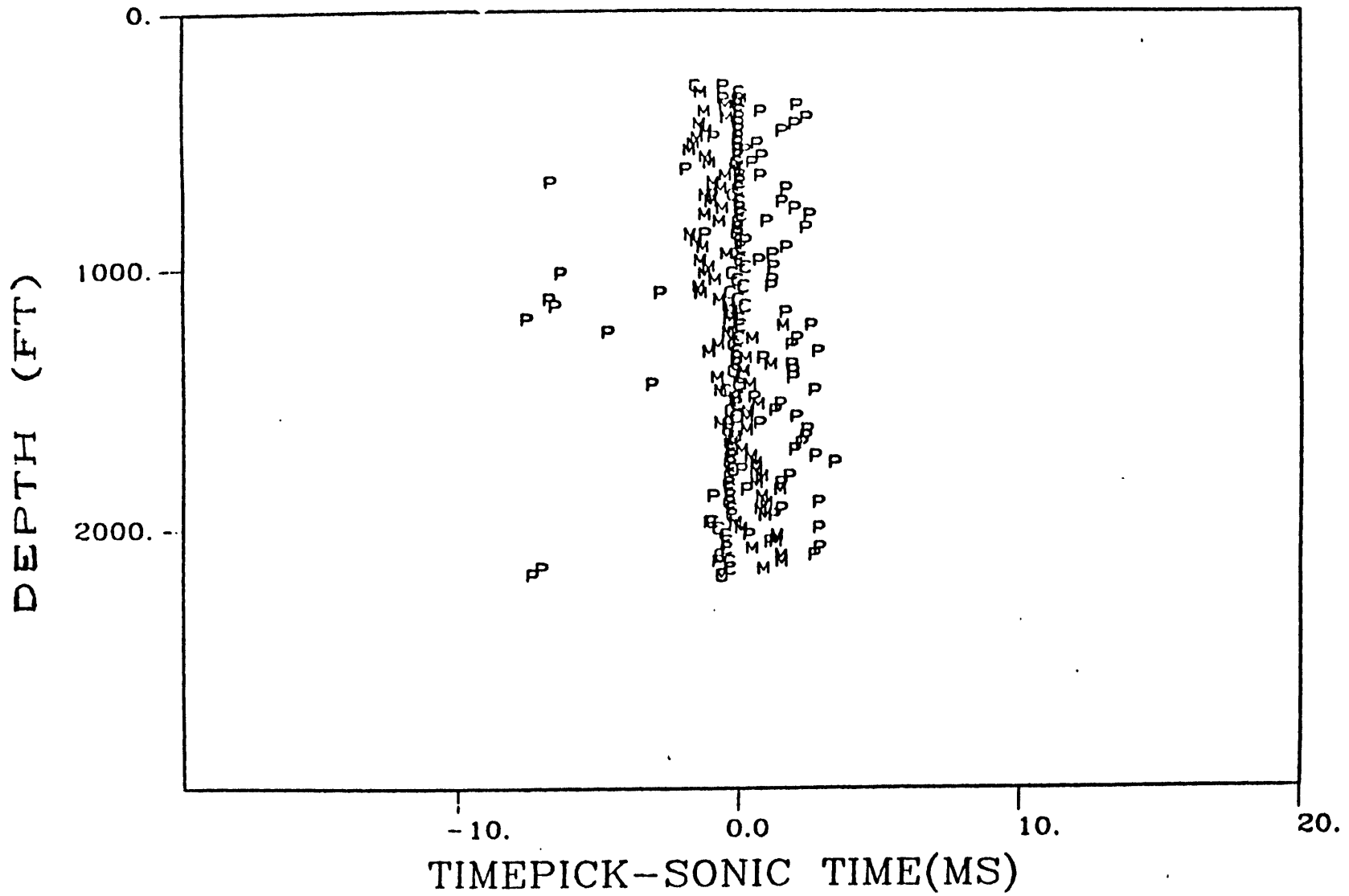

Figure 13.

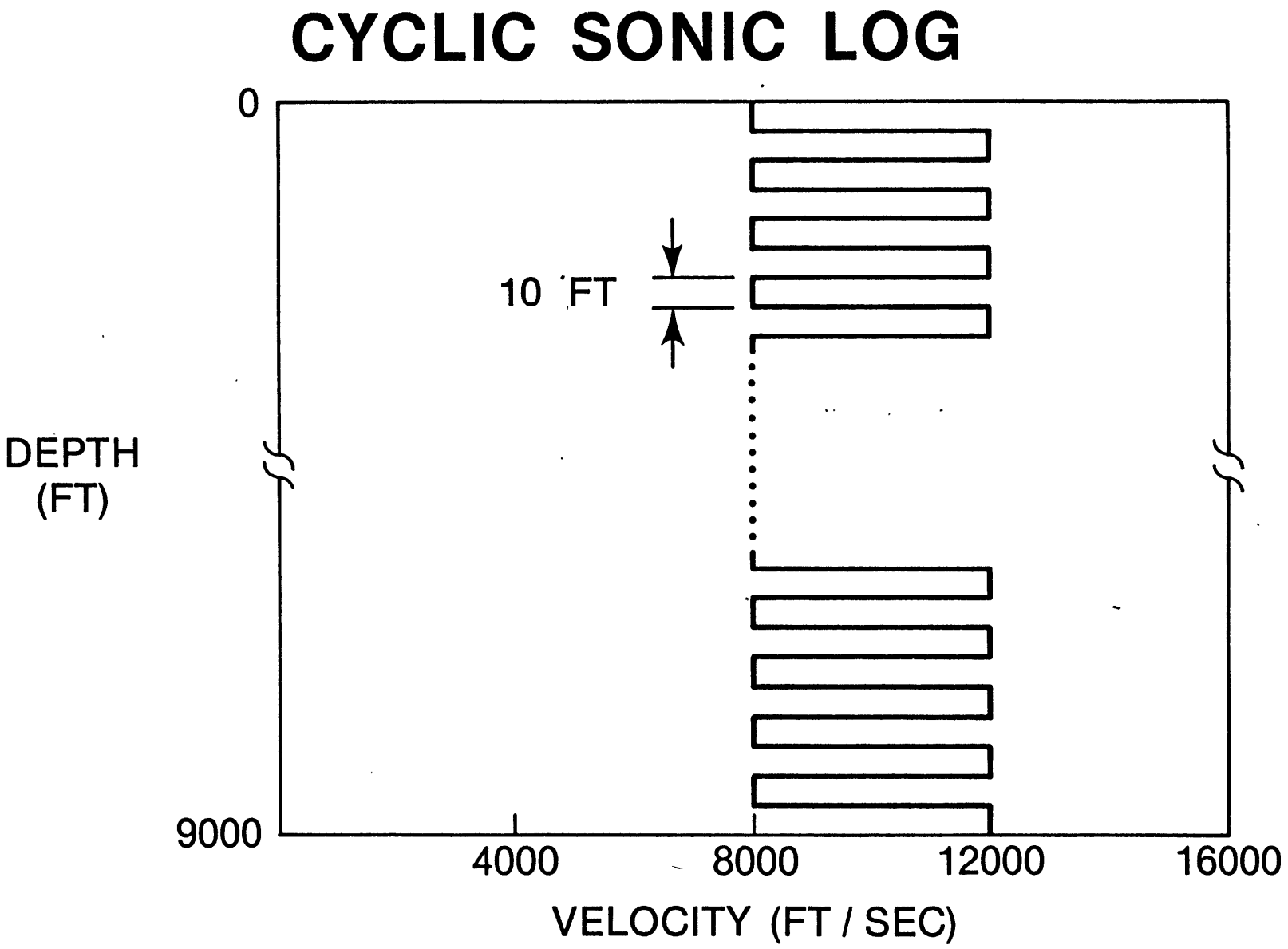
CYCLIC SONIC LOG
0
10 FT
DEPTH
(FT)
9000
4000
8000
12000
16000
VELOCITY (FT / SEC)

Figure 14.

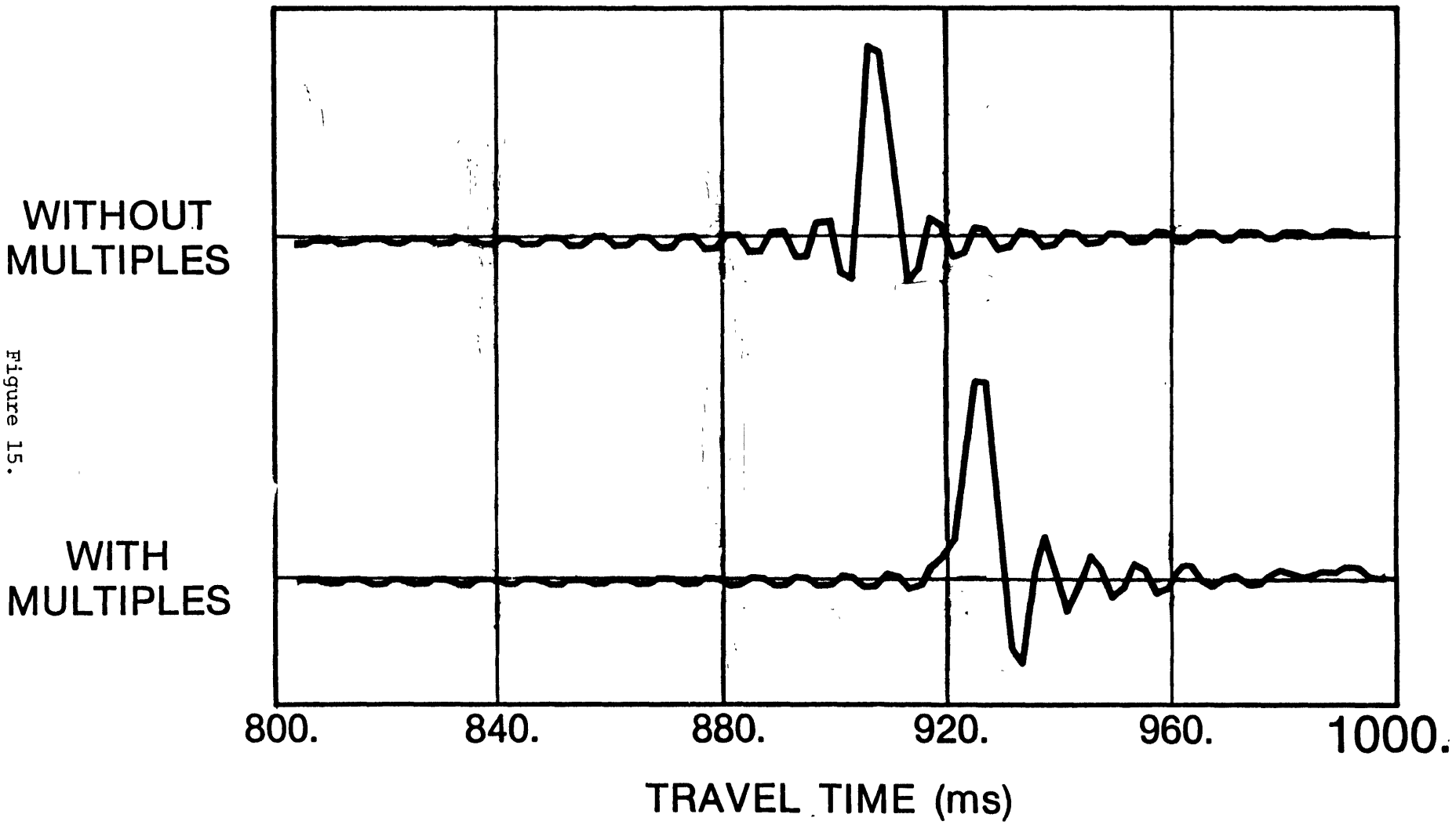
WITHOUT MULTIPLES
WITH MULTIPLES
800.
840.
880.
920.
960.
1000.
TRAVEL TIME (ms)

Figure 15.

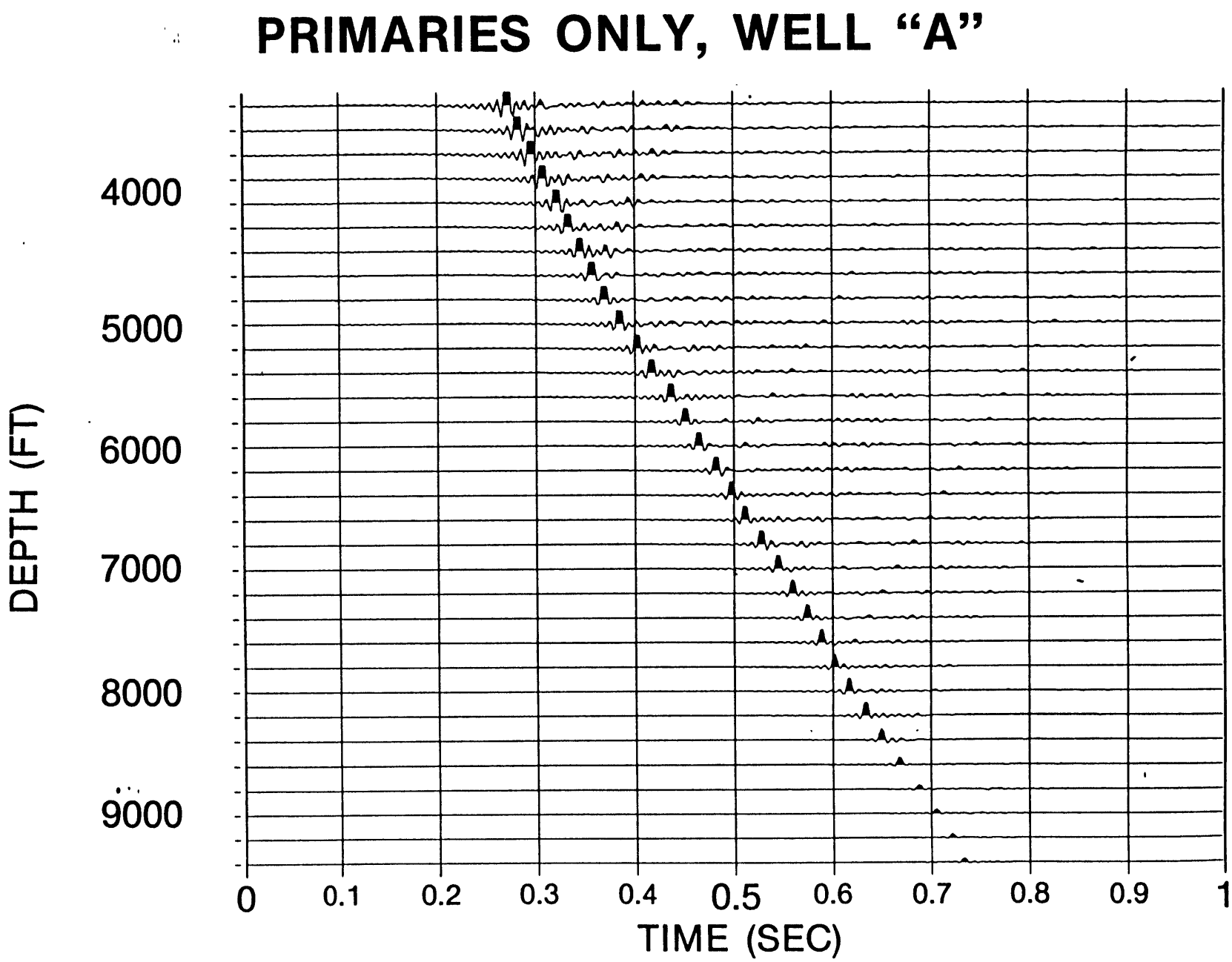
PRIMARIES ONLY, WELL "A"
DEPTH (FT)
4000
5000
6000
7000
8000
9000
0
0.1
0.2
0.3
0.4
0.5
0.6
0.7
0.8
0.9
1
TIME (SEC)

Figure 16.

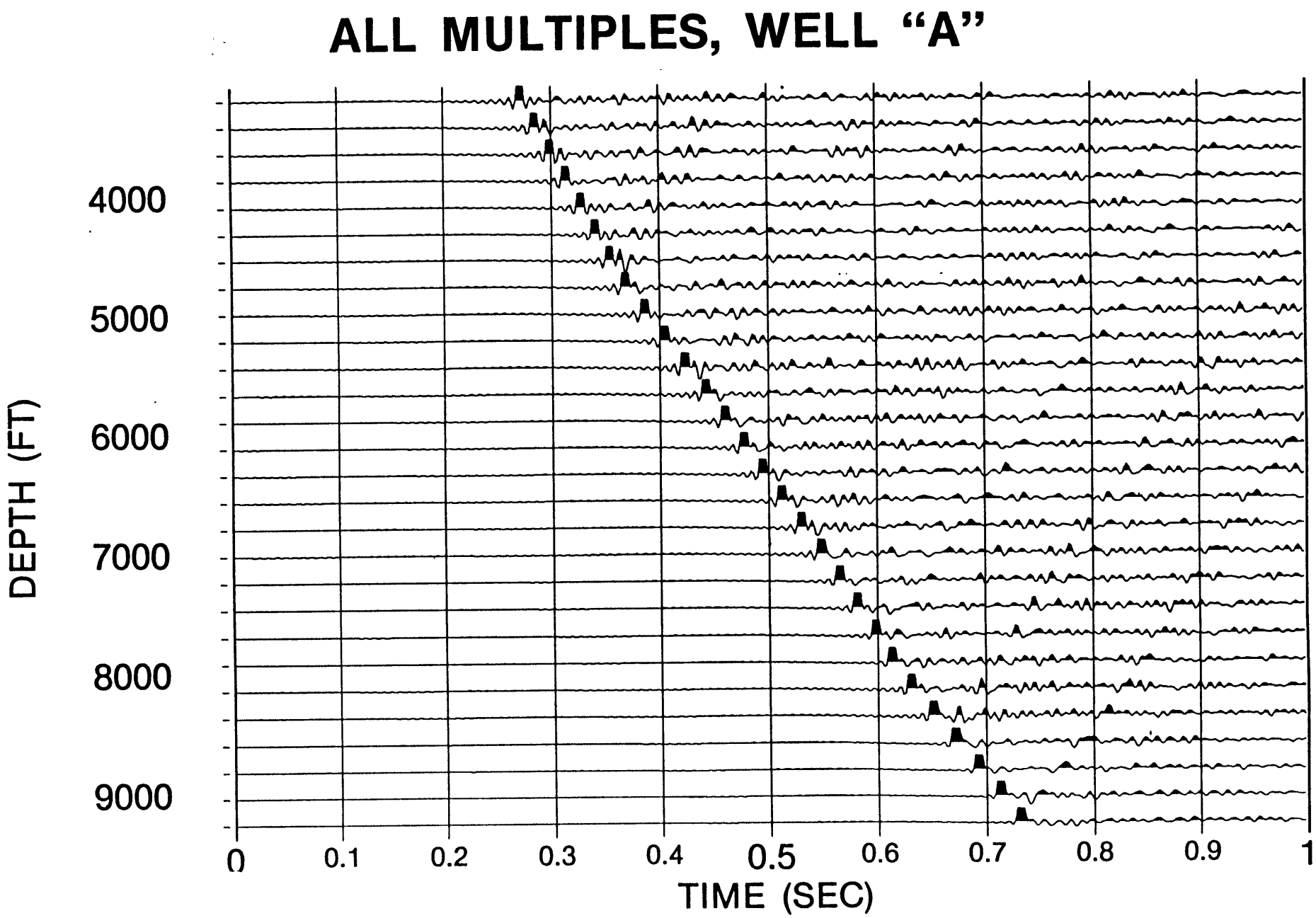
ALL MULTIPLES, WELL "A"
DEPTH (FT)
4000
5000
6000
7000
8000
9000
0
0.1
0.2
0.3
0.4
0.5
0.6
0.7
0.8
0.9
1
TIME (SEC)

Figure 17.

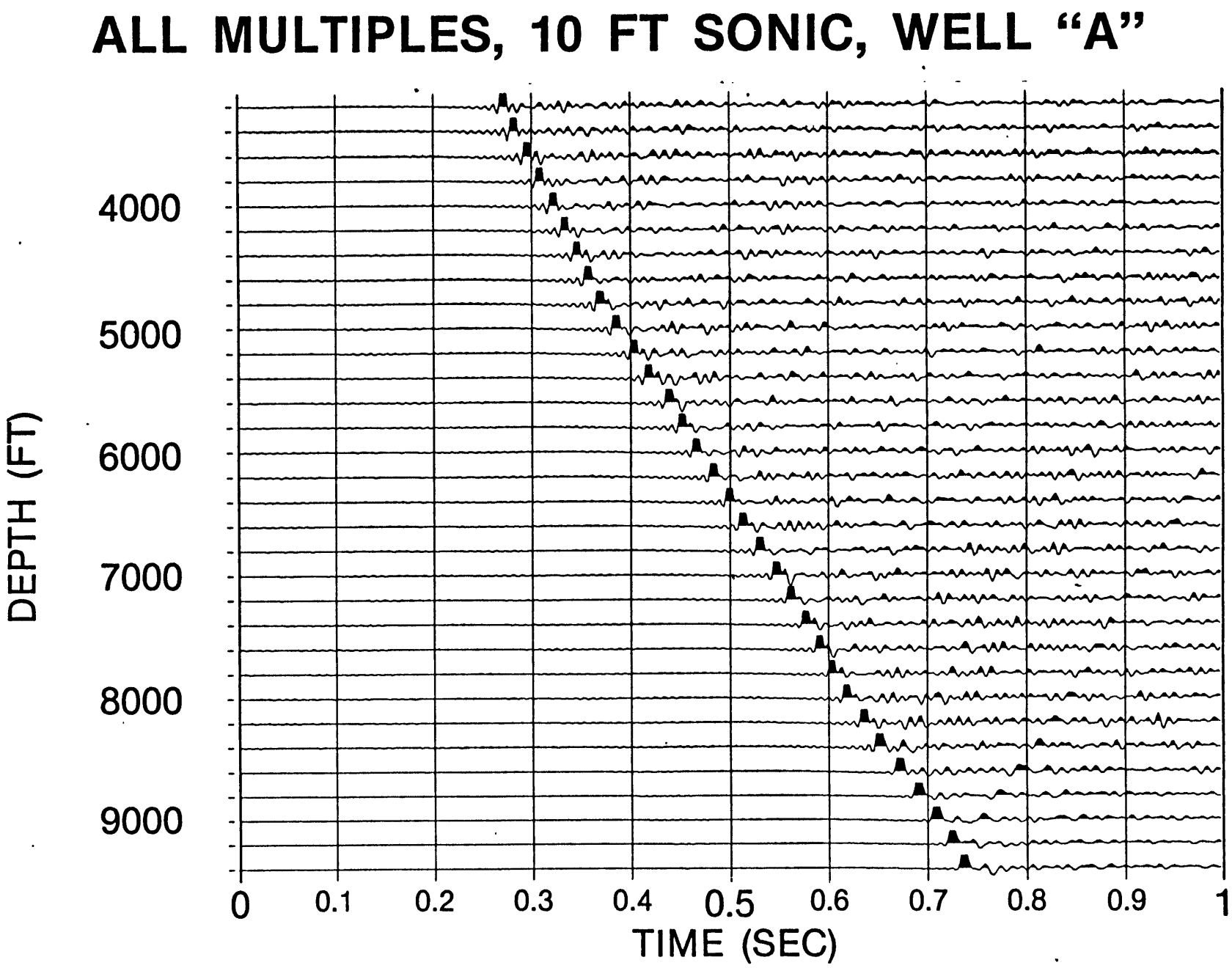
ALL MULTIPLES, 10 FT SONIC, WELL "A"
DEPTH (FT)
4000
5000
6000
7000
8000
9000
0
0.1
0.2
0.3
0.4
0.5
0.6
0.7
0.8
0.9
1
TIME (SEC)

Figure 18.

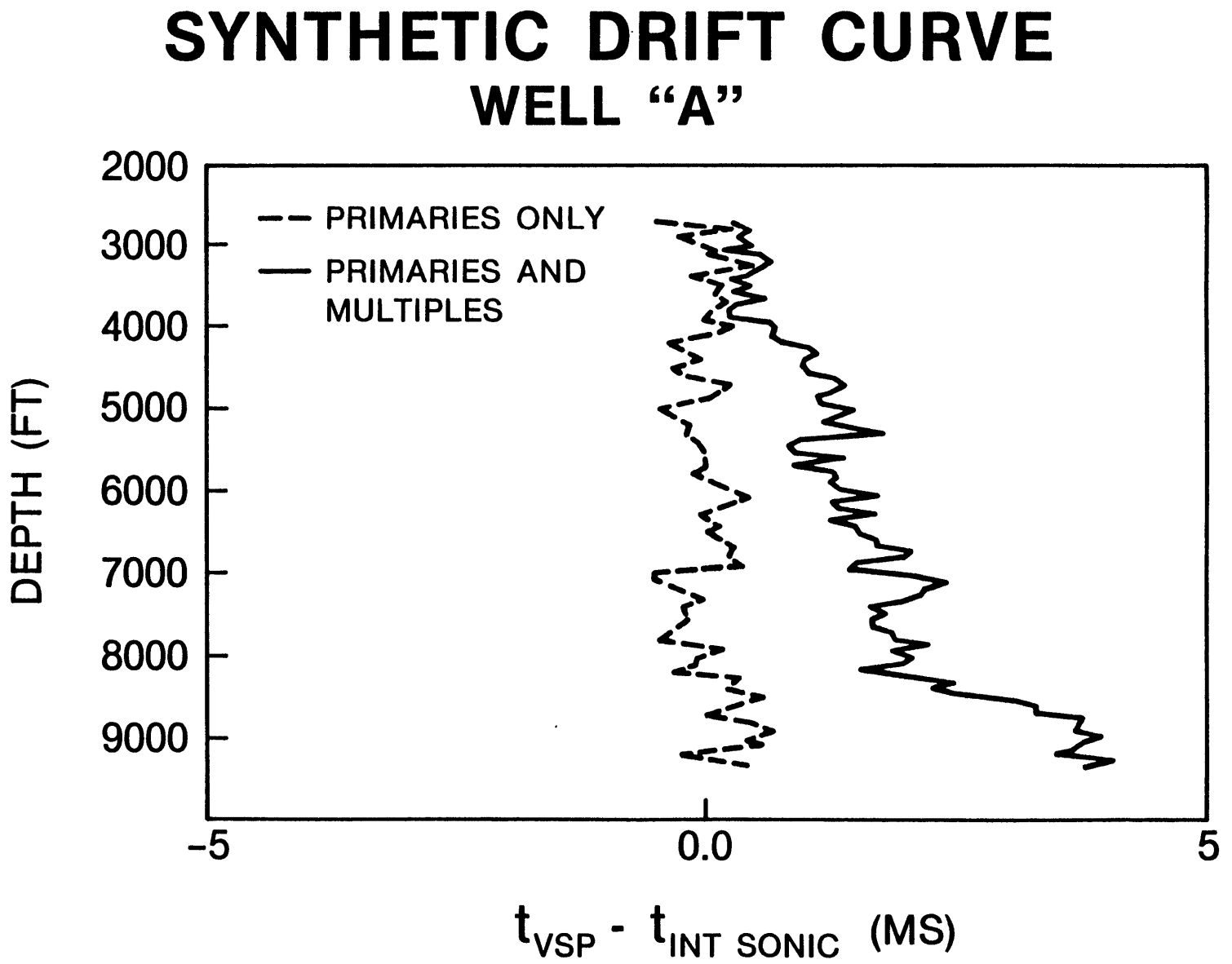
SYNTHETIC DRIFT CURVE
WELL "A"
PRIMARIES ONLY
PRIMARIES AND MULTIPLES
DEPTH (FT)
2000
3000
4000
5000
6000
7000
8000
9000
-5
0.0
5
$t_{VSP} - t_{INT\ SONIC}$ (MS)

Figure 19.

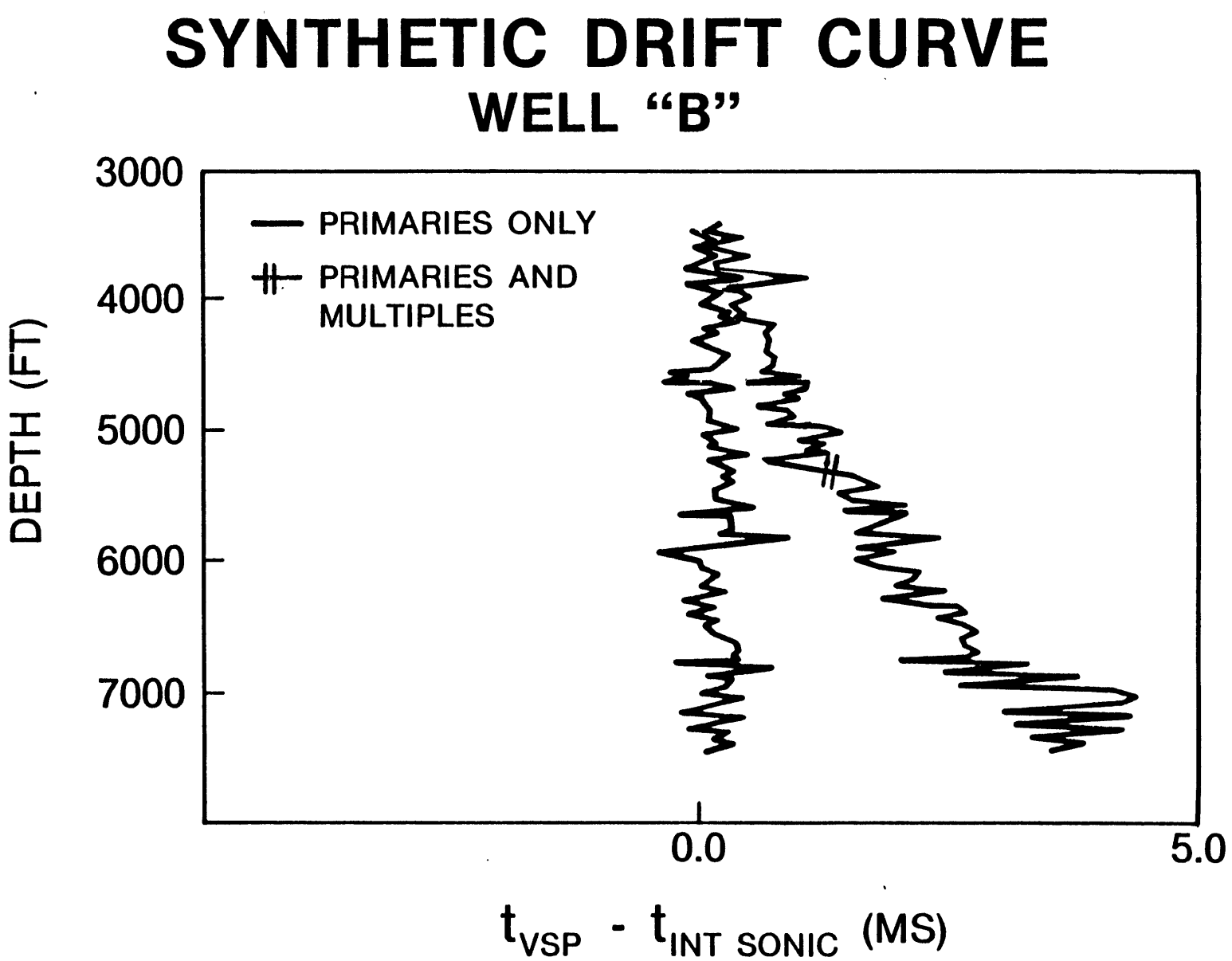
SYNTHETIC DRIFT CURVE
WELL "B"
PRIMARIES ONLY
PRIMARIES AND MULTIPLES
DEPTH (FT)
3000
4000
5000
6000
7000
0.0
5.0
$t_{VSP} - t_{INT\ SONIC}$ (MS)

Figure 20.

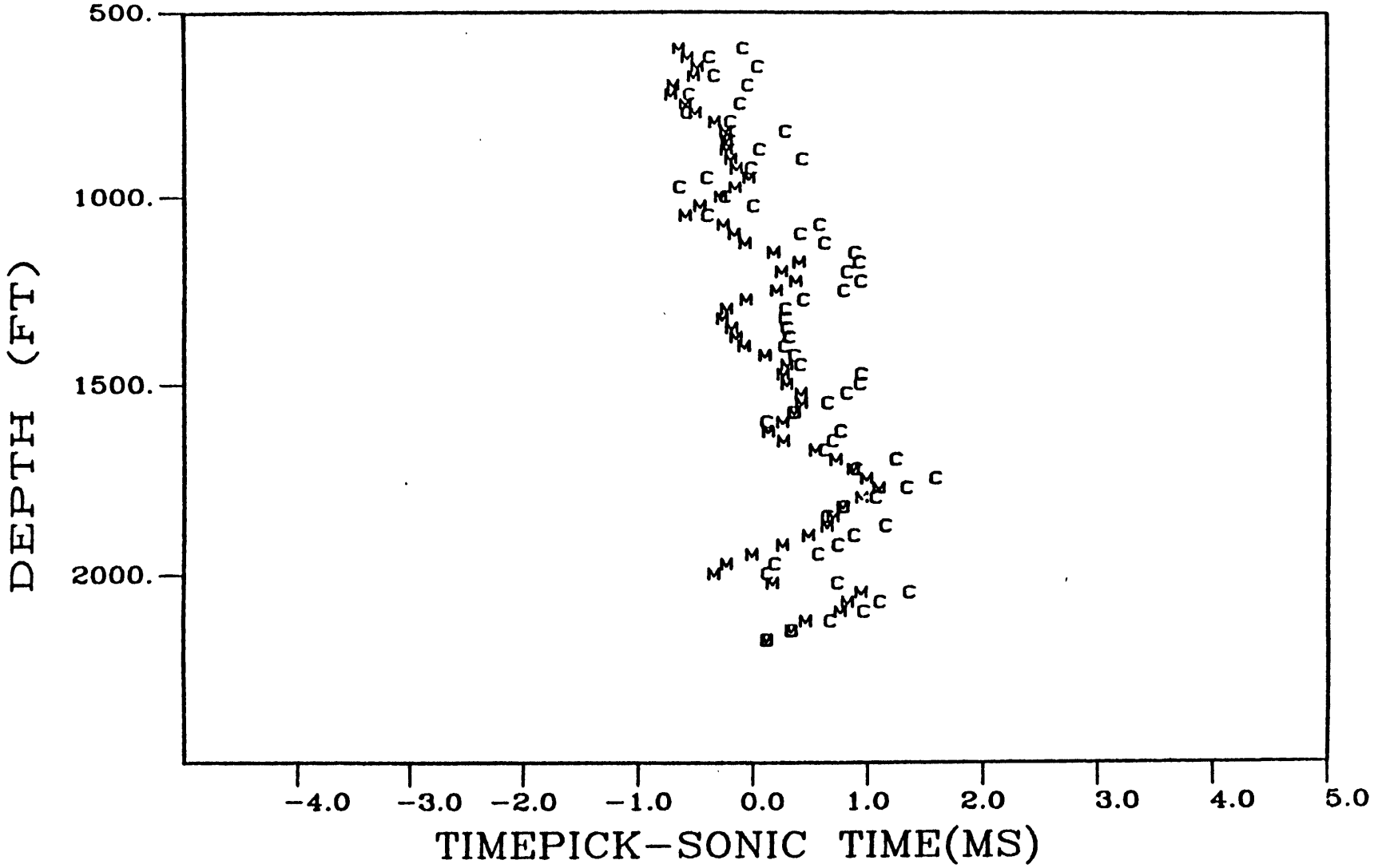
500.
1000.
1500.
2000.
DEPTH (FT)
-4.0
-3.0
-2.0
-1.0
0.0
1.0
2.0
3.0
4.0
5.0
TIMEPICK-SONIC TIME(MS)

Figure 21.

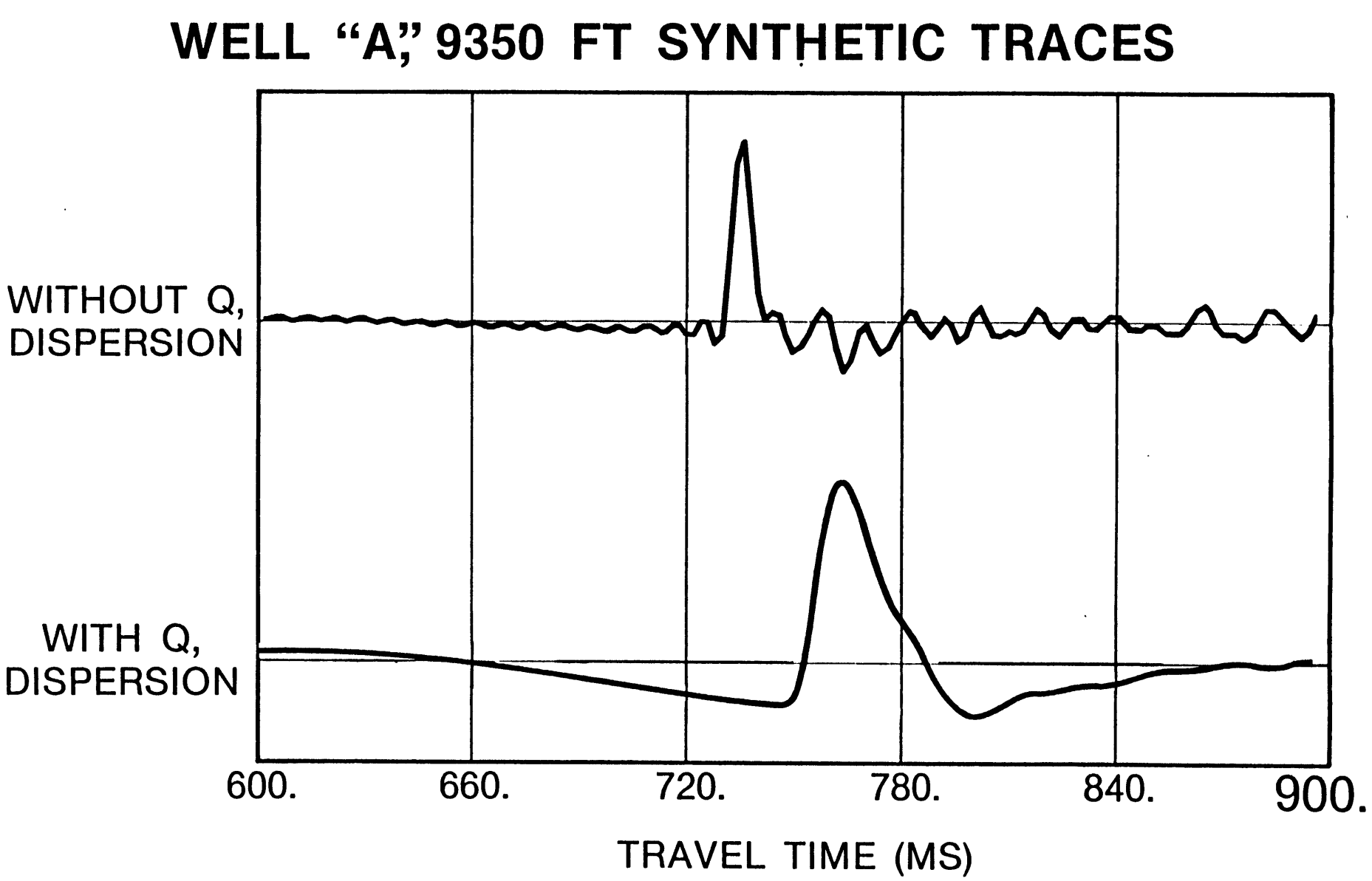
WELL "A," 9350 FT SYNTHETIC TRACES
WITHOUT Q, DISPERSION
WITH Q, DISPERSION
600.
660.
720.
780.
840.
900.
TRAVEL TIME (MS)

Figure 22.

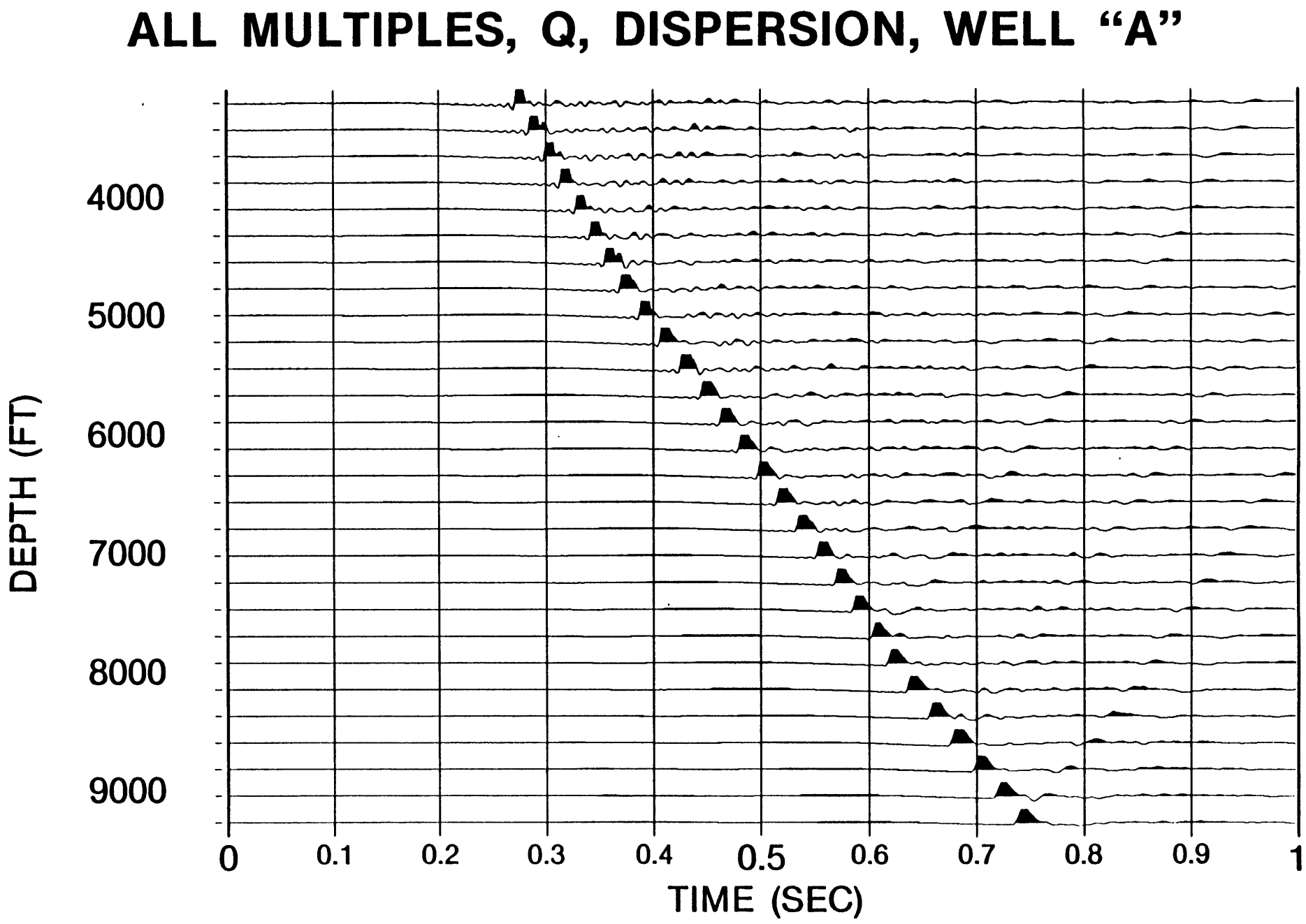
ALL MULTIPLES, Q, DISPERSION, WELL "A"
DEPTH (FT)
4000
5000
6000
7000
8000
9000
0
0.1
0.2
0.3
0.4
0.5
0.6
0.7
0.8
0.9
1
TIME (SEC)

Figure 23.

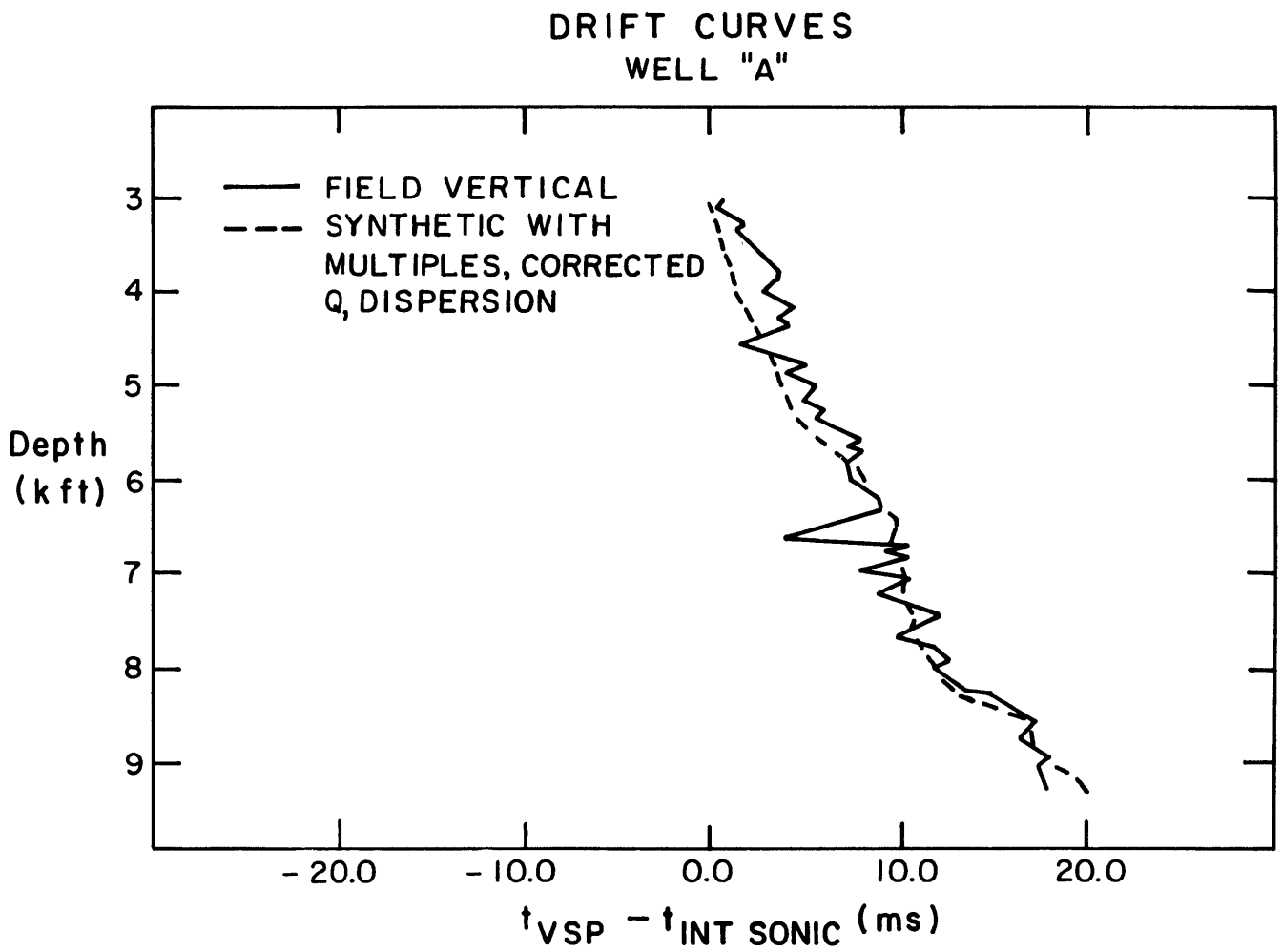
DRIFT CURVES
WELL "A"
FIELD VERTICAL
SYNTHETIC WITH
MULTIPLES, CORRECTED
Q, DISPERSION
Depth
(k ft)
3
4
5
6
7
8
9
- 20.0
- 10.0
0.0
10.0
20.0
$t_{VSP} - t_{INT\ SONIC}$ (ms)

Figure 24.

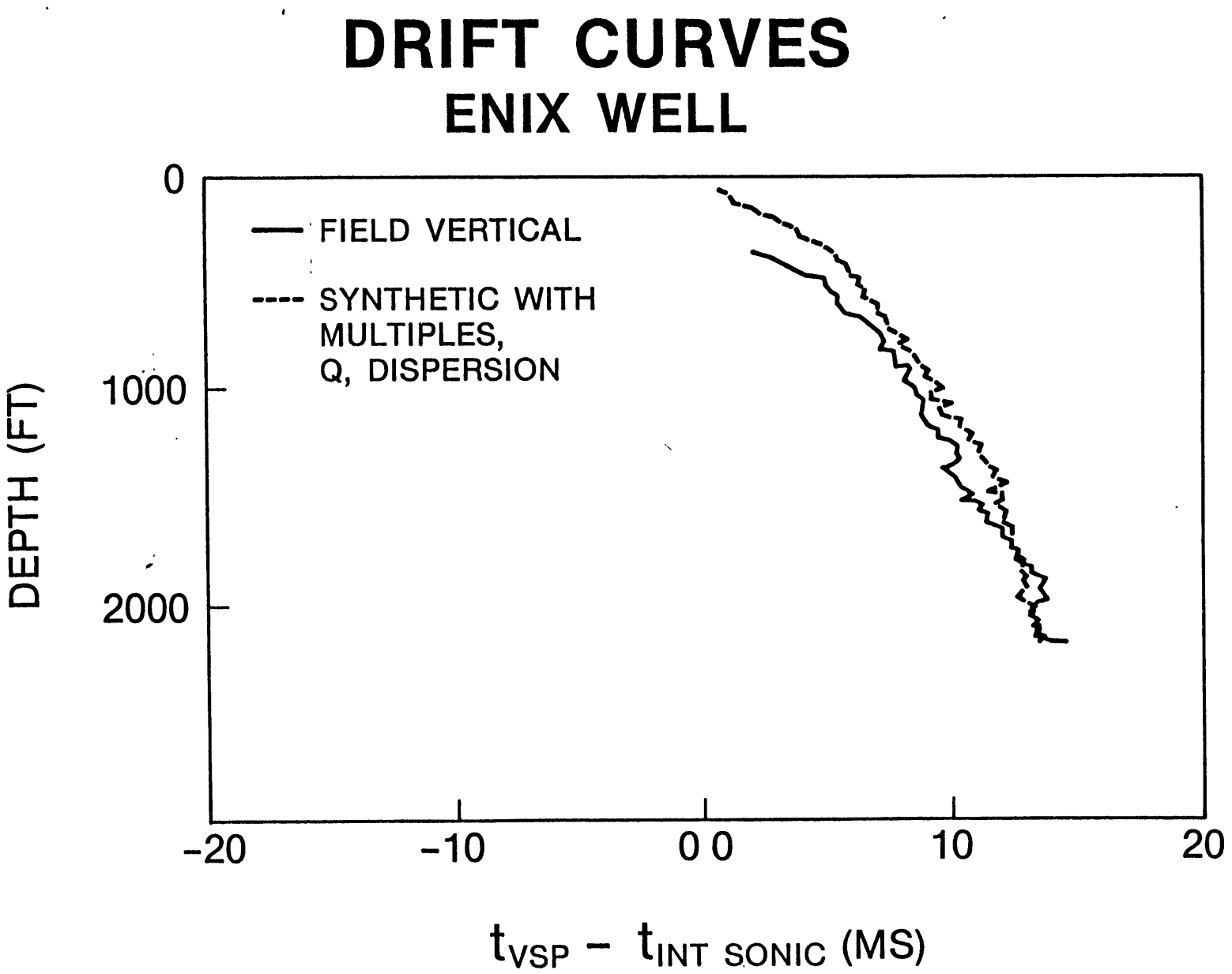
DRIFT CURVES
ENIX WELL
0
1000
2000
DEPTH (FT)
FIELD VERTICAL
SYNTHETIC WITH MULTIPLES, Q, DISPERSION
-20
-10
0 0
10
20
$t_{VSP} - t_{INT\ SONIC}$ (MS)

Figure 25.

Chapter 4

WAVEFORM INVERSION

...what would happen if you told them that all reflection seismology is really a special case of the VSP?

J.P. DiSiena
Dallas, Texas
Oct. 1981

4.1 INTRODUCTION

The inversion of seismic data for the lithologic parameters of direct interest (velocity, density and attenuation as opposed to reflection coefficients) has been the somewhat unrealized goal of surface seismic processing for some time (Rice et al., 1981; Johnson and Nogami, 1982). The vertical seismic profile (VSP) provides an opportunity to accurately measure these parameters. Unlike the sonic and density logs, the VSP measures parameters laterally over a several hundred foot distance from the borehole. This provides a sample of these parameters in the unaltered formation.

VSP traveltime inversions have been used successfully to find velocities (Grant and West, 1965; Stewart, 1982) but these techniques do not use the full seismic trace. Earthquake seismologists have been developing time domain inversions for the first several cycles of teleseismic traces, with the intention of finding details of the earthquake source (Kikuchi and Kanamori, 1982) and gross earth structure (Mellman, 1980). These studies have proved useful in the analysis of subsurface events monitored by surface receivers (Nabelek, 1983).

There is considerable coherent energy in the later part of the VSP waveform (Jolly, 1953; DiSiena et al., 1981; Gaiser et al., 1982). As it is these later times which contain the upgoing wavefield and have further

information constraining the seismic parameters, it is compelling to develop techniques to utilize the full trace.

Iterative full waveform inverse techniques are developed and examined here. The forward model consists of a one-dimensional frequency domain wave equation (Ganley, 1981) operating near the boundary of two half-spaces. Because of source and receiver variability in real data, groups of four traces are inverted at one time.

Two distinct inversions are considered. The first procedure uses a weighted, least-squares formulation similar to that of Marquardt (1963) to find velocity, attenuation and the up and downgoing waves from the four trace group. The second procedure also finds the impedances of the half-spaces using the stochastic inverse formulation. These impedances and the velocity estimates are then used to find the densities. In both cases the initial guesses at the velocity, attenuation and upgoing and downgoing waves are iteratively updated. The initial guesses at impedance in the stochastic inverse are critical to the final densities computed. The inversion process is repeated for groups of traces from the bottom to the top of the VSP section.

Several synthetic examples as well as a field VSP are analyzed using the above algorithms.

4.2 THEORY

There are numerous approaches with various levels of complexity that may be used to describe a propagating wavefield. Because many VSP surveys are conducted through largely horizontal layers which may number in the hundreds, a simple, fast method to calculate the forward problem is required. A one-dimensional, frequency domain, wave equation approach is used here to model the wavefield (Claerbout, 1976; Aki and Richards, 1980;

Robinson and Treitel, 1980; Ganley, 1981; Kan et al., 1981). The wavefield is calculated in the frequency domain so that the attenuation may be included across the frequency band. Otherwise the problem could be formulated and solved in the time domain.

Consider first the acoustic wave equation solution with waves propagating at normal incidence to a boundary.

At any depth in the section the seismic displacement trace $S(\omega)$, may be represented in frequency domain ω as the sum of an upgoing wave $U(\omega)$ and a downgoing wave $D(\omega)$

$$S(\omega) = D(\omega) + U(\omega) \tag{1}$$

where all waves are in the complex frequency domain.

The downgoing wave at one depth is related to itself $D'(\omega)$ at a greater depth (see Figure 1) in the same attenuating layer by

$$D'(\omega) = D(\omega)\, e^{\frac{-i\omega d}{v}}\, e^{-\alpha\omega d} \tag{2}$$

where d is the difference in depths

ω is the angular frequency

v is the phase velocity

α is the attenuation coefficient

Similarly the upgoing wave at a given depth may be related to the wave $U'(\omega)$ at another depth by

$$U'(\omega) = U(\omega)\, e^{\frac{i\omega d}{v}}\, e^{\alpha\omega d} \tag{3}$$

where d, ω, v, α are as above

At a given interface the displacement reflection coefficient R and transmission coefficient T are related by

$$1 + R = T \tag{4}$$

These coefficients are functions of the layer impedances

$$Z_i = \rho_i v_i \tag{5}$$

$$R = \frac{Z_i - Z_{i+1}}{Z_i + Z_{i+1}} \tag{6}$$

$$T = \frac{2Z_i}{Z_i + Z_{i+1}} \tag{7}$$

where the density (ρ_i) and velocity (v_i) are in the i^{th} layer.

Note that because of equation (4), R and T are functionally related. But they are composed of two impedances. As will be considered later in the section on the inverse problem, this means that there is one observable (R or T) depending on two parameters (Z_1 and Z_2).

The upgoing and downgoing waves in layer i are related to those of layer i+1 (Figure 1) by

$$D_{i+1}(\omega) = -R_i U_{i+1}(\omega) + T_i D'_i(\omega) \tag{8}$$

$$U'_i(\omega) = R_i D'_i(\omega) + (2-T_i) U_{i+1}(\omega) \tag{9}$$

For several reasons, as mentioned previously and discussed later, it is reasonable to take a group of four traces for analysis. We suppose that there is an interface between the second and third recording levels (Figure 2). It is also assumed that the traces are equally spaced in depth (VSP surveys usually are) and that there are no sources in the depths under consideration. Having variable receiver spacing poses no theoretical problem but is avoided here for simpilicity.

From Figure 2, we note that the only parameters required to specify the seismograms at the four levels are the downgoing wavefield across the relevant frequency band at the first depth, the upgoing wavefield at the fourth depth, the two velocities, two impedances and the attenuation.

The vertical displacement field at each depth is

$$S_1(\omega) = D(\omega)+R\cdot D(\omega)\cdot P(3d,v1,\alpha)+(2-T)\cdot U(\omega)\cdot P(3d,v_2,v_1,\alpha)$$

$$S_2(\omega) = D(\omega)\cdot P(d,v_1,\alpha)+R\cdot D(\omega)\cdot P(2d,v_1,\alpha)+(2-T)\cdot U(\omega)\cdot P(2d,v_2,v_1,\alpha) \quad (10)$$

$$S_3(\omega) = T\cdot D(\omega)\cdot P(2d,v_1,v_2,\alpha)+U(\omega)\cdot P(d,v_2,\alpha)-R\cdot U(\omega)\cdot P(2d,v_2,\alpha)$$

$$S_4(\omega) = T\cdot D(\omega)\cdot P(3d,v_1,v_2,\alpha)+U(\omega)-R\cdot U(\omega)\cdot P(3d,v_1,v_2,\alpha)$$

where $D(\omega)$ is the downgoing wave at the uppermost receiver

$U(\omega)$ is the upgoing wave at the deepest receiver

v_1, v_2 are the velocities of the half-spaces

α is the attenuation coefficient

d is the distance between the receivers

R, T are the reflection and transmission coefficients

P is the propagation function

e.g. $P(2d,v_1,v_2,\alpha) = \exp(-2\alpha\omega d)\ \exp^{-i\omega(\frac{3d}{2v_1}+\frac{d}{2v_2})}$

The above formulations are for plane waves. However, field data are generally collected from a point source. Thus spherical waves are more realistic. To correct the model for this spreading, a spherical spreading term $\frac{z}{z+d}$ at depth z+d referenced to depth z is included in the propagation function.

While only the above model will be used to process data here several extensions to this basic forward model are considered.

A somewhat more complex case is encountered if the incident P waves are at some angle to the normal (see Figure 3). Reflected and transmitted S waves are now generated both from the downgoing wave and upgoing wave impinging on the interface. These waves are included in the elastic formulation below for the four receivers shown in Figure 2. In this case the wavefield is described in terms of potentials at x=0 (after Pilant, 1979).

$$S_1(\omega) = D(\omega)+T_p'\cdot U(\omega)\cdot P(3d,kz',k_{z2}',\alpha)+T_s'\cdot U(\omega)\cdot P(3d,k_{z2}',k_z^{s'},\alpha)$$
$$+ Rp\cdot D(\omega)\cdot P(3d,k_z,\alpha) + R_s\cdot D(\omega)\cdot P(3d,k_z,k_z^s,\alpha)$$

$$S_2(\omega) = D(\omega)\cdot P(d,k_z,\alpha)+T_p'\cdot U(\omega)\cdot P(2d,k_{z2}',k_z',\alpha)+T_s'\cdot U(\omega)$$
$$P(2d,k_{z2}',k_{z1}^{s'},\alpha)$$
$$+ Rp\cdot D(\omega)\cdot P(2d,k_z,\alpha) \quad + R_s\cdot D(\omega)\cdot P(2d,k_z,k_z^s,\alpha) \qquad (11)$$

$$S_3(\omega) = T_p\cdot D(\omega)\cdot P(2d,k_z,k_{z2},\alpha)+U(\omega)\cdot P(d,k_{z2}',\alpha)+T_s\cdot D(\omega)\cdot$$
$$P(2d,k_z,k_{z2}^s,\alpha)$$
$$+R_p'\cdot U(\omega)\cdot P(2d,k_{z2}',\alpha) \quad + R_s'\cdot U(\omega)\cdot P(2d,k_{z2}',k_{z2}^{s'},\alpha)$$

$$S_4(\omega) = T_p\cdot D(\omega)\cdot P(3d,k_z,k_{z2},\alpha) + U(\omega) + T_s\cdot D(\omega)\cdot P(3d,k_z,k_{z2}^s,\alpha)$$
$$+ Rp'\cdot U(\omega)\cdot P(2d,k_{z2}',\alpha) \quad + R_s'\cdot U(\omega)\cdot P(3d,k_{z2}',k_{z2}^{s'},\alpha)$$

where $U(\omega)$, $D(\omega)$ are the upgoing and downgoing potentials

d is the distance between receivers

P is the propagation function as in equations (10)

θ_1 is the incidence angle of the downgoing P wave

θ_2 is the incidence angle of the upgoing P wave

R_p, R_s are the downgoing wave P and converted S reflection coefficients for angle θ_1

T_p, T_s are the downgoing wave P and converted S transmission coefficients for angle θ_1

R_p', R_s', T_p', T_s' are the coefficients for the upgoing wave at angle θ_2

k_z, k_z^s are the vertical P and S components of the wavenumber in the upper layer for the downgoing wave $D(\omega)$

k_{z2}, k_{2z}^s are the vertical P and S components of the wavenumber in the lower layer for the downgoing wave

k_z', $k_z^{s'}$, k_{z2}', $k_{z2}^{s'}$ are the vertical wavenumbers for the upgoing wave $U(\omega)$ for P and S waves in the upper and lower layers respectively.

Pilant (1979) has given expressions for the transmission and reflection coefficients as well as the angles of emergence of the various waves. Even for this relatively simple geometry the coefficients are extremely complicated and generally require a numerical solution.

The previous equations (11) can be reinterpreted to provide a forward model which has a dipping interface (see Figure 4). For simplicity let the incident upgoing P wave be zero. If equations (11) are considered as rotated coordinates then by using a rotation matrix through the angle θ_1, the problem for waves propagating vertically or at some angle, but incident on a dipping bed, may be solved.

Including both upgoing and downgoing incident P and S waves presents no conceptual difficulty in the four trace model. Again, however the computational problem is somewhat complex. Pilant (1979) has given formulae for the relevant coefficients. These extensions to the basic forward model could be used in an inversion scheme involving more complex geology or surveys.

Note that this analytic model of one boundary and four traces may be easily altered. For example, two more traces could be included by propagating the waves given in equations (10) a distance d farther on top and below the depths given. Because no new parameters are required to describe the new traces, the problem would have more observed data constaining the parameters. However, depth resolution has been degraded as parameters are averaged over a greater distance.

In a similar manner, two interfaces could be included inside the six traces, say between the second and third, and fourth and fifth traces. This would allow greater structural resolution (3 velocities and impedances) but still constrain $U(\omega)$, $D(\omega)$ and α.

Returning to the normal incidence acoustic problem, it is possible to connect the observed data to the model through a Taylor expansion. The difference between the resultant calculated spectra and observed spectra is assumed to be linearly related to the change that needs to be made in the parameters. That is, equations (10) are linearized and the observed data are regarded as neighboring points of the model. If the problem is actually non-linear the process will need to be repeated.

In the present case

$$O_i(\omega_k) - S_i(\omega_k) \approx \sum_j \frac{\partial S_i(\omega_k)}{\partial p_j} \Delta p_i \qquad \begin{matrix} i = 1,4 \\ j = 1,N \\ k = 1,NF \end{matrix} \qquad (12)$$

where $O_i(\omega_k)$ is the observed spectral value at frequency ω_k and level i

$S_i(\omega_k)$ is the calculated seismogram at level i

p_j is the jth parameter

Δp_j is change required in p_j.

N is the total number of parameters

NF is the number of discrete frequencies to be used.

The actual data recorded are in the time domain thus the four seismograms (i=1,4) are Fourier transformed to the frequency domain (K=1,N) to find the observation $O_i(\omega_k)$. The observations are left in their real and imaginary parts (as opposed to amplitude and phase) as are the synthetic seismograms. To describe the four traces, eight times the number of frequencies used for each trace are required. The cases analyzed here use 32 frequency points and thus 256 observations.

The parameters in the problem consist of the downgoing spectra $D(\omega)$, the upgoing spectra $U(\omega)$, the layer velocities and impedances plus the attenuation. Thus 133 parameters are required. Recall that this procedure is flexible as to how many observations and parameters are used. One of the goals of the data processing discussed later will be to analyze what parameters are required or resolvable.

The parameters are related to the synthetic total trace by equations (10). These are the relations that are used to find the partial derivatives. The derivatives of $S(\omega)$ are strictly linearly related to $D(\omega)$ and $U(\omega)$. As α is very small, $\exp(-\alpha\omega x)$ is quite close to one and the derivative is essentially linear with α also. The derivatives with respect to velocity are more complex. They are the source of non-linearity in the problem. Nonetheless the velocity derivatives can be approximated well by using just a first order term in the expansion of the complex exponential and reflection coefficients. If impedances are used then they effect the seismograms only through the reflection and transmission coefficients. Thus the derivatives of the seismograms with respect to impedance just involve the derivatives of the reflection and transmission coefficients. The magnitude of higher order derivatives falls off slowly.

After separating the observations and parameters into real and imaginary parts, equation (12) may be written as

$$
\begin{bmatrix} O_1^R(\omega_1)-S_1^R(\omega_1) \\ \vdots \\ O_2((\omega_2)-S_2R(\omega_2) \\ \vdots \\ O_4^I(\omega_{NF})-S_4^I(\omega_{NF}) \end{bmatrix}
=
\begin{bmatrix}
\frac{\partial S_1^R}{\partial D^R} & \frac{\partial S_1^R}{\partial U^I} & \frac{\partial S_1^R}{\partial V_1} & \frac{\partial S_1^R}{\partial V_2} & \frac{\partial S_1^R}{\partial \alpha} & \frac{\partial S_1^R}{\partial Z_1} & \frac{\partial S_1^R}{\partial Z_2} \\
\vdots & \vdots & & & & & \\
\frac{\partial S_4^I}{\partial D^R} & \frac{\partial S_4^I}{\partial U^I} & \frac{\partial S_4^I}{\partial V_1} & \frac{\partial S_4^I}{\partial V_2} & \frac{\partial S_4^I}{\partial \alpha} & \frac{\partial S_4^I}{\partial Z_1} & \frac{\partial S_4^I}{\partial Z_2}
\end{bmatrix}
\bullet
\begin{bmatrix} \Delta D^R(\omega_1) \\ \Delta D^R(\omega_{NF}) \\ \Delta D^I(\omega_1) \\ \Delta D^I(\omega_{NF}) \\ \Delta U^R(\omega_1) \\ \vdots \\ \Delta U^I(\omega_{NF}) \\ \Delta V_1 \\ \Delta V_2 \\ \Delta \alpha \\ \Delta Z_1 \\ \Delta Z_2 \end{bmatrix}
\tag{13}
$$

Cast in matrix form equation (13) becomes

$$Y = AX \tag{14}$$

Y - column vector of $O_i(\omega) - S_i(\omega)$

A - matrix of partial derivatives $\frac{\partial S_i}{\partial p_j}$

X - column vector of parameter changes Δp_j

By altering the parameters of this model, the observed data may be matched in some specified sense by the calculated seismograms.

4.3 INVERSE METHOD

Because of error in the data and model inadequacy, it will not be possible to find parameters for equation (14) which make the observed and calculated wavefields identical. It remains to find the change in parameters $\hat{X}$ which brings the calculated seismograms closest to the real data. There are numerous ways to do this. The standard method is to find $\hat{X}$ which minimizes the least-square error in the data; that is find $\hat{X}$ such that Y^TY is minimized. If there were no ambiguity in the model parameters and no weighting was required, then the simplest solution would be the straightforward least-squares estimate $\hat{X}$ as shown in Chapter 2 and given below

$$\hat{X} = (A^TA)^{-1}A^TY \tag{15}$$

where A^T is the transpose of $\tilde{A}$.

In the present case the parameters and observed data can be of radically different numeric size and thus should be scaled first to be dimensionless

$$X' = GX \tag{16}$$

where G is a matrix of the guesses at the reciprocals of the standard deviation of the parameters (a priori deviation)

$$Y' = EY \tag{17}$$

where E is a matrix of the reciprocals of the standard deviation of the data.

The following problem is solved for X'

$$A'X' = Y' \tag{18}$$

where $A' = EAG^{-1}$

and

$$\hat{X} = G^{-1}(A'^TA')^{-1}A'^TY' \tag{19}$$

The solution given in equation (19) corresponds to the purely overdetermined case. This gives the classical weighted least-squares (WLS) solution with perfect parameter resolution. The matrix V of errors in the parameters due to error in the data (the a posteriori covariance matrix [Hoversten et al., 1982; Tarantola and Valette, 1982]) is evaluated at the data error minimum and is given by

$$V = \sigma^2 G^{-1}(A'^T A')^{-1} G^{-1} \tag{20}$$

$$\sigma^2 = \frac{Y'^T Y'}{8*NF-N}$$

In practice a small number is often added to the diagonal of $A'^T A'$ in equation (19) for numerical stability. The strategy to achieve a solution is to continually reduce the damping on the diagonal.

The matrix $A'^T A'$ may be decomposed using eigenvector analysis (e.g. the Jacobi rotations method [JCEIGS, 1971]) as

$$A'^T A' = V \Lambda^2 V^T \tag{21}$$

where Λ^2 is the matrix of the square of the eigenvalues

V is the matrix of associated eigenvectors.

The relative size of the eigenvalues can aid in determining whether the problem has been scaled to make all parameters of similar significance.

When the inverse problem is not purely overconstrained, as when impedance is included in the problem, a somewhat different formulation is used. Recall from equations (10) that the impedances are represented in the observed data through the reflection coefficient R (as T=1+R). But R is a function of the two impedances. Thus the solution will not be unique.

To consider the inversion with impedance, the stochastic formulation is used (Aki and Richards, 1980; Tarantola and Valette, 1982). In this case, the data mismatch is minimized but so is the parameter change. It is

this minimization of the parameter change which allows a unique solution to be picked when parameters are unresolved. In principal the algorithms will be able to constrain R. This defines a linear relationship [via equation (6)] between Z_1 and Z_2. The final values for Z_1 and Z_2 will be those values which fall on the line defined by R and which are very close to the original guesses. Clearly a good initial guess is important. The a priori data and parameter estimates are used in the stochastic formulation as follows

$$\hat{X} = (A^T E^T EA + \varepsilon G^T G)^{-1} A^T E^T EY \tag{22}$$

where ε is a damping parameter usually taken to be 1.0.

Because this problem is not purely overconstrained there is some non-uniqueness in the parameters or trade-off between them. Thus the resolution matrix R, which relates the calculated estimates to the true values, is useful

$$R = (A^T E^T EA + \varepsilon G^T G)^{-1} A^T E^T EA \tag{23}$$

The estimates of parameter variance are taken as the square roots of the diagonal of the covariance matrix

$$V = \sigma^2 LL^T \tag{24}$$

where $L = (A^T E^T EA + \varepsilon G^T G)^{-1} A^T E^T E$

and $$\sigma^2 = \frac{Y^T Y}{8*NF-N}$$

The strategy in applying (22) to the VSP problem including density is to first make good a priori guesses at E and G. The algorithm iteratively finds the best solution by updating A but keeping ε, E and G constant.

These inversion techniques basically "fine-tune" reasonable initial guesses. The initial velocities may be determined either from the traveltime inversion discussed in Chapter 2 or the sonic log. Attenuation

values may be found using a spectral ratio of the total traces at two different depths. As outlined later, the downgoing wave can be reasonably started as just the total top trace of the group. The upgoing wave may be initially started, for example, as a time shifted fraction of the downgoing wave. As the algorithm progresses up the section, it is possible to use the extracted traces from one group as input into the next group inversion. The next section discusses some of the details of implementing equations (15)-(24) on a digital computer.

4.4 COMPUTATION

The basic problem shown in equation (14) incorporates a large matrix of partial derivatives. These are calculated either by forward differencing or analytically, whichever is faster. As mentioned previously, the problem is strictly linear with respect to $\bar{U}$ and D, thus these derivatives are evaluated analytically.

Because $\alpha\omega d$ is much less than one, the problem is almost linear with respect to α also. The α partial derivative may be evaluated either analytically or by forward differencing. The partial derivatives with respect to velocity are analyzed most easily by forward differencing while the impedance derivatives are calculated analytically.

The arrays in this inversion problem are quite large. For example the A matrix in equation (14) is 256 x 133 for the four level, thirty-two frequency case. The matrix to invert is symmetric and positive definite (with sufficient damping). Thus storage space is reduced by about one-half. This matrix is then inverted using a Cholesky decomposition. This fast decomposition expresses the matrix as the product of a triangular matrix and its transpose. The triangular matrix inversion is rapidly accomplished. As mentioned earlier, there are two inversions used here.

When impedance is not considered, the simple WLS formulation is used. The strategy adopted to find a solution (after Marquardt, 1963) in the WLS algorithm is to first introduce a large damping term in equation (19). This inverse then gives a parameter change direction which corresponds to the gradient direction of the error surface. This damping is decreased with further iterations and the inverse parameter change direction takes on the form of the Gauss-Newton step. The damping is almost reduced to zero. When impedances are used as parameters, the stochastic inverse is employed. The Cholesky algorithm is again used to find the inverse matrix.

The process of updating the parameters is usually repeated until the calculated spectra match the observed spectra to a predetermined accuracy or the parameters are not changing significantly. In practice this usually requires from five to ten iterations. Most of the cases discussed here are given a maximum of ten iterations.

4.5 SYNTHETIC DATA

The WLS and stochastic algorithms are first tested on synthetic data. The testing is accomplished by generating (via the wave equation) a set of four "observed" traces with given velocities, attenuation and upgoing and downgoing waves. In the stochastic case, impedances are also included. Noise may be added to the observed traces. The algorithm is then given a "guessed" set of parameters differing substantially from those of the observed traces. The procedures attempt to match the noisy traces by altering the guessed parameters.

4.5.1. WLS Inverse

Four of the numerous trials with the WLS algorithm are discussed in this section. In the first case, noise free data are inverted. In the

second case, traces mixed with substantial noise are processed. The initial and final traces are compared to the observed data.

In the next example, a small amount of noise is added to the observed data, but the extracted upgoing and downgoing waves are also displayed. The fourth example shows the problems incurred when the velocity contrast is between the first and second traces in the observed data as opposed to the second and third traces as is assumed in the model.

In the noise-free case, upper and lower observed velocities and attenuation are 4,000 ft/s, 7,000 ft/s and 4.0×10^{-6} Neper(N)-s/radian-ft. The initial guessed velocities are 6,000 ft/s, 9,000 ft/s and 1.0×10^{-6} Neper-s/radian-ft. The traces are separated by 40.0 ft. A sinusoidal downgoing wave and a smaller, shifted sinusoidal upgoing wave are used in observed seismograms sets. They have periods of 24 ms. The guessed sinusoids have periods of 16 ms.

Deciding on what values to use in the scaling matrices is a somewhat subjective task. The data scaling factor, in this case, is given a value of about 0.1% of the maximum observed trace amplitude. This data scaling is taken to be the same for all of the observations. The model parameter scalings are different for each type of parameter. Recall that the inversion is performed for 64 downgoing wave spectral amplitudes, 64 upgoing spectral amplitudes, 2 velocities and an attenuation. The spectral parameter scalings are chosen to be slightly smaller than the data variance. The magnitude of the spectral parameters is about 10.0 in the synthetic cases calculated, thus the parameter scalings are chosen as about 0.01. The velocity and attenuation scalings that were used are approximately the magnitude of the step required to achieve the true solution.

After six iterations the calculated velocities and attenuation are well within 1.0% of the observed values. The "observed" data and initial guess are shown in Figure 5. The final calculated trace and the noise free observed trace are shown in Figure 6. To within the width of the lines drawn, they are identical.

As the added damping is quite small, the resolution matrix is very close to the identity matrix. The velocities and attenuation are well resolved. Each iteration of the routine requires approximately 1-2 minutes of CPU time on the VAX 11/780 system.

The same observed data in the frequency domain are mixed with considerable white noise (S/N = 20 dB) and shown in Figure 7. The inversion is now performed. The results after 10 iterations are shown in Figure 8. The algorithm is able to match the observed traces quite closely. In fact as there is little signal at high frequencies, there appears to be some matching of the noise also.

For the third and fourth examples, five synthetic traces are generated. A velocity contrast is placed between the second and third traces. The third case processes these data with the model velocity contrast in the same position. The fourth case shifts down one trace so that the observed velocity contrast is one level spacing above the contrast assumed in the model.

The upper layer (2000 - 2060 ft) has a velocity of 4000 ft/s while the lower layer (2060 - 2160 ft) has a 7000 ft velocity. The attenuation coefficient is given a value of 2.0×10^{-6} Nepers-s/rad-ft. The downgoing source is a sinusoid with a 32.0 ms period. An upgoing sinusoid, delayed 80.0 ms from the downgoing arrival at the deepest trace, is also included. A signal-to-noise ratio of 26.0 dB is used.

The initial guesses (zero upgoing trace, downgoing trace equal to the uppermost trace) and observed data are shown in Figure 9. After ten iterations, the final calculated traces (Figure 10) are very close to identical to the observed traces. The residual in this case is 0.6, and the velocities and attenuation estimates are close to those of the original data (see Table 1). Figure 11 shows the downgoing trace, which as expected, is close to a pure sine cycle. The upgoing waves are displayed in Figure 12. The intersection of first-breaking downgoing and upgoing energy gives the depth of generation of the primary reflection (about 2060 ft here). The later upgoing energy has also been extracted.

The next trace group inversion is shifted down one level. Now, the model does not fit the data. The observed data and initial guesses are displayed in Figure 13. After ten iterations, the correspondence of the calculated data to the observed is only moderate (Figure 14). The value of the residual is 1.7, which is twice as large as the previous case. The upper calculated velocity is 5316 ft/s which is close to the average of the two observed layers weighted according to the present geometry (table 2). There is a substantial overestimate of the attenuation coefficient. This is largely due to the decrease in the amplitude of the observed traces due to the original velocity contrast. In the model, there is a much smaller contrast causing a smaller reflection (r.c. = -0.12). Thus the disappearance of amplitude is ascribed to attenuation. It is seen in Figure 15 that the reflection itself in the top trace is partially modelled as the source waveform. This too must be attenuated in the lower three traces.

To match the top trace some upgoing energy is required. But aside from the small amount of reflected energy, upgoing waves must come in from

the bottom trace. This upwardly propagating energy is seen leading the first downgoing arrivals in the bottom two traces. Clearly this is contamination due to the model misfit. Thus two indicators, unrealistic arrivals and a large residual, are diagnostic of a mismatch of the model to the data.

4.5.2 Impedance Stochastic Inverse

The WLS algorithm has been able to extract seismic parameters rather well from the previous synthetic examples. It is of great interest however to be able to gain some information on the impedances underlying the observations. As discussed previously there is theoretically no unique solution for the impedances. It is possible to estimate the impedance ratio or approximately the impedance difference, but not the impedances themselves. Thus the stochastic method is used.

Seismograms with the same values as Figure 5, but now including impedances of $9.2*10^3$ g-ft/cc-s and $17.5*10^3$ g-ft/cc-s for the upper layer and lower layer, are calculated. They are mixed with noise (S/N=20 dB). Data and parameter scalings are also taken as before with the scaling factors for the impedance set to 5.0% of the initial guesses. These values and the final results are given in Table 3. Even with the large amount of noise in the data the velocities are well estimated. The impedance difference is also reasonable. The impedances themselves are too high. This is because the initial guess was too large. The algorithm brought these guesses into agreement with the relationship defined by the reflection coefficient by moving them a minimal distance.

Supposing that there are better guesses at the impedance and the data are mixed with less noise (10,000 g-ft/cc-s , 16,000 g-ft/cc-s; S/N=60 dB)

then the final impedances, after 10 iterations, are much closer to the actual values (see Table 4).

Thus some information on impedance and then density may be extracted. However, a good initial guess is required to fix the impedance estimates absolutely.

4.6 FIELD DATA

The WLS and stochastic algorithms are now used on real data. The observed data are from the ARCO geophysical test site near Sulphur Springs, Texas. As discussed in previous chapters this VSP survey (called the ENIX VSP) used an impulsive source placed 100 ft away from the wellhead. Recordings were made every 25 ft from T.D. at 2175 ft to the surface. A sonic log from the same well is shown in Figure 17. Note the large velocity contrast apparent at 2000 ft. This is the contact between a Taylor group marl and the Pecan Gap limestone.

4.6.1 WLS Inverse

To illustrate the inversion procedure, four traces straddling the velocity contrast at 2000 ft are taken and processed with the WLS inversion. Their depths are 2100 ft, 2025 ft, 1950 ft and 1875 ft. They are shown in Figure 18. The initial guess at the downgoing wave is taken to be identical to the uppermost trace. The upgoing trace is started at zero. Average velocities are taken from the sonic log. The spectral amplitudes of the field data vary from 0.0 to about 100.0. They are weighted (the E matrix) with standard deviations of 1.0. The guessed traces are also shown in Figure 18.

To make all the eigenvalues about equal to 1.0 it is found that a standard deviation of 5% of the guessed attenuation value and 0.5% of the velocities is necessary for the parameter weights. The guessed spectral

amplitudes are given a standard deviation of 0.5. This weighting is thus quasi-logarithmic. Ten iterative updates of the parameters were performed The resolution matrix was very close to diagonal (.998 on the diagonal; zeroes elsewhere). The final parameter estimates and standard deviations are given in Table 5.

Note that the standard deviations for the velocity of this full waveform inverse are about 39 ft/s and 104 ft/s while with the traveltime inverse on the same data the standard deviations are on the order of 500 ft/s. The full waveform algorithm is able to constrain the velocities better than the traveltime inverse, as would be expected from the greater quantity of data used. The observed traces and final calculated time domain traces after 10 iterations are shown in Figure 19. The fit is quite good. The velocities determined from the inversion are 7485 ft/s and 10,870 ft/s for the upper and lower layers respectively. The average sonic log values for these depths are 7530 fts/ and 11,000 ft/s.

It is instructive to plot the extracted downgoing and upgoing waves which add together to give the total observed seismograms. Figure 20 shows the observed traces as well as the total downgoing wavefield. Note that below the interface most of the trace is composed of downgoing energy. Effectively there is a long source function. Above the interface there is some other energy. The extraction of the upgoing waves is an important goal of VSP data processing. In Figure 21, the observed traces and the total upgoing wavefields are plotted. Note the significant reflected energy in the top two traces. Following this reflection back to its intersection with the downgoing wave shows at what depth it was generated. This procedure gives a generation depth at 1995 ft. This corresponds rather well to the sonic log contrast centered at 2000 ft. The upgoing

waveform is very close to the negative polarity of the downgoing wave (as expected from the positive impedance contrast). This provides further evidence of the efficacy of the process as downgoing and upgoing energy are independently estimated. Note also the upgoing energy at the tail end of the traces. This is a reflection from below the bottom of the borehole. While it is difficult to guess by eye at the underlying structure in the traces of Figure 18, the inversion performed here is able to simultaneously estimate the velocities and extract the downgoing and upgoing waves. The attenuation coefficient determined for these four traces was 3.5×10^{-6}, which corresponds to a Q value of about 16. This Q value is quite low indicating high attenuation. The data seems to demand it however. If the peak-to-peak decay across the traces in Figure 18 is calculated for the dominant frequency of 28.0 Hz then a Q value of 5 is determined.

As mentioned earlier this inversion technique is applied to a group of four traces, then applied to an adjacent group of traces and so on from the bottom of the data upwards. The process is started from the bottom because the data correspond best to the normal incidence model at depth. Starting from the data top or bottom should make little difference to the final answer.

Ten groups of traces separated by 75 ft are next sequentially processed. The results are shown in Table 6. Q values are from about 8 to 80. Where alf = 1.0×10^{-8} no attenuation was resolvable. A good fit is judged by the residual being around 1% of the maximum spectral value (residual less than 2 for the lower traces; 4 for the upper traces). The attenuation in the bottom trace group is fairly large (as is the residual). This may be due to the complex stratigraphy evident on the sonic and density logs. Short path multiples are generated by the impedance

mismatches. Using the time delay formula from Chapter 3 and the ENIX sonic log for this region suggests that there will be only 0.05 ms seismic delay. This corresponds to a very large Q value. The actual data nonetheless will still contain longer path multiples as well as other interferences. This effectively adds noise into the data and probably some attenuation (as compared to the two layer model). As was noted in the section dealing with synthetics, a misplaced boundary can cause an anomalously high attenuation coefficient to be estimated. This appears to be very similar to the present case as there is a contrast at 2000 ft while the top trace of this group is at 1950 ft.

The velocities determined are similar to the averages of the sonic log across the corresponding regions but slightly lower. Anticipating later results, these velocities are also close to the averages of the VSP velocities from trace groups separated by 25 ft and 50 ft.

Ten groups of traces now separated by 25 ft are processed. Table 7 shows the inversion results. Again the velocities are similar to the sonic values in the same areas.

Comparing the 75 ft inverse with the 25 ft case, shows that the 25 ft case generally has smaller residuals. This is partially because less velocity structure and other noise is introduced into the observed data. However the errors on the parameters are generally several times larger than in the 75 ft case. For example errors in the attenuation coefficient are from 1.0-2.1 x 10^{-6} N-s/rad-ft. This is often as large as the attenuation coefficient itself. In the 75 ft case the errors are from 0.4-1.0 x 10^{-6} N-s /rad•ft which shows a considerable better estimate. The errors in the velocity for the 25.0 ft case are generally from 100-250

ft/s, while in the 75.0 ft case from 30-200 ft/s. The 50 ft separation case has errors intermediate to these previous two cases.

If for example, attenuation is the parameter of interest, then an inversion using 75 ft spacing is the best choice. If velocity resolution is required then the 25 ft case is more appropriate.

The next example gives the results of inverting traces separated by 50.0 ft from 2175 ft to 1075 ft. The parameter estimates and residuals for 20 trace groups of the ENIX data are given in Table 8. Ten iterations were performed for each group. Figure 22 shows the observed data and the calculated results of a four group inversion for ten depths. Spectral data have values ranging from 0.0 to 100.0. The final spectral RMS residuals are from 0.8 to 4.9 (see Table 8). The resolution matrix in all cases is exceedingly close to the identity matrix (all diagonal entries are greater than 0.98). The velocities from this inversion are plotted with the sonic log in Figure 17. Note that the seimic velocities are somewhat lower than the sonic values.

In Chapter 3 it was observed that the ENIX data had a traveltime residual of about 7.0 ms/1000 ft. It is interesting to see if this agrees with the slightly lower velocities observed from the waveform inversion. Consider for example the depths 1675-1875 ft which had reasonably good velocity inversion. The slownesses were about 7.0 μs/ft larger than the sonic slownesses (see Figure 17). This gives a traveltime residual of 7.0 ms/1000 ft, just as found before using the total traveltimes as opposed to interval velocities. Thus traveltime residuals and interval velocity differences agree for this region.

Once the inversion is complete and all the seismic parameters have been estimated, they are put back into the model and the total upgoing and

downgoing waves are calculated. The downgoing waves are displayed in Figure 23. Note that the waveforms are fairly consistent from trace group to trace group, but are losing the high frequencies with downward propagation. A slight bend in the arrival time line is visible at around 1975 ft, indicating the velocity change. There is no upgoing energy apparent. Note also the loss of amplitude between the 1975 ft depth and the 2025 ft depth. This is due to the reflected energy loss.

There is great interest in the upgoing wavefield as lithologic structure has more obvious effects on it than the downgoing wave. Figure 24 displays the extracted upgoing waves. These are calculated in the same manner as before; the inversion estimates the seismic parameters and these are put back into the model and the total upgoing wavefield is generated. Apparent in Figure 24, is a large upgoing event generated between 1975 ft and 2025 ft. The traces 2075-1925 ft are from one inversion. They indicate only a moderate fit after 10 iterations, with a residual of 2.1. Normally this particular group would be removed, but is included here to show a substandard fit. Nonetheless, it is still clear that the major reflector is somewhere just below 1975 ft. The previous example in Figures 10-13 is from this same region. In this previous case though, the traces were separated by 75 ft. The fit was much better with a residual of 1.37. This may be so because of the gradient nature of the velocity. The sonic log (Figure 17) shows that the velocity change occurs from about 1990 ft to 2040 ft. Because of this there is probably still downgoing energy being reflected at the 2025 ft trace. But in this group inversion the reflector is put at 2000 ft. Thus the algorithm must assume that the upgoing energy at 2025 ft is coming from below at 2075 ft thus some of the reflected energy is put into the incident upgoing wave. This contamination can be

seen on the trace at 2075 ft. Again this problem is evident in the large data residual and indicates that the fit is poor. This group could be left out or reanalyzed with a different spacing. Thus traces spaced farther apart are more likely to correspond to the one interface model than those closely spanning a transitional zone.

The upgoing wave at the tail end of the traces is again evident. This is a reflection from below the bottom of the borehole. By the polarity of the event, it too appears to have been generated by a positive impedance contrast. If the velocities were, on the average 9000 ft/s (approximately the average velocity over the bottom 400 ft of the ENIX well), then this reflection would meet the direct arrival at a depth of about 2700 ft. This would locate the impedance contrast. This result is surprisingly well corroborated from a well-log in a closely neighboring well. The high velocity Austin Chalk at a 2690 ft depth is found to underlie a shaley low velocity section (DiSiena, 1983). This explains the event and its polarity.

4.6.2 Impedance Stochastic Inverse

The stochastic inverse is now used with real data. The traces shown in Figure 18 are again inverted. The impedances are guessed to be 2.4 g/cc x their corresponding layer velocities. The standard deviations are 1.0% of this. The other parameters are taken as before.

The results of this inversion are displayed in Table 9. Note that the residual has been reduced slightly and that velocity estimates are again similar to those of Table 5. They are now well resolved (0.95 on the resolution matrix diagonal). The impedance estimates are 17150 g•ft/cc.s and 25533 g•ft/cc.s. Dividing these by their respective layer velocities gives density values of 2.28 g/cc and 2.37 g/cc. Interpreting these values

in light of the previous discussion, gives confidence that a significant density contrast (0.1 g/cc) does in fact exist. Assuming that the initial impedance guesses were reasonable allows some confidence to be put in this result. The corresponding resolution diagonals for the impedances still sum to one. But because the residual has been reduced and the values bear some correspondence to those observed on the density log, it appears that a good solution has been reached. The ten groups of four traces with 75 ft spacing are again processed. The results are given in Table 10. For most of these depths there is little impedance contrast and density estimation is poor. The densities estimated are from 2.0 g/cc to 3.0 g/cc but bear little resemblance to the density log. The values from the 25 ft spaced trace inversion are given in Table 11. This spacing appears to be too small to constrain the reflection coefficients and thus the densities.

The 50.0 ft separation as noted previously does not perform as well at the 2000 ft area as does the 75.0 ft separation. Nonetheless an eight group inversion is performed with a 50.0 ft trace separation. The results are given in Table 12. The solution is not enhanced where the large reflection coefficient occurs, but is somewhat better at the 1975 ft level. It appears that the 50 ft model corresponds to the small change evident on the well-logs. At this depth, the density estimates of 2.16 g/cc and 2.13 g/cc are similar to those observed on the density log (2.23 g/cc and 2.19 g/cc). Again the differences are resolved due to a correct spacing, good initial guess and the presence of a reflection coefficient.

Generally, the inversion with impedance can provide reasonable constraint on the densities but only in areas of impedance contrast with the appropriate receiver spacing when a good initial guess may be made.

4.7 LIMITATIONS

There are a number of bounds on the applicability of the previous algorithms. As written the forward model requires normal incidence plane waves (corrected for spherical divergence) on a horizontal interface. In areas of complex geology, this will obviously not apply. If the source is offset a significant distance from the well-head, relative to the depth of consideration, the model again will not apply. It is important to consider the limits of the forward model in correspondence to field data. First, suppose that the source is offset some distance from the well head, causing an angle of incidence θ at the receiver group. Now considering just interval velocities the actual velocity V is related to the apparent (measured) velocity V_{app} by

$$V_{app} = \frac{V}{\cos\theta} \tag{25}$$

Assuming that θ is small then

$$V_{app} = V(1+\frac{\theta^2}{2})$$

Suppose the limit of applicability of the model is defined as that θ such that V_{app} is only 1% different than V. Then $\theta<8°$. For receiver depths below about 700 ft the ENIX source offset (100 ft) is within the bounds developed above.

Another concern is the suitability of the amplitude-corrected plane wave model as applied to actual results from a point source. Generally, it is conceived that far enough from the point source the wavefronts will be approximately planar. One way to quantize this is through the Fresnel zone concept. It is reasonable to suppose that if a plane wave and spherical wave are very similar over the first Fresnel zone of an area above the receivers, then the receivers are insonated in a similar manner.

Consider first the Fresnel zone radius X. As shown in Appendix V

$$X = \left(\frac{\lambda R R_s}{R+R_s}\right)^{1/2}$$

where λ is the wavelength

R is the interface to receiver distance

R_s is the interface to source distance

It will be assumed that if the traveltimes from the edge of the Fresnel zone for the spherical and plane wave are not significantly different relative to the wave period then the spherical wave is well-approximated by the plane wave.

In Appendix V it is shown that distance difference between the wave types at the Fresnel radius is

$$r = \frac{X^2}{R_s}$$

If $\frac{r}{V} \ll T$ then the plane wave assumption is appropriate. In the ENIX case r is about 10 ft, $V \sim 10^4$ ft/s and $T = 4 \times 10^{-2}$ sec. Thus the above condition is well-satisfied.

The algorithm guesses the downgoing and upgoing waveforms for each group. Thus the effect of short-path multiples on the downgoing wave will always be included but never isolated in the extracted downgoing wave. That is, the extracted downgoing wave may change shape slightly in a manner not predicted by the attenuation and transmission coefficients.

Attenuation is modeled as varying linearly with frequency, thus a constant Q value is always calculated.

Another limitation concerning the forward model is that the interface is put in the middle of the observations. As noted in previous sections, when this is not the case the solution is degraded. A way to partially ameliorate this would be to have the interface position as an adjustable parameter.

4.8 DISCUSSION

In many cases the VSP is conducted in regions of largely horizontal sedimentary strata. The survey generally uses sources which are offset from the well-head only a small distance (especially relative to the receiver depth). Thus for a great deal of data the zero-offset one-dimensional limitation is not severe. As shown previously, an offset source, computationally more demanding, requires no conceptual changes in the inversion procedure.

The VSP data set often has several limitations which have motivated the piecewise inversion method. While some care is usually taken to ensure a constant source, results are varied. There are a number of reasons for this; source-to-ground coupling varies, the source itself is inconsistent, several sources in a multiple source array may not always function or may behave erratically.

Likewise, the receiver output may be variable because of a change in the clamping of the geophone to the borehole wall or if the well is cased, a poor bond of the casing to the formation. The data itself then is often only piecewise similar.

Similarly, data are sometimes collected over only specific intervals in the subsurface. This too requires that an inversion technique need only specific intervals of data and not samples of the whole section.

Recall that f-k filtering has been used successfully to separate upgoing and downgoing waves. However there are edge effects to these filters as well as problems associated with non-uniform vertical trace spacing. The waveform inverse described previously does not suffer from these difficulties and furthermore needn't use more than four traces at a time.

For a full VSP section this algorithm finds the parameters of groups of traces independently. To find the upgoing wave at the surface, the upgoing waves extracted from each trace group can be added together (stacked) to form a complete surface trace. A similar procedure can be adopted for the downgoing traces.

As mentioned before, some trace groups will be in vertical positions that have an interface but, contrary to assumption, not between the second and third traces. This will shows up as a poor fit, according to the residuals. On this basis that particular estimation could be rejected. Recall that the algorithm will shift upward one trace at a time, thus there is an excess of parameter estimates. This allows rejection or weighting of some of the poorer estimates. Also if the source waveform or receiver response varies through the four traces, a poor solution will likely be achieved again. This solution could be rejected.

4.9 CONCLUSIONS

Iterative modeling of full waveform seismic data is a viable approach to the estimation of the parameters of a medium. Synthetic data show that the velocity and attenuation of a simple medium may be recovered using the weighted damp least-squares approach. The spectral parameters of the upgoing and downgoing waves may also be estimated. Results from the synthetic seismograms are good. The traces inverted from the ENIX VSP

demonstrate the viability of the algorithm and its use in separating upgoing and downgoing energy. The estimated velocities are very well constrained and after considering velocity dispersion, agree closely with those of the sonic log. Attenuation values are in the normal range for the sediments encountered.

Attempts to invert the traces for density have been partially successful. In regions of high impedance contrast a reasonable density estimate may be achieved with an appropriate model layer spacing and initial guess.

Table Captions

Table 1. WLS inversion results for noisy synthetic data.

Table 2. WLS inversion results for noisy synthetic data using erroneous model.

Table 3. Stochastic inversion results for noise-free synthetic data including impedances.

Table 4. Stochastic inversion results for synthetic data including impedances and noise (S/N=20dB).

Table 5. WLS inversion results for ENIX traces spaced 75 ft apart with bottom depth at 2100 ft. This set straddles a large impedance contrast.

Table 6. WLS inversion results for ENIX traces spaced 75 ft apart with bottom depth at 2175 ft and top depth at 1275 ft.

Table 7. WLS inversion results for ENIX traces spaced 25 ft apart with bottom depth at 2175 ft and top depth at 1875 ft.

Table 8. WLS inversion results for ENIX traces spaced 50 ft apart with bottom depth at 2175 ft and top depth at 1075 ft.

Table 9. Stochastic inversion results for ENIX traces spaced 75 ft apart with bottom depth at 2100 ft. This group straddles a large impedance contrast. Impedances are estimated and densities calculated from them.

Table 10. Stochastic inversion results for ENIX traces spaced 75 ft apart with bottom depth at 2175 ft and top depth at 1275 ft. Impedances are estimated and densities calculated from them.

Table 11. Stochastic inversion results for ENIX traces spaced 25 ft apart with bottom depth at 2175 ft and top depth at 1425 ft. Impedances are estimated and densities calculated from them.

Table 12. Stochastic inversion results for ENIX traces spaced 50 ft apart with bottom depth at 2175 ft and top depth at 1525 ft. Impedances are estimated and densities calculated from them.

Figure Captions

Figure 1. Normal incidence wave propagation in an attenuating medium across a boundary.

Figure 2. Upgoing and downgoing waves for four equally-spaced receiver positions on either side of a boundary.

Figure 3. Incident P waves at some angle to the boundary of two attenuating media. Note the converted waves.

Figure 4. Incident P waves on an interface dipping at an angle θ, with the horizontal.

Figure 5. Synthetic traces (solid lines) and initial guessed traces (broken lines).

Figure 6. Synthetic traces (solid lines) and final calculated traces which are indistinguishable from them.

Figure 7. Noisy synthetic traces (solid line) and the initial guess (broken line).

Figure 8. Noisy synthetic traces (solid line) and final calculated traces (broken line) after 10 iterations.

Figure 9. Noisy synthetic traces (solid line) and initial guess (broken line).

Figure 10. Noisy synthetic traces (solid line) and calculated traces after 10 iterations. The two are largely indistinguishable.

Figure 11. Noisy synthetic traces (solid line) and extracted downgoing event (broken line).

Figure 12. Noisy synthetic traces (solid line) and extracted upgoing event (broken line).

Figure 13. Noisy synthetic traces (solid line) and initial guess (broken line) using erroneous model.

Figure 14. Noisy synthetic traces (solid line) and calculated traces after 10 iterations using gerroneous model.

Figure 15. Noisy synthetic traces (solid line) and extracted downgoing event (broken line) using erroneous model.

Figure 16. Noisy synthetic traces (solid line) and extracted upgoing event (broken line) using erroneous model.

Figure 17. ENIX sonic log. Note velocity contrast at 2000 ft.

Figure 18. ENIX field traces (solid line) and initial guessed traces (broken line).

Figure 19. ENIX field traces (solid line) and final calculated traces (broken line).

Figure 20. ENIX field traces (solid line) and total estimated downgoing wavefield (broken line).

Figure 21. ENIX field traces (solid line) and total estimated upgoing wavefield (broken line).

Figure 22. ENIX field traces (solid line) and final calculated traces (broken line).

Figure 23. ENIX total downgoing wavefield.

Figure 24. ENIX total upgoing wavefield. Dots indicate first arrivals from Figure 23. One cycle of the upgoing reflection is shaded. An upgoing reflection from below the well is also shaded.

```
bottom depth= 212Ø ft  top depth= 2ØØØ ft  trace spacing= 4Ø ft

INPUT:
data weight= 1.ØØØØØ
spectral parameter weight= Ø.5ØØØØØ
v1 scale= 2ØØ.ØØØØ   v2 scale= 2ØØ.ØØØØ   alf scale= 1.ØØØØØe-Ø7
marquardt parameter= 5.ØØØØØ

v1 observed= 4ØØØ.ØØ  v2 observed= 7ØØØ.ØØ  alf observed= 2.ØØØØØe-Ø6
# iterations= 1Ø

RESULTS:
v1= 3977.81 ft/s   v2= 7153.1Ø ft/s    alf= 3.19Ø47e-Ø6 N-s/rad*ft

v1 err= 23.8171   v2 err= 94.1Ø35   alf err= 9.14Ø25e-Ø7
r.c.= -Ø.2855Ø37   t.c.= Ø.7144963
resid=  Ø.686955
```

Table 1.

```
bottom depth= 216Ø ft  top depth= 2Ø4Ø ft  trace spacing= 4Ø ft

INPUT:
data weight= 1.ØØØØØ
spectral parameter weight= Ø.5ØØØØØ
v1 scale= 2ØØ.ØØØØ   v2 scale= 2ØØ.ØØØØ   alf scale= 1.ØØØØØe-Ø7
marquardt parameter= 5.ØØØØØ

v1 observed= 4ØØØ.ØØ  v2 observed= 7ØØØ.ØØ  alf observed= 2.ØØØØØe-Ø6
# iterations= 1Ø

RESULTS:
v1= 5315.95 ft/s   v2= 6659.31 ft/s    alf= 1.8Ø98Øe-Ø5 N-s/rad*ft

v1 err= 155.651    v2 err= 3ØØ.834     alf err= 3.1Ø943e-Ø6
r.c.= -Ø.1167ØØ3   t.c.= Ø.8832997
resid=    1.73676
```

Table 2.

```
bottom depth = 2120 ft  top depth= 2000 ft  trace spacing= 40 ft

"observed" parameters
 v1= 4000.00 ft/s  v2= 7000.00 ft/s  alf=4.000000e-06 N*s/ft*rad
 z1= 9200.00 g*ft/cc*s   z2= 17500.0 g*ft/cc*s
 period= 32.0 sec
 S/N= 20dB

data weight= 1.000000
spectral parameter weight= 0.800000
v1 scale= 200.000  v2 scale= 200.000   alf scale= 2.000000e-07
z1  scale= 550.000   z2 scale= 550.000
marquardt param.= 0.150000
v1 start=5000.0 ft/s  v2 start= 8500.0  alf start= 1.000e-06 N*s/rad*ft
z1 start= 8000.00 g*ft/cc*s  z2 start= 20000.0 g*ft/cc*s
# iteratons=10

resid=    2.04796
v1=    4020.32   ft/s    v2=    6974.58   ft/s   alf=    2.52322e-06
z1=    10225.4  z2=    19327.3
d1=    2.54344   g/cc     d2=    2.77111   g/cc
r.c.=  -0.304   t.c.=  0.696
typical parm err.=1.37190
v1 err=58.4623  v2 err= 235.033  alf err= 6.49182e-07
z1 err=473.697  z2 err= 252.906

resolution diagonal
spec. =0.9463  v1 =0.9983  v2=0.9741  alf=0.3088  z1=0.7633  z2=0.2176
```

Table 3.

```
bottom depth = 2120 ft  top depth= 2000 ft  trace spacing= 40 ft

"observed" parameters
 v1= 4000.00 ft/s  v2= 7000.00 ft/s  alf=4.000000e-06 N*s/ft*rad
 z1= 9200.00 g*ft/cc*s   z2= 17500.0 g*ft/cc*s
 period= 32.0 sec
 S/N= 20dB

data weight= 1.000000
spectral parameter weight= 0.800000
v1 scale= 200.000  v2 scale= 200.000   alf scale= 2.000000e-07
z1  scale= 550.000   z2 scale= 550.000
marquardt param.= 0.150000
v1 start=5000.0 ft/s  v2 start= 8500.0  alf start= 1.000e-06 N*s/rad*ft
z1 start= 10000.00 g*ft/cc*s  z2 start= 16000.0 g*ft/cc*s
# iteratons=10

resid=    0.02459
v1=    4000.14   ft/s    v2=    6995.52   ft/s   alf=    3.96595e-06
z1=    9052.3  z2=    17204.0
d1=    2.26049   g/cc     d2=    2.45929   g/cc
r.c.=  -0.311   t.c.=  0.689
typical parm err.=1.37190
v1 err=0.631223  v2 err= 2.93883  alf err= 2.50288e-08
z1 err=4.96221   z2 err= 2.64040

resolution diagonal
spec. =0.9434  v1 =0.9999  v2=0.9984  alf=0.9666  z1=0.7814  z2=0.2183
v1=    4000.14   ft/s    v2=    6995.52   ft/s   alf=    3.96595e-06
z1=    9042.28  z2=    17204.0
d1=    2.26049   g/cc     d2=    2.45929   g/cc
```

Table 4.

bottom depth= 2100 ft top depth= 1375 ft trace spacing= 75 ft

INPUT:
data weight= 1.000000
spectral parameter weight= 0.500000
v1 scale= 30.0000 v2 scale= 40.0000 alf scale= 1.000000e-07
marquardt parameter= 5.00000
v1 start= 9315.00 v2 start= 9376.15 alf start= 7.39706e-06
iterations= 10

RESULTS:

v1= 7484.62 ft/s v2= 10869.6 ft/s alf= 3.52325e-05 N/rad*ft

v1 err= 38.5869 v2 err= 103.690 alf err= 4.07307e-07
typical param. err= 1.25743
r.c.= -0.1846599 t.c.= 0.8153400
resid= 1.06558

Table 5.

dep=	2175.ØØ ft	resid=	2.81762		
v1=	9315.Ø8 ft/s	v2=	9376.15 ft/s	alf=	7.397Ø6e-Ø6
dep=	21ØØ.ØØ ft	resid=	1.36558		
v1=	7484.62 ft/s	v2=	1Ø869.6 ft/s	alf=	3.52325e-Ø6
dep=	2Ø25.ØØ ft	resid=	2.98295		
v1=	7198.42 ft/s	v2=	8929.41 ft/s	alf=	8.36Ø73e-Ø7
dep=	195Ø.ØØ ft	resid=	2.17655		
v1=	7462.Ø2 ft/s	v2=	7129.84 ft/s	alf=	1.16522e-Ø6
dep=	1875.ØØ ft	resid=	2.Ø6189		
v1=	7389.Ø3 ft/s	v2=	7228.11 ft/s	alf=	1.ØØ[illegible]e-Ø8
dep=	18ØØ.ØØ ft	resid=	1.98838		
v1=	7235.73 ft/s	v2=	7447.55 ft/s	alf=	1.Ø28Ø7e-Ø6
dep=	1725.ØØ ft	resid=	2.12584		
v1=	7123.49 ft/s	v2=	7567.46 ft/s	alf=	1.Ø9659e-Ø6
dep=	165Ø.ØØ ft	resid=	2.58Ø4Ø		
v1=	7661.Ø7 ft/s	v2=	7129.92 ft/s	alf=	3.6583Øe-Ø6
dep=	1575.ØØ ft	resid=	3.1Ø262		
v1=	7854.Ø6 ft/s	v2=	7384.3Ø ft/s	alf=	1.61276e-Ø6
dep=	15ØØ.ØØ ft	resid=	4.89218		
v1=	8167.94 ft/s	v2=	7681.93 ft/s	alf=	1.58916e-Ø6

Table 6.

```
dep= 2175.ØØ ft   resid= Ø.695ØØ4
v1=    1Ø22Ø.2 ft/s   v2=     84Ø7.6Ø ft/s   alf=    5.43825e-Ø7 N/rad*ft

dep= 215Ø.ØØ ft   resid= Ø.62Ø757
v1=    1Ø59Ø.3 ft/s   v2=     1Ø946.7 ft/s   alf=    3.Ø1827e-Ø6

dep= 2125.ØØ ft   resid= Ø.5Ø9799
v1=    11396.2 ft/s   v2=     1Ø839.Ø ft/s   alf=    6.Ø2845e-Ø8

dep= 21ØØ.ØØ ft   resid= Ø.6Ø8741
v1=    1Ø81Ø.7 ft/s   v2=     1Ø252.9 ft/s   alf=    1.53533e-Ø6

dep= 2Ø75.ØØ ft   resid= Ø.616873
v1=    1Ø898.1 ft/s   v2=     9873.6Ø ft/s   alf=    2.39954e-Ø6

dep= 2Ø5Ø.ØØ ft   resid= 1.25229
v1=    9866.1Ø ft/s   v2=     12Ø26.9 ft/s   alf=    1.13887e-Ø6

dep= 2Ø25.ØØ ft   resid= 1.33624
v1=    7451.Ø9 ft/s   v2=     11613.3 ft/s   alf=    4.51972e-Ø6

dep= 2ØØØ.ØØ ft   resid= 1.36458
v1=    6921.33 ft/s   v2=     9192.42 ft/s   alf=    4.52725e-Ø6

dep= 1975.ØØ ft   resid= Ø.757961
v1=    7146.45 ft/s   v2=     7513.Ø9 ft/s   alf=    1.2Ø338e-Ø6

dep= 195Ø.ØØ ft   resid= Ø.7ØØØ69
v1=    7322.55 ft/s   v2=     7199.59 ft/s   alf=    3.95733e-Ø6
```

Table 7.

dep= 2175.ØØ ft	resid= Ø.955811		
v1= 1Ø895.7 ft/s	v2= 9279.Ø6 ft/s	alf=	2.38783e-Ø6 N/ft^5*rad
dep= 2125.ØØ ft	resid= 1.47669		
v1= 1Ø13Ø.6 ft/s	v2= 1Ø43.Ø.3 ft/s	alf=	2.ØØØ26e-ØS
dep= 2Ø75.ØØ ft	resid= 2.31Ø47		
v1= 7882.53 ft/s	v2= 11348.Ø ft/s	alf=	5.454Ø3e-Ø6
dep= 2Ø25.ØØ ft	resid= 2.6Ø212		
v1= 6548.55 ft/s	v2= 1Ø282.7 ft/s	alf=	1.ØØØØØe-Ø8
dep= 1975.ØØ ft	resid= 1.3424Ø		
v1= 75ØØ.46 ft/s	v2= 72ØØ.Ø8 ft/s	alf=	1.82679e-ØS
dep= 1925.ØØ ft	resid= 1.74317		
v1= 7216.51 ft/s	v2= 724Ø.21 ft/s	alf=	5.Ø9182e-Ø7
dep= 1875.ØØ ft	resid= 2.15173		
v1= 73Ø1.25 ft/s	v2= 7314.24 ft/s	alf=	1.ØØØØØe-Ø8
dep= 1825.ØØ ft	resid= 1.93727		
v1= 7287.7Ø ft/s	v2= 7386.9Ø ft/s	alf=	1.11Ø62e-Ø6
dep= 1775.ØØ ft	resid= 2.Ø4741		
v1= 7486.58 ft/s	v2= 7361.59 ft/s	alf=	1.ØØØØØe-Ø8
dep= 1725.ØØ ft	resid= 2.143Ø5		
v1= 74Ø3.94 ft/s	v2= 7216.41 ft/s	alf=	2.56633e-Ø6
dep= 1675.ØØ ft	resid= 1.9739Ø		
v1= 7319.52 ft/s	v2= 761Ø.91 ft/s	alf=	2.46565e-Ø6
dep= 1625.ØØ ft	resid= 1.98842		
v1= 7684.77 ft/s	v2= 7241.99 ft/s	alf=	1.8Ø627e-Ø6
dep= 1575.ØØ ft	resid= 2.36561		
v1= 7458.3Ø ft/s	v2= 7391.47 ft/s	alf=	1.51874e-Ø6
dep= 1525.ØØ ft	resid= 2.23811		
v1= 7712.55 ft/s	v2= 7291.66 ft/s	alf=	2.62846e-Ø6
dep= 1475.ØØ ft	resid= 4.59676		
v1= 822Ø.25 ft/s	v2= 7521.31 ft/s	alf=	2.Ø2688e-Ø6
dep= 1425.ØØ ft	resid= 4.85825		
v1= 7981.Ø5 ft/s	v2= 813Ø.Ø9 ft/s	alf=	1.52638e-Ø6
dep= 1375.ØØ ft	resid= 4.77693		
v1= 7497.63 ft/s	v2= 8Ø74.63 ft/s	alf=	1.549Ø3e-Ø6
dep= 1325.ØØ ft	resid= 3.Ø9711		
v1= 822Ø.25 ft/s	v2= 7521.31 ft/s	alf=	2.Ø2688e-Ø6
dep= 1275.ØØ ft	resid= 2.9Ø698		
v1= 84Ø3.35 ft/s	v2= 7265.6Ø ft/s	alf=	2.17497e-Ø6
dep= 1225.ØØ ft	resid= 3.Ø7155		
v1= 8112.79 ft/s	v2= 7618.35 ft/s	alf=	2.62Ø14e-Ø6

Table 8.

top dep= 1875.ØØ ft bottom dep= 21ØØ.ØØ ft trace sep= 75.ØØ ft

v1= 7518.84 ft/s v2= 1Ø759.46 ft/s alf= 3.18833e-Ø6

err v1= 3Ø.9442 ft/s err v2= 92.2765 ft/s err alf= 2.4172Øe-Ø7

z1= 1715Ø.4 g*ft/cc*s z2= 25533.4 g*ft/cc*s

err z1= 165.Ø32 g*ft/cc*s err z2= 11Ø.936 g*ft/cc*s

>d1= 2.28 g d2=2.37 g

r.c.= -Ø.196Ø426

t.c.= Ø.8Ø39573

resid= 1.34834

Table 9.

```
 bottom depth= 2175 ft  top depth= 675 ft  trace spacing= 75 ft
 data weight= 1.000000
 spectral parameter weight=0.500000
 v1 scale=200.000   v2 scale=200.000   alf scale=2.000000e-07
 z1 scale=550.000   z2 scale=550.000
 marquardt parameter=5.000000e-02
 # iterations= 10

depth=    2175.00   ft     resid=    2.61564
v1=     8968.50   ft/s    v2=     9922.29   ft/s   alf=     1.04716e-05
z1=     23796.0  z2=     19844.6
d1=     2.65328   g/cc     d2=     2.000000   g/cc
r.c.=0.0900482   t.c.=1.0900482
v1 err=129.847   v2 err=246.484   alf err=9.01745e-07
z1 err=449.111   z2 err=538.177
typical param. error= 2.83530

depth=    2100.00   ft     resid=    1.34737
v1=     7516.90   ft/s    v2=     10758.4   ft/s   alf=     3.14868e-06
z1=     15424.2  z2=     22987.2
d1=     2.05193   g/cc     d2=     2.13666   g/cc
r.c.=-0.1968801   t.c.=0.8031198
v1 err=36.2738   v2 err=108.234   alf err=3.54279e-07
z1 err=173.705   z2 err=116.606
typical param.err= 1.15734

depth=    2025.00   ft     resid=    2.39578
v1=     7010.26   ft/s    v2=     9371.04   ft/s   alf=     3.01025e-06
z1=     18959.1  z2=     19456.1
d1=     2.70448   g/cc     d2=     2.07620   g/cc

depth=    1950.00   ft     resid=    2.16739
v1=     7436.83   ft/s    v2=     7151.44   ft/s   alf=     1.49652e-06
z1=     19838.2  z2=     18561.4
d1=     2.66756   g/cc     d2=     2.59548   g/cc

depth=    1875.00   ft     resid=    2.13700
v1=     7442.79   ft/s    v2=     7169.85   ft/s   alf=     1.000000e-08
z1=     19085.1  z2=     19355.0
d1=     2.56425   g/cc     d2=     2.69950   g/cc

depth=    1800.00   ft     resid=    1.88045
v1=     7170.95   ft/s    v2=     7537.41   ft/s   alf=     1.92298e-06
z1=     19496.3  z2=     18904.7
d1=     2.71879   g/cc     d2=     2.50812   g/cc

depth=    1725.00   ft     resid=    2.05284
v1=     7191.30   ft/s    v2=     7494.20   ft/s   alf=     3.39619e-07
z1=     18187.9  z2=     20201.5
d1=     2.52915   g/cc     d2=     2.69562   g/cc

depth=    1650.00   ft     resid=    2.57770
v1=     7649.33   ft/s    v2=     7147.59   ft/s   alf=     3.83023e-06
z1=     19987.0  z2=     18414.3
d1=     2.61290   g/cc     d2=     2.57629   g/cc

depth=    1575.00   ft     resid=    2.93455
v1=     7934.57   ft/s    v2=     7314.08   ft/s   alf=     1.07298e-06
z1=     19071.1  z2=     19328.7
d1=     2.40354   g/cc     d2=     2.64267   g/cc

depth=    1500.00   ft     resid=    4.88218
v1=     8230.31   ft/s    v2=     7621.03   ft/s   alf=     1.20972e-06
z1=     19517.7  z2=     18895.2
d1=     2.37144   g/cc     d2=     2.47935   g/cc

depth=    1425.00   ft     resid=    5.10713
v1=     7774.11   ft/s    v2=     7993.85   ft/s   alf=     1.86228e-06
z1=     19108.2  z2=     19298.6
d1=     2.45792   g/cc     d2=     2.41418   g/cc

depth=    1350.00   ft     resid=    4.25733
v1=     7843.39   ft/s    v2=     8009.36   ft/s   alf=     1.00846e-06
z1=     19162.3  z2=     19239.7
d1=     2.44311   g/cc     d2=     2.40215   g/cc

depth=    1275.00   ft     resid=    2.97772
v1=     8265.17   ft/s    v2=     7501.36   ft/s   alf=     2.75295e-06
z1=     20824.4  z2=     17569.4
d1=     2.51954   g/cc     d2=     2.34216   g/cc

depth=    1200.00   ft     resid=    3.97690
v1=     7274.38   ft/s    v2=     8161.27   ft/s   alf=     3.65720e-06
z1=     18304.0  z2=     20079.8
d1=     2.51623   g/cc     d2=     2.46038   g/cc

depth=    1125.00   ft     resid=    4.71453
v1=     6720.60   ft/s    v2=     8072.79   ft/s   alf=     1.85124e-06
z1=     18292.9  z2=     20209.0
d1=     2.72191   g/cc     d2=     2.50335   g/cc

depth=    1050.00   ft     resid=    3.73467
v1=     6631.39   ft/s    v2=     7318.90   ft/s   alf=     1.66117e-06
z1=     19544.1  z2=     18818.5
d1=     2.94721   g/cc     d2=     2.57122   g/cc

depth=    975.000   ft     resid=    4.05135
v1=     6752.59   ft/s    v2=     6773.19   ft/s   alf=     5.09925e-07
z1=     18949.6  z2=     19493.1
d1=     2.80627   g/cc     d2=     2.87798   g/cc

depth=    900.000   ft     resid=    4.79887
v1=     6613.66   ft/s    v2=     6808.99   ft/s   alf=     4.53279e-06
z1=     19760.9  z2=     17848.2
d1=     2.98789   g/cc     d2=     2.62127   g/cc
```

Table 10.

```
bottom depth= 2175 ft  top depth=1625 ft   trace spacing= 25 ft
data weight= 1.00000
spectral parameter weight= 0.500000
v1 scale= 50.0000   v2 scale=50.0000   alf scale=1.000000e-07
z1 scale=250.000   z2 scale=250.000
marquardt parameter= 0.100000
# iterations= 10

 depth=2175 ft
 v1=    10465.9  v2=    8250.10  alf=    2.24141e-07
 z1=    23243.5  z2=    19885.1
 d1=    2.22088  d2=    2.41029
 resid=   0.689131

 depth=2150 ft
 v1=    11229.2  v2=    10315.8  alf=    3.13971e-07
 z1=    22886.3  z2=    27283.2
 d1=    2.03812  d2=    2.63703
 resid=   0.558813

 depth=2125 ft
 v1=    11462.4  v2=    10778.1  alf=    6.79618e-08
 z1=    27497.5  z2=    26394.9
 d1=    2.39894  d2=    2.45076
 resid=   0.510259

 depth=2100 ft
 v1=    10384.5  v2=    10710.4  alf=    8.68449e-07
 z1=    28838.5  z2=    26126.1
 d1=    2.77700  d2=    2.43750
 resid=   0.591086

 depth=    2000.00
 v1=    10632.2  v2=    10285.8  alf=    8.75774e-07
 z1=    26186.1  z2=    23663.9
 d1=    2.46980  d2=    2.31868
 resid=   0.620115

 depth=    1975.00
 v1=    10387.0  v2=    11298.0  alf=    4.93134e-07
 z1=    21602.9  z2=    28955.6
 d1=    2.07900  d2=    2.56290
 resid=    1.23196

 depth=    1950.00
 v1=    7151.24  v2=    12857.3  alf=    5.71684e-06
 z1=    21172.9  z2=    28977.6
 d1=    2.96074  d2=    2.25378
 resid=    1.27884

 depth=    1925.00
 v1=    6885.81  v2=    9457.41  alf=    6.70755e-06
 z1=    15611.3  z2=    19336.3
 d1=    2.26717  d2=    2.04457
 resid=    1.36252

 depth=    1900.00
 v1=    7162.61  v2=    7521.60  alf=    3.75234e-06
 z1=    16698.4  z2=    16476.7
 d1=    2.31877  d2=    2.19059
 resid=   0.778213

 depth=    1875.00
 v1=    7451.67  v2=    7869.87  alf=    3.94295e-06
 z1=    17177.4  z2=    17206.1
 d1=    2.38517  d2=    2.43373
 resid=   0.737235

 depth=    1850.00
 v1=    7522.16  v2=    7164.78  alf=    3.03220e-06
 z1=    18492.3  z2=    17266.0
 d1=    2.45837  d2=    2.48984
 resid=   0.829381

 depth=    1825.00
 v1=    7587.88  v2=    7162.05  alf=    8.17720e-07
 z1=    18401.2  z2=    17719.2
 d1=    2.42511  d2=    2.47404
 resid=   0.693699

 depth=    1800.00
 v1=    6915.12  v2=    7607.20  alf=    1.000000e-08
 z1=    18430.9  z2=    17993.2
 d1=    2.66530  d2=    2.36520
 resid=    1.17594

 depth=    1775.00
 v1=    7814.98  v2=    7176.46  alf=    2.22601e-06
 z1=    16517.0  z2=    16600.3
 d1=    2.35456  d2=    2.32431
 resid=    1.07775

 depth=    1750.00
 v1=    7364.74  v2=    6940.93  alf=    1.55370e-06
 z1=    16746.7  z2=    16925.7
 d1=    2.27391  d2=    2.43854
 resid=    1.01606

 depth=    1725.00
 v1=    7656.21  v2=    7339.99  alf=    1.000000e-01
 z1=    17653.1  z2=    17709.2
 d1=    2.30572  d2=    2.41270
 resid=    1.78072

 depth=    1700.00
 v1=    7385.42  v2=    7705.97  alf=    1.000000e-08
 z1=    18156.8  z2=    18585.0
 d1=    2.46171  d2=    2.41177
 resid=    2.00708

 depth=    1675.00
 v1=    7009.35  v2=    7698.46  alf=    1.94987e-06
 z1=    17710.0  z2=    17754.9
 d1=    2.52675  d2=    2.30868
 resid=    1.66820

 depth=    1650.00
 v1=    7648.64  v2=    6884.28  alf=    3.98482e-06
 z1=    17167.9  z2=    16476.4
 d1=    2.24457  d2=    2.39333
 resid=    1.49883

 depth=    1625.00
 v1=    7717.72  v2=    7853.31  alf=    4.46215e-07
 z1=    19773.7  z2=    16875.3
 d1=    2.56211  d2=    2.39253
 resid=    1.11562
```

Table 11.

```
dep=  2175      resid= Ø.784Ø15
v1=    11360.1  v2=     9006.12  alf=     1.ØØØØØe-Ø8
z1=    22692.7  z2=     2190Ø3.9
d1=    2.ØØØØØ  d2=     2.43212

dep=  2125      resid= 1.47479
v1=    10112.3  v2=     10519.2  alf=     2.51175e-Ø6
z1=    27284.5  z2=     2730Ø4.8
d1=    2.69815  d2=     2.59572

dep=  2075      resid= 2.138Ø4
v1=    7699.83  v2=     12161.7  alf=     1.Ø3376e-Ø5
z1=    21939.8  z2=     26984.8
d1=    2.84939  d2=     2.21883

dep=  2025      resid= 2.26Ø3Ø
v1=    6562.77  v2=     10920.Ø  alf=     3.78362e-Ø6
z1=    17722.7  z2=     22Ø52.5
d1=    2.7ØØ5Ø  d2=     2.Ø1946

dep=  1975      resid= 1.3416Ø
v1=    7496.18  v2=     72Ø4.33  alf=     2.ØØ284e-Ø6
z1=    16175.Ø  z2=     1537Ø.4
d1=    2.15777  d2=     2.1335Ø

dep=  1925      resid= 1.66Ø54
v1=    7126.16  v2=     7336.1Ø  alf=     1.79657e-Ø6
z1=    18551.Ø  z2=     17447.4
d1=    2.6Ø322  d2=     2.3783Ø

dep=  1875      resid= 2.125Ø1
v1=    7442.13  v2=     7179.34  alf=     1.ØØØØØe-Ø8
z1=    16729.2  z2=     17472.1
d1=    2.24791  d2=     2.43366

dep=  1825      resid= 1.93782
v1=    726Ø.93  v2=     7415.62  alf=     1.43Ø12e-Ø6
z1=    17883.8  z2=     17841.8
d1=    2.463Ø2  d2=     2.4Ø598
```

Table 12.

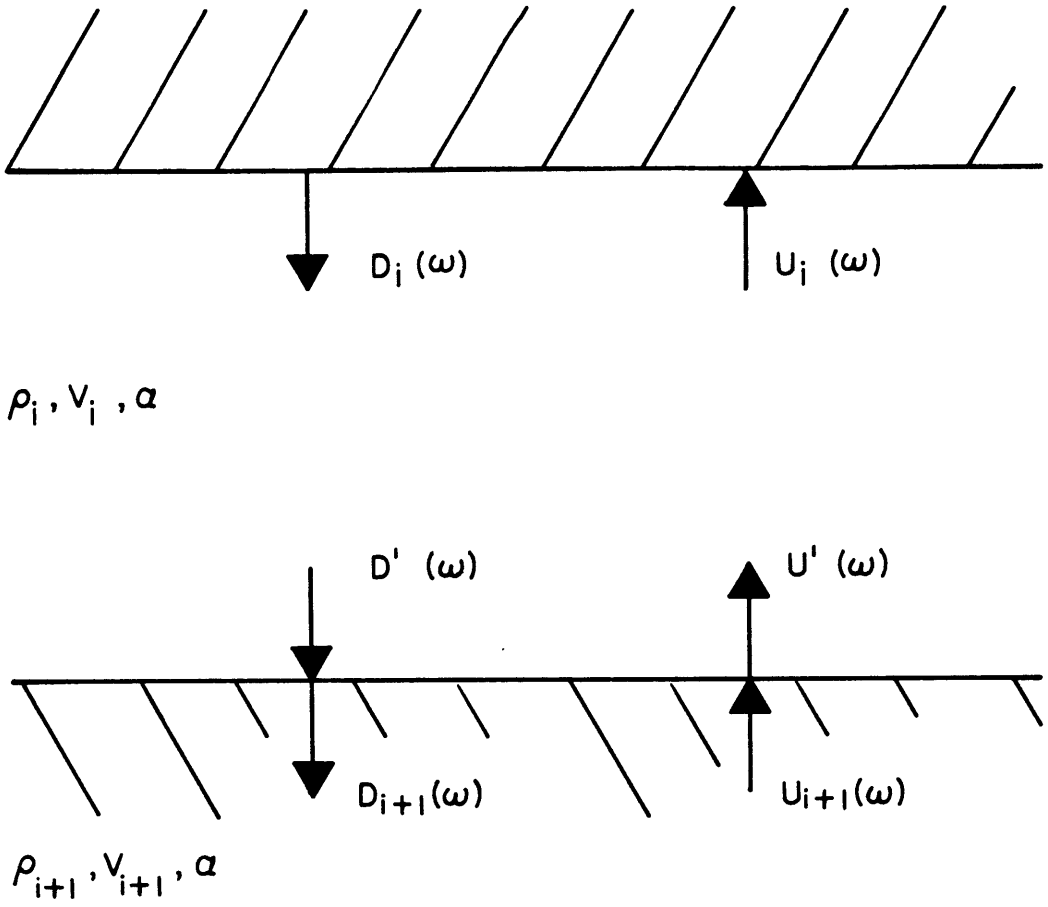
$D_i(\omega)$
$U_i(\omega)$
ρ_i, V_i, α
$D'(\omega)$
$U'(\omega)$
$D_{i+1}(\omega)$
$U_{i+1}(\omega)$
$\rho_{i+1}, V_{i+1}, \alpha$

Figure 1.

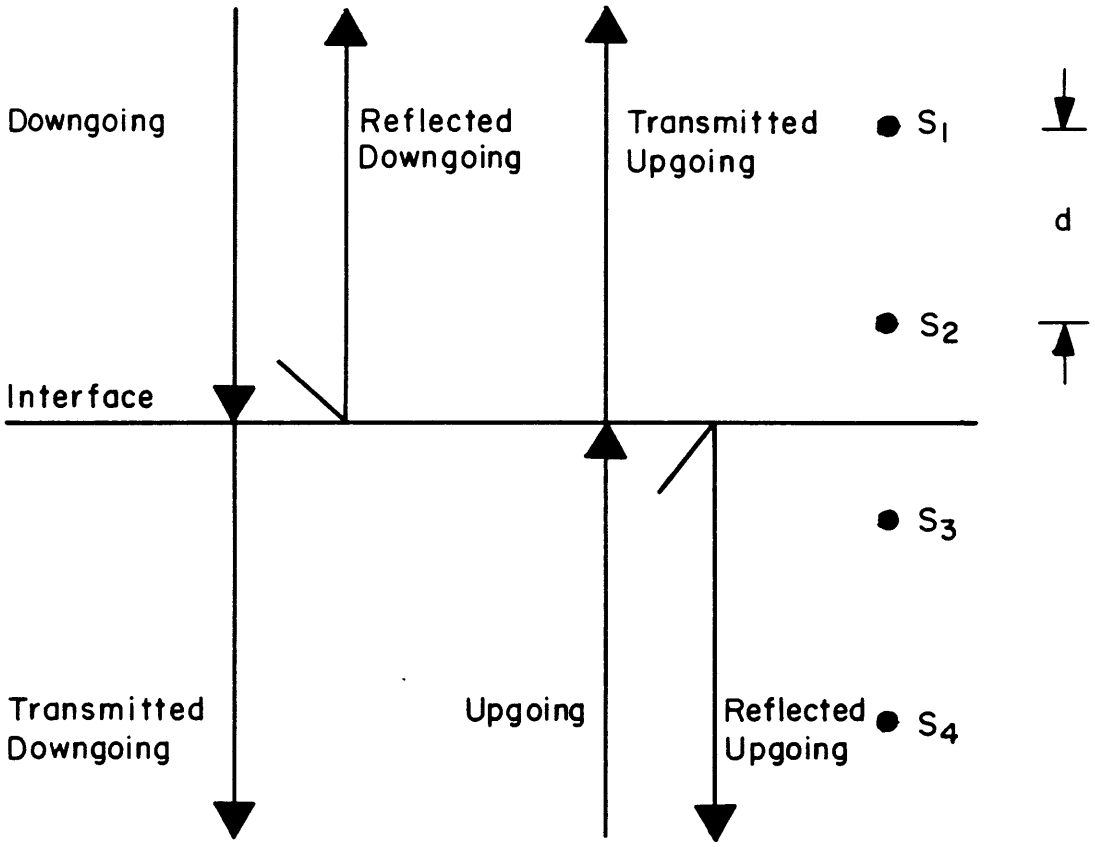
Downgoing
Reflected
Downgoing
Transmitted
Upgoing
S_1
d
S_2
Interface
S_3
Transmitted
Downgoing
Upgoing
Reflected
Upgoing
S_4

Figure 2.

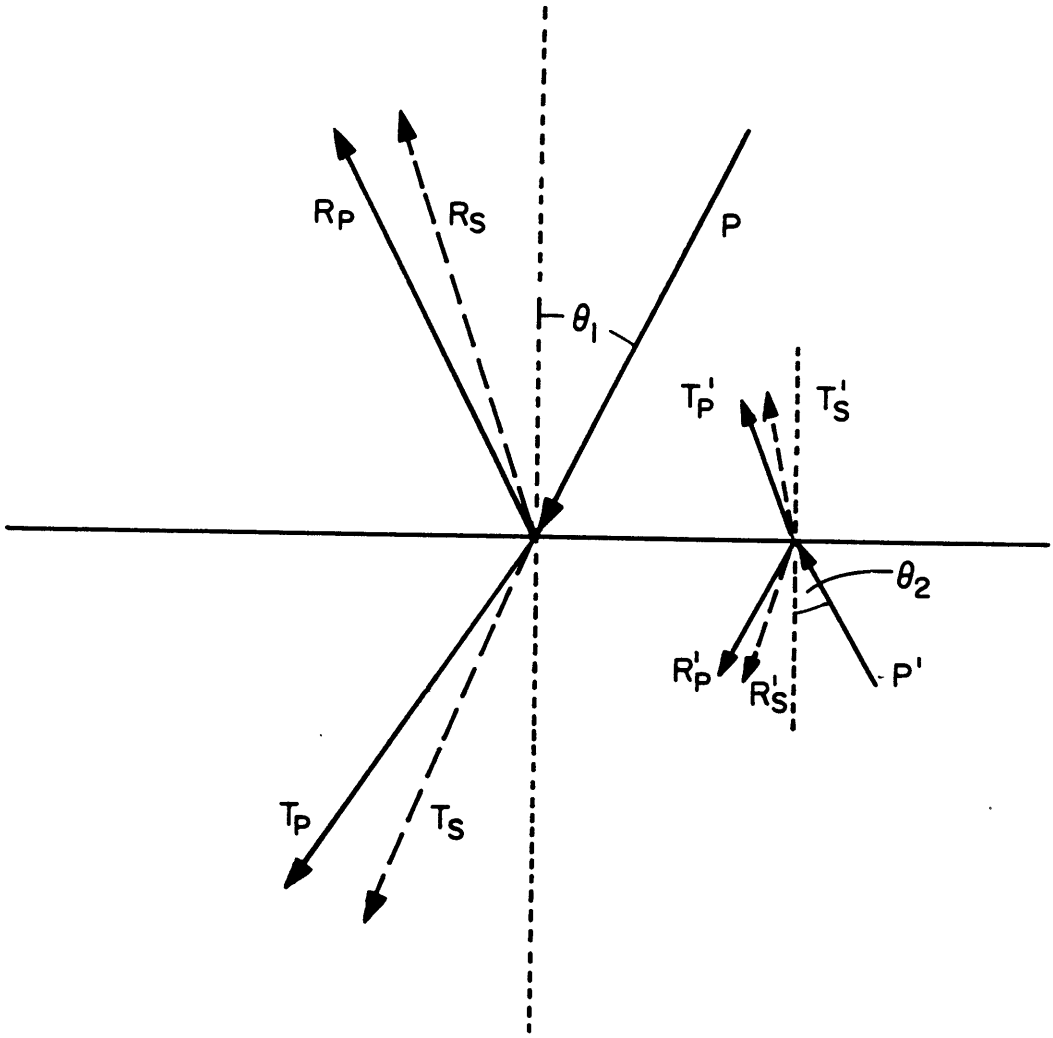

Figure 3.

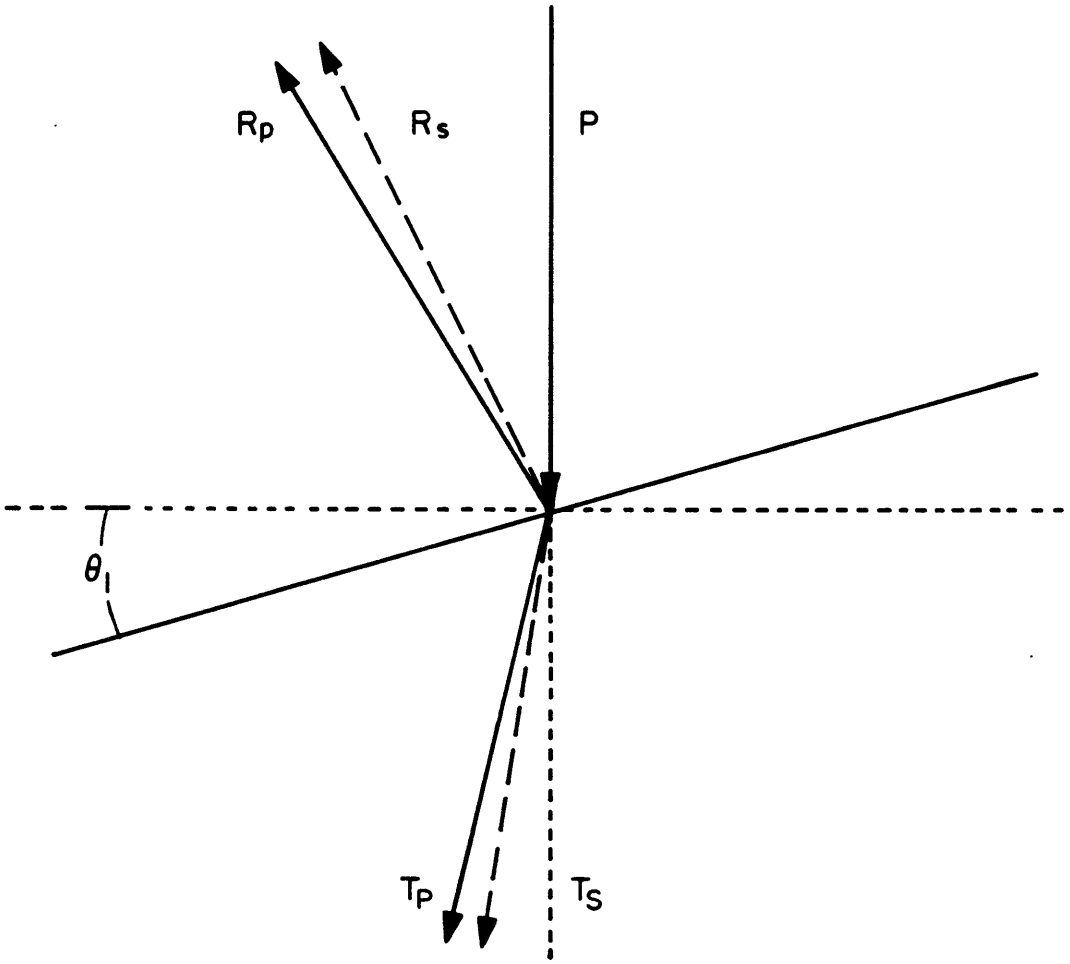

Figure 4.

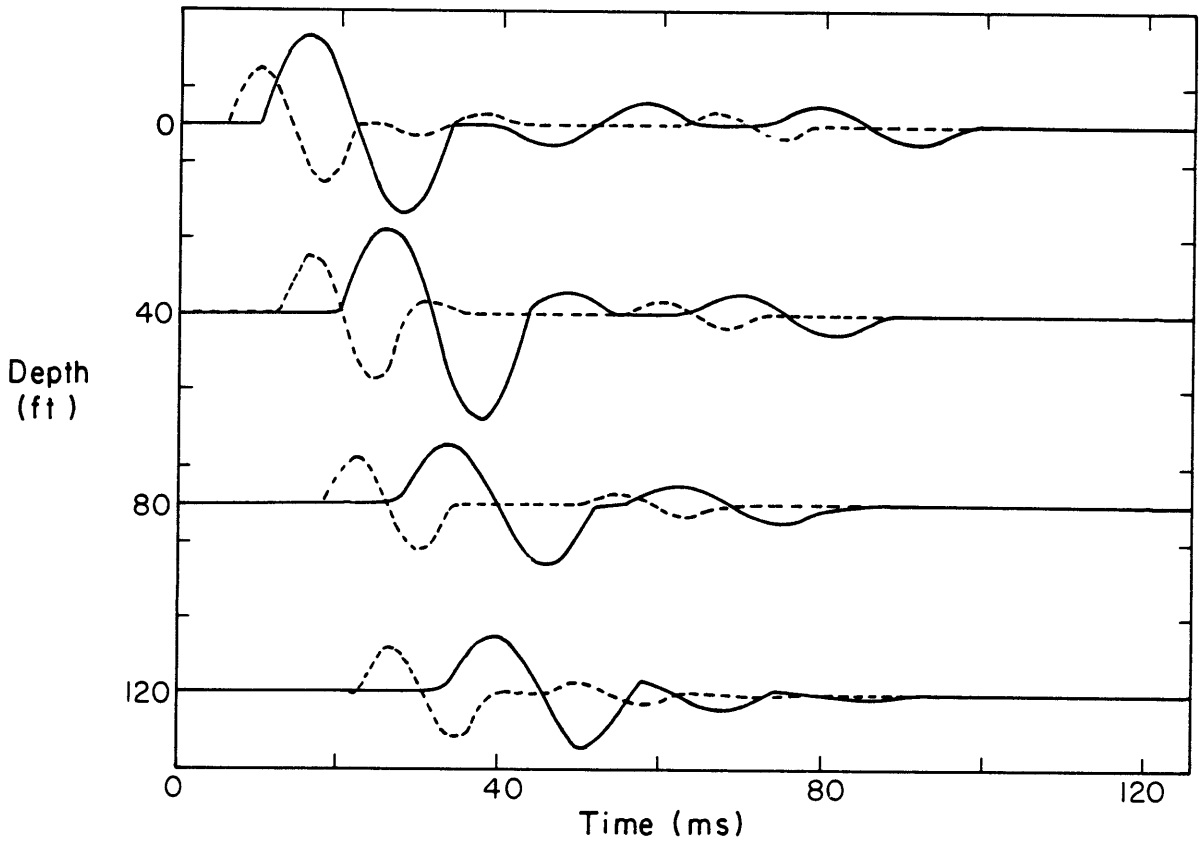

Figure 5.

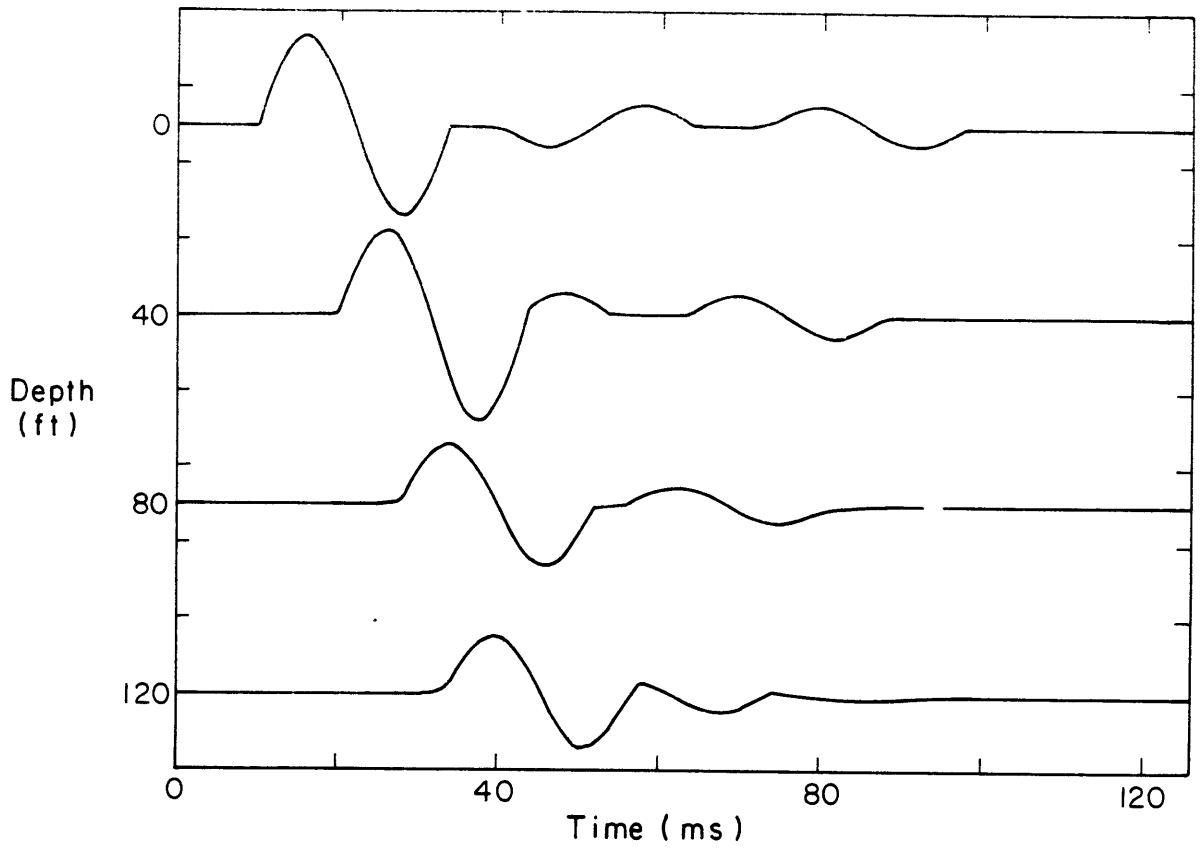

Figure 6.

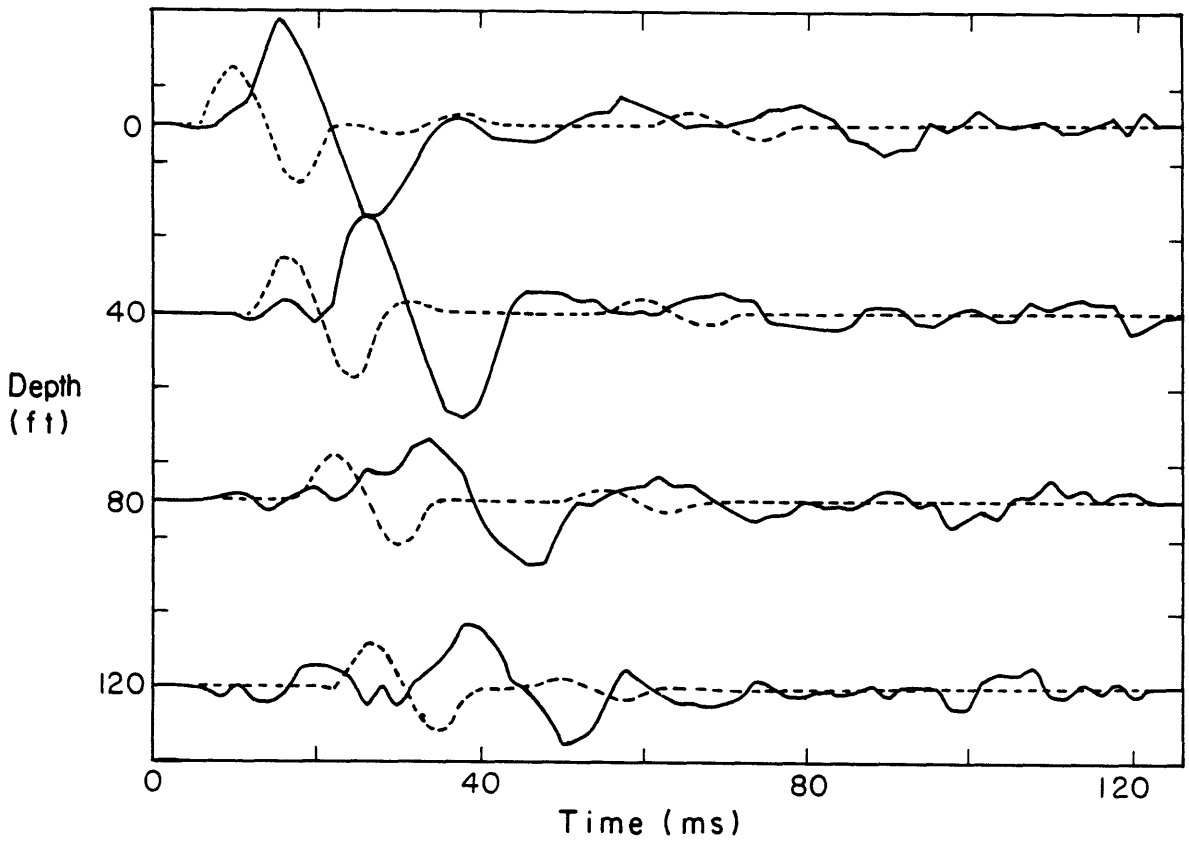

Figure 7.

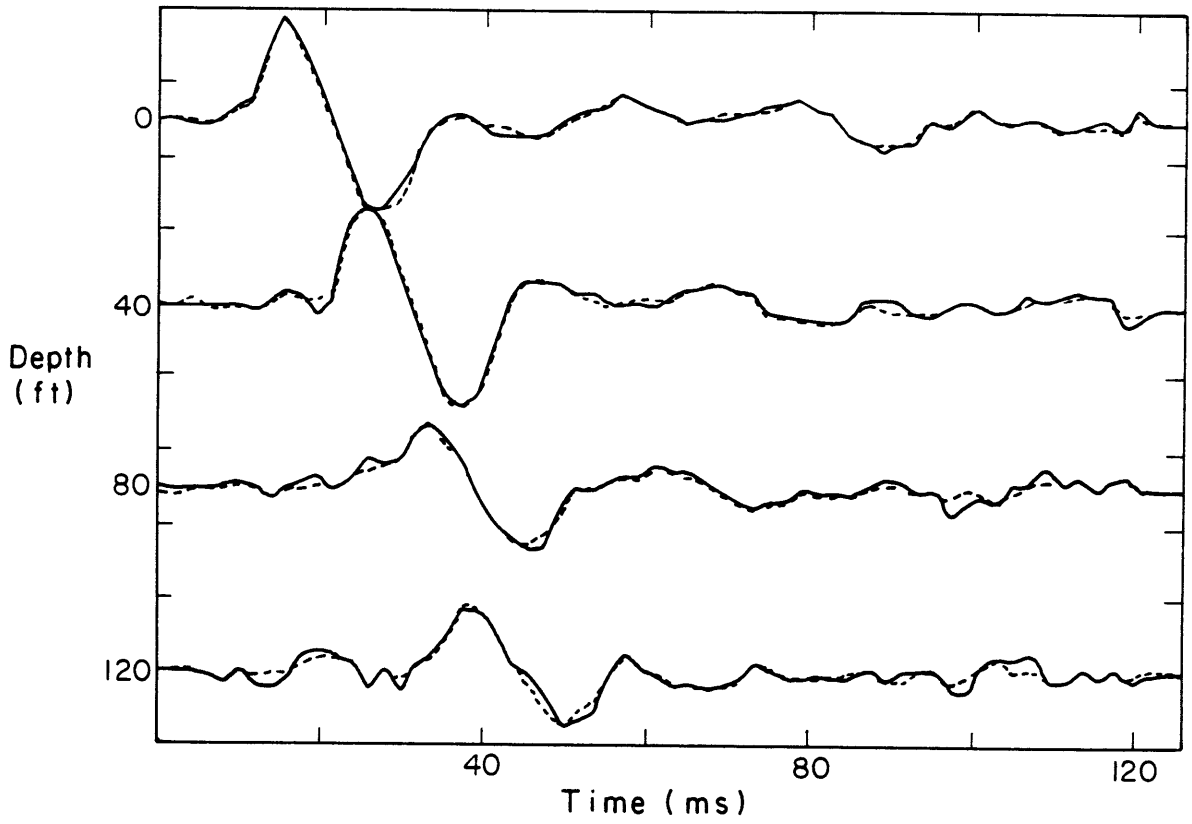

Figure 8.

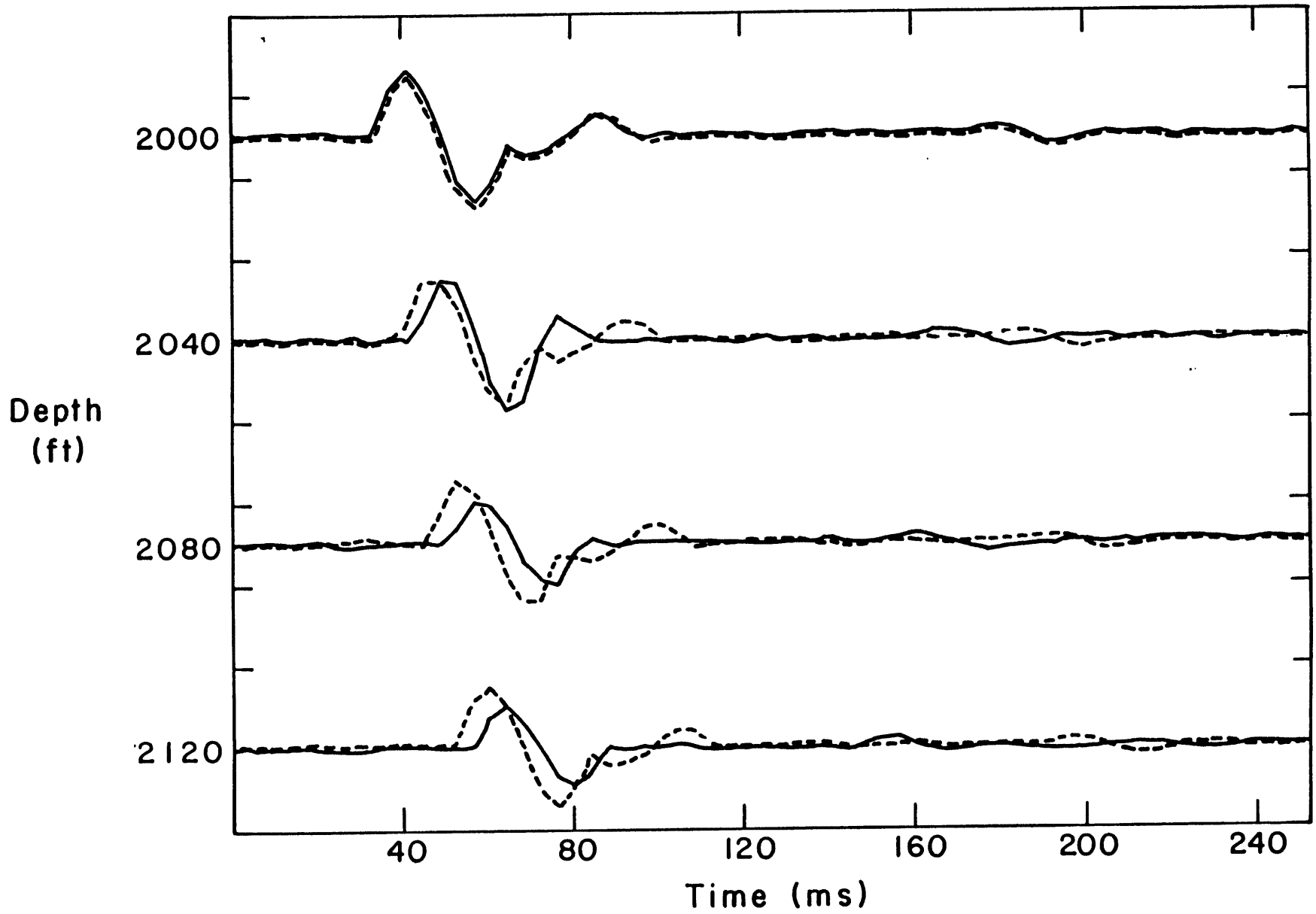

Figure 9.

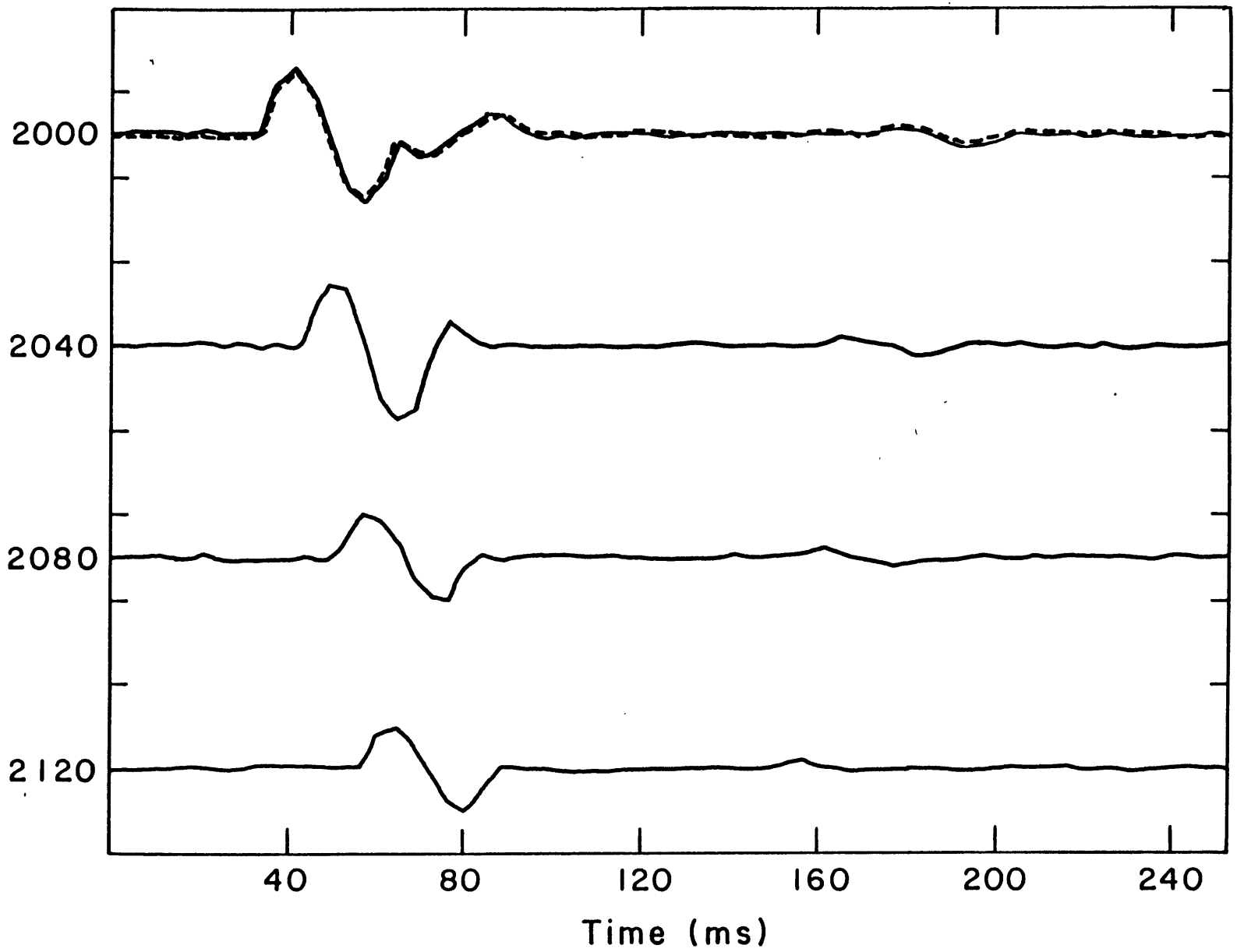

Figure 10.

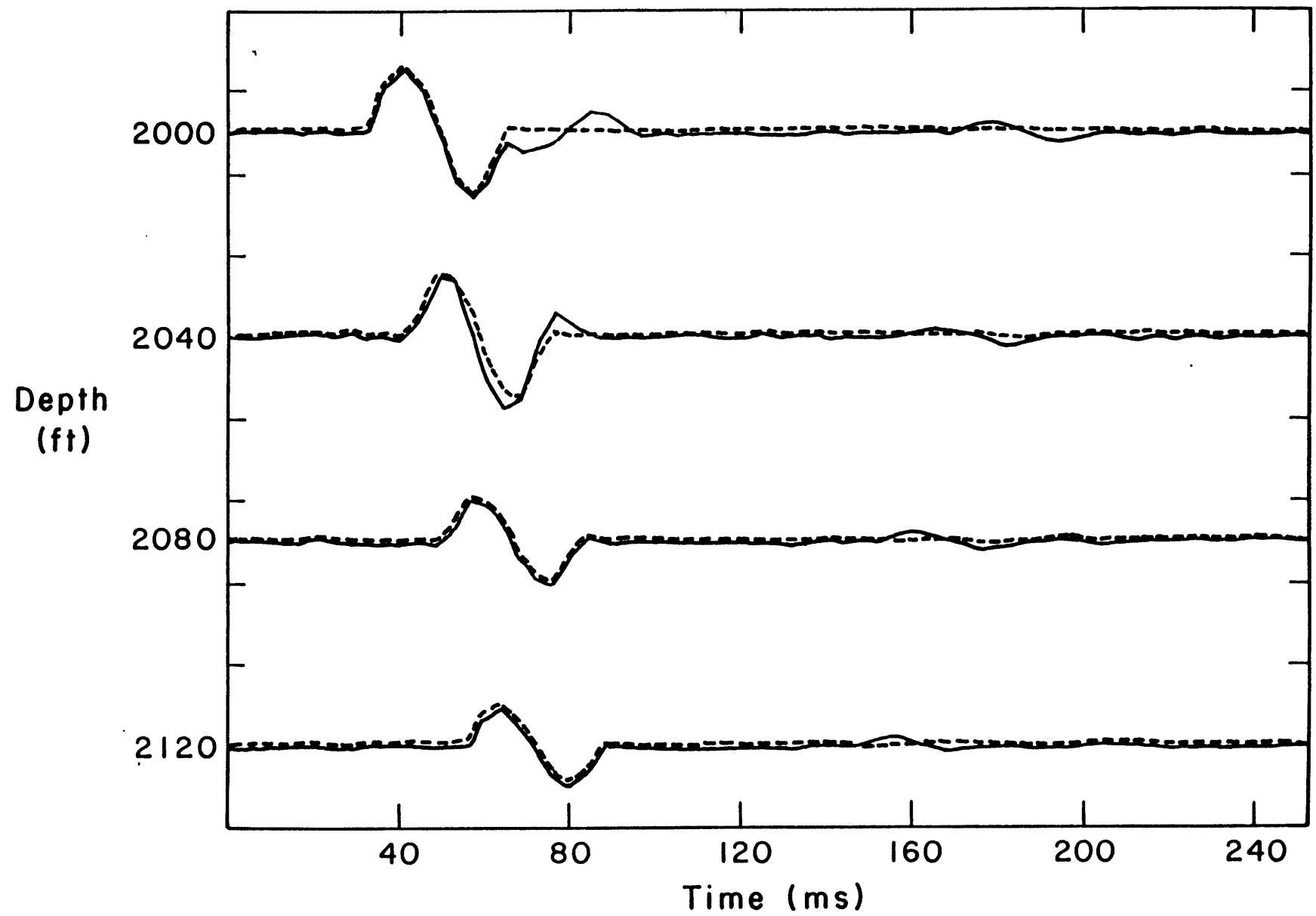

Figure 11.

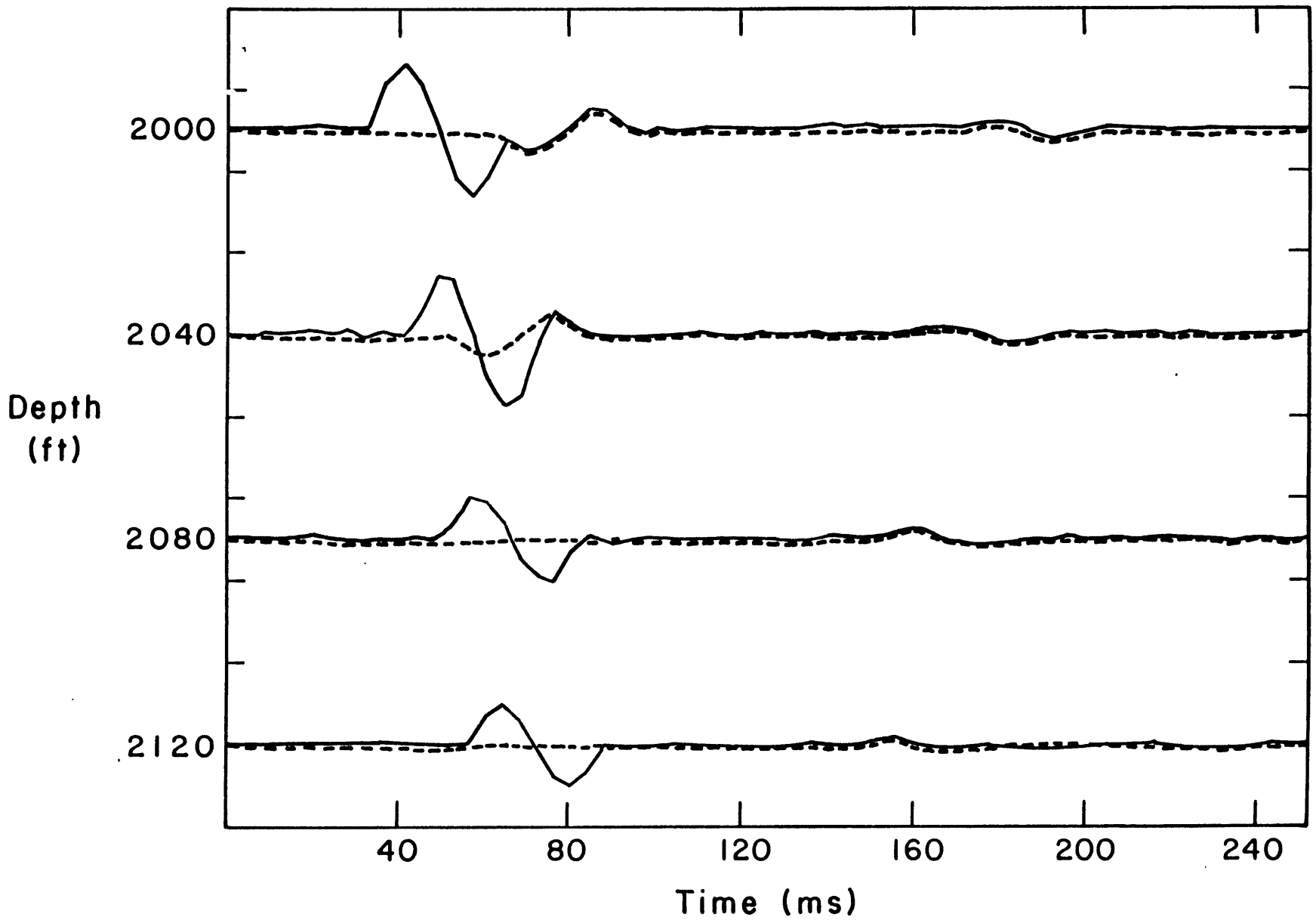

Figure 12.

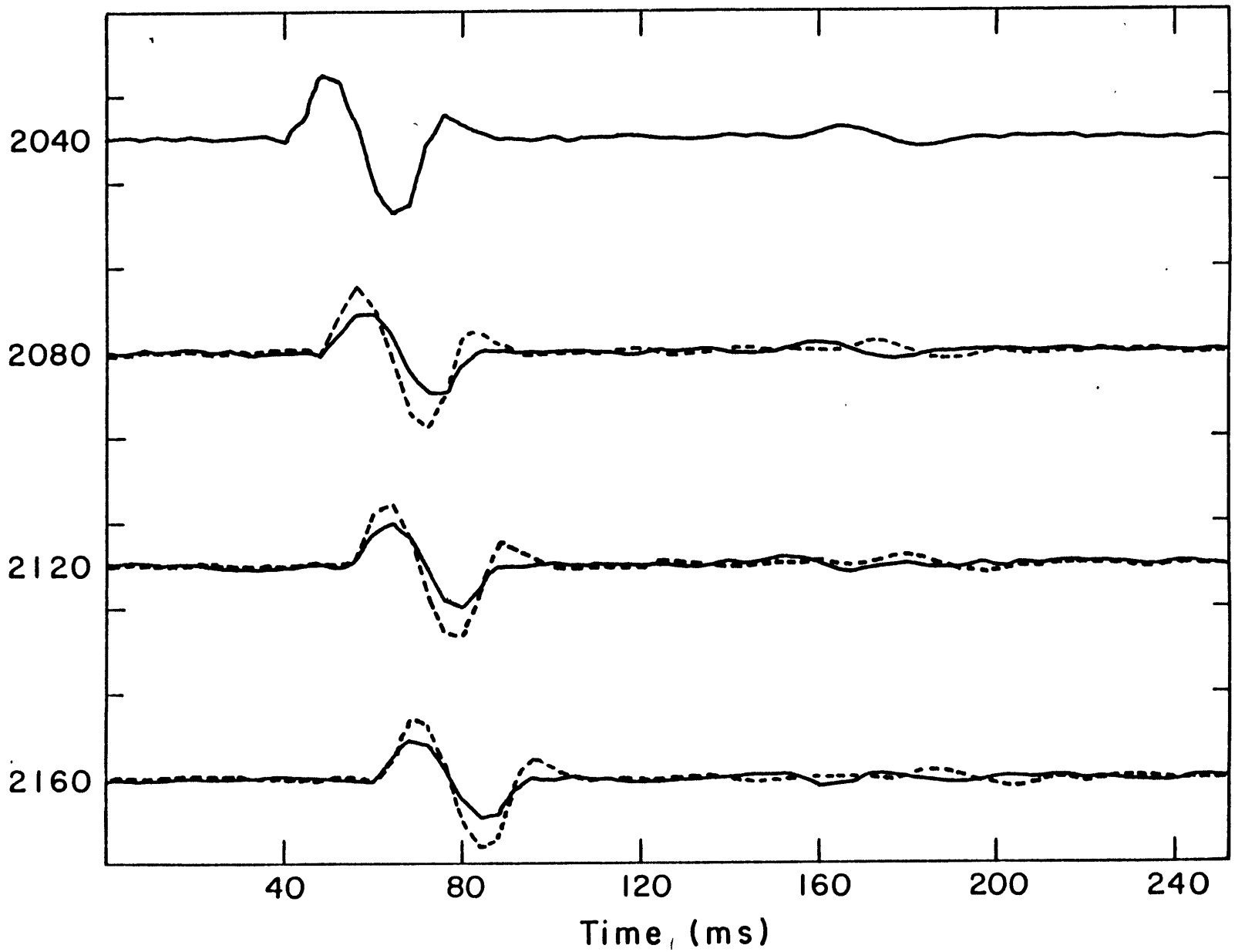

Figure 13.

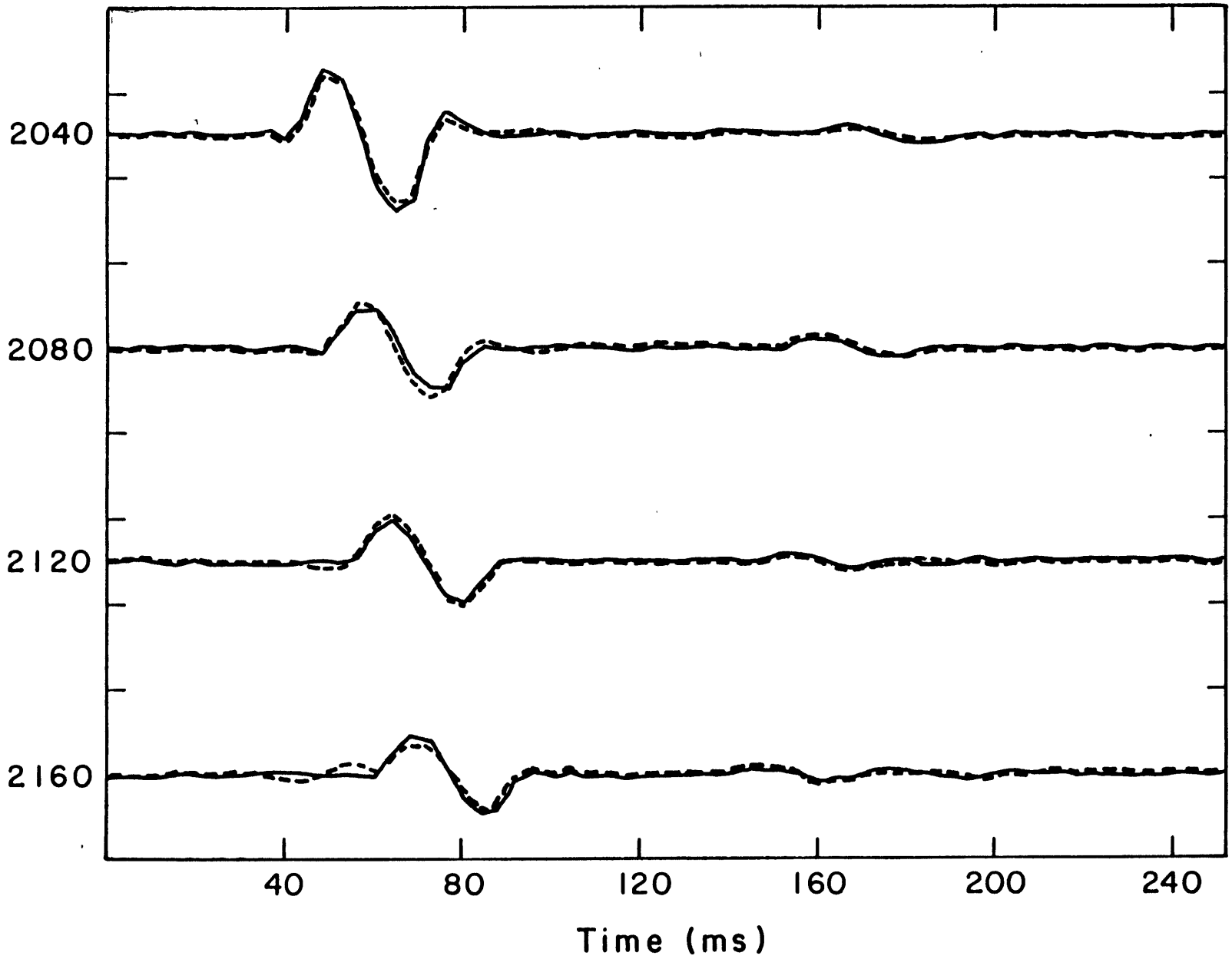

Figure 14.

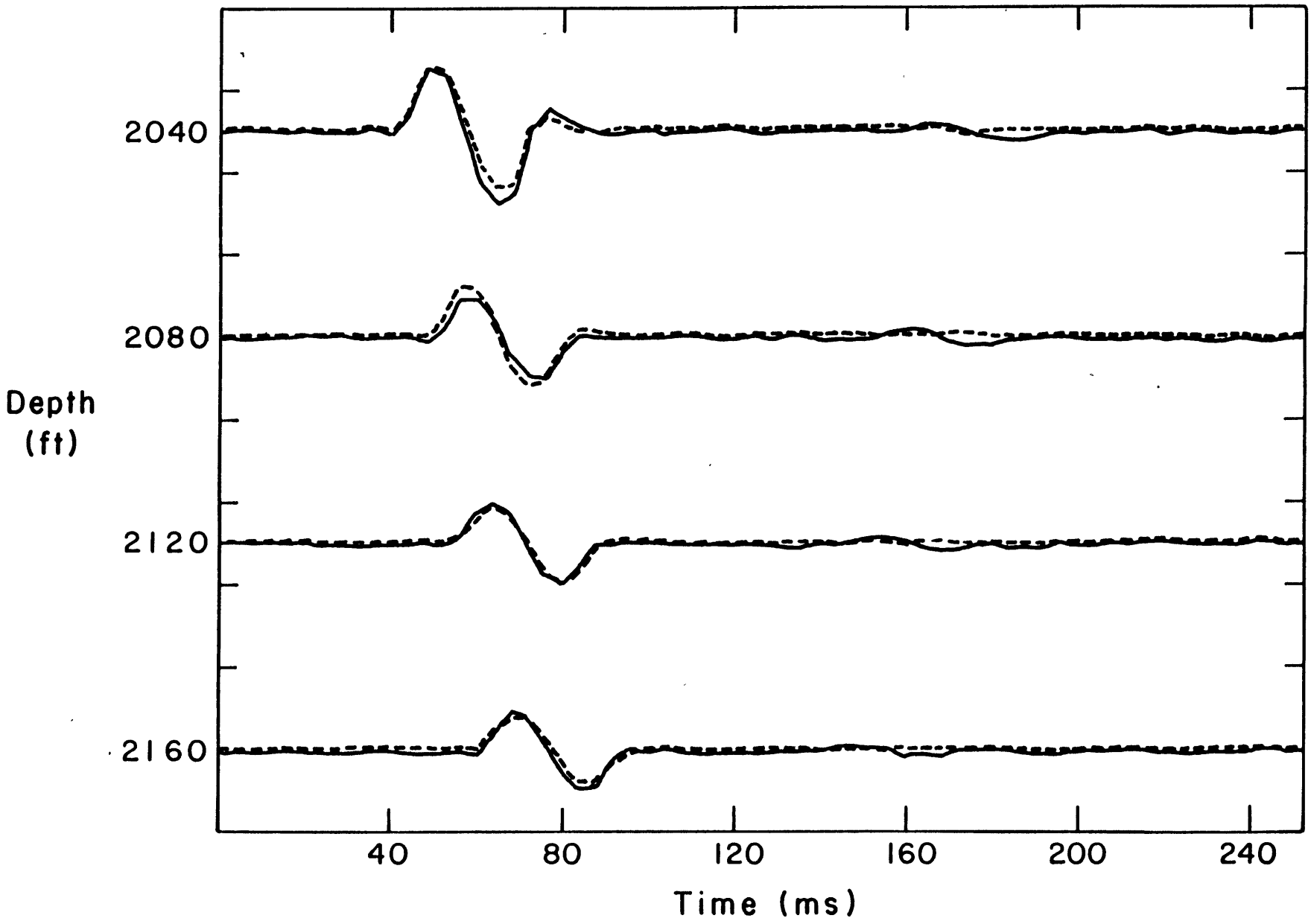

Figure 15.

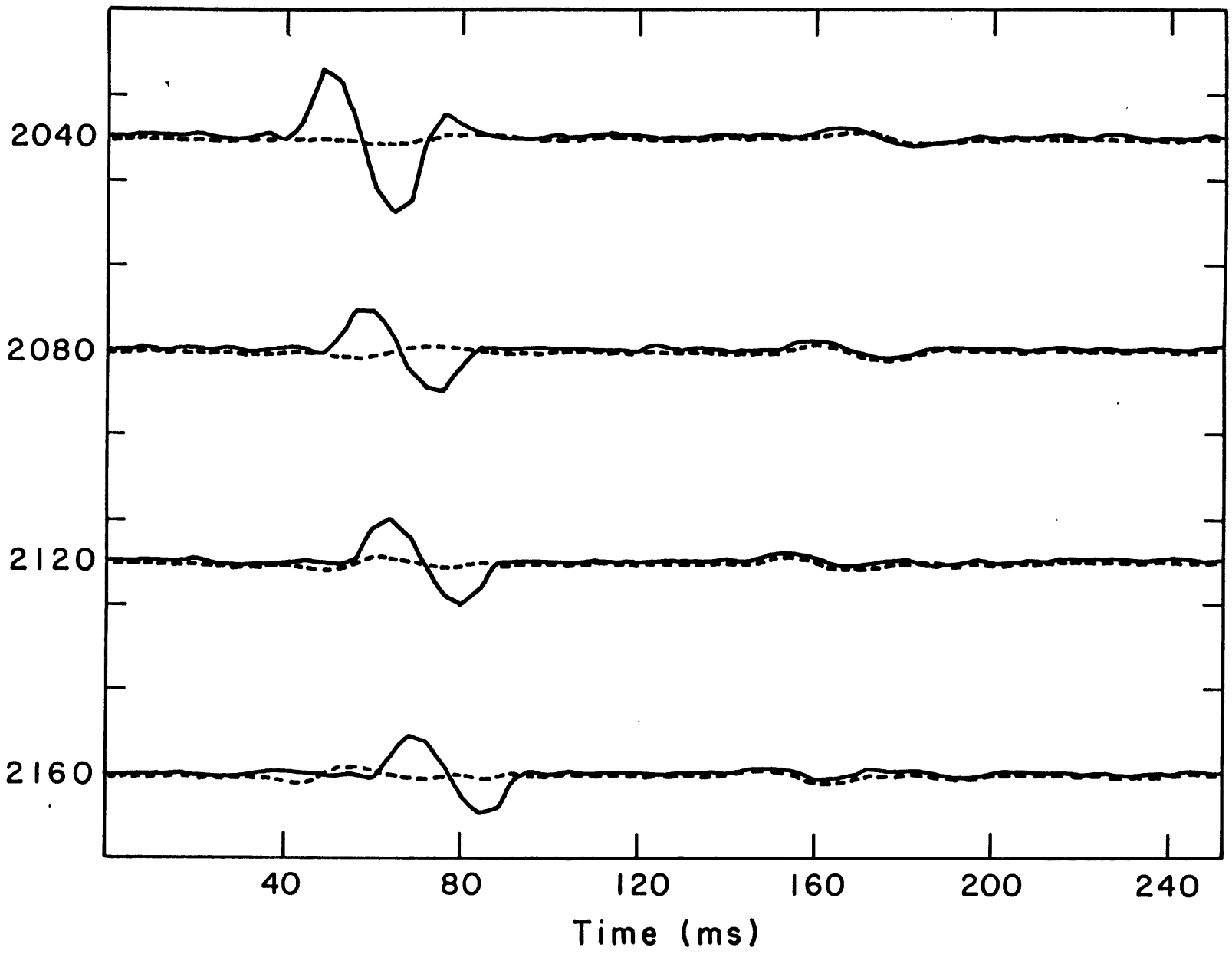

Figure 16.

SONIC AND DENSITY LOGS
ENIX WELL

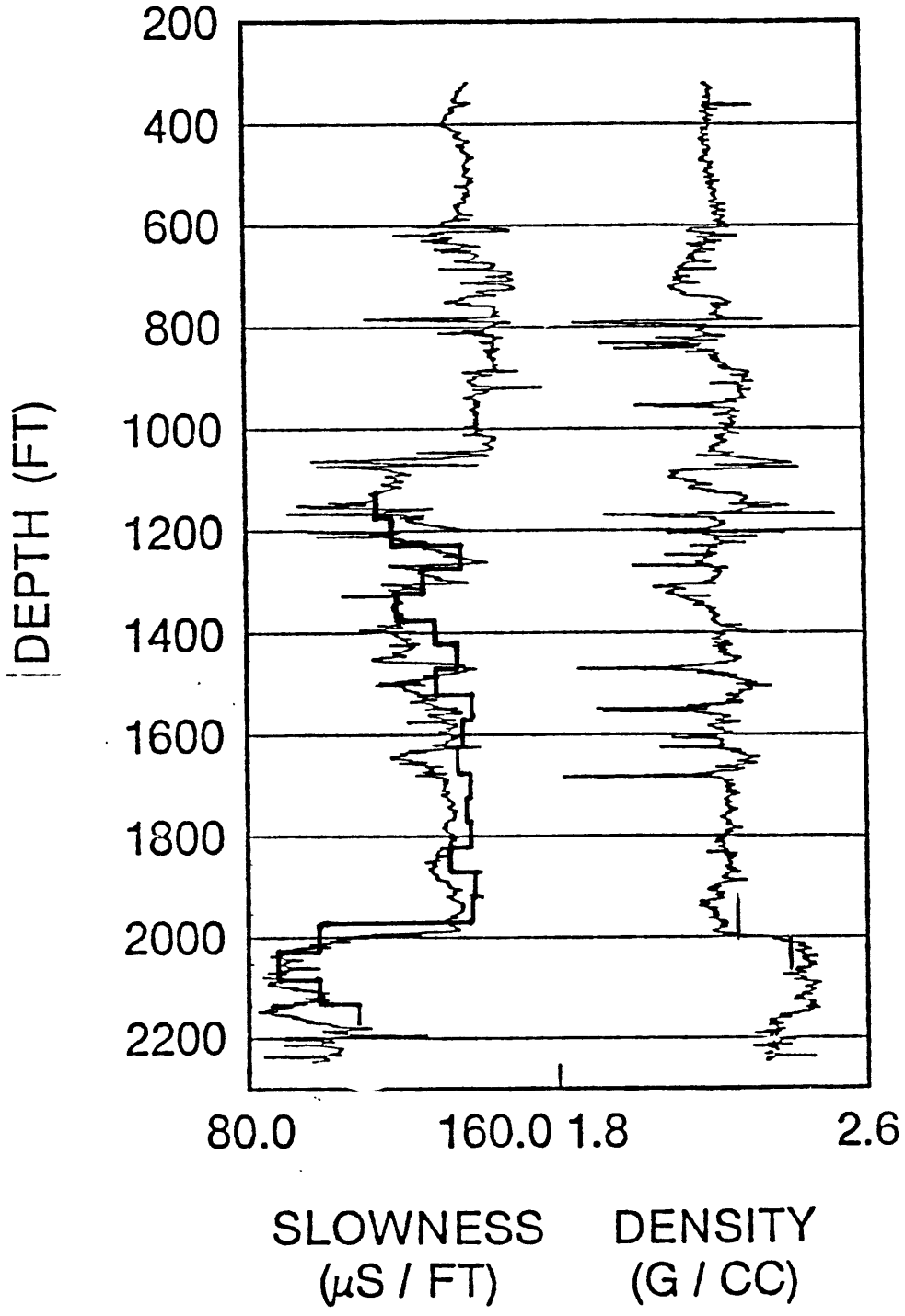

Figure 17.

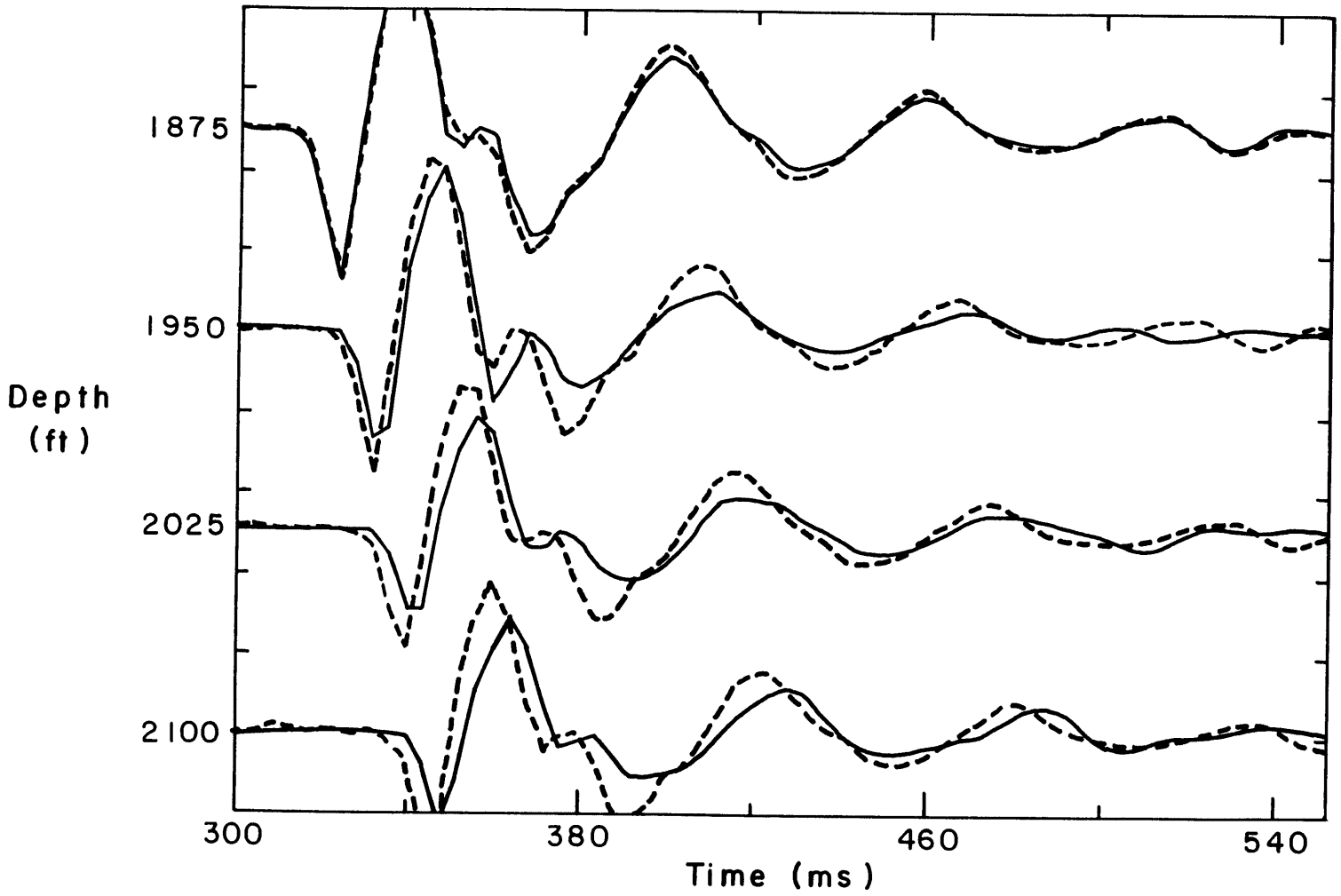

Figure 18.

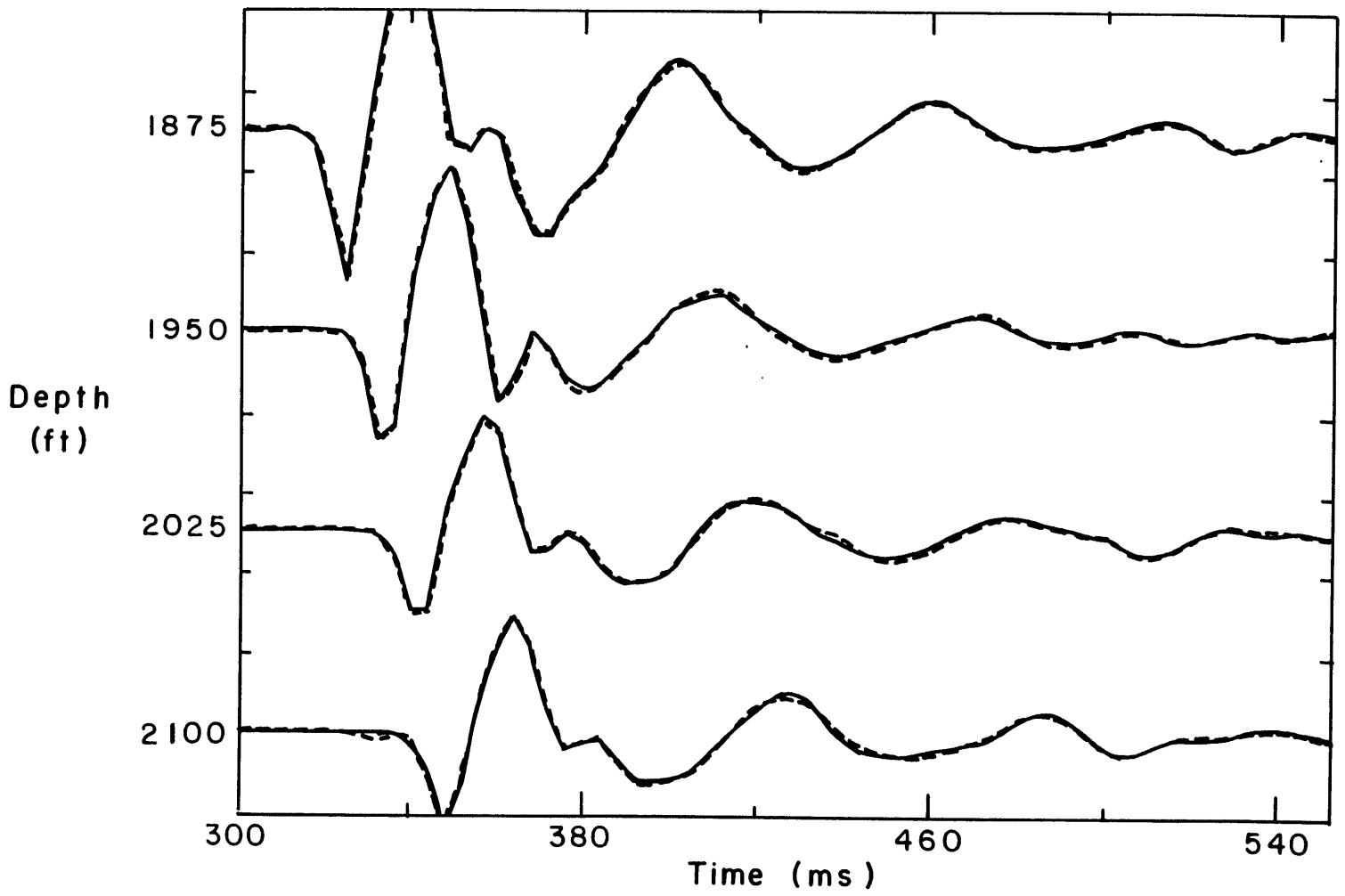

Figure 19.

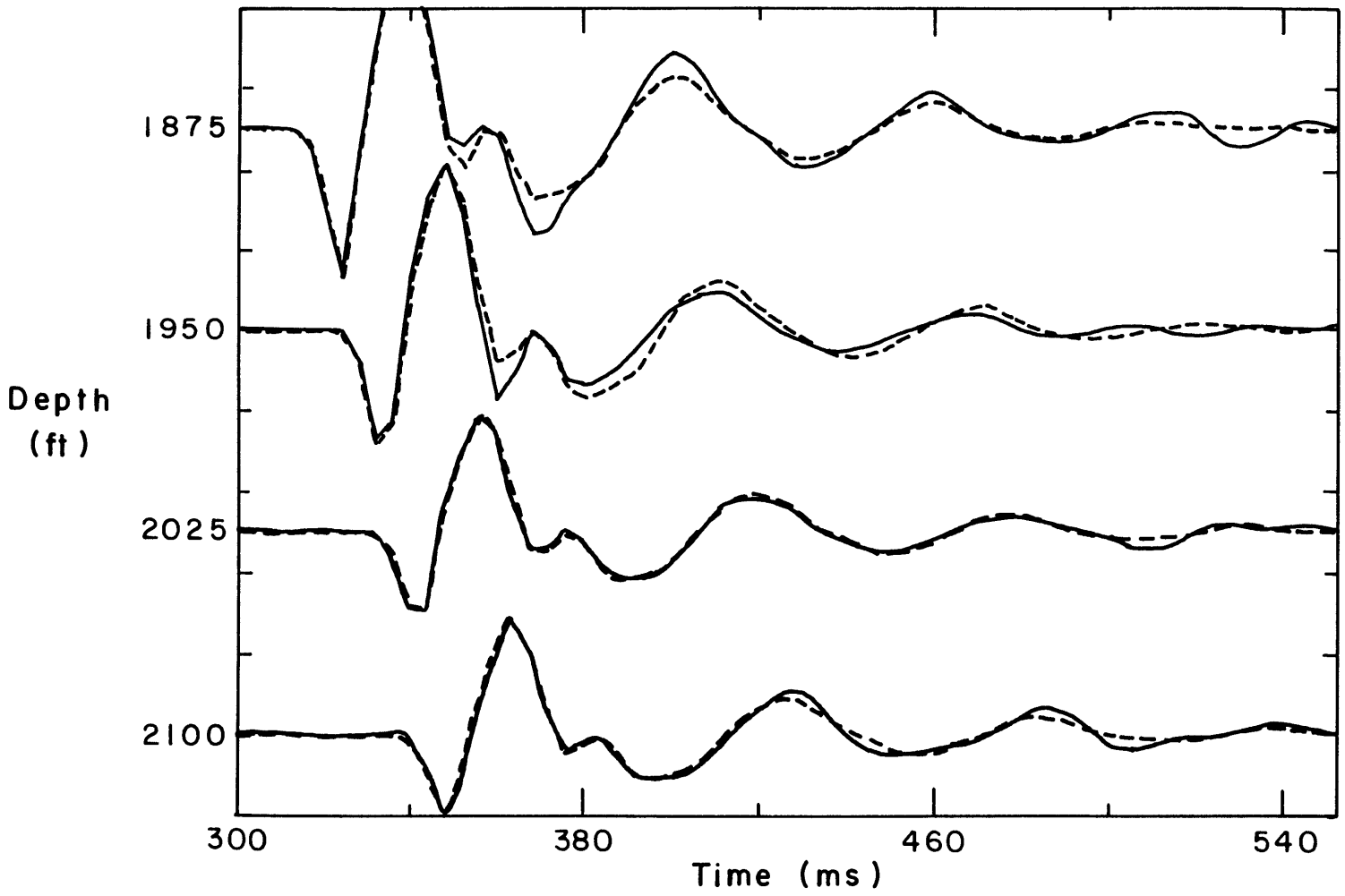

Figure 20.

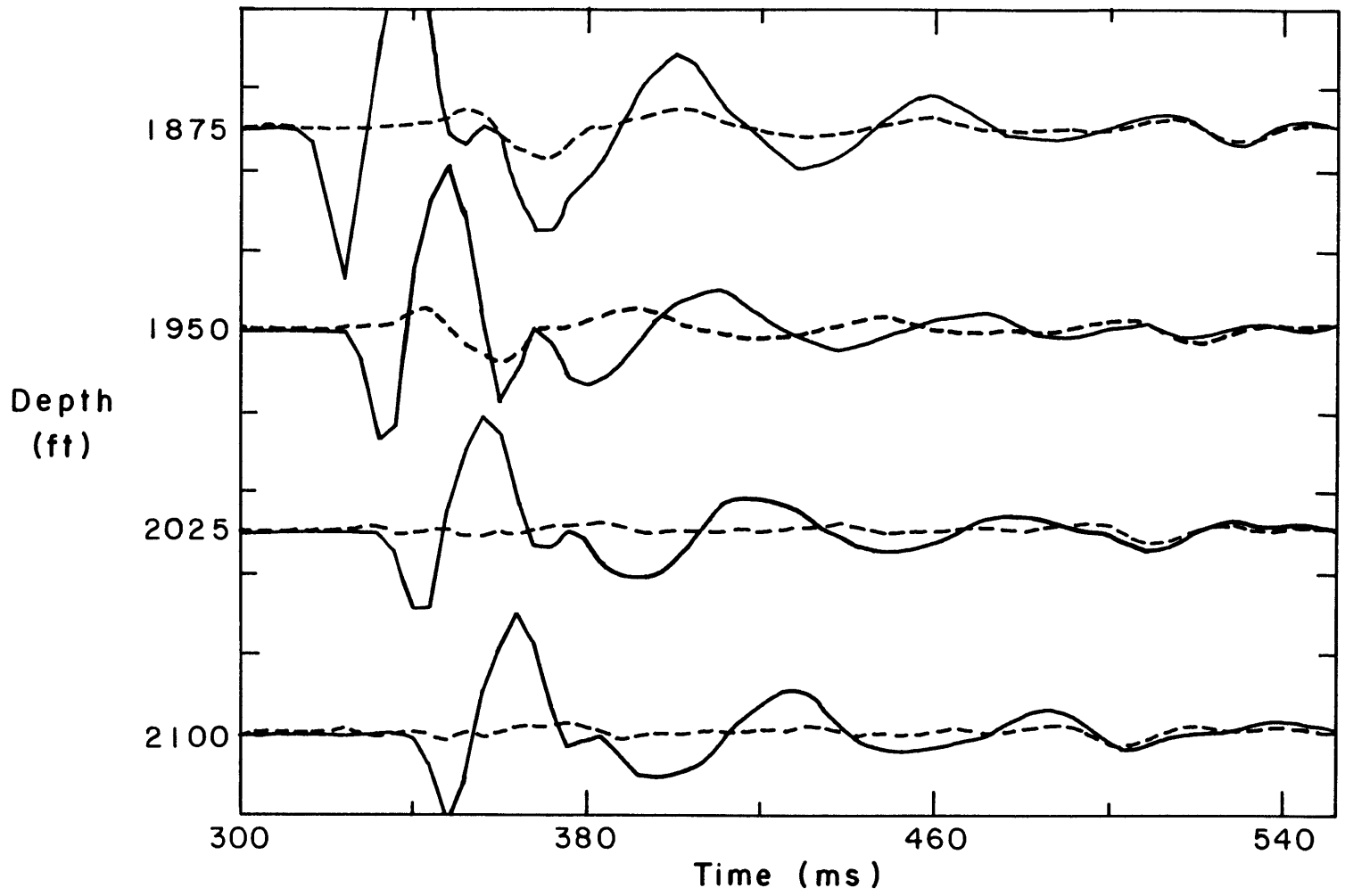

Figure 21.

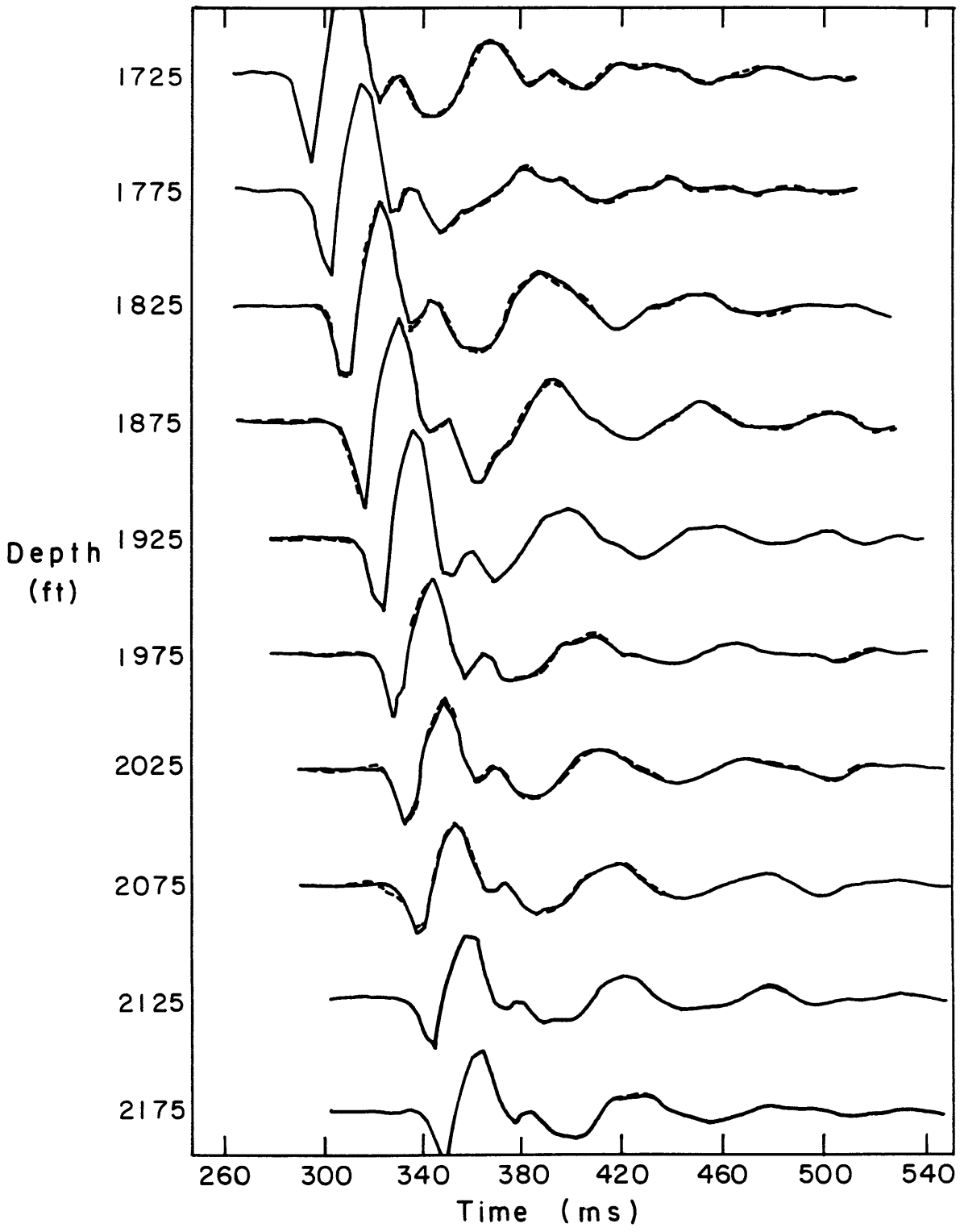
1725
1775
1825
1875
1925
1975
2025
2075
2125
2175
Depth
(ft)
260
300
340
380
420
460
500
540
Time (ms)

Figure 22.

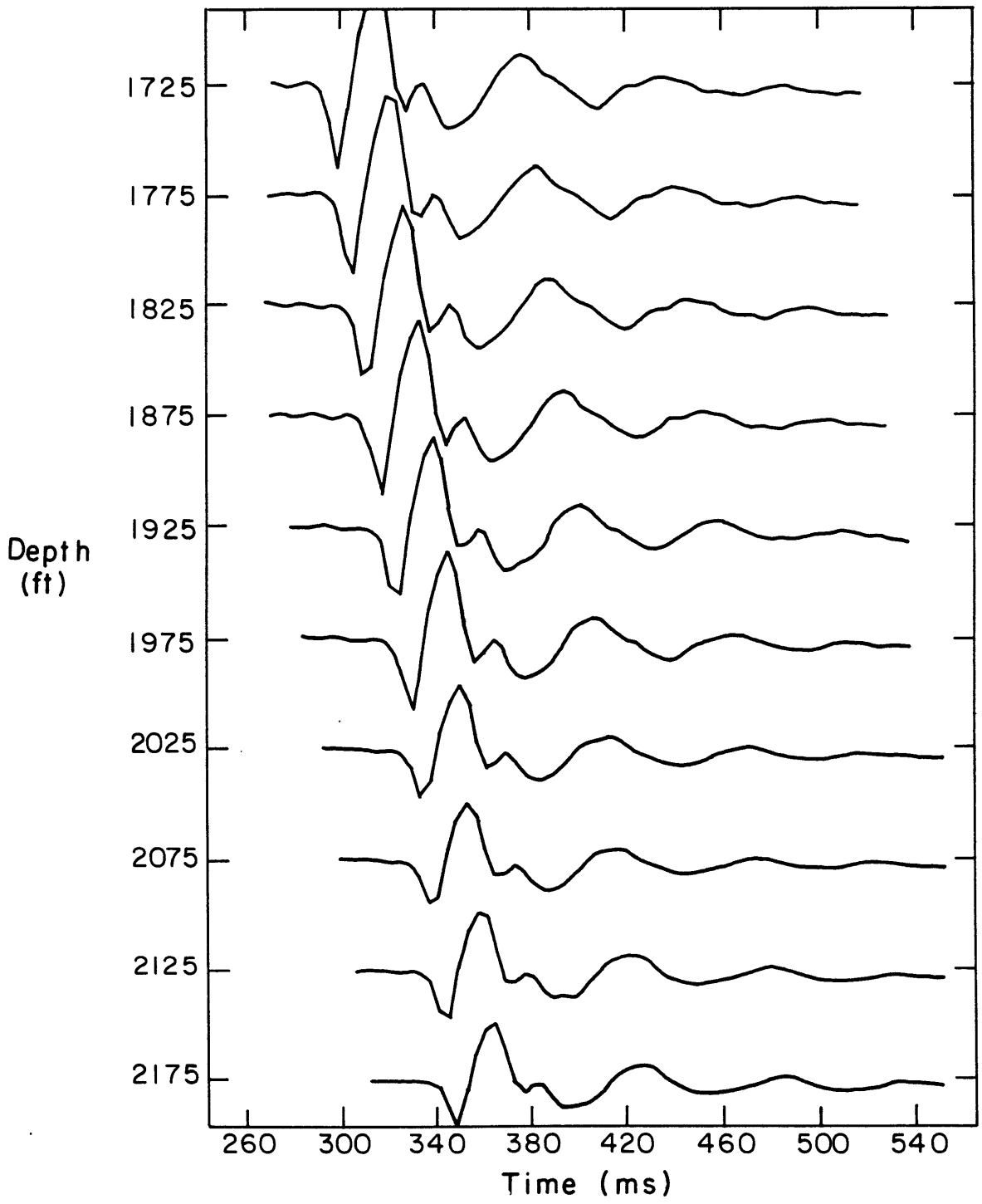
Depth
(ft)
1725
1775
1825
1875
1925
1975
2025
2075
2125
2175
260
300
340
380
420
460
500
540
Time (ms)

Figure 23.

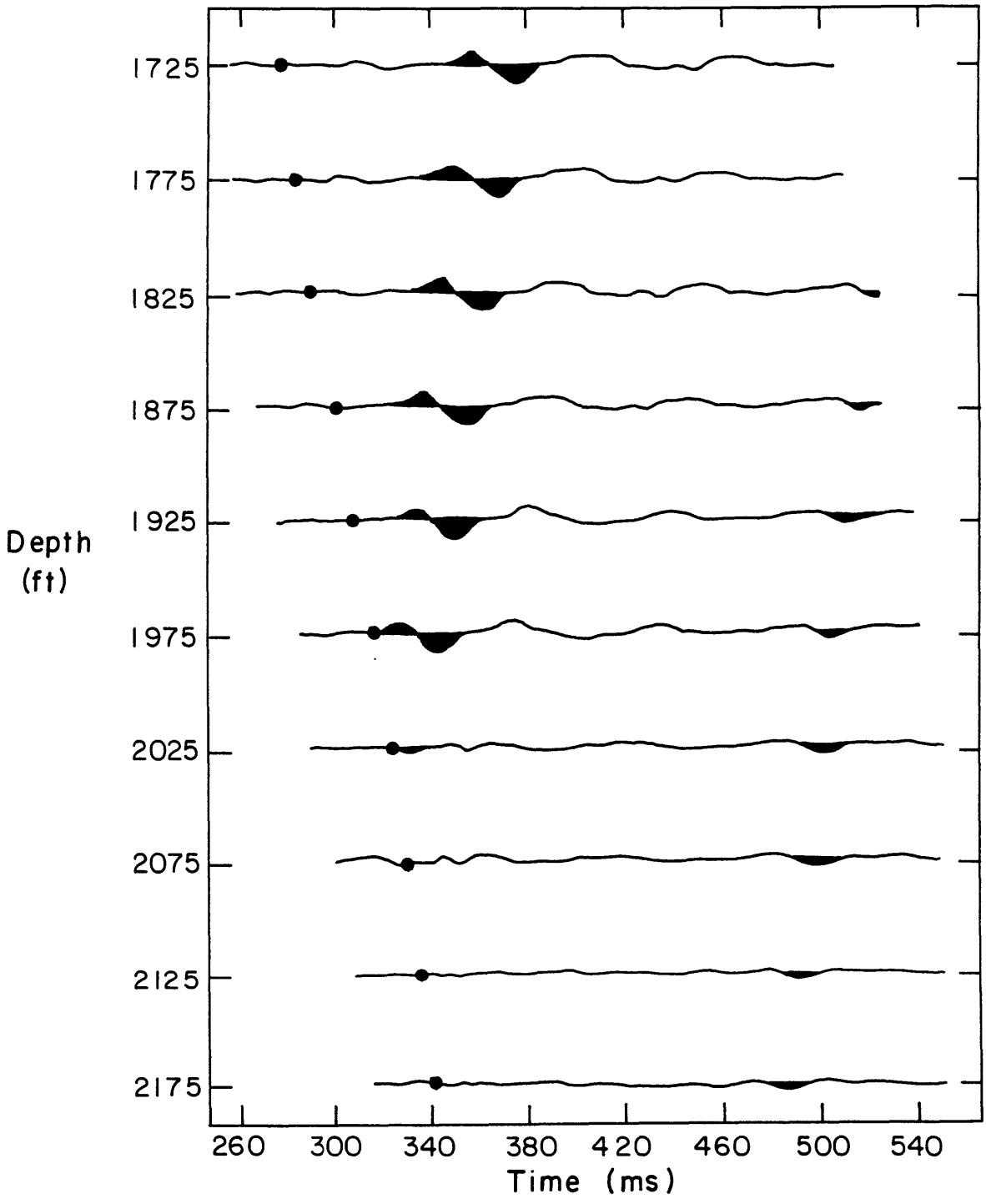
1725
1775
1825
1875
1925
1975
2025
2075
2125
2175
Depth
(ft)
260
300
340
380
420
460
500
540
Time (ms)

Figure 24.

Chapter 5

CONCLUSIONS

What we do here is nothing to what we dream of doing.

D.A.F. de Sade in Justine

In the course of this work the 1-D VSP has been analysed. As outlined in the introduction, there is considerable room for development in the quantitative analysis of in situ seismic data. These analyses are and will be computer intensive and will no doubt borrow many techniques from reflection processing and earthquake seismology. There is great potential for the VSP method to provide constraint on the lithologic parameters.

Using only the first breaks in the VSP provides a simple data set from which the velocity section may be found. For the single source offset survey in areas of approximately layered strata, with inevitable noise in the traveltimes, a straightforward traveltime inversion is quite effective. The Levenberg-Marquardt scheme with 1-D ray-tracing has been applied to synthetic data and three field experiments. It provides a stable and accurate 1-D velocity section. Several layers may have estimated velocities even when there are no observations present in them. The velocity errors aid in deciding how much significance may be attached to a particular value. The inverse algorithm operating on a Gulf Coast VSP data set has elucidated two low velocity zones associated with over-pressure gas. Velocity layers from 40 -150 ft are associated with reasonable errors and traveltime residuals in the field experiments.

In the previous data sets, it is noticed that the seimic velocities are often somewhat less than the sonic velocities. This discrepancy and many others in the literature have led to the proposal that seismic traveltimes are generally longer than their corresponding integrated sonic times. It appears from the study of synthetics and data from a number of wells in Texas that this discrepancy may be explained by the effect of attenuation and its associated velocity dispersion and to a lesser degree by short path multiple delay. Apparently and significantly, 1) body wave dispersion exists and 2) a nearly constant Q model describes it. Simple formulae to estimate the effects of short-path multiples and Futterman (1962) velocity dispersion on the seismic traveltimes have been given and applied to the field data with good results.

As is evident from but a glance at a VSP section, using only traveltime values neglects a great deal of information later in the VSP traces. With this in mind the full waveform inversion has been developed. Using the one-dimensional acoustic wave equation and groups of four traces at a time, the VSP section can be inverted for the underlying seismic parameters. Both the weighted least-squares and stochastic inverses have been used. In particular, velocity is very well estimated. The upgoing and downgoing waves are extracted and may be used to find the depths of large impedance contrasts. Attenuation estimates are reasonable for the sediments involved. Impedances are not well resolved theoretically or computationally. However, given a large reflection coefficient, appropriate receiver spacing and good initial guess, reasonable impedances may be calculated. The impedances and velocities may be used to estimate the density.

This waveform inversion is significant for several reasons: 1) Because of the geometry and wavelengths involved in the VSP survey, all parameters represent averages of the lithology several hundreds of feet from the well; 2) seismic velocities are determined (as opposed to sonic velocities); 3) an attenuation value is determined without the contaminating effect of reflected energy; 4) upgoing energy is extracted without the use of f-k filtering; 5) various statistical parameters are generated which allow critical analysis of the quality of the solution; 6) in areas of high impedance contrast, densities may be estimated.

This thesis has attempted to present a coherent and complete set of methods to analyse the one-dimensional VSP. Many of the techniques are extendable to higher dimensions. Traveltime inversions provide a velocity structure to be "fine-tuned" by the full waveform inverse. The inverse separates the wavefields while estimating velocity, attenuation and density. These techniques have illuminated the underlying geology in the eight VSP experiments discussed here.

Chapter 6

FUTURE WORK

6.1 TRAVELTIME INVERSION

The 1-D ray trace traveltime inversion has been developed and used in Chapter 2. Keho (1982) extended this algorithm to include refractions. Including primary reflections would add further constraint. Thurber (1981) developed an approximate 3-D ray tracing technique and inversions. Thurber's (1981) formulation could be adapted to the VSP case to provide a tomographic type inversion if a number of VSP source offsets were available. Extending these ray-tracing forward models to one which included amplitude information would be very useful. One eligible forward model is the Gaussian beam method (Cerveny, 1981). This method may be used to trace rays through a complex medium and to calculate the amplitude of the arrival. An inversion using traveltime and arrival amplitude as parameters could clearly utilize more of the VSP data.

6.2 SEISMIC VS. SONIC TRAVELTIMES

Using the traveltimes has helped to unravel wave propagation effects in a layered earth. Velocity dispersion was found to be particularly significant when comparing seismic and sonic times. It would be interesting to confirm velocity dispersion across the seismic bandwidth using the phase spectrum. Because of interfering reflection this is perhaps best accomplished by introducing frequency dependent velocity in the full waveform inversion.

Also worthy of consideration is the dependence of Q on frequency. Chapter 3 shows that the data may be explained by a nearly constant Q model. Further analysis of the amplitude spectra may reveal greater complexity in Q.

6.3 WAVEFORM INVERSION

The method of trace inversion discussed in Chapter 4 is one viable technique. However, if the full VSP section is very consistent (no source or receiver variations) another type of inversion could prove useful. Envisioned is a simultaneous inversion of the whole VSP. While this may seem like a very large computational task, there are some compelling reasons to attempt it. First, no upgoing wave parameters are required as all energy originates with the surface downgoing pulse. Thus the only parameters needed are the initial downgoing spectra, the velocities, and densities and attenuation. This would be approximately the same number of parameters as the present inversion. As the inverse matrix has the dimensions of the number of parameters by number of parameters the inversion itself will be manageable.

Secondly, suppose that the traces are 128 points long for example and that there are 50 levels. Then there is a great deal of data constraining the parameters for a particular inversion. This should decrease the parameter variance considerably.

The problem with the full VSP section inversion is computing the partial derivatives. Again considering the above example, with 6400 data points and say 200 parameters, gives about 1.3×10^6 partial derivatives to compute per iteration. There may be however some cunning methods to find these. One possible approach to the calculation of the partial derivatives with respect to the medium is outlined below (after Madden and Park, 1983).

Consider first the propagation of normally-incident acoustic waves in a horizontally-layered medium. The basic equations are as follows

$$\frac{\partial P}{\partial z} = - \rho \frac{\partial V}{\partial t} \qquad (1)$$

$$\frac{\partial V}{\partial z} = - k \frac{\partial P}{\partial t} \qquad (2)$$

where V is the particle velocity in the z direction
P is the pressure in the z direction
ρ is the density
k is the inverse elastic modulus $(\rho \cdot c^2)^{-1}$
c is the acoustic velocity of the medium

Assuming that V and P have exponential time dependences then equations (1) and (2) can be written in matrix form as

$$D \cdot Y \equiv \begin{bmatrix} \frac{\partial}{\partial z} & i\omega\rho \\ i\omega k & \frac{\partial}{\partial z} \end{bmatrix} \cdot \begin{bmatrix} P \\ V \end{bmatrix} = 0 \qquad (3)$$

where D is the operator matrix
Y is the observation matrix

The problem is to relate perturbations in the model parameters ($\delta\rho, \delta k$) to the resulting changes in the observations ($\delta P, \delta V$)

Now $$(D+\delta D)\ (Y+\delta Y) = 0 \qquad (4)$$

And assuming that the operation $\delta D \delta Y$ is negligible

$$S \cdot \delta Y = -\delta D \cdot Y \qquad (5)$$

The solution to equation (5) can be expressed in terms of a Green's function. The Green's function G(r,s) gives the effect at receiver position r caused by an impulsive source at s. That is

$$D \cdot G(r,s) = \delta(z-s) \tag{6}$$

where $\delta(z-s)$ is the source delta function for the observations

Ganley (1981) has given the Green's function for the VSP case of a buried source and subsurface receiver. His solution is in the form of a product of propagator matrices for a source at η and a receiver at depth ζ.

Because D is linear, equation (5) may be solved by

$$\delta Y_k(\zeta) = \int_{z_i}^{z_{i+1}} G_k(\zeta,\eta)_j [\delta D \cdot Y]_j d\eta \tag{7}$$

where $\delta Y_k(\zeta)$ is the perturbation of the k^{th} observable (k=1,2) in the ith layer at ζ

z_{i+1}, z_i are the ith layer boundaries containing the perturbed parameters

$G_k(\zeta,\eta)_j$ is the Green's function for the kth component of a receiver at ζ and the jth component (j=1,2) of a source at η

More explicitly

$$\begin{aligned} \delta P(\zeta) &= \int_{z_i}^{z_{i+1}} (i\omega V G_1(\zeta,\eta)_1 \delta\rho + i\omega P G_1(\zeta,\eta)_2 \delta k) d\eta \\ \delta V(\zeta) &= \int_{z_i}^{z_{i+1}} (i\omega V G_2(\zeta,\eta)_1, \delta\rho + i\omega P G_2(\zeta,\eta)_2 \delta k) d\eta \end{aligned} \tag{8}$$

The partial derivatives $\frac{\partial P}{\partial \rho}$, $\frac{\partial P}{\partial k}$, $\frac{\partial V}{\partial \rho}$ and $\frac{\partial V}{\partial k}$ are found from equation (8).

Assuming that the problem is well-posed allows reciprocity to be invoked for the Green's functions

$$G_i(s,r)_j = G_j(r,s)_i \tag{9}$$

This will make all the partial derivatives of the problem available by computing only one-half of them.

Having found the model partial derivatives in a manner outlined as above, the inverse problem can be solved as in equations (13)-(15) in Chapter 4.

REFERENCES

Aki, K. and W.H.K. Lee, Determination of three-dimensional velocity anomalies under a seismic array using first P arrival times from local earthquakes, J. Geophys. Res., 81, 4381-4399, 1976.

Aki, K. and P.G. Richards, Quantitative Seismology: Theory and Methods, Vols. I and II, W.H. Freeman Co., San Francisco, CA, 1980.

Alam, M.A., "Processing Uphole Surveys," personal communication, 1981.

Aminzadeh, F. and Mendel, J.M., Non-normal incidence state-space model and line source reflection synthetic seismogram, Geophys. Prosp., 30, 541-568, 1982.

Azimi, S.A., A.V. Kalinin, V.V. Kalinin, and B.L. Pivovurov, Impulse and transient characteristics of media with linear and quadratic absorption laws, Izv., Phys. Solid Earth, February, 88-93, 1968.

Balch, A.H., M.W. Lee, J.J. Miller, and R.T. Ryder, The use of vertical seismic profiles in seismic investigations of the earth, Geophysics, 47, 6, 1982.

Balch, A.H., Vertical Seismic Profiling, IHRDC, Boston, Mass., to be published in 1983.

Bamberger, A., G. Chavent, C. Hemon, and P. Lailly, Inversion of normal incidence seismograms, Geophysics, 47, 5, 757-770, 1982.

Becquey, M., M. Lavergne, and C. Willm, Acoustic impedance logs computed from seismic traces, Geophysics, 44, 9, 1485-1501, 1979.

Beeston, H.E. and T.V. McEvilly, Shear wave velocities from downhole measurements, Earthquake Engineering and Structural Dynamics, 5, 2, 181-190, 1977.

Berzon, I.S., Some results of a study of seismic waves from well shooting, Izv. Geophys. Ser., 9, 1308-1333, 1964.

Beydoun, W.B., Sources of seismic noise in boreholes, M.S. Thesis, Department of Earth and Planetary Sciences, M.I.T., Cambridge, Mass., 1982.

Bickle, S., A rapid search algorithm, personal communication, 1981.

Borcherdt, R.D., Energy and plane waves in linear viscoelastic media, J. Geophys. Res., 78, 14, 2442-2453, 1973.

Boss, F.E., How the sonic log is used to enhance the seismic reference service velocity survey, Canadian Well Logging Soc. Journal, 3, 1, 17-31, 1970.

Bouchon, M. and K. Aki, Discrete wave-number representation of seismic-seismic-source wave fields, Bull. Seism. Soc. Am., 67, 2, 259-277, 1977.

Bouchon, M., Discrete wavenumber VSP FORTRAN Program, Personal communication, 1982.

Brennan, B.J. and D.E. Smylie, Linear viscoelasticity and dispersion in seismic wave propagation, Rev. Geophys. Space Phys., 19, 2, 233-246, 1981.

Brown, B.J. and D.E. Smylie, Linear viscoelasticity and dispersion in seismic wave propagation, Rev. Geophys. Space Phys., 19, 2, 233-246, 1981.

Brown, K.M. and J.E. Dennis, Derivative-free analogues of the Levenberg-Marquardt and Gauss algorithms for nonlinear least-squares approximation, Numer. Math, 18, 289-297, 1972.

Brewer, H.L. and J. Holtzscherer, Results of subsurface investigations using seismic detectors and deep bore holes, Geophysical Prospecting, 6, 2, 81-100, 1958.

Castagna, J., On problems with the sonic log, Personal communication, 1982.

Cerveny, V., Seismic wavefields in structurally complicated media, Notes from lectures given at the Venig Meinesz Laboratory, Utrecht, April-May 1981.

Cerveny, V., I.A. Molotkov, and I. Psencik, Ray Method in Seismology, Univerzita Karlova, Prague, Czechoslovakia, 1977.

Cheng, C.H. and M.N. Toksoz, Inversion of seismic velocities for the pore aspect ratio spectrum of a rock, J. Geophys. Res., 84, 7533-7543, 1979.

Cheng, C.H. and M.N. Toksoz, Generation, propagation and analysis of the tube waves in a borehole, Trans. SPWLA 23rd Annual Logging Symposium, 1982.

Chun, J. and D.G. Stone, Extrapolation and interpolation of VSP data, Proc. 52nd Annual SEG Meeting, Oct. 17-21, Dallas, Texas, 1982.

Claerbout, J.F., Synthesis of a layered medium from its acoustic transmission response, Geophysics, 33, 264-269, 1968.

Claerbout, J.F., Fundamentals of Geophysical Data Processing: With Applications to Petroleum Prospecting, McGraw-Hill, Inc., New York, N.Y., 1976.

Comer, R., Algorithms for one-dimensional ray tracing, Personal communication, 1981.

Crampin, S., R. McGonigle and D. Bamford, Estimating crack parameters from observations of P wave velocity anisotropy, Geophysics, 45, 3, 345-360, 1980.

Crosson, R.S., Crustal structure modelling of earthquake data 1. Simultaneous least-squares estimation of hypocenter and velocity parameters, J. Geophys. Res., 81, 17, 3036-3046, 1976.

Deeming, T., Synthetic seismograms and vertical seismic profiles, presented at the 49th Annual SEG Meeting, No. RW-18, New Orleans, LA, 1979.

DeGolyer, E., Notes on the early history of applied geophysics in the petroleum industry, J. Soc. Petrol. Geophys., 6, 1, 1-10, 1935.

Demidenko, Y.B., Vertical seismic profiling, Internat. Geology Rev., 11, 7, 1964.

DiSiena, J.P., B.S. Byun, and J.E. Fix, Vertical seismic profiling: a processing analysis case study, presented at the 50th Annual SEG Meeting, Houston, Texas, 1980.

DiSiena, J.P., J.E. Gaiser, and D. Corrigan, Three component vertical seismic profiles: Orientation of horizontal components for shear wave analysis, presented at the 51st Annual SEG Meeting, Oct. 11-15, Los Angeles, CA, 1981.

DiSiena, J.P., Depth of Austin Chalk near Sulphur Springs, TX, personal communication, 1983.

Dix, C.H., The interpretation of well-shot data I, Geophysics, 4, 1, 24-32, 1939.

Dix, C.H., The Interpretation of Well-Shot Data II, Geophysics, 10, 2, 160-170, 1945.

Dix, C.H., The Interpretation of Well-Shot Data III, Geophysics, 11, 4, 457-461, 1946.

Dix, C.H., Seismic Prospecting for Oil, Harper and Row, Publishers, Inc., New York, N.Y., 1952.

Dix, C.H., Seismic Prospecting for Oil, 2nd edition, Int. Human Resources Development Corp., Boston, Mass., 1981.

Domenico, S.N., Elastic properties of unconsolidated porous sand reservoirs, Geophysics, 42, 7, 1339-1368, 1977.

Douze, F.J., Signal and noise in deep wells, Geophysics, 29, 5, 1964.

Dunlap, H.F., Deep well seismic refraction, Canadian Patent No. 838308, Mar. 31, 1970.

Evans, J.L., Major structural and stratigraphic features of the Anadarko Basin, in Proceedings of the Natural Gas Resources Development in Mid-Continent Basins: Production and Exploration Techniques Symposium, Univ. of Tulsa, Tulsa, Okla., March 11-12, 1980.

Fehler, M., R.M. Turpening, C. Blackway and M. Mellen, Detection of a hydrofrac with shear wave vertical seismic profiles1, Proc. 52nd Annual SEG Meeting, Oct. 17-21, Dallas, Texas, 1982.

Fitch, A.A., Vertical seismic profile, V.S.P. Short Course, Southeastern Geophysical Society, New Orleans, Louisiana, March 25, 1981.

Flinn, E.A., Local earthquake location with an electronic computer, Bull. Seismol. Soc. Am., 50, 3, 467-470, 1960.

Fulp, T.J., J.P. DiSiena and J.E. Gaiser, Personal communication, 1981.

Futterman, W.I., Dispersive body waves, J. Geophys. Res., 67, 13, 1962.

Gaiser, J.E., R.W. Ward and J.P. DiSiena, Three component vertical seismic profiles: polarization measurements of P-wave particle motion for velocity analysis, Proc. 52nd Annual SEG Meeting, Oct. 17-21, Dallas, Texas, 1982.

Gallagher, J.N. and C.C. Lash, Seismic attenuation studies at Mounds, Oklahoma, Presented at the 48th Annual SEG Meeting, San Fransisco, CA, 1978.

Galperin, E.I., Detailed investigation of a velocity model of the upper part of a profile under conditions of weak velocity differentiation, Izv., Geophys. Ser., 4, 456-474, 1964.

Galperin, E.I., The intensity of head and transcritically reflected waves from vertical seismic profiling data, Izv., Earth Physics, 10, 9-24, 1966.

Galperin, E.I., All Union Seminar, Experience, results and prospects of the use of vertical seismic profiling (VSP) for the purpose of increasing the effectiveness of seismic prospecting, Izv., Earth Physics, 11, 107-109, 1970.

Galperin, E.I., Vertical Seismic Profiling, Society of Exploration Geophysicists, Special Publication No. 12, Tulsa, Okla., 1974 (originally published in Russian by Nedra, Moscow, USSR, 1971).

Galperin, E.I., Polarization of seismic waves and the possibility of increasing the efficiency of seismic investigations, Izv., Earth Physics, 2, 107-121, 1975.

Galperin, E.I. and A.V. Frolova, The study of converted waves by vertical seismic profiling, Izv., Earth Physics, 9, 93-104, 1966.

Galperin, E.I., A.N. Amirov, and P.A. Troitskiy, A method of selecting waves in vertical seismic profiling, Izv., Earth Physics, 6, 92-95, 1970.

Galperin, E.I. and A.V. Frolova, Three component seismic observations in boreholes, Parts 1 and 2, Bull. Acad. Sci. USSR, Geophys. Ser., English Trans., 519-528, 644-653, 1961.

Galperin, E.I. and A.V. Frolova, Three component seismic observations in boreholes, 1, Vertical Seismic Profiling, Izv. Geophys. Ser., 793-809, 1961.

Galperin, E.I., L.M. Vorovskiy and R.M. Galperina, Seismological observations in wells and possibilities of increasing the useful sensitivity of the equipment, Izv. Earth Physics, 2, 79-89, 1976.

Gamburtsev, A.G., Determining velocity characteristics of a medium using well shooting with observation points inside the meidum, Exploration Geophysics, vol. 99, ed. G.V. Keller, Consultants Bureau, N.Y., 1969 (Trans. of Prikladnaya Geofiz., v. 49, 45-58, 1967, in Russian).

Ganley, D.C., A method for calculating synthetic seismograms which include the effects of absorption and dispersion, Geophysics, 46, 8, 1100-1107, 1981.

Ganley, D.C. and E.R. Kanawewich, Measurement of attenuation and dispersion from Check Shot Surveys, J. Geophys. Res., 85, 5219-5226, 1980.

Gardner, L.W., Seismograph determination of salt-dome boundaries using well detection deep on zone flanks, Geophysics, 14, 1, 1949.

Garriott, J.C., Vertical seismic profiling data acquisition, Seismograph Service Corp. Tech. Memo No. D26, Tulsa, Okla., 1981.

Gilbert, F. and A.M. Dziewonski, An application of inverse theory to the retrieval of structural parameters and source mechanisms from seismic spectra, Phil. Trans. Roy. Soc., A278, 1975.

Gladwin, M.T. and F.D. Stacey, Anelas ic degradation of acoustic pulses in rocks, Phys. Earth Plan. Int., 8, 332-336, 1974.

Goetz, J.F., L. Dupal and J. Bowles, An investigation into the discrepancies between sonic log and seismic check shot velocities, Australian Petrol. Explor. Assoc. Journal, 19, 1, 131-141, 1979.

Goupillaud, P.L., An approach to inverse filtering of near surface layer effects from seismic records, Geophysics, 26, 6, 754-760, 1961.

Grant, F.S. and G.F. West, Interpretation Theory in Applied Geophysics, McGraw-Hill Co., N.Y., 1965.

Gregory, A.R., Aspects of rock physics from laboratory and log data that are important in seismic interpretation, in Seismic Stratigraphy - Applications to Hydrocarbon Exploration, AAPG Memoir Publication 26, ed. by C.A. Payton, Tulsa, OK, 1977.

Gretener, P.E.F., An analysis of the observed time discrepancies between continuous and conventional well velocity surveys, Geophysics, 26, 1, 1-11, 1961.

Hardage, B.A., The user/interpreter awareness of VSP data, presented at SEG/Southeastern Geophysical Society Short Course, New Orleans, LA, March 25, 1981.

Hardage, B.A., An examination of tube wave noise in vertical seismic profiling data, Geophysics, 46, 6,892-903, 1981.

Hardage, B.A., Vertical Seismic Profiling, Geophysical Press, to be published in 1983.

Hauge, P.S., Measurements of attenuation from vertical seismic profiles, Geophysics, 46, 11, 1981.

Hays, D.B., R.N. Shurtleff, and C.B. Wason, Applications of rigorous seismic inversion, SEG Convention Paper, S-64, 1979.

Hays, D.B., A.D. McAulay, R.N. Shurtleff and C.B. Wason, Seismic inversion by modeling, presented at the 50th Annual SEG Meeting, Houston, Texas, No. W-1, 1980.

Henderson, J.B. and R. Brewer, Borehole velocity surveys, Geophysics, 18, 2, 1953.

Hilterman, F.J., Amplitudes of seismic waves - a quick look, Geophysics, 40, 5, 1975.

Holste, W., Problems and results with reflection and refraction seismics in boreholes, Geophysical Prospecting, 7, 2, 1959.

Hoversten, G.M., A. Dey and H.F. Morrison, Comparison of five least-square inversion techniques in resistivity sounding, Geophys. Prosp., 30, 688-715, 1982.

Huang, C. and J.A. Hunter, The correlation of 'tube wave' events with open fractures in fluid-filled boreholes, Geological Survey of Canada Report, 1980.

Huang, C. and J.A. Hunter, The 197Ɛ progress report on the seismic and downhole surveys at the Chalk River and Whiteshell research areas, Atomic Energy of Canada Limited, TR- 31 May 1980.

Hubbard, T.P., Deconvolution of surface recorded data using vertical seismic profiles, presented at 49th Annual SEG Meeting, no. S-46, New Orleans, LA, 1979.

Jackson, D.D., Interpretation of inaccurate, insufficient and inconsistent data, Geophys. J. Roy. astr. Soc., 28, 1972.

JCEIGS, Jacobi Rotations Algorithm, Univ. of Waterloo Computing Center, Waterloo, Ontario, Canada, 1971.

Johnson, W.W. and H.H. Nogami, One-dimensional inversion of seismic data, presented at 52nd Annual SEG Meeting, Oct. 17-21, paper no. S15.2, Dallas, Texas, 1982.

Jolly, R.N., Deep-hole geophone study in Garvin County, Oklahoma, Geohysics, 19, 662-670, 1953.

Kan, T.K., Personal communication, 1981.

Kan, T.K., D. Corrigan, and P.D. Huddleston, Attenuation measurements from vertical seismic profiles, presented at the 51st Annual SEG Meeting, Los Angeles, Oct. 11-15, 1981.

Karus, E.V., L.A. Ryabinkin, E.I. Gal'perin, V.A. Teplitskiy, Y.B. Demidenko, K.A. Mustafayev and M.B. Rapoport, Detailed investigations of geologic structures by seismic well surveys, 9th World Petroleum Congress Proc., v. 3, 247-257, 1975.

Keho, T., Traveltime inversion with refractions, Personal communication, 1982.

Keho,T., Dynamics of in situ (VSP) wave fields, M.I.T. internal paper, Cambridge, MA., 1982.

Kennett, P. and R.L. Ireson, Recent developments in well velocity surveys and the use of calibrated acoustic logs, Geophys. Prosp., 19, 395-411, 1971.

Kennett, P., R.L. Ireson and P.J. Conn, Vertical seismic profiles: their applications in exploration geophysics, Geophys. Prosp., 28, 5, 676-699, 1980.

Kikuchi, M. and H. Kanamori, Inversion of complex body waves, Bull. Seism. Soc. Am., 57, 1017-1023, 1982.

Kokesh, F.P., The development of a new method of seismic velocity determination, Geophysics, 3, 560-574, 1952.

Koefoed, O., Aspects of vertical seismic resolution, Geophys. Prosp., 29, 21-30, 1981.

Kunetz, G., and I. D'Erceville, Sur certaines proprieties d'une onde plane de compression dans un milieu stratific, Ann. Geophysique, 18, 351-359, 1962.

Lamb, H., On the velocity of sound in a tube as affected by the elasticity of the walls, Manchester Memoirs, 42, 1-16, 1898.

Lang, D.G., Downhole seismic: Technique exands borehole data, Part 1, Oil and Gas Journal, 77, 28, 1979a.

Lang, D.G., Downhole seismic: Combination of technques sees nearby features, Conclusion, Oil and Gas Journal, 77, 29, 1979b.

Lash, C.C., Shear waves, multiple reflections and converted waves formed by a deep vertical wave test (Vertical Seismic Profiling), Geophysics, 45, 9, 1373-1411, 1980.

Lash, C.C., Investigation of multiple reflections and wave conversions by means of vertical wave test (Vertical Seismic Profiling) in Southern Mississippi, Geophysics, 47, 7, 977-1000, 1982.

Laverge, M. and C. Willm, Inversion of seismograms and pseudo-velocity logs, Geophys. Prosp., 25, 231-250, 1977.

Lee, M.W. and A.H. Balch, Computer processing of vertical seismic profiling data, Geophysics, 48, 3, 272-287, 1983.

Levin, F.K. and R.D. Lynn, Deephole geophone studies, Geophysics, 23, 4, 1958.

Lindseth, R.O., Stratigraphic traps with synthetic sonic logs, Dallas Geophysical Society Short Course, Dallas, TX, December 10, 1979.

Lindseth, R.O., Synthetic sonic logs - a process for stratigraphic interpretation, Geophysics, 44, 1, 1979.

Lomnitz, C., Creep meausurements in igneous rocks, J. Geology, 64, 473-479, 1956.

Lomnitz, C., Linear dissipation in solids, J. Applied Physics, 28, 201-205, 1957.

Madden, T. and S. Park, Formulation of the 1-D Inverse Problem, Personal Communication, 1983.

Marquardt, D.W., An algorithm for least-squares estimation of nonlinear parameters, J. Soc. Indust. Appl. Math., 11, 2, 1963.

McCaslin, J.C., Independents step up exploration pace, Oil Gas J., 77, 44, 1979.

McCaslin, J.C., Anadarko play heads busy mid-continent campaign, Oil Gas J., 79, 21, 1981.

McCollum, B. and W.W. LaRue, Utilization of existing wells in seismograph work, Bull. Am. Assoc. Petro.. Geol., 15, 12, 1409-1417, 1931.

McCormack, M.D., R.G. Quay, and R.W. Verm, A study of the time variant character of source signatures in boreholes, presented at the 49th Annual SEG Meeting, No. S-51, New Orleans, LA, 1979.

McDonal, F.J., F.A. Angona, R.L. Mills, R.L. Sengbush, R.G. Van Nostrand, and J.E. White, Attenuation of shear and compressional waves in Pierre shale, Geophysics, 23, 421-439, 1958.

Mellman, G.R., A method of body-wave waveform inversion for the determinates of earth structure, Geophys. J. R. astr. Soc., 62, 481-504, 1980.

Mellen, M.H., VSPRT: A FORTRAN program to generate synthetic vertical seismic profiles in two-dimensional media using asymptotie ray theory, Earth Resources Lab, M.I.T. Internal Report, Cambridge, MA, 1982.

Michon, D., Presidential Address, Geophys. Prosp., 30, i-v, 1982.

Michon, D., P. Tariel and Y. Ollivier, Le Film sismique vertical en tant qu'outil complememtaire des diagraphies, Trans. 7th SPWLA European Logging Symposium, Paris, Oct. 21-23, 1981.

Miller, G.F. and H. Pursey, The field and radiation impedance of mechanical radiators on the free surface of a semi-infinite isotropic solid, Proc. Roy. Soc., A, 223, 521-530, 1954.

Mons, F., Vertical seismic exploration and profiling technique, United Kingdom Patent Application No. 2029016, March 12, 1980.

Mons, F. and K. Babour, Vertical seismic profiling: recording, processing, applications, Schlumberger Technical Memo, M-083425, 1981.

Mooney, H.M., Seismic shear waves in engineering, J. Geotechnical Eng. Div., ASCE, No. GT8, 905-923, August, 1974.

Morris, J.L., Jr., Attenuation estimates from seismograms recorded in a deep well, M.S. Thesis, Graduate College of Texas A & M University, College Station, TX, 1979.

Nabelek, J., Inversion of body waves for the earthquake source, Ph.D. Thesis, Dept. of Earth and Planetary Sciences, M.I.T., Cambridge, MA, 1983.

Newman, P., Divergence effects in a layered earth, Geophysics, 38, 3, 1973.

Newman, P.J., and M.H. Worthington, In situ investigation of seismic body wave attenuation in heterogeneous media, Geophys. Prosp., 30, 377-400, 1982.

O'Brien, P.N.S. and A.L. Lucas, Velocity dispersion of seismic waves, Geophys. Prosp., 19, 1-26, 1971.

O'Doherty, R.F. and N.A. Anstey, Reflections on amplitudes, Geophys. Prosp., 19, 430-458, 1971.

Ohta, Y., N. Goto, F. Yamamizu, and H. Takahashi, S-wave velocity measurements in deep soil deposit and bedrock by means of an elaborate down-hole method, Bull. Seism. Soc. Am., 70, 1, 363-377, 1980.

Omnes, G., Vertical seismic profiling: A bridge between velocity logs and surface seismograms, 53rd Annual SPE Fall Conference, SPE Paper No. 7436, Houston, TX, Oct. 1-3, 1978.

Omnes, G., Logs from P and S vertical seismic profiles, Journal of Petroleum Technology, 32, 10, 1980.

Omnes, G., Personal communication, January, 1983.

Parker, R.K., Understanding seismic inverse theory, Ann. Rev. Earth Plan. Science, 5, 1977.

Peyret, O. and F. Mons, Sonic versus seismic velocities: positive drift study, recording frequency effect, Schlumberger Technical Memo, M-083210, 1981.

Pilant, W.L., Elastic Waves in the Earth, Elsevier, Sci Publ. Co., Amsterdam, The Netherlands, 1979.

Prange, M.D., Calculation of synthetic VSP seismograms using the discrete wavenumber method, M.I.T. Earth Resources Lab Memo, January 1983.

Rice, R.B., S.J. Allen, O.J. Gant, Jr., R.N. Hodgson, D.E. Larson, J.P. Lindsey, J.R. Patch, T.R. LeFehr, G.R. Pickett, W.A. Schneider, J.E. White, and J.C. Roberts, Developments in exploration geophysics, 1975-1980, Geophysics, 46, 8, 1981.

Richards, P.G. and W. Menke, The apparent attenuation of a scattering medium, to be submitted to Bull. Seis. Soc. Am., 1982.

Ricker, N., The form and laws of propagation of seismic wavelets, Geophysics, 18, 1, 10-40, 1953.

Riggs, E.D., Seismic wave types in a borehole, Geophysics, 20, 1, 53-67, 1955.

Robertson, J.D. and D. Corrigan, Radiation patterns of a shear-wave vibrator in near-surface shale, Geophysics, 48, 1, 19-26, 1983.

Robinson, E.A. and S. Treitel, Geophysical Signal Processing, Prentice-Hall, Englewood Cliffs, NJ, 1980.

Rudnitskiy, V.P., Vertical travel-time curves of refracted waves and multiply refracted waves, Izv., Earth Physics, 12, 89-93, 1968.

Sabatier, P.C., On the geophysical inverse problem, J. Geophys. Res., 43, 1977.

Schepers, R., High resolution near surface reflection measurements using a vertical array technique, J. Geophys., 43, nos. 5-6, 791-806, 1977.

Schlumberger, Schlumberger Seismic Services, Technical Memo No. SMP-5031, 1982.

Schoenberger, M. and F.K. Levin, Apparent attenuation due to intrabed multiples, Geophysics, 39, 3, 278-291, 1974.

Schoenberger, M. and F.K. Levin, Apparent attenuation due to intrabed multiples II, Geophysics, 43, 4, 730-737, 1978.

Seeman, B. and L. Horowicz, Vertical seismic profiling: separation of upgoing and downgoing acoustic waves in a stratified medium, Schlumberger Technical Paper, M-083424, 1981.

Seismograph Service Limited, The V.S.P. Modelling Atlas, 2nd edition, Holwood, Keston, Kent, U.K., 1980.

Sheriff, R.E., Factors affecting seismic amplitudes, Geophys. Prosp., 23, 125-138, 1975.

Sheriff, R.E., Limitations on resolution of seismic reflections and geologic detail derivable from them, in Seismic stratigraphy - Applications to hydrocarbon exploration, Memoir 26, Am. Assoc. Petroleum Geol., Tulsa, OK, 1977.

Sherwood, J.W.C. and A.W. Trorey, Minimum-phase and related properties of the response of a horizontally stratified absorptive earth to plane acoustic waves, Geophysics, 30, 2, 191-197, 1965.

Simaan, M. and D. Jovanovich, Optimum filters for vertical array seismic data processing, presented at the 50th Annual SEG Meeting, Houston, TX, No. R-20, 1980.

Slotnick, M.M. On seismic computations, with applications I, Geophysics, 1, 1, 9-22, 1936a.

Slotnick, M.M., On seismic computations, with applications, II, 1, 3, 299-305, 1936b.

Spencer, T.W., J.R. Sonnad and T.M. Butler, Seismic Q-stratigraphy or dissipation, Geophysics, 47, 1, 16-24, 1982.

Stacey, F.D., M.T. Gladwin, B. McKavanaugh, A.T. Linde and L.M. Hastie, Anelastic damping of acoustic and seismic profiles, Geophysical Surveys, 2, 133-151, 1975.

Stewart, R.R., R.M. Turpening and M.N. Toksoz, Study of a subsurface fracture zone by vertical seismic profiling, Geophysical Research Letters, 8, 11, 1132-1135, 1981.

Stewart, R.R., P.D. Huddleston, and T.K. Tan, Traveltime analysis and vertical seismic profiles, Proc. 52nd Annual SEG Meeting, Oct. 17-21, Dallas, TX, 1982.

Stewart, R.R., Interval velocities from vertical seismic profiles: A review and least-squares traveltime inversion, submitted to Geophysical Prospecting, December, 1982.

Stewart, R.R., Velocity analysis and vertical seismic profiles, ARCO Oil and Gas Research Report, No. RR81-50, 45 pp., Dallas, TX, 1982.

Stone, D.G., Prediction of depth and velocity on VSP data, Proc. 52nd Annual SEG Meeting, Oct. 17-21, Dallas, TX, 1982.

Strick, E., An explanation of observed time discrepancies between continuous and conventional well surveys, Geophysics, 36, 2, 285-295, 1971.

Tango, G.J., Vertical Seismic Profiling: An overview, V.S.P. Short Course, Southeastern Geophysical Society, New Orleans, Louisiana, March 25, 1981.

Tarantola, A. and B. Valette, Generalized nonlinear inverse problems solved using the least squares criterion, Rev. Geophys. Space Phys., 20, 2, 219-232, 1982.

Temme, P. and G. Muller, Numerical simulation of vertical seismic profiling, J. Geophys., 50, 177-188, 1982.

Thomas, D.H., Seismic applications of sonic logs, The Log Analyst, 19, 1, 1978.

Thurber, C.H., Earth structure and earthquake locations in the Coyote Lake Area, Central California, Ph.D. Thesis, Department of Earth and Planetary Sciences, M.I.T., Cambridge, MA, 1981.

Toksoz, M.N., R.M. Turpening and R.R. Stewart, Assessment of the Antrim oil shale fracture zone by vertical seismic profiling, U.S. Dept. of Energy Report No. FE-2346-91, September, 1980.

Tullos, F.H. and A.C. Reid, Seismic attenuation in Gulf Coast sediments, Geophysics, 34, 516-528, 1969.

Turpening, R.M., Seismic wave generator and method of geophysical prospecting using the same, U.S. Patent No. 4059820, Nov. 22, 1977.

Turpening, R.M., Tube wave attenuation in Michigan VSP, Personal communication, 1980.

Van der Stoep, D.M., Velocity anisotropy measurements in wells, Geophysics, 31, 1966.

Van Sandt, D.R. And F.K. Levin, A study of cased and open holes for deep-hole seismic exploration, Geophysics, 28, 1963.

Walling, D. and C. Savit, Interpretation methods for well velocity surveys, Geophysical Prospecting, 5, 1, 1957.

Ward, R.W. and M.R. Hewitt, Monofrequency borehole traveltime survey, Geophysics, 42, 6, 1137-1145, 1977.

Weaver, P., Relations of geophysics to geology, Bull. Am. Assoc. Petrol. Geol., 18, 1, 3-12, 1934.

White, J.E. and R.L. Sengbush, Velocity measurements in near-surface formations, Geophysics, 18, 1, 54-69, 1953.

White, J.E., Seismic Waves: Radiation, Transmission and Attenuation, McGraw-Hill Book Co., New York, 1965.

Widess, J., How Thin is a Thin Bed?, Geophysics, 38, 6, 1176-1180, 1973.

Wiggins, R.A., The general linear inverse problem: implication of surface waves and free oscillations for earth structure, Rev. Geophys. Space Phys., 10, 1, 251-285, 1972.

Wingo, J.R., Velocity and attenuation determinations from a vertical seismic profile, M.S. Thesis, Department of Earth and Planetary Sciences, M.I.T., Cambridge, MA, 1981.

Willis, M.E., Seismic velocity and attenuation from full waveform acoustic logs, Ph.D. Thesis, Department of Earth and Planetary Sciences, M.I.T., Cambridge, MA, 1983.

Wright, C. and P. Johnson, On the generation of P and S wave energy in crystalline rocks, Geophys. Prosp., 30, 58-70, 1982.

Wuenschel, P.C., Seismogram synthesis including multiples and transmission coefficients, Geophysics, 25, 1, 106-129, 1960.

Wuenschel, P.C., Dispersive body waves - an experimental study, Geophysics, 30, 4, 539-551, 1965.

Wuenschel, P.C., The vertical array in reflection seismology, Geophysics, 41, 2, 219-232, 1976.

Wyatt, K.D., Synthetic vertical seismic profile, Geophysics, 46, 6, 880-891, 1981.

Wyatt, K.D. and S.B. Wyatt, Downhole vertical seismic profile survey reveals structure near borehole, Oil and Gas Journal, 80, 42, 77-82, 1982.

Zeitvogel, M.E., Investigation of frequency dependent attenuation in a vertical seismic profile, M.S. Thesis, Graduate College, Texas A & M University, College Station, TX, 1982.

Appendix I.

FRACTURE ZONE DELINEATION

GEOPHYSICAL RESEARCH LETTERS, VOL. 8, NO. 11, PAGES 1132-1135, NOVEMBER 1981

STUDY OF A SUBSURFACE FRACTURE ZONE BY VERTICAL SEISMIC PROFILING

Robert R. Stewart, Roger M. Turpening, and M. Nafi Toksoz

Department of Earth and Planetary Sciences,
Massachusetts Institute of Technology, Cambridge, MA, 02139

Abstract. Remotely estimating the properties of subsurface fracture zones is important in characterizing the structure of the shallow earth. We present a vertical seismic profiling (VSP) technique to make this fracture zone estimation and discuss the results of a VSP experiment performed in the upper 770 m of the Michigan Basin. Both P and SH waves were used to observe an explosively-fractured volume of Antrim shale. The experiment was divided into two parts: a "before" survey run on the unaltered rock, then an identical "after" survey executed across the fractured volume. A seismic velocity structure of the basin was calculated from the "before" survey. Comparison of the "after" observations to the "before" data, elucidated the fracture volume and its effective elastic parameters. From travel-time delays, amplitude attenuation, converted and scattered waves, we estimated the depth (395 m), shape (ellipsoidal), size (10 m x 20 m x 30 m) and porosity (20%) of the fracture zone.

Introduction

The characterization of subsurface fracture zones is of fundamental importance in a number of pursuits such as geothermal energy production, the recovery of hydrocarbons and waste disposal. As direct access (such as a mine shaft) to the total fracture volume is generally unavailable, remote measurements must be made. Presented here is a vertical seismic profiling (VSP) method for making such measurements. This VSP technique (Figure 1) uses both P and S wave surface sources and a down-hole receiver. The receiver is clamped at a desired depth in the well and the waves from the surface source are recorded. The receiver is then moved to new depths where the measurements are repeated (McDonal et al., 1958; Gal'perin, 1974; Lash, 1980; Toksoz et al., 1980).

In particular, we use the VSP technique to elucidate the characteristics of a subsurface explosively-fractured volume of Antrim oil shale. To determine the parameters (size, orientation, velocity, porosity) of the fracture zone, "before" and "after" fracturing measurements were taken. The before data was collected prior to any explosive alteration of the earth. Careful comparison of the after data (the post-fracturing survey run exactly as the before survey) to the before data allowed us to make an estimation of the parameters relating to the fracture zone.

Location and Procedure

This project was conducted near Peck, Michigan about 100 km north of Detroit. In this region the Antrim oil shale extends through the depths 370 m to 430 m. It is one of the area's numerous nearly horizontal beds of shale, limestone and sandstone (Washington, 1978).

Four VSP surveys were accomplished. The surface geometry of these surveys is shown in Figure 2. The source was kept in a fixed location while the wall-clamping three-component borehole seismometer (receiver) was winched up the well, stopping at 7.6 m (25 ft.) intervals. At each of the positions, a P wave and right and left polarized shear wave were generated by the source. The S wave generator was fired first at a 90° angle, then a 270° angle to the line joining the source and the well-head. This generated predominantly P and SH wave energy (see Toksoz et al., 1980 for a full discussion of the SH generation process). These three "shots" were recorded sequentially and without stacking by the down-hole receiver and by a three-component surface monitor geophone. A 1.0 ms sampling rate was used by the digital recording equipment.

Velocity Profiles

From the first-arriving P and SH waves in the H line survey (the complete SH section is shown in Figure 3), we deduced the P and SH interval velocities. The use of polarized SH waves (the SV waves generated weren't polarized) greatly

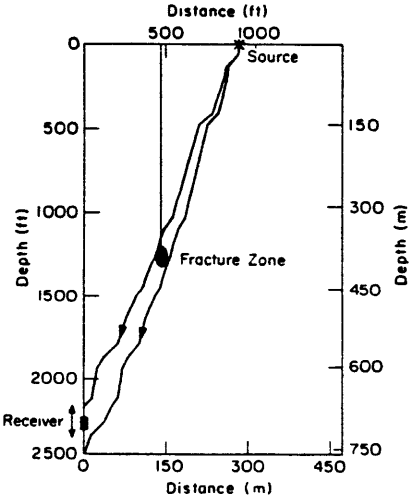

Fig. 1. Schematic cross-section (D line) of VSP survey. Two seismic rays are shown which bound the fracture zone. The source generates seismic energy which propagates through the medium and is recorded by the down-hole geophone (receiver). The source fires for each receiver depth.

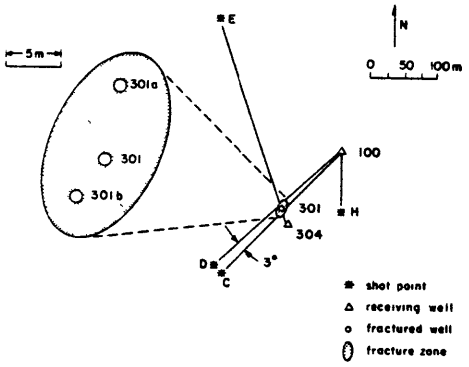

Fig. 2. Surface geometry of VSP survey lines and wells. The fracture zone, in plan view, is shown enlarged at left.

facilitated the identification of first-arriving shear energy. Preliminary velocity sections were computed using a simple inversion scheme (Dix, 1945). These velocities were altered, by a standard two-dimensional ray-tracing computer program, until the ray-traced travel times agreed with the observed times to within experimental error (2.0 ms for P waves, 3.0 ms for SH waves). Errors in the travel times were a result of inaccurate zero-time breaks and inexact time-picks. Tool slippage in the well (erroneous depths) and two-dimensional modelling are further sources of error in the final velocity section.

The VSP velocity section and sonic log are shown in Figure 4. Also graphed is the regional geologic section. We note that the seismic P and SH interval velocities correlate well. The sonic log and VSP velocities are also generally in accord, although some discrepancies exist. This may be due to VSP or sonic log error or the fact that the two techniques sample different rock volumes (Gretener, 1961).

The seismic P and SH velocities in the Antrim shale were 3078 m/s and 1945 m/s, respectively. These are at worst 8% different from the sonic log values. Ultrasonic core analysis gave V_p values ranging from 3180 m/s to 4825 m/s. Ultrasonic V_s values ranged from 2073 m/s to 2814 m/s (Humphrey, 1978).

Fracturing

After the VSP surveys had been done on the unaltered ground, the central well and two nearby wells (#301, 301a, 301b -shown in Figure 2) were explosively fractured. Approximately 700 kg of explosive slurry was used in each well. This liquid explosive occupied a column of about 15 m above the average well depth of 405 m. The same set of VSP surveys was done again, now including the fracture zone. Careful comparison of the before and after data revealed a number of differences associated with the fracture zone.

On the receiver close to the fracture zone (E line) we observed both P and SH time delays (Figure 5). The maximum P delay (the difference between after and before travel times) was 3.0 ms. The maximum SH delay was 6.4 ms. Both of these delays tapered to zero at their upper and lower ends. The consistency of these time differences inspired confidence in them. From these delays we deduced that the vertical extent of the altered zone was from about 380 m to 410 m depth. The tapered delays indicated that the fracture zone itself was tapered (perhaps ellipse-like in cross-section). P wave attenuation was also noted in this same vertical area. Plotted in Figure 5 is the ratio of the peak-to-peak value of the first cycle of the after waveform to the value of the before waveform. This ratio reaches a minimum value of 0.5. Spectral ratio comparisons of before and after waveforms in the fracture zone gave exceedingly small Q values around 2.0. This low Q is consistent with the attenuating effect on seismic waves of a highly fractured rock. Using before waveforms 30 m and 60 m apart, the spectral ratio method gave a Q of about 20 for the unaltered shale.

Other evidence of the fracture zone came from the lines which had the fractured region half-way between the source and receiver (C and D lines). One observation on these records was that the vertical geophone received polarized energy from the SH sources over a certain depth on the after records but not on the before traces. From ray-tracing this interval was found to be that directly in the shadow area of the postulated

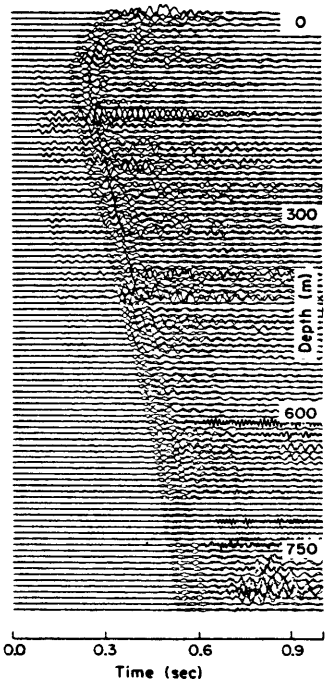

Fig. 3. Complete SH seismic section overlay (H line) for right and left polarized sources.

fracture zone (centered at 395 m depth, 30 m high with a 20 m length, refer to Figure 1). The magnitude of these events was puzzling , but it appears that some type of complicated conversion is occurring. As both C and D lines showed this conversion, they are consistent with a minimum fracture zone width (NW-SE dimension) of 7 m and minimum length (NE-SW dimension) of 20 m.

Unfortunately there wasn't a fan of lines surveyed which could have directly determined the fracture zone width. In light of this we applied the scattering theory of Yamakawa (1962) in attempt to further constrain the fracture zone width. Yamakawa's theory presents an analytic solution for the scattered wave generated by a plane P wave incident on a spherical anomaly (low velocity zone) in a half-space. In the present case, the fracture zone was in a thick layer of shale and was a number of wavelengths from the source, as is assumed by Yamakawa's theory. The fracture zone was not spherical however, so we use the anomaly diameter as just an approximation to the fracture zone width. As the amount of wave scattering varies with the cube of the diameter of the scatterer, we used the decrease in the amplitude ratio, shown in Figure 5, to compute the fracture zone width. Knowing the impinging wavelength and approximate velocity anomalies (from previous width estimates and time delays), the theory predicted a diameter of about 10 m. We note also that the local amplitude minimum at 373 m depth agreed with the position of a secondary scatter lobe, as postulated by the Yamakawa theory. Now supposing that each borehole was fractured equally (10 m fracture diameter for each well), then the three boreholes give a combined length of about 20 m (see Figure 2). This is in accord with the C and D line observations.

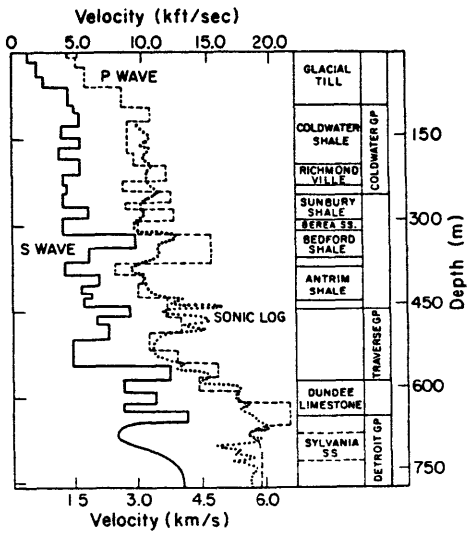

Fig. 4. Compendium of VSP P and SH velocities, sonic log and geologic section for experimental site near Peck, Michigan.

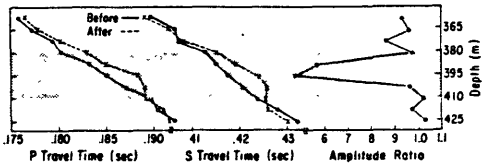

Fig. 5. Before versus after P and SH wave travel times and amplitude ratios.

If we consider all of the above information together, then an approximate, but cogent interpretation is possible. Because the wavelength of the seismic energy is long (about 75 m) and our vertical sampling is coarse (7.6 m), we do not expect a highly resolved zone. Nevertheless the observations are consistent with the interpretation that the fracture zone has a vertical dimension of 30 m, a length in the NE direction of 20 m, and a width of 10 m. As the fractured region with these dimensions appears to taper toward its extremities, it is simplest to describe it as approximately ellipsoidal.

Non-Seismic Observations

Numerous theoretical formulations have been devised to relate explosive yield to the resulting diameter of permanent rock deformation for nuclear events (Mueller and Murphy, 1971) and shallow chemical explosions (Gurvich et al., 1966). We combined these formulations (by introducing depth dependence into the shallow explosion equation) to describe an intermediate-depth chemical explosion. It states that

$$D = \frac{16.0\, W^{1/3}}{h^{0.42}} \qquad (1)$$

where D is the diameter of permanent deformation (m)
W is the weight of explosive (kg)
h is the explosion depth (m)
For the explosive weight of 712 kg (in well 301), this formulation predicts a fracture zone diameter of 12 m, slightly larger than the seismic estimate of 10 m. Caliper logs were run which showed an enlarged borehole over the depths from 384 m to 412 m. Pressurized air flow tests were also performed (Kim, 1978). These indicated that the wells 5 m away from the fractured well were in communication. Well 304 (line E receiver) was not in communication with the fracture zone. Generally, wells greater than 8 m away from the fracture zone center were not in communication.

Porosity

Cracks and pores in a rock lower its P and S wave velocities. Several formulations have been developed to invert lowered velocities for the causative crack density and porosity (Cheng and Toksoz, 1979; Crampin et al., 1980). In the present case, knowing the thickness of the fracture zone and the travel-time delays we calculated the reduced velocity values. P and SH velocities were found to be 1600 m/s and 870 m/s, respectively. Using the reduced velocities as

representative of a uniformly cracked medium, the pre-fracture velocities as the cracked medium's matrix velocities, and saturated cracks we calculated (after Cheng and Toksoz, 1979) the fracture zone properties. The P and SH velocity reductions require a crack aspect ratio of 0.03 and porosity of 20%. . This is an extremely large increase from the pre-fracture porosity of 3% (Washington, 1978). Again the zone appears to be highly fractured, but this high porosity estimate strains the validity of the velocity inversion formulations.

Conclusions

The VSP method has established the P and SH velocity structure in the Michigan Basin to a depth of 770 m. P and SH interval velocities show a good degree of correlation. The VSP velocities are in accord with the laboratory and sonic log measurements.

By using the "before" and "after" VSP technique and observing the differences between the two data sets, the fracture zone parameters have been estimated. The zone appears to be a highly fractured (20% porosity) ellipsoidal volume with its major axis (height) in the vertical direction and minor axis (width) facing NW. The dimensions of the zone are about 30 m x 20 m x 10 m and it is centered at 395 m depth. It has reduced seismic velocities (about one-half the unaltered values) and a very high attenuation (Q = 2.0). The VSP interpretation is internally consistent and is supported by the non-seismic observations. The VSP results gave the overall extent and porosity of the fracture zone, complementing the non-seismic techniques which gave cavity size and communication information.

Acknowledgements. This work was performed under contract 770154-M0853-51 with Dow Chemical, U.S.A. under Prime Contract D.O.E. EX76-C-01-2346.

References

Cheng, C.H. and M.N. Toksoz, Inversion of seismic velocities for the pore aspect ratio spectrum of a rock, J. Geophys. Res., 84, 7533-7543, 1979.

Crampin, S., R. McGonigle, and D. Bamford, Estimating crack parameters from observations of P wave velocity anisotropy, Geophysics, 45, 345-360, 1980.

Dix, C.H., The interpretation of well-shot data, Geophysics, 10, 160-170, 1945.

Gal'perin, E.I., Vertical Seismic Profiling, Society of Exploration Geophysicists Special Publication No. 12, Tulsa, Okla., 1974.

Gretener, P.E.F., An analysis of the observed time discrepancies between continuous and conventional well velocity surveys, Geophysics, 26, 1-11, 1961.

Gurvich, I.I. et al., Experimental amplitude characteristics of an explosion, Izv. Earth Phys., 3, 33-43, 1966.

Humphrey, J.P., Energy from in situ processing of Antrim oil shale, U.S. Dept. of Energy Report No. FE-2346-20, January 1978.

Kim, K., Mechanical characteristics of Antrim shale, U.S. Dept. of Energy Report No. FE-2346-24, 1978.

Lash, C.C., Shear waves, multiple reflections, and converted waves formed by a deep vertical wave test (vertical seismic profiling), Geophysics, 45, 1373-1411, 1980.

McDonal, F.J. et al., Attenuation of shear and compressional waves in Pierre shale, Geophysics, 23, 421-439, 1958.

Mueller, R.A. and J.R. Murphy, Seismic characteristics of underground nuclear detonations, Part I and II, Bull. Seis. Soc. Am., 61, 1675-1713, 1971.

Toksoz, M.N., R.M. Turpening, and R.R. Stewart, Assessment of the Antrim Oil Shale fracture zone by vertical seismic profiling, U.S. Dept. of Energy Report No. FE-2346-91, September, 1980.

Washington, L.J., Energy from in situ processing of Antrim oil shale, U.S. Dept. of Energy Report No. FE-2346-34, July 1978.

Yamakawa, N., Scattering and attenuation of elastic waves, Geophysical Magazine (Tokyo), 31, 63-103, 1962.

(Received April 21, 1981;
revised June 22, 1981;
accepted July 14, 1981.)

ATTENUATION MEASUREMENT

JOURNAL OF GEOPHYSICAL RESEARCH, VOL. 88, NO. B1, PAGES 546–554, JANUARY 10, 1983

Strain Dependent Attenuation: Observations and a Proposed Mechanism

ROBERT R. STEWART AND M. NAFI TOKSOZ

Earth Resources Laboratory, Department of Earth and Planetary Sciences, Massachusetts Institute of Technology Cambridge, Massachusetts 02139

A. TIMUR

Chevron Oil Field Research Company, La Habra, California 90631

The measured attenuation (Q^{-1}) of a rock is a function of a number of parameters, one of those being the applied strain amplitude. It is important to understand the effect that strain amplitude has on Q^{-1} for several reasons: different measurement techniques use differing strain amplitudes and may measure a dissimilar Q^{-1}, near source (large strain) wave propagation may behave highly non-linearly, and the strain amplitude dependence can provide insight into the attenuation mechanism. A physical model based on the contact friction between crack surfaces in the rock has been developed to describe rock deformation and dissipation under large applied strain. The three-dimensional crack surfaces are characterized by a statistical distribution of asperity heights. The sliding contact of these spherically-tipped asperities dissipates frictional energy. Hertzian theory is applied to the average asperity contact and predicts that the large strain attenuation is given by $Q^{-1} = k\zeta\varepsilon/P^{+3}$, where k is a constant consisting of the matrix elastic parameters, ζ is the crack density, ε is the strain amplitude, and P is the confining pressure. The total attenuation measured appears to be the sum of this strain dependent term and a strain independent term. The results of ultrasonic pulse transmission experiments are compared with the model's prediction. Both P and S waves with strain amplitudes from 10^{-8} to 10^{-5} were employed. Frequencies from 0.4 to 1.5 MHz were used in conjunction with rock confining pressures of 2 to 580 bars on dry Berea sandstone and lucite samples. The spectral ratio method and rise time technique were applied to deduce the Q^{-1} values. The observed data and other observations from the literature compare well with the model's prediction for the dependence of Q^{-1} on large strain amplitude, crack density, and pressure.

INTRODUCTION

The understanding and usage of seismic wave attenuation (Q^{-1}) as a rock parameter require knowledge of the behavior of Q^{-1} under various conditions. The pressure, temperature, saturation state of the rock, and the frequency of the propagating wave are all factors known to affect Q^{-1} [*Johnston et al.*, 1979; *Toksoz et al.*, 1979; *Kovach and Nur*, 1980; *Spencer*, 1981]. The effect of the amplitude of the propagating strain on Q^{-1} has been the subject of increasing research [*Peselnick and Outerbridge*, 1961; *Gordon and Davis*, 1968; *Gordon and Rader*, 1971; *Mavko*, 1979; *Winkler et al.*, 1979; *Johnston and Toksoz*, 1980; *Tittmann et al.*, 1981]. Attenuation in rocks generally increases with increasing strains once a certain threshold strain value has been reached (Figure 1). Similarly, strain amplitudes have been recognized by engineers as exerting a dominant influence on the dynamic moduli of soils [*Richart et al.*, 1970; *Imai et al.*, 1979; *Stoll*, 1979].

In this paper we propose a model of rock deformation and dissipation that predicts the effect that large strain amplitudes, pressure, and crack density have on attenuation. The model is based on Hertzian contact friction theory (after *Mavko* [1979]) and statistically defined crack surfaces [*Walsh and Grosenbaugh*, 1979] that are used to develop a mechanism for large-strain wave attenuation.

Also presented are the results of experiments designed to elucidate the strain effect. All measurements were made by using the ultrasonic pulse transmission technique [*Timur*, 1977]. Attenuation values were determined by the spectral ratio method [*Toksoz et al.*, 1979] and the rise time technique [*Gladwin and Stacey*, 1974; *Sears*, 1980]. These observations and those of other investigators are summarized and compared with the predictions of the proposed model.

Paper number 2B1618.
0148-0227/83/002B-1618$05.00

THEORETICAL MODEL

We first construct a simple physical rock model and then describe the work loss in it as a large strain wave passes. In the model we assume a homogeneous elastic matrix material with randomly oriented dry cracks, pore spaces, or grain boundaries. Only the work loss associated with the frictional sliding of adjacent surfaces (hereinafter called cracks) as a large strain wave propagates is considered. To study the dissipation at a single crack, we use a particular crack model [*Greenwood and Williamson*, 1966; *Gangi*, 1978, *Walsh and Grosenbaugh*, 1979] in conjunction with the Hertzian contact theory [*Mindlin and Deresiewicz*, 1953; *Mavko*, 1979]. *Greenwood and Williamson* [1966] supposed that the crack surfaces are covered with a statistical distribution of asperity, or bump, heights (Figure 2*a*). By assuming that these asperities have spherical tips that come in Hertzian contact (Figure 2*b*) and slide upon one another, a frictional work loss may be calculated [*Mindlin and Deresiewicz*, 1953; *Mavko*, 1979]. Summing up the frictional work loss from individual asperity contacts on a crack and then summing over all cracks gives a total work loss and thus a large strain Q^{-1} value.

Greenwood and Williamson [1966] considered a microscopic rough surface with a reference plane and a smooth surface a distance d from it (Figure 3). Given an asperity

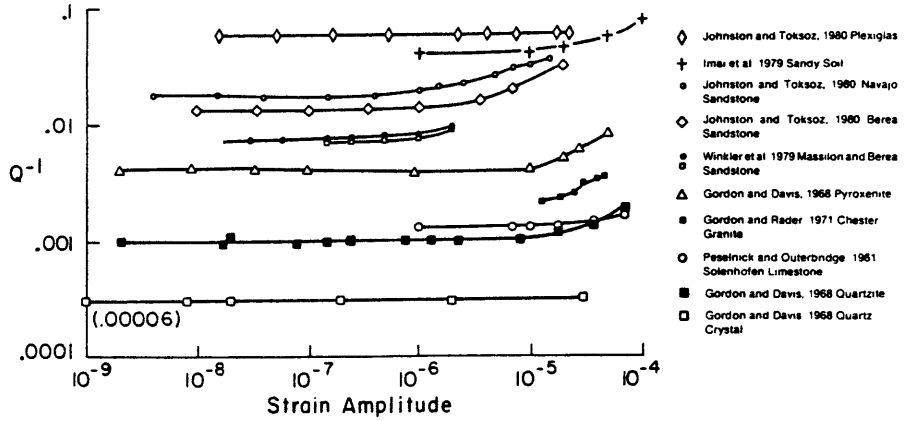

Fig. 1. Compendium of attenuation values as a function of strain amplitude. Results are from numerous investigators but most of the experiments were performed at atmospheric pressure.

height distribution $\phi(z)$ with standard deviation σ, the probability of contact between the plane and an asperity tip of height z is

$$\text{prob}\,(z \geq d) = \int_d^\infty \phi(z)dz \tag{1}$$

If there are η asperities on the crack surface then the expected number of contacts n will be

$$n = \eta \int_d^\infty \phi(z)dz \tag{2}$$

The relationship between the total load N on the volume V and the separation of the surfaces d (Figures 2 and 3) is

$$N = 2/3\eta \frac{ER^{1/2}}{(1-\nu^2)} \int_d^\infty (z-d)^{3/2}\phi(z)dz \tag{3}$$

where E is the Young's modulus of the matrix material, R is the tip radius, and ν is the Poisson's ratio for the matrix material.

Using a dimensionless asperity height variable s, and a normalized plane separation $h = d/\sigma$, and assuming an exponential asperity distribution e^{-s} (the exponential distribution is used instead of the more realistic Gaussian distribution to simplify the mathematics, as discussed by *Greenwood and Williamson* [1966]) then

$$n = \eta e^{-h} \tag{4}$$

and the load is given by

$$N = \eta(\pi R\sigma^3)^{1/2} \frac{E}{2(1-\nu^2)} e^{-h} \tag{5}$$

then from (4) and (5)

$$n = n_0 N \tag{6}$$

where

$$n_0 = \frac{2(1-\nu^2)}{(\pi R\sigma^3)^{1/2}E}$$

Also the expected area of contact C, for the exponential height distribution, is given by

$$C = \pi\eta R\sigma e^{-h} \tag{7}$$

Thus the number of contacts and the total contact area increase linearly with the load. Because both the total contact area and the number of asperities that are expected to touch increase linearly with the load, the average individual contact radius a is independent of the load. We note here

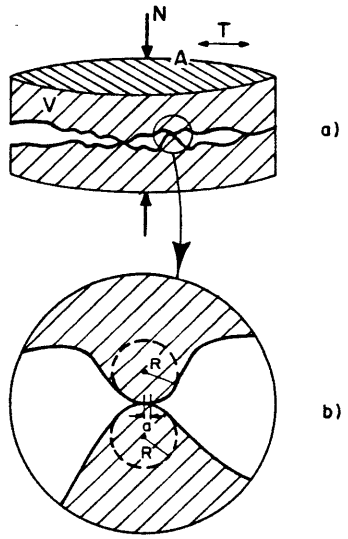

Fig. 2. (*a*) Schematic view of a small volume V of rock containing a single crack. This small volume is under a normal confining force N with an oscillating force T. The nominal area of the crack face is given by A. (*b*) A microscopic schematic view of the contact between the two sides of the crack. The asperity tips have radius R and a radius of contact a.

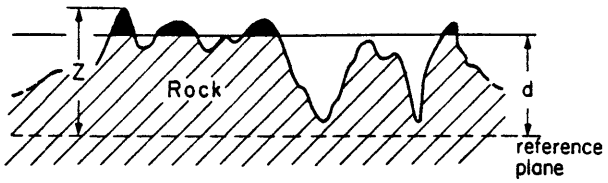

Fig. 3. Schematic view of the crack surface. The height of an asperity tip above the reference plane is given by Z. The height of the planar surface from the reference plane is d.

that there are actually two rough surfaces in contact, not one smooth surface and one rough one. It is more correct then to consider σ as one-half the standard deviation of the aperture between the two crack surfaces [*Walsh and Grosenbaugh*, 1979].

Now let us consider the work loss at an average contact. Given a load N on the volume V, then we take the expected load on each asperity contact to be N/n, with an expected oscillating shear force of T/n. Using these forces in the formulation of *Mindlin and Deresiewicz* [1953], the work loss per cycle ΔW, at the contact area of two spheres will be

$$\Delta W = \frac{(2 - \nu)T^3}{36\mu n^2 a f N} \tag{8}$$

where μ is the shear modulus of the matrix material and f is the coefficient of friction. We note that in the formulation of *Mindlin and Deresiewicz* [1953], the shear force T/n must be smaller than fN/n. This is so that the spheres do not slide completely across one another. Thus the central part of the circular area of contact does not slip while an annulus of area around it does. Assuming that $\mu \approx 0.25$ Mb and $f \approx 0.1$ [*Mavko*, 1979] and that T is given as in (16), then this condition is generally satisfied in our experiments.

Summing up the work losses at the n expected contacts, in a simple linear manner, gives the work loss for the total crack

$$\Delta W_T = n\Delta W \tag{9}$$

$$= \frac{(2 - \nu)T^3}{36\ \mu n a f N} \tag{10}$$

We now assume that the effective shear modulus μ^*, for this volume V, behaves like that of a sphere pack [*White*, 1965]

$$\mu^* = \mu_0 P^{1/3} \tag{11}$$

where

$$\mu_0 = \frac{[3(1 - \nu^2)E^2]^{1/3}}{2(2 - \nu)(1 + \nu)}$$

P is the confining pressure on V and

$$P = N/A \tag{12}$$

where A is the area of the reference plane contained in V. The total work done W_L, in a large volume V_L of rock is

$$W_L = 1/2\ V_L \mu^* \varepsilon^2 \tag{13}$$

where ε is the applied strain.

If we assume that V_L is composed of a number of small volumes V, containing a single crack and sum work losses as before, then the total work loss ΔW_L in the volume V_L will be

$$\Delta W_L = \zeta V_L \Delta W_T \tag{14}$$

where ζ is the crack density, but

$$Q^{-1} = \frac{\Delta W_L}{2\pi W_L} \tag{15}$$

Supposing that the sample confining pressure is the same as the pressure on the small volume (as in *Walsh and Grosenbaugh* [1979]) and substituting (6) through (14) into (15), then

$$Q^{-1} = \frac{k\zeta\varepsilon}{P^{4/3}} \tag{16}$$

where

$$k = \frac{(2 - \nu)\mu_0^2 A}{36\pi a f \mu n_0}$$

and

$$T = \mu^* \varepsilon A$$

As with previous models [*Mavko* 1979], this model predicts that attenuation increases linearly with strain amplitude, but it also postulates a linear increase of attenuation with crack density as well as an inverse variance to the four-thirds power with pressure.

Experimental Measurements

To supplement the sparse data available on attenuation values at varying strains and pressures, we conducted further experiments. The ultrasonic pulse transmission technique was used with the apparatus described by *Timur* [1977]. *Toksoz et al.* [1979] have presented further discussion concerning the experimental procedure involved in a pulse transmission experiment. The present apparatus was thoroughly tested for electronic linearity and repeatability.

Velocity data was collected concurrently with the attenuation data. This was accomplished by measuring the difference between the pulse generation time on one side of the sample and its time of reception on the other side. The sample length was accurately measured previous to the experiment and monitored while the experiment was in progress. Vacuum dried and Argon flushed Berea sandstone was used under both hydrostatic confining pressure and axial pressure. Experiments were also conducted with lucite as a sample.

Q^{-1} values were determined by the spectral ratio method, in conjunction with an aluminum standard, for the hydrostatically confined case. Unfortunately, attenuation calculations

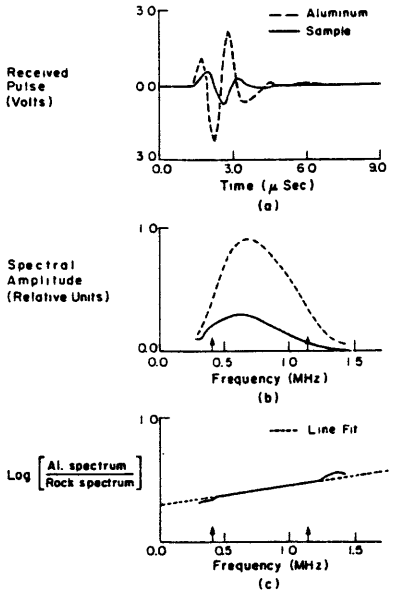

Fig. 4. Signal processing steps for attenuation measurement. (*a*) The output of the transducer that has received the pulses transmitted through the samples. The dotted line is the aluminum transmitted pulse, while the solid line is the rock transmitted pulse. The widths of the first cycles of the waveforms were used for the modified rise time Q^{-1} determination. (*b*) The Fourier transforms of the above pulses. (*c*) The logarithmic ratio of the above two spectra for the spectral ratio Q^{-1} determination. The dotted line is the least-square fit to the data points over the frequency range indicated by the vertical arrows.

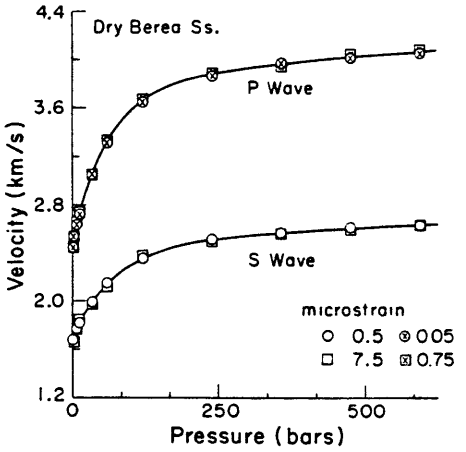

Fig. 5. *P* and *S* wave velocities of dry Berea sandstone as a function of hydrostatic confining pressure and strain amplitude. The *S* velocity values with strain amplitudes of 7.5×10^{-6} (squares) are almost identical to those with strain amplitudes of 0.5×10^{-6} (circles). The *P* velocities with smaller strains of 0.75×10^{-6} and 0.05×10^{-6} are very close also.

are notoriously variable. Pulse window lengths and the frequency intervals over which the calculations are performed are several factors that may have a large effect on the final attenuation value. We used a computer code that stepped through a number of window lengths and frequency intervals to arrive at the best attenuation line fit (i.e., the line with the least standard deviation from the data; see Figure 4). The variance of the data from this best fitting line was used to estimate the error in the Q^{-1} value. *Millahn* [1982] has given a realistic assessment of some of the errors involved with the estimation of Q^{-1}. For the experiments run under axial pressure a modified rise time method (discussed later) was used to calculate a Q^{-1} value.

Estimating the maximum strain amplitude of a wave propagating in a rock is another subtle problem [*Stoll*, 1979]. Indeed, in the ultrasonic case due to the apparatus and propagation complexity, we can arrive at only a rough estimate of the strain amplitude. We have used the approximate piezoelectric equations from *Hueter and Bolt* [1955] and the transducer manufacturer's specifications (Gulton Industries, Glennite Piezoceramics Bulletin H-500) to derive a voltage-strain relationship. It states that the strain amplitude generated by the piezoelectric transmitter is a linear function of the voltage applied to it. Similarly, the voltage produced by the receiving transducer is a linear function of the strain impinging upon it. The estimated strain amplitude radiated from the transmitter into the sample is corrected for the different impedance contrasts that are crossed as the pulse propagates from the transmitter to the receiver. We assume that these contrasts or interfaces are frequency

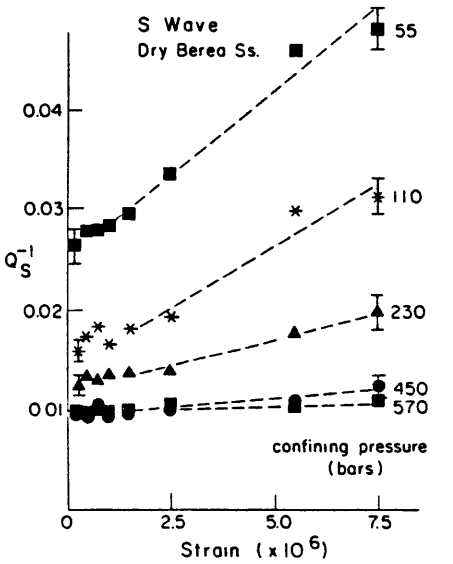

Fig. 6. *S* wave attenuation versus strain amplitude for dry Berea sandstone. The pulse transmission technique was used with the samples at various hydrostatic confining pressures. The error bars shown give the 99.5% confidence limits as determined from the best attenuation line fit.

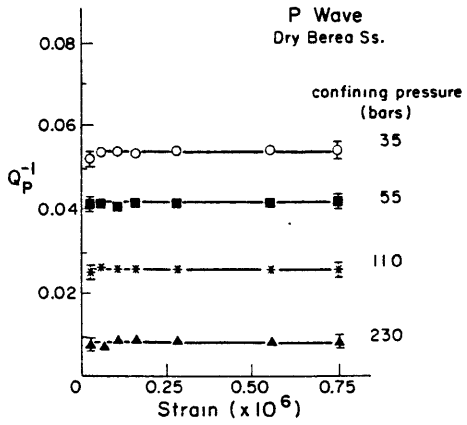

Fig. 7. *P* wave attenuation versus strain amplitude for dry Berea sandstone (the same sample as in Figure 6) at various pressures. Note the smaller strain amplitudes. The error bars shown give the 99.5% confidence limits as determined from the best attenuation line fit.

independent. The strain amplitude was varied in the system by changing the voltage applied to the transmitter. The voltage was taken in several steps from 12 V to 750 V.

All the received waveforms were recorded digitally on magnetic tape and computer processed. Good, but not uncommon, examples of the waveforms and their frequency content are shown in Figure 4. Generally, the lower end of the attenuation line was restricted to frequencies above about 0.4 MHz to avoid problems associated with ultrasonic beam diffraction [*Stewart*, 1981].

Dry Berea Sandstone

S waves with incident strain amplitudes from approximately 0.1×10^{-6} to 7.5×10^{-6} were used with a 5.0 cm thick dry Berea sample. The jacketed sample was hydrostatically confined at pressures varying from 2 bars to 580 bars. For the received waveforms to be consistent pressures in excess of 25 bars were generally required. This is due to poor or variable transducer coupling to the sample at low pressures. The shear wave velocity changed from 1.70 km/s at 2 bars to 2.65 km/s at 570 bars. Applied strain amplitudes had no observable effect on the velocity (Figure 5). The calculated Q_s^{-1} values (from the spectral ratio of the sample and aluminum) as a function of strain and pressure are shown in Figure 6. The error bars shown give the 99.5% confidence limits on Q^{-1} determined from the best line fit, as was discussed previously. We first note that the Q^{-1} value is fairly constant below strains of about 10^{-6}. As strain increases past 10^{-6} the Q_s^{-1} values increase linearly with strain. At low confining pressures (55 bars), Q_s^{-1} is almost doubled over the strain range used here. As the confining pressure is increased, the changes in the Q_s^{-1} values are diminished.

The transmitter and receiver contained both *P* and *S* wave transducers. Thus it was possible to perform a *P* wave experiment concurrently with the previously described *S* wave experiment at all pressures and voltage levels. Unfortunately the *P* transducer generated strains that were about an order of magnitude smaller (about 1×10^{-8} to 1×10^{-6}) than the *S* transducer. Referring to Figure 5, we see that there is again no effect of strain amplitude on *P* wave velocity. Likewise, at these small strain amplitudes there is no apparent dependence of attenuation on strain amplitude (Figure 7).

Because we were unable to achieve high enough strain amplitudes in this *P* wave experiment, we used a different set of high-output *P* wave transducers for another suite of measurements. In this experiment a dry Berea sandstone (a different sample but with the same dimensions as before) was kept under axial pressure. In this case, data were recorded from 25 bars to 600 bars. Again, because of transducer coupling problems the measurements made at 25 bars axial pressure are not as reliable as the higher pressure measurements. *P* waves were used with strain amplitudes from about 1×10^{-7} to 1×10^{-5}. The Q^{-1} values were calculated from the difference between the half-width t_s of the sandstone transmitted pulse and the half-width t_a of an aluminum transmitted pulse. The rise times of the sample and aluminum transmitted pulses are empirically related to the attenuation [*Gladwin and Stacey*, 1974; *Stacey et al.*, 1975] by the equation

$$t_s = t_a + CtQ^{-1} \tag{17}$$

where t is the sample propagation time and C is a constant given by *Gladwin and Stacey* [1974] as 0.53.

We use the pulse half-width as an approximation to the rise time. This modified rise time technique was used because the high output (air backed) transmitters generated waveforms that were ringy and not amenable to windowing and spectral ratio analysis. Again we observe the increase of Qp^{-1} with large strain amplitude and the reduction of the effect with increasing axial pressure (Figure 8). The low

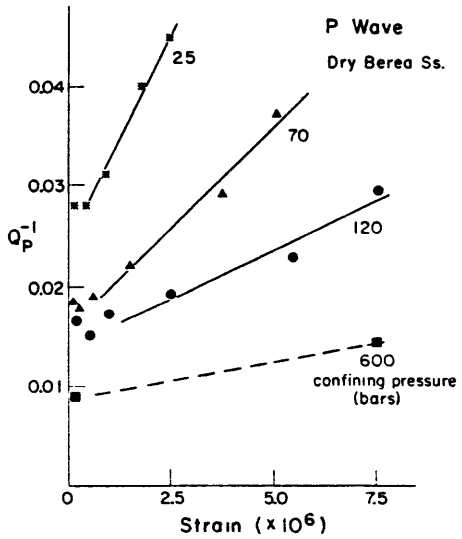

Fig. 8. *P* wave attenuation versus strain amplitude for dry Berea sandstone. The pulse transmission technique was used with the samples at various axial pressures.

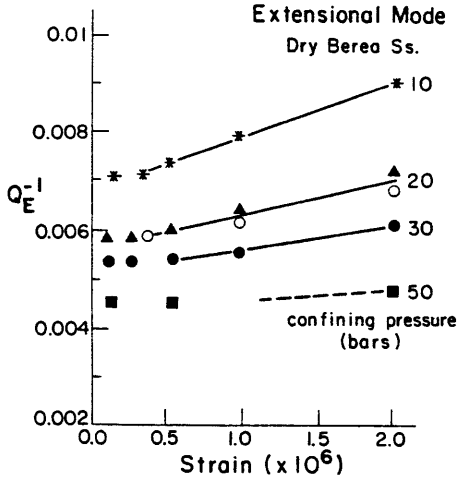

Fig. 9. Attenuation versus strain amplitude for Berea sandstone from *Winkler et al.* [1979]. The extensional mode vibrations of a resonating bar, at various pressures, were used to calculate a Q^{-1} value. The Q^{-1} values shown with open circles were made with a confining pressure of 50 bars but also a helium pore pressure of 30 bars.

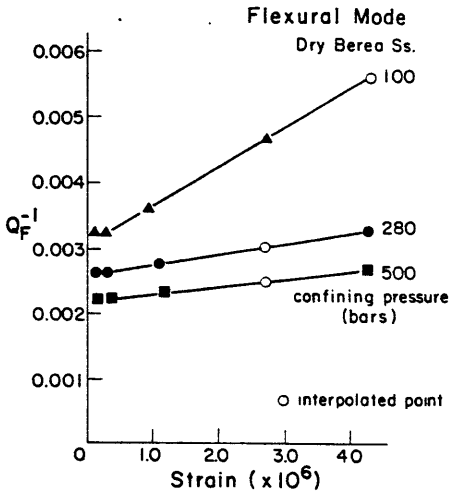

Fig. 10. Attenuation as a function of strain and confining pressure for dry Berea sandstone [from *Tittmann et al.*, 1981]. The flexural mode of a resonating bar under various pressures has been used to determine a Q^{-1} value. The empty circles are interpolated or extrapolated points.

strain axial Qp^{-1} values were somewhat different from the previous Qp^{-1} values. These differences may be due to the dissimilar type of confining pressure used (axial versus hydrostatic), the error inherent in the experiment and processing sequence, or the fact that a different rock sample had been used.

Two data sets from the literature are also included here. *Winkler et al.* [1979] performed an extensional mode, bar resonance experiment on dry Berea sandstone. Their results are shown in Figure 9. The onset of the strain dependence in their bar resonant experiment is at a strain value of about 0.3 × 10^{-6}. The linear increase of Q^{-1} with strain is again observed and the amount of the increase diminishes as the confining pressure increases. *Tittmann et al.* [1981] conducted a resonating bar experiment on dry Berea sandstone. They used the flexural mode of the bar at several confining pressures and strains. Their results are shown in Figure 10. Attenuation increases linearly with strain past a threshold value of about 0.3 × 10^{-6} and again the magnitude of the increase diminishes with increasing confining pressure. The magnitude of the attenuation of *Tittmann et al.* [1981] at low strains is also smaller than the ultrasonic attenuation. This will be discussed later in the paper.

From the previous Figures 6, 8, 9, and 10 we observe that greater confining pressures cause a decrease in the strain effect. To observe the effect of confining pressure on the magnitude of the strain dependent attenuation, we subtract the intercept or 'zero strain' value of Q^{-1} from the total Q^{-1} measured. This change in the Q^{-1} value from the intercept is called ΔQ^{-1}. The data from Figures 6, 8, 9, and 10 are now plotted as functions of pressure for constant strain amplitudes in Figures 11, 12, 13, and 14. The inverse dependence of ΔQ^{-1} on pressure is evident. The dotted line in the figures is ΔQ^{-1} varying exactly with pressure to the minus four-thirds power.

In Figure 11, the ΔQ^{-1} with the largest strains have dependences well-approximated by the inverse four-thirds power of confining pressure. At a strain amplitude of 1.5 × 10^{-6} the strain effect is beginning to decrease. At lower

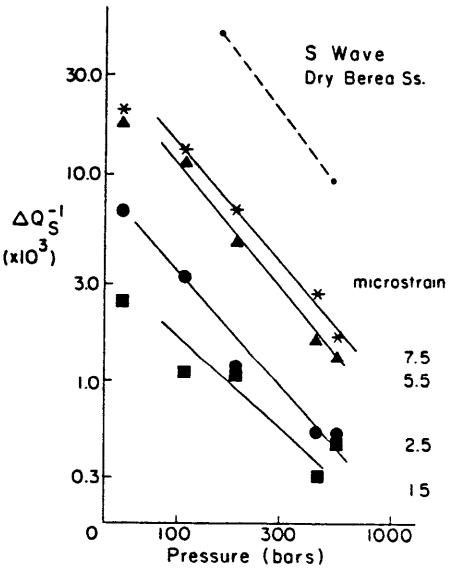

Fig. 11. The strain dependent part of the total attenuation as a function of confining pressure and strain amplitude for the same data as plotted in Figure 6. The data are plotted on a log-log scale and the broken line has an inverse four-thirds power dependence of ΔQ^{-1} on pressure.

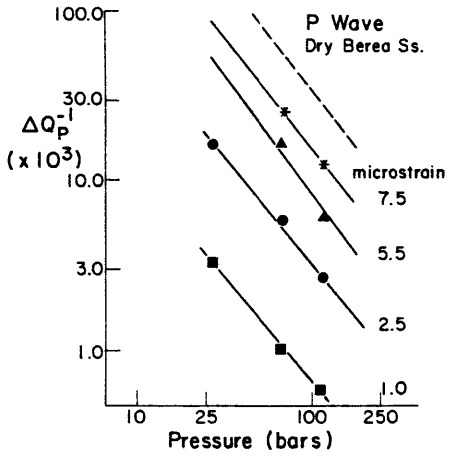

Fig. 12. The strain dependent part of the total attenuation versus confining pressure and strain amplitude for the data shown in Figure 8. The data are plotted on a log-log scale and the broken line has an inverse four-thirds power pressure dependence.

strains there is only scatter around a constant Q_s^{-1} value. Figure 12 has ΔQ_p^{-1} plotted versus axial pressure. All the strain levels here have a similar four-thirds dependence on pressure. The bar resonant data of *Winkler et al.* [1979] have been plotted in Figure 13. Generally, these values decrease with pressure to an exponent somewhat less than −4/3 except at the lowest pressure (10 bars). The pressure dependence of Q_E^{-1} begins to decrease at strains of about 0.3×10^{-6}. The results of *Tittmann et al.* [1981] for a bar resonance experiment are shown in Figure 14. These data depend inversely on pressure with a power between minus four-thirds and minus one.

Other Results

A lucite sample was run in our apparatus at several different pressures with a full suite of strains (1×10^{-7} to 1×10^{-5}). Q_s^{-1} values were distributed from 0.015 to 0.013 over the confining pressure range of 25 bars to 580 bars. Strain amplitude in this case had no consistent effect on the Q_s^{-1} values. *Johnston and Toksoz* [1980] report similar strain independence in their Plexiglas experiments (Figure 1) as do *Winkler et al.* [1979] in their lucite results. In another experiment, *Gordon and Davis* [1968] report the results of measurements made on a single quartz crystal. They found no strain dependence of Q^{-1} with strains from 1×10^{-9} to 1×10^{-5}.

One other relevant experiment in the literature is that reported by *Batzle et al.* [1980]. They made stress-strain measurements on several igneous rocks with various thermally induced fracture porosities ranging from 0.0% to 0.6%. They used very large (about 10^{-3}) quasi-static strains. From their hysteresis curves they deduced a Q^{-1} (the hysteresis loop defines ΔW, while the total area under the curve defines W, which gives Q^{-1} via (15)). Figure 15 reproduces their results. We note that $\Delta W/W$ or $2\pi Q^{-1}$ increases approximately linearly with fracture porosity. Assuming that fracture porosity is linearly related to crack density, then these results indicate that attenuation increases linearly with crack density. *Batzle et al.* [1980] quote other results which claim that at low strains porosity has no effect on $\Delta W/W$. *Johnston and Toksoz* [1980] attempted to demonstrate this also. They

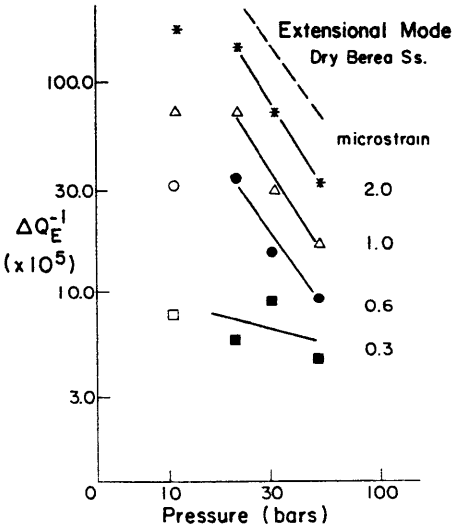

Fig. 13. The strain dependent part of the total attenuation plotted against the confining pressure and the strain amplitude for the data shown in Figure 9. The data are plotted on a log-log scale and the broken line has an inverse four-thirds power pressure dependence.

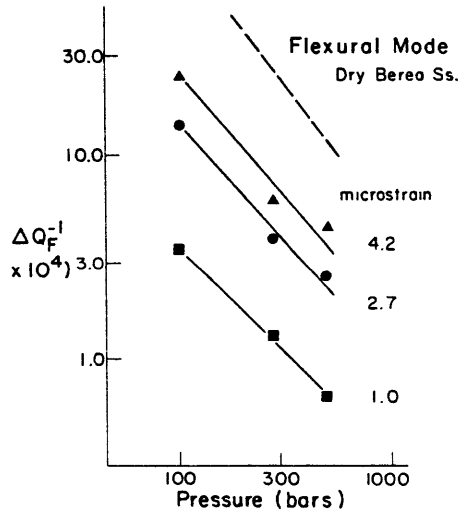

Fig. 14. The strain dependent part of the total attenuation as a function of the confining pressure and strain amplitude for the data shown in Figure 10. The data are plotted on a log-log scale and the broken line has an inverse four-thirds power pressure dependence.

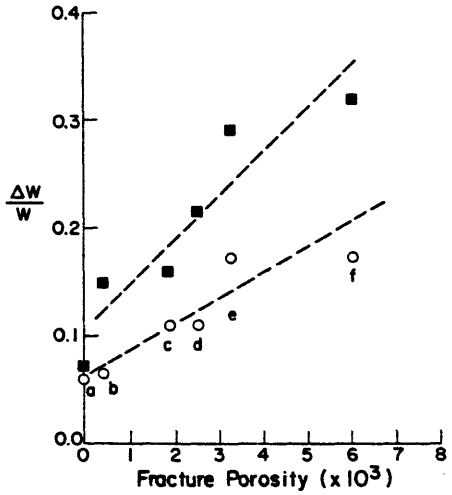

Fig. 15. The attenuation ($\Delta W/W$) from the work loss ratio on stress-strain curves as a function of porosity for a granite and diabase [from *Batzle et al.*, 1980]. Squares and open circles are for the first and second stress cycles, respectively. The samples were thermally cycled as follows: (*a*) diabase, no heating; (*b*) diabase to 500°C; (*c*) granite, unheated; (*d*) granite to 300°C; (*e*) diabase to 700°C; (*f*) granite to 500°C.

made Q^{-1} measurements on rocks before and after cracks had been induced by thermal cycling. The thermally-cracked rocks showed a large strain dependence effect. The virgin samples have much smaller dependencies. Thus, like the data of *Batzle et al.* [1980] these data suggest that Q^{-1} should increase with increasing fracture porosity (and thus crack density).

Discussion

It appears that materials that are not cracked or porous (lucite, Plexiglas, quartz crystals) do not display an increasing attenuation with increasing strain amplitude, while cracked materials do exhibit the strain effect. The observations support the original contention that cracks or pore wall contacts are the localities of large strain work loss. Furthermore, it appears that large strain attenuation is linearly related to the crack density.

As was mentioned earlier, the differences between the Q^{-1} values determined by the different techniques are somewhat worrisome. Several possible causes are apparent. For example, assuming that Poisson's ratio equals 0.25 and that Q_p^{-1} equals Q_s^{-1}, then Q_E^{-1} should be about equal to Q_p^{-1} [*Winkler and Nur*, 1979]. Still the Q_E^{-1} values in Figure 9 are much less than the Q_p^{-1} values in Figure 8. Different Berea sandstone samples have been used, however. As variation exists in the rock itself we would expect some variance in its properties. Also important is the effect on Q^{-1} of the trace amounts of moisture in otherwise 'dry' samples [*Clark et al.*, 1981].

In addition, the experiments themselves are different. The bar resonance and ultrasonic pulse measurements are made at very different frequencies. Even in dry rocks there may be some frequency dependence of attenuation.

As demonstrated, strain amplitudes clearly have an effect on the attenuation value. It appears though from the magnitude of the differences in the measured Q^{-1} values that the strain amplitudes are not the only cause of difference between the attenuation values determined by different laboratory techniques.

The predicted pressure dependence of the large strain effect is based on the sphere pack model of *White* [1965]. Thus while it appears to be a reasonable assumption for the sandstones considered here, it may be a poor assumption for other rocks.

Another point to discuss is that the attenuation loss was previously derived for only shear forces. It may be shown though [*Mindlin and Deresiewicz*, 1953; *Mavko*, 1979] that for oscillatory forces at oblique angles to the loading pressure on the two spheres of Figure 2b, the Q^{-1} determined will be multiplied by a constant. Thus for randomly-oriented cracks, the k in (16) will include an orientation constant.

The Fourier transform analysis involved in the spectral ratio method is generally applied to linearly propagating waves [*Stacey et al.*, 1975]. However, as our theory and experiments show at large strains, wave propagation is nonlinear. Nonetheless, from the quality of the data in Figure 6, it appears that Fourier transforms may be used at least approximately to analyze the time domain pulses, while (18) governs the propagation loss of a Fourier frequency component. This is probably because the aluminum-transmitted pulse propagates linearly and is taken to be the input pulse, while the output pulse from the rock is attenuated enough that it is in the linear propagation region also. In general, the subject of linear or nonlinear attenuation for different conditions still remains a topic of some contention [*McKavanagh and Stacey*, 1974].

Finally, when small strains ($< 1 \times 10^{-6}$) are used there does not seem to be a strain dependent effect, but there is nonetheless still a nonzero attenuation. Thus perhaps the total attenuation Q_{total}^{-1}, may be the sum of several terms (ΣQ_i^{-1}) representing different types of strain independent losses plus the strain dependent term (as suggested by *Johnston et al.* [1979]; *Mavko* [1979])

$$Q_{\text{total}}^{-1} = \Sigma Q_i^{-1} + k\zeta e/P^{4/3} \tag{18}$$

Because of this lack of strain dependence in Q^{-1} at small strains, it appears that contact friction (as described by *Mindlin and Deresiewicz* [1953]) is not dominant or operable. This is perhaps because the normal force on the contact does not go to zero on the perimeter of the contact area, as is assumed by *Mindlin and Deresiewicz* [1953]. Other possibilities exist. Perhaps with only fractions of microstrains applied, the static coefficient of friction may not be overcome, or indeed the concepts of macroscopic friction may not apply [*Savage*, 1969].

Although the notions of contact friction may not apply to small strain attenuation, the statistical crack description holds great potential for the description of large and small strain attenuation as well as other rock properties [*Walsh and Grosenbaugh*, 1979; *Palmer and Traviolia*, 1980; *Walsh*, 1981].

Conclusions

In summary, we have presented both theoretical analysis and experimental verification of the large strain amplitude ($>1 \times 10^{-6}$), pressure and crack density dependence of

attenuation. The observations and model suggest that attenuation in dry rocks, for this strain regime, is caused by frictional work dissipation from the rubbing together of asperities on crack surfaces. For large strain amplitudes, attenuation increases linearly with strain amplitude and crack density. Attenuation varies approximately with the minus four-thirds power of confining pressure.

Because different experiments for measuring attenuation may operate at different strain levels, care must be exercised when comparing the respective data sets. Large strains will attenuate much more rapidly than small strains, thus increasing the applied strain amplitude does not increase the propagated wave amplitude proportionally.

Acknowledgments. We are grateful to the Chevron Oil Field Research Company (COFRC), La Habra, California, for releasing the ultrasonic data presented here. This research was partly supported by Geophysical Service, Inc., under grant P06077-W63550.

REFERENCES

Batzle, M. J., G. Simmons, and R. W. Siegfried, Microcrack closure in rocks under stress: Direct observation, *J. Geophys. Res.*, *85*, 7072–7090, 1980.

Clark, V. A., T. W. Spencer, and B. R. Tittmann, The effect of thermal cycling on the seismic quality factor Q of some sedimentary rocks, *J. Geophys. Res.*, *86*, 7087–7094, 1981.

Gangi, A. F., Variation of whole and fractured porous rock permeability with confining pressure, *Int. J. Rock Mech. Mining Sci.*, *15*, 249–257, 1978.

Gladwin, M. T., and F. D. Stacey, Anelastic degradation of acoustic pulses in rock, *Phys. Earth Planet. Int.*, *8*, 332–336, 1974.

Gordon, R. B., and L. A. Davis, Velocity and attenuation of seismic waves in imperfectly elastic rock, *J. Geophys. Res.*, *73*, 3917–3935, 1968.

Gordon, R. B., and D. Rader, Imperfect elasticity of rock: Its influence on the velocity of stress waves, in *The Structure and Physical Properties of the Earth's Crust, Geophys. Monogr. Ser.*, vol. 14, edited by J. G. Heacock, p. 235, AGU, Washington, D. C., 1971.

Greenwood, J. A., and J. B. P. Williamson, Contact of nominally flat surfaces, *Proc. R. Soc. London Ser. A*, *295*, 300, 1966.

Hueter, T. F., and R. H. Bolt, *Sonics: Techniques for the Use of Sound and Ultrasound in Engineering and Science*, John Wiley, New York, 1955.

Imai, T., T. Kanamori, and K. Tonouchi, Determination of dynamic deformation characteristics of soils by seismic methods and laboratory tests, *Tech. Rep. RP-4106*, OYO Corp., Tokyo, Japan, 1979.

Johnston, D. H., and M. N. Toksoz, Thermal cracking and amplitude dependent attenuation, *J. Geophys. Res.*, *85*, 937–942, 1980.

Johnston, D. H., M. N. Toksoz, and A. Timur, Attenuation of seismic waves in dry and saturated rocks, II, Mechanisms, *Geophysics*, *44*, 691–711, 1979.

Kovach, R. L., and A. M. Nur, Stanford Q Conference, *J. Geophys. Res.*, *85*, 5171, 1980.

Mavko, G. M., Frictional attenuation: An inherent amplitude dependence, *J. Geophys. Res.*, *84*, 4769–4775, 1979.

McKavanagh, B., and F. D. Stacey, Mechanical hysteresis in rocks at low strain amplitudes and seismic frequencies, *Phys. Earth Planet. Int.*, *8*, 246, 1974.

Millahn, K. O., Comment on 'Measurement of absorption and dispersion from check shot surveys' by D. C. Ganley and E. K. Kanasewich, *J. Geophys. Res.*, *87*, 1784–1785, 1982.

Mindlin, R. D., and H. Deresiewicz, Elastic spheres in contact under varying oblique forces, *J. Appl. Mech.*, *20*, 327–344, 1953.

Palmer, I. D., and M. L. Traviola, Attenuation by squirt flow in undersaturated gas sands, *Geophysics*, *45*, 1780–1792, 1980.

Peselnick, L., and W. F. Outerbridge, Internal friction and rigidity modulus of Solenhofen limestone over a wide frequency range, *U.S. Geol. Surv. Prof. Pap. 400B*, 1961.

Richart, F. E., J. R. Hall, and R. D. Woods, *Vibrations of Soils and Foundations*, Prentice-Hall, Englewood Cliffs, N. J., 1970.

Savage, J. C., Comment on 'Velocity and attenuation of seismic waves by imperfectly elastic rock' by R. B. Gordon and L. A. Davis, *J. Geophys. Res.*, *74*, 726–728, 1969.

Sears, F. M., Analysis of microcracks in dry polycrystalline NaCL by ultrasonic signal processing, *Rep. UCRL-52975*, Lawrence Livermore Lab., Livermore, Calif., 1980.

Spencer, J. W., Stress relaxation at low frequencies in fluid-saturated rocks: Attenuation and modulus dispersion, *J. Geophys. Res.*, *86*, 1803–1812, 1981.

Stacey, F. D., M. T. Gladwin, B. McKavanagh, A. T. Linde, L. M. Hastie, Anelastic damping of acoustic and seismic pulses, *Geophys. Surv.*, *2*, 131–151, 1975.

Stewart, R. R., Ultrasonic beam diffraction and its effect on attenuation measurement, *Geophysics*, in press, 1981.

Stoll, R. D., Experimental studies of attenuation in sediments, *J Acoust. Soc. Am.*, *66*, 4, 1979.

Timur, A., Temperature dependence of compressional and shear wave velocities in rocks, *Geophysics*, *42*, 1977.

Tittmann, B. R., J. R. Bulau, M. Abdel-Gawad, L. Ahlberg, C. Salvado, and H. Nadler, Experimental results on seismic losses in porous rocks over a wide range of frequencies and physical states of rocks, paper presented at the 51st Annual SEG Meeting, Los Angeles, Calif., Oct. 11–16, 1981.

Toksoz, M. N., D. H. Johnston, and A. Timur, Attenuation of seismic waves in dry and saturated rocks, I, Laboratory measurements, *Geophysics*, *44*, 681–690, 1979.

Walsh, J. B., Effect of pore pressure and confining pressure on fracture permeability, *Int. J. Rock Mech. Mining Sci.*, *18*, 429–935, 1981.

Walsh, J. B., and M. A. Grosenbaugh, A new model for analyzing the effect of fractures on compressibility, *J. Geophys. Res.*, *84*, 3532–3535, 1979.

White, J. E., *Seismic Waves: Radiation, Transmission, and Attenuation*, McGraw-Hill, New York, 1965

Winkler, K., and A. Nur, Pore fluids and seismic attenuation in rocks, *Geophys. Res. Lett.*, *6*, 1–4, 1979

Winkler, K., A. Nur, and M. Gladwin, Friction and seismic attenuation in rocks, *Nature*, *277*, 528–531, 1979.

(Received April 23, 1982;
accepted October 15, 1982.)

APPENDIX III

Ray Trace Integral Derivation

Assuming Snell's Law, we derive (after Grant and West, 1965) the traveltime integral shown in equation (3) of Chapter 2 . The horizontal ray path increment dx is related to the vertical increment dz and incidence angle θ by

$$dx = \tan\theta \, dz \qquad \theta<\pi/2 \tag{1}$$

Integrating equation (1) over some depth, H, gives the total horizontal distance traveled by the ray

$$X = \int_o^H \tan\theta \, dz \tag{2}$$

But Snell's Law states that

$$\frac{\sin\theta(z)}{V(z)} = p \tag{3}$$

where $\sin\theta(z)$ is the sine of the angle-of-incidence at a depth, z

V(z) is the velocity at the depth, z

p is the ray parameter which is constant for a given ray

Substituting equation (3) into equation (2) gives

$$X(H) = \int_o^H \frac{pV(z)\,dz}{[1-p^2V^2(z)]^{1/2}} \tag{4}$$

Now

$$dt = \frac{dz}{V(z)\cos\theta(z)} \tag{5}$$

Upon integrating equation (5) to depth, H, and substituting equation (3) into that integral, we arrive at

$$T(H) = \int_o^H \frac{dz}{V(z)[1-p^2V^2(z)]^{1/2}} \tag{6}$$

To solve the above equation, we must find p as a function of depth. That is, as measurements are made down the well, we need to know what ray parameters are required to have a ray from a given offset arrive at a given depth. Now differentiating equation (6)

$$\frac{dT}{dH} = \frac{d}{dH} \int_o^H \frac{dz}{V(z)[1-p^2(H)V^2(z)]^{1/2}} \tag{7}$$

$$= p(H)\left(\frac{dp}{dH}\right) \int_o^H \frac{V(z)dz}{[1-p^2(H)V^2(z)]^{3/2}} + \frac{1}{V(H)[1-p^2(H)V^2(H)]^{1/2}} \tag{8}$$

But the source offset is constant so that

$$dX = 0 \tag{9}$$

then differentiating equation (4) to find $\frac{dX}{dH}$ and substituting this into equation (9) gives

$$\frac{p(H)V(H)}{[1-p^2(H)V^2(H)]^{1/2}} = -\int_o^H \frac{V(z)\left(\frac{dp}{dH}\right)dz}{[1-p^2(H)V^2(z)]^{3/2}} \tag{10}$$

and substituting equation (10) into (8)

$$p^2(H) = \frac{1}{V^2(H)} - \left(\frac{dT}{dH}\right)^2 \tag{11}$$

Then putting equation (11) in (6) gives us the desired result

$$T(H) = \int_o^H \{1-V^2(z)\left[\frac{1}{V^2(H)} - \left(\frac{dT}{dz}\right)_H^2\right]\}^{-1/2} \frac{dz}{V(z)} \tag{12}$$

APPENDIX IV

Seismogram Manual Picking Error

Intuitively, one expects that the accuracy of a first-break pick on a seismogram will be related to the frequency of the arrival, f_m, and the signal-to-noise ratio (S/N).

Aki and Richards (1980) have given a formula to quantify the above intuitions. They suggest that the time-picking error, Δt, is as follows

$$\Delta t = \frac{1}{f_m \log_2\left(1+\left(\frac{S}{N}\right)^2\right)} \qquad (1)$$

The signal-to-noise ratio for a first break, though, is difficult to define. Aki and Richards (1980) empirically determined that the RMS amplitude, S, should be set equal to 1/20 of the maximum height of the arrival. N is the standard RMS amplitude of the noise.

Suppose, for example, that f_m = 100 Hz and S/N = 3, then Δt = 3 ms. This value is probably realistic for a single seismogram but perhaps too large for the hand-picked VSP case, as there is some type of eye correlation between VSP traces at consecutive depths which gives a pick with less error.

APPENDIX V

VSP Lateral Resolution

Using the Fresnel zone concept (Sheriff, 1977) we may attempt to find approximately what area of a reflector (or transmitter in this case) contributes to the transmitted pulse received at a point at some distance below the reflector. The first Fresnel zone is that area of a reflector from which energy arrives and constructively interferes with the transmitted pulse. To calculate the VSP Fresnel zone, we consider the very simple case shown in Figure 1. In this case, there is a point source directly above the receiver on a constant velocity (V) section with a single density contrast interface. The distance from the source to the interface is R_s, and the interface to receiver distance is R. The first Fresnel zone radius X is that distance on the interface from which waves are recorded at the receiver up to 1/2 a period (or equivalently 1/2 wavelength) behind those waves which propagated in a straight line between the source and receiver.

Equating the direct travel path plus a half-period delay with the maximum delay Fresnel zone path gives the following

$$\frac{R-r}{V} + \frac{T}{2} = \frac{(R^2 + X^2)^{1/2}}{V} \tag{1}$$

but

$$T = \frac{1}{f} = \lambda \tag{2}$$

then

$$R-r + \frac{\lambda}{2} = (R^2 + X^2)^{1/2} \tag{3}$$

and

$$r = (R_s^2 + X^2)^{1/2} - R_s$$

suppose $X \ll R_s$, then $r = \frac{X^2}{2R_s}$ (4)

From equation (3) and assuming that $X \ll R$

$$R - \frac{X^2}{2R_s} + \frac{\lambda}{2} = R + \frac{X^2}{2R} \tag{5}$$

or simplifying

$$X^2 = \frac{\lambda R R_s}{R+R_s}$$

$$X = \left(\frac{\lambda\, RR_s}{R+R_s}\right)^{1/2} \tag{6}$$

This is approximately the farthest lateral distance on the interface which may affect the first arriving wave at some receiver below the interface.

Consider the following example with R_s = 2000 ft, R = 1000 ft, λ = 200 ft, then putting these values into equation (6) gives a first Fresnel zone radius of about 350 ft. Thus, the spherical wave can sample a rock volume a considerable distance from the borehole.

Figure 1. Schematic diagram for VSP Fresnel zone. Velocity is constant in the section, but there is a density contrast at a depth R_s from the surface source (s). The receiver is at a depth R below the interface. The path from the source to the Fresnel radius X on the interface inscribes an arc (dotted line) which cuts the vertical at a distance r below the interface.

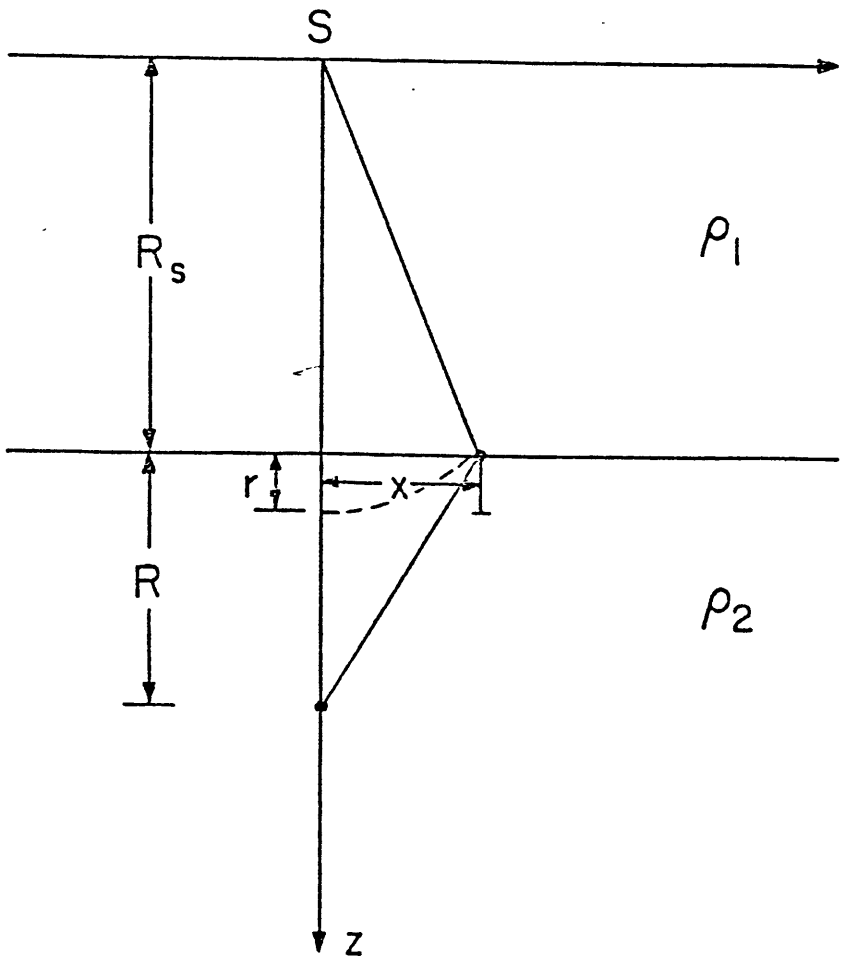

Figure 1.

APPENDIX VI

Seismic and Sonic Survey Problems

Discussed here are the effects which cause the sonic log interval transit time (Δt) and the VSP traveltime (t) to be different from each other and some true value. Brief comments are given on ways to overcome these difficulties.

Δt TOO LONG

(a) A noise spike occurring on the closest receiver before the actual pulse arrives may cause an early time pick from that receiver.

(b) The pulse detection algorithm may miss the first arriving energy on the far receiver entirely and pick a later arrival (cycle skipping).

(c) The amplitude of the waveform may be smaller on the far receiver than on the near receiver; thus, a constantly biased pulse height picker will pick later on the far receiver's waveform than on that of the near receiver (Δt stretch).

Note that the above may be largely resolved by muting, despiking, and suitable gain control.

(d) If the borehole diameter is too large, the traveltime will be that of the mud which is generally longer than that of the formation.

(e) In a formation that is not gas filled, the drilling-induced alteration generally lowers the velocity of the adjacent formation with corresponding increase in the sonic time.

These latter problems are severe ones but may be overcome, at least theoretically, by a long spacing between receivers.

Δt TOO SHORT

(f) A noise spike on the far receiver channel causes the picking algorithm to trigger before the pulse arrives and thus gives an early time pick.

(g) Cycle skipping may occur on the closest receiver causing a delayed time pick.

These problems are overcome as before with muting, etc.

(h) Drilling mud may displace gas in a formation and thus cause a higher compressional velocity than that of the virgin formation with corresponding shortened traveltime (Gregory, 1977).

(i) The drilling mud may have a velocity higher than the formation [gas-bearing shales, near-surface sediments (Goetz et al., 1979)], causing the first arrivals on both receivers to be mud transmitted and thus faster than the energy which travels through the formation.

A multireceiver sonic tool and careful analysis may be necessary to correct these difficulties which are presently becoming recognized and researched.

(j) As energy follows the fastest path between points, highly dipping thin beds may cause velocities to be measured slightly too high.

It is claimed that excentering the sonic tool reduces this effect (Goetz et al., 1979; Castagna, 1982).

(k) Intrinsic dispersion causes the high sonic frequencies to travel faster than seismic waves (discussed later in the paper) which may give sonic times consistently less than the check shot times.

The check shot traveltime (from source to receiver) has errors associated with it also. Again, we separate these effects into categories which make the check shot times either too long or too short with respect to some correct value and the sonic log. Included are very brief comments on methods to overcome these discrepancies.

$t_{seismic}$ TOO LONG

(a) An insensitive picking algorithm may give a positive shift to the time picks.

This problem may be corrected by a careful utilization of picking techniques (e.g., manually-constrained trace crosscorrelation).

(b) The check shot cable and instruments may introduce time delays.

These instrument delays may be accounted for and calibrated previous to the experiment.

(c) Dispersion, Q, and multiples all cause apparent time delays of the maximum energy in a waveform.

These effects require modeling to determine their magnitude and structure and are discussed earlier in the paper.

$t_{seismic}$ TOO SHORT

(d) A deviated well may have a considerably longer total length than actual depth. Thus, the seismic energy may have appeared to travel farther than it actually has. The uncorrected traveltime will be too short relative to the integrated sonic (which equivalently has been integrated over a distance too long).

Corrections using a deviated borehole survey can minimize this problem.

(e) Curved ray propagation or refraction in a layered medium gives a traveltime which is generally made too short after reducing it to the vertical time by simple straight ray assumptions in relation to the true vertical traveltime.

(f) Rays follow the fastest path between two points, thus highly dipping thick beds can cause seismic traveltimes to be considerably shorter than the integrated sonic times (Goetz et al., 1979).

Using an adequate ray trace correction gives a more accurate vertical traveltime.

(g) Anisotropy with higher horizontal than vertical velocities will also make seismic energy appear to arrive too fast with respect to the sonic log.

(h) Lateral formation changes with higher velocities will allow the seismic energy to follow a faster path.

(i) High velocity waves propagating in the near-surface casing may give a small but measureable first break.

Again, these effects require rather careful analysis, perhaps with offset sources, to determine the nature of the anisotropy, lateral inhomogeneity or wave type. They are areas of current research.

APPENDIX VII

SHORT-PATH MULTIPLE-INDUCED TIME DELAY

It is reasonable to suspect that the time delay caused by short-path multiples is somehow related to the number of reflecting layers, the strength of the reflectors, and the traveltime in each layer.

For a given time after the directly transmitted impulse, there will be a number of multiples arriving. As the number of layers and the time after the direct arrival increases, there are an increasing number of paths (multiple bounces) that a wave could follow to arrive at that particular time. However, as the number of layers increases, the magnitude of the reflection coefficients between the layers will decrease. Thus there will be a time, generally some time after the direct arrival, which has the largest amplitude (the trade-off time between greatest number of multiples arriving and transmission losses).

For example, suppose a time is picked in the impulse response that is 4 two-way time units after the direct arrival. A spike arriving at this time can occur in a number of ways, three of which are shown (for equal times in a layer) in Figure 1.

Thus, the longer the delay is from the direct arrival, the greater the possible number of arrivals. Also, for a greater number of layers, there is a greater number of any given multiple type. Again, though, the amplitude of a given multiple is decreased for every reflection or transmission.

If there is a bandlimited input used as opposed to the delta function, the transmitted response will be smoothed. However, as the bandlimited pulse is considerably longer than the traveltimes of the short-path multiples which contribute to the early impulse response, the bandwidth is

not expected to shift the time of the maximum arrival. That is, we are assuming that the wavelengths are much larger than the layer thicknesses and, thus, are not a first order effect.

Schoenberger and Levin (1978) showed empirically that traveltime delays due to multipathing were linearly related to the apparent cumulative attenuation. Richards and Menke (1982) proposed an expression for the apparent attenuation due to multipathing (scattering) based on the mean square value of the reflection coefficients σ^2 in a set of layers and the average velocity $\overline{V}$

$$Q^{-1} = 5 \times 10^{-4} \sigma^2 \overline{V} \tag{1}$$

These results suggest that the apparent attenuation is dependent on the reflection coefficients and the cumulative apparent attenuation is related to the number of layers. On this basis the following formula for time delay is proposed.

$$t_{delay} = K \sum_{i}^{N} |R_i|^2 \Delta t_i \tag{2}$$

where K is an empirically-determined constant

N is the number of layers

$|\overline{R}_i|$ is the magnitude of the reflection coefficient at the bottom of layer i

Δt_i is the average traveltime in a layer i

FIGURE CAPTION

Figure 1. Diagram of several multiple bounces in a layered (Goupillaud) medium. The energy arrives at the same time in these three cases.

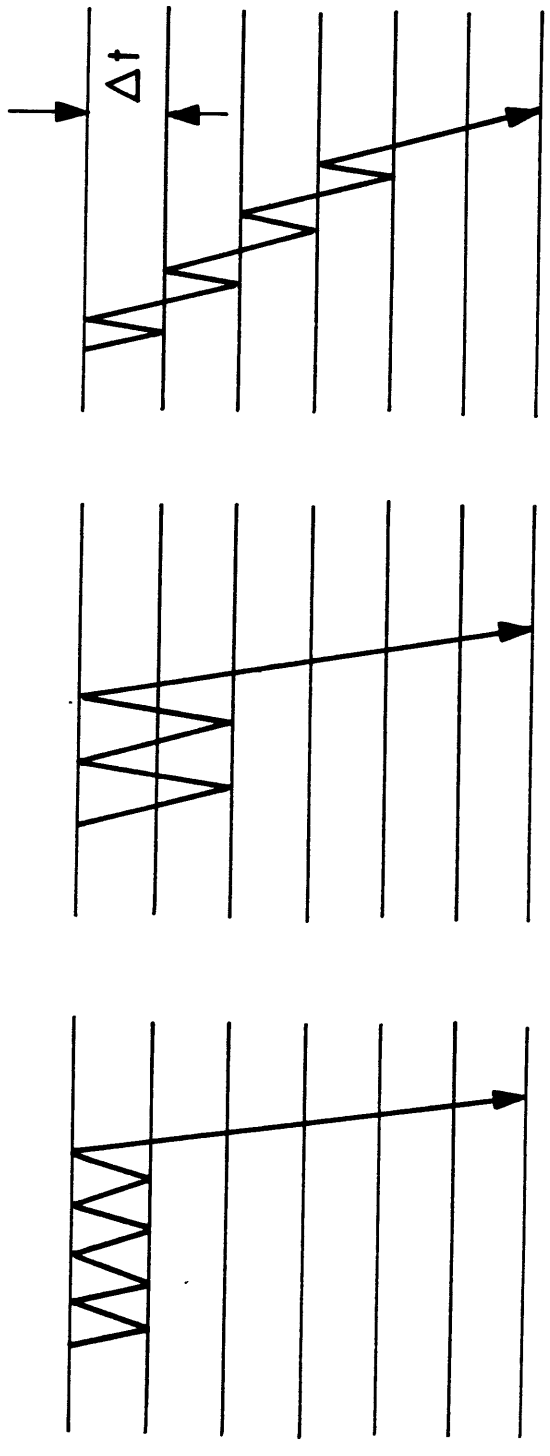

Figure 1

APPENDIX VIII

Dispersion-Induced Time Delay

Aki and Richards (1980) use the laboratory observations of creep in rocks (Lomnitz, 1956; 1957) and stress strain relations to derive a frequency-dependent velocity. In their formulation, Q is nearly constant. They show that

$$c(\omega) = c(a)\ \{1 - \frac{1}{\pi Q}\ [\gamma + \ln\ (\frac{\omega}{a})]\}^{-1} \qquad (1)$$

where $c(\omega)$ is the phase velocity at some frequency ω

Q is the quality factor at ω

γ is Euler's constant ($\simeq .577$)

c is velocity at some very high frequency a

For two arbitrary frequencies ω_1, ω_2, and assuming that πQ is large then equation (1) reduces to

$$\frac{c(\omega_1)}{c(\omega_2)} = 1 + \frac{1}{\pi Q} \ln\ (\frac{\omega_1}{\omega_2}) \qquad (2)$$

Equation (2) is that of Azimi et al. (1968) who suggested it as part of their causal-linear (Hilbert transform) theory. It is also the same as that of Futterman (1962) who found it by insisting on a linearly propagating causal pulse with constant attenuation factor α. Some care is required, however, in defining Q which is nearly constant in some formulations while varying in others. Note that the second term in equation (2) is the first order correction to a constant velocity. Q is also a function of frequency and to first order has an equation similar to equation (2). Thus variations in Q may be neglected to find the velocity equation correct to the first order only.

The group velocity in an elastic medium V is defined as follows

$$V(\omega) = \frac{c(\omega)}{1 - \frac{\omega}{c(\omega)} \frac{dc(\omega)}{d\omega}} \tag{3}$$

Assuming that the group velocity is approximately the same in an attenuative medium and using equation (1) substituted into (3) for two frequencies gives

$$\frac{V(\omega_1)}{V(\omega_2)} \approx 1 + \frac{1}{\pi Q} \ln \left(\frac{\omega_1}{\omega_2}\right) \tag{4}$$

Thus, the group velocities are related in a similar manner as are the phase velocities.

If we are interested in finding the traveltime delay between two pulses or wave packets centered at frequencies ω_1, ω_2, after having traveled some distance d through a homogeneous medium, then the following equation is of use

$$t_{delay} = \frac{d}{V(\omega_1)} - \frac{d}{V(\omega_2)} \tag{5}$$

and substituting equation (4) into (5) gives

$$t_{delay} = \frac{d}{V(\omega_2)} \frac{1}{1 + \frac{1}{\pi Q} \ln \left(\frac{\omega_1}{\omega_2}\right)} - 1 \tag{6}$$

and simplifying equation (6) with the assumption that $\frac{1}{\pi Q} \ln(\frac{\omega_1}{\omega_2})$ is small

$$t_{delay} = \frac{d \ln \left(\frac{\omega_2}{\omega_1}\right)}{V(\omega_2)\ \pi Q} \tag{7}$$

Equation (7) predicts the amount of time delay between two pulses propagating with two different frequencies.

For a consolidated section with a sonic velocity of 15,000 ft/s and a a Q of 100 over a 2000 ft distance, equation (7) predicts a delay of only 2.5 ms. Even so, propagation to 10,000 ft and back to the surface would give a dispersive delay of 25.0 ms.